การกำหนดบริเวณที่เป็นไปได้ของโหลดด้วยวิธีการตามรอยขอบเขต

นายสถาพร ลิมป์ปัทมปาณี

วิทยานิพนธ์นี้เป็นส่วนหนึ่งของการศึกษาตามหลักสูตรปริญญาวิศวกรรมศาสตรดุษฎีบัณฑิต
สาขาวิชาวิศวกรรมไฟฟ้า ภาควิชาวิศวกรรมไฟฟ้า
คณะวิศวกรรมศาสตร์ จุฬาลงกรณ์มหาวิทยาลัย
ปีการศึกษา 2554

# LOAD FEASIBLE REGION DETERMINATION USING BOUNDARY TRACING METHOD

Mr. Sataporn Limpatthamapanee

A Dissertation Submitted in Partial Fulfillment of the Requirements

for the Degree of Doctor of Philosophy Program in Electrical Engineering

Department of Electrical Engineering

Faculty of Engineering

Chulalongkorn University

Academic year 2011

| | |
|---|---|
| Thesis Title | LOAD FEASIBLE REGION DETERMINATION USING BOUNDARY TRACING METHOD |
| By | Mr. Sataporn Limpatthamapanee |
| Field of Study | Electrical Engineering |
| Thesis Advisor | Assistant Professor Sotdhipong Phichaisawat, Ph.D. |

---

Accepted by the Faculty of Engineering, Chulalongkorn University in Partial Fulfillment of the Requirements for the Doctoral Degree

…….. Dean of the Faculty of Engineering

(Associate Professor Boonsom Lerdhirunwong, Dr.Ing.)

THESIS COMMITTEE

……..Chairman

(Professor Bundhit Eua-arporn, Ph.D.)

……. Thesis Advisor

(Assistant Professor Sotdhipong Phichaisawat, Ph.D.)

…….. Examiner

(Chanarong Banmongkol, Ph.D.)

…….. Examiner

(Surachai Chaitusaney, Ph.D.)

…….. External Examiner

(Pradit Fuangfoo, Ph.D.)

สถาพร ลิมป์ปัทมปาณี : การกำหนดบริเวณที่เป็นไปได้ของโหลดด้วยวิธีการตามรอยขอบเขต. (LOAD FEASIBLE REGION DETERMINATION USING BOUNDARY TRACING METHOD) อ. ที่ปรึกษาวิทยานิพนธ์หลัก: ผศ. ดร. โสตถิพงศ์ พิชัยสวัสดิ์, 173 หน้า.

วิทยานิพนธ์นี้นำเสนอวิธีการกำหนดบริเวณที่เป็นไปได้ของโหลดบนระนาบระหว่างแกนกำลังไฟฟ้าจริงและแกนกำลังไฟฟ้ารีแอกทีฟ โดยปัญหาที่พิจาณาในงานวิจัยนี้คือการตรวจสอบความสามารถส่งผ่านกำลังไฟฟ้าจากพื้นที่ต้นทางไปยังพื้นที่ปลายทางใด ๆ ของระบบไฟฟ้ากำลัง ทั้งนี้วิธีการที่นำเสนอใช้กระบวนการตามรอยขอบเขตโดยการกำหนดจุดขอบของบริเวณที่เป็นไปได้ของโหลดด้วยการหาระยะทางสั้นที่สุดจากจุดโหลดที่เป็นไปไม่ได้ หลังจากนั้นจึงติดตามหาขอบเขตด้วยกระบวนการทางเวกเตอร์และการหาระยะทางสั้นสุดสลับกันไปจนกว่าจะได้รูปวงปิดของบริเวณที่เป็นไปได้ของโหลดออกมา วิธีการที่นำเสนอได้รับการทดสอบกับระบบ 2 บัส ระบบ 6 บัส ระบบ IEEE 24 บัส และระบบไฟฟ้ากำลังของประเทศไทย ซึ่งผลการทดสอบแสดงให้เห็นว่าวิธีการนี้สามารถกำหนดบริเวณที่เป็นไปได้ของโหลดสำหรับการส่งกำลังไฟฟ้าระหว่างต้นทางและปลายทางต่าง ๆ ได้ ซึ่งบริเวณที่เป็นไปได้ของโหลดจะบ่งบอกถึงขีดจำกัดในการเปลี่ยนแปลงโหลดด้วยปัจจัยต่าง ๆ เช่น การเพิ่มโหลด การตัดโหลด และการชดเชยกำลังไฟฟ้ารีแอกทีฟ เป็นต้น วิธีการนี้ทำให้เห็นสภาวะความเป็นไปได้ของโหลดอย่างชัดเจนมากกว่าวิธีการกำหนดขอบเขตของโหลดแบบดั้งเดิม อาทิ การคำนวณเพาเวอร์โฟลว์แบบซ้ำและการคำนวณเพาเวอร์โฟล์วแบบต่อเนื่องเป็นต้น นอกจากนี้วิธีการที่นำเสนอยังสามารถหาขอบเขตนอกสุดของพื้นที่เป็นไปได้ของโหลดอันเนื่องมาจากพารามิเตอร์ของระบบที่สนใจได้อีกด้วย

ภาควิชา...วิศวกรรมไฟฟ้า... ลายมือชื่อนิสิต.....
สาขาวิชา..วิศวกรรมไฟฟ้า.....ลายมือชื่อ อ.ที่ปรึกษาวิทยานิพนธ์หลัก.....
ปีการศึกษา....2554.....

# # 5171832021 : MAJOR ELECTRICAL ENGINEERING
KEYWORDS : TRANSFER CAPABILITY / POWER FLOW SOLUTION SPACE/ SECURITY REGION/ SOLVABLE REGION / FEASIBLE REGION

SATAPORN LIMPATTHAMAPANEE : LOAD FEASIBLE REGION DETERMINATION USING BOUNDARY TRACING METHOD. ADVISOR: ASSIST. PROF. SOTDHIPONG PHICHAISAWAT, Ph.D., 173 pp.

This dissertation proposes a method for determining load feasible region on a plane between real power axis and reactive power axis. The considered problem in this research is the transfer capability determination from a source to a sink area in a power system. The proposed method uses the boundary tracing process by determining a boundary point of load feasible region with the distance minimization from an unfeasible loading point. Then, next boundary points are traced using vector operations and the distance minimization repeatedly until obtaining a closed contour of load feasible region. The proposed method has been tested with 2-bus system, 6-bus system, IEEE 24-bus system, and Thailand power system. The results show that this method can determine load feasible regions for several source-sink pairs. The load feasible region shows limits of load changes due to several activities, e.g. load increment, load shedding, and reactive power compensation. This method can visualize feasible load conditions more obviously than the conventional load margin determination methods, e.g. repeated power flow and continuation power flow. Moreover, the proposed method can determine the outermost boundary of load feasible region affected by the considered system parameters.

Department : Electrical Engineering Student's Signature .....
Field of Study : Electrical Engineering Advisor's Signature .....
Academic Year : 2011 .....

# Acknowledgements

My deepest gratitude goes to my advisor, Assistant Professor Dr. Sotdhipong Phichaisawat who has given invaluable advice and wisdom in both academic and practical aspects since my master degree. I also express my thankfulness to Professor Dr. Bundhit Eua-arporn, the chairman of thesis committee, and examiners Dr. Chanarong Banmongkol, Dr. Surachai Chaitusaney, Dr. Pradit Fuangfoo for their helpful comments on this research.

I would like to extend my thankfulness to all of my supervisors in Srinakarind Hydro Power Plant at EGAT who provide me a great opportunity to continue my study in which I have a strong willingness to apply my knowledge from the research for benefits of the organization.

I would like to express my gratitude to Dr. Somphop Asadamongkol for his helpful suggestion to my research.

In addition, I would like to thank my father, Mr. Viboon Limpatthamapanee and my mother, Mrs. Somkid Limpatthamapanee for their moral support and undying love.

# Contents

Page

Page

# List of Tables

# List of Figures

Figure Page

Figure Page

# CHAPTER I

# INTRODUCTION

## 1.1 Problem Statement

In power system analysis, an operating condition must satisfy power flow equations and all system values must be within acceptable ranges. In order to evaluate system conditions, the power flow solution can be solved by Newton-Raphson method. Then, the power flow solution provides detailed system values, i.e. nodal voltages, transmission line flows. Nevertheless, the power system has some limitations to supply load demands. The load increment might cause the violation of power systems, e.g. the violation of nodal voltages and the overload of transmission lines, etc. Moreover, the load increment is limited by a critical point of steady-state voltage stability [1], [2]. Thus, the determination of load margin receives much attention in the power system analysis. Especially in the modern power system, the load margin of power transfer between a given source-sink pair is taken into account [3], [4].

The load margin can be evaluated by increasing an existing load condition until the system parameters reach their limits. The load margin can be determined by several methods [5]-[7], e.g. repeated power flow, continuation power flow, and optimal power flow methods. In the load margin determination, the bus power factor is assumed to be fixed. In general, the load margin just represents the maximum loading point in a specific direction of load changes. In practice, the load margin can be varied according to loading directions. Furthermore, an operation of reactive power devices can change the load conditions which then result in the change of load margin. The variation of load margin can be explained through the concept of security regions in the multi-dimensional parameter space, comprising bus injections, generator voltage settings, and MW interchange, etc [8]. The parameter space is bounded by the boundary of security regions. The existing load condition can be represented as a point which can move inside the region. The size of load margin depends on the position of an existing loading point and the direction of load change. However, the boundary of security regions can be expanded or shrunk by system parameters. In order to enhance the load margin monitoring, the purpose of this research is to develop the method for determining the boundary of the security regions under a condition of power transfer between a given source-sink pair.

The security regions are classified into several types, i.e. unsolvable region, infeasible region, and feasible region. The unsolvable region is a set of operating points where the power flow solution does not exist. The infeasible region is a set of operating points where the power flow solutions exist, but at least one device limit is violated. The feasible region is a set of power flow solutions that all parameters are within their limits. The feasible and infeasible regions are totally called the solvable region [8]-[12]. The method to determine the boundary of solvable region is based on the predictor-corrector process. The solvable boundary point tracing method called "continuation method" is proposed in [13]. The continuation method is to predict the next solution point by a tangent vector and then correct the prediction point to be the boundary point. The boundary points of a solvable region are the power flow solutions, of which the Jacobian matrix is singular [14]-[16]. The boundary points of solvable region must satisfy nonlinear equations consisting of the power flow equations and the equations corresponding to the singularity condition of the Jacobian matrix.

The key components of the boundary tracing method are the boundary point determination and the prediction of the next boundary point. The continuation method in [13] determines the solvable boundary point by solving the system of nonlinear equations. The solvable boundary point can be determined by another approach. The minimization approach in [8] finds the solvable boundary point by minimizing the Euclidean distance from a point outside the solvable region. It can be adapted for finding the solvable boundary points in the boundary tracing process [17]. However, the boundary tracing methods in [13] and [17] do not focus on the boundary bounded by the operational limits, called the feasible region. The security region determination has never been applied for the power transfer between the source-sink pair in a power system.

This research proposes a method for tracing the boundary points of a feasible region in order to determine the feasible region of the power transfer between a source-sink pair. The proposed method consists of the feasible boundary point determination and the tracing process implemented on the plane of apparent power. This research also presents impact of system parameters on the boundary of a feasible region by utilizing a boundary curve obtained by the proposed method.

## 1.2 Objective

1. To develop a method for tracing the boundary of load feasible region under a condition of a power transfer between a given source-sink pair.
2. To provide the fundamental concept to utilize the obtained feasible region in power system analysis.
3. To analyze the effects of system parameters to the shape of load feasible region.

## 1.3 Scope of the thesis

1. The study considers only power system in steady state operation.
2. The feasible region studied in this work is under the condition of the power transfer between a given source-sink pair.
3. The study considers takes into account only the following
   3.1 Nodal voltage limits,
   3.2 Generator limits, and
   3.3 Transmission line limits.
4. The load and generation models used in this work are based on classical models.

## 1.4 Step of Implementation

1. Studying literature works related to the load margin determination.
2. Studying literature works related to the power flow solution space.
3. Formulating the problem in order to determine boundary points of a feasible region.
4. Developing the tracing method in order to determine the boundary curve of feasible region.
5. Studying the effects of system parameters to the feasible region.
6. Illustrating the proposed method on test systems.

# CHAPTER II

# LOAD MARGIN DETERMINATION

In order to verify power system availability, the basic requirements of the solution are that the considered conditions are solvable and all system parameters are within their limits. The load margin determination is to find the incremental load condition satisfying these requirements. For the solvability of power systems, the load level must be less than a point where the power flow Jacobian is singular. For the feasibility of power systems, the system parameters, e.g. nodal voltages, and transmission line flows, etc, must not violate its corresponding limits. The tools used for determining the load margin are based on power flow equations. In this chapter, the mathematical backgrounds of power flow equations and load margin determinations are reviewed.

## 2.1 Power Flow Problem

The power flow equation is the fundamental problem for power system engineers. For the system operation, the operating condition must satisfy the power flow equations. The power flow problem consists of: to determine voltage at each bus and to calculate power flows in each transmission line. In power flow problem, variables for each bus are the real power ($P$), reactive power ($Q$), the voltage magnitude ($V$), and the voltage phase angle ($\delta$). The fixed variables are different depending on the bus type. The power flow problem is the system of nonlinear equations expressed as

$$\boldsymbol{f}(\boldsymbol{x}) - \boldsymbol{S} = \boldsymbol{0} \tag{2.1}$$

where $\boldsymbol{S}$ is a vector of real and reactive power injections, which are known variables

$$\boldsymbol{S} = [\boldsymbol{P}_{pv}\ \boldsymbol{P}_{pq}\ \boldsymbol{Q}_{pq}]^T . \tag{2.2}$$

And then $\boldsymbol{x}$ is a vector of unknown variables expressed as

$$\boldsymbol{x} = [\boldsymbol{\delta}_{pv}\ \boldsymbol{\delta}_{pq}\ \boldsymbol{V}_{pq}]^T \tag{2.3}$$

The nonlinear function $\boldsymbol{f}(\boldsymbol{x})$ consists of the real and reactive power functions ($\boldsymbol{f}_P(\boldsymbol{x})$ and $\boldsymbol{f}_Q(\boldsymbol{x})$), which can be presented as

$$\boldsymbol{f}(\boldsymbol{x}) = [\boldsymbol{f}_{Ppv}(\boldsymbol{x})\ \ \boldsymbol{f}_{Ppq}(\boldsymbol{x})\ \ \boldsymbol{f}_{Qpq}(\boldsymbol{x})]^T \tag{2.4}$$

The subscript "*pv*" and "*pq*" are the associated variables of generator bus and load bus, respectively. In the power flow problem, *N* defined as a number of equations equals to *npv+2npq* where *npv* and *npq* are a number of generators and load buses consecutively. The power flow problem has *N* unknowns and *N* equations. The solution of power flow problem is a point in the power flow solution space. The solution can be solved by the Newton-Raphson method.

### 2.2 Load Margin Determination

The load margin is an ability to increase the load from the existing condition. The problem of the load margin determination usually considers the power transfer between the source-sink pair. In the modern power market, the load margin is the basis for many quantities, i.e. the total transfer capability (TTC), the available transfer capability (ATC), etc [3]. The load margin determination methods are classified into three categories, i.e. the repeat power flow method (RPF), the continuation power flow method (CPF), and the optimal power flow method (OPF) [5]-[7]. Both RPF and CPF calculate the sequence of power flow solutions by increasing the sink bus load until the solution touches a critical point or an operational limit. The RPF method directly solves the power flow solution in each load increment step. In a different way, the CPF method repeats determining the power flow solutions with the augmented Jacobian matrix to avoid the ill-conditioned matrix, in which the load increment is close to the critical point. The OPF method is to maximize the incremental load parameter subjected to the power system constraints [6].

### 2.2.1 Repeated Power Flow

The method treats the source bus as the reference bus and then determines the power flow solution. If the solution does not violate the operational limit, the considered load is increased by the following way,

$$P_{di} = P_{di}^{0} + \lambda \tag{2.5}$$

$$Q_{di} = (P_{di}^{0} + \lambda)\tan(\cos^{-1}(\psi_i)) \tag{2.6}$$

Where

$\lambda$ is a scalar parameter corresponding to the load increment at the sink bus;

$P_{di}$ is the real power at sink bus *i*;

$P_{di}^{0}$ is the base case real power at sink bus *i*;

$Q_{di}$ is the reactive power at sink bus *i*;

$\psi_i$ is the power factor angle of load change at bus *i*;

The power flow is repeated with the increment step of the scalar parameter $\lambda$ until the system reaches the operational limit. The load margin is the difference between the base case load and the maximum load as the following,

$$Load\ Margin = P_{di}(\lambda) - P_{di}^{0} \tag{2.7}$$

### 2.2.2 Continuation Power Flow

The continuation power flow (CPF) is a tool for determining the curve of power flow solutions. The obtained curve presents the margin from the existing load condition to the critical point where the power system reaches an unstable condition. The critical load point is called the saddle-node-bifurcation point (SNB). In the problem, the load parameter $\lambda$ is added to the power flow problem as an unknown variable. An increment of parameter $\lambda$ corresponds to an increment of load in the specified proportion of real and reactive power. The continuation power flow can determine the load margin and the voltage characteristic of the power transfer scenarios between a given source-sink pair.

The sink bus load ($P_{di}$, $Q_{di}$) and the source bus generation ($P_{gj}$) are the functions of $\lambda$, as the following:

$$P_{di}(\lambda) = P_{di}^{0} + \lambda[K_{di} S_{\Delta BASE} \cos(\psi_i)] \tag{2.8}$$

$$Q_{di}(\lambda) = Q_{di}^{0} + \lambda[K_{di} S_{\Delta BASE} \sin(\psi_i)] \tag{2.9}$$

$$P_{gj}(\lambda) = P_{gj}^{0}(1 + \lambda K_{gj}) \tag{2.10}$$

Where

$P_{di}^{0}$, $Q_{di}^{0}$ are the original load at bus $i$, active and reactive respectively;

$P_{gj}^{0}$ is the original active generation at bus $j$;

$K_{di}$ is the multiplier designating the rate of load change at bus $i$ as $\lambda$ change;

$K_{gi}$ is the constant specifying the rate of change in generation as $\lambda$ varies;

$\psi_i$ is the power factor angle of load change at bus $i$;

$S_{\Delta BASE}$ is the apparent power, which is chosen to provide appropriate scaling of $\lambda$.

The power flow equation is also the function of $\lambda$ as the following,

$$\boldsymbol{f}(\boldsymbol{x}) - \boldsymbol{S}(\lambda) = \boldsymbol{g}(\boldsymbol{x}, \lambda) = \boldsymbol{0}. \tag{2.11}$$

The number of unknowns is $N$+1 because of the additional variable $\lambda$, while the number of equations is $N$, the solution is a curve, consequently. The way to quantify this curve is to use the predictor-corrector continuation process [1], [2].

The predictor process is to calculate the tangent vector ($\boldsymbol{t}$) from the following linear system:

$$[\boldsymbol{J}_{Aug}][\boldsymbol{t}] = \begin{bmatrix} \boldsymbol{g}_x & \boldsymbol{g}_\lambda \\ & \boldsymbol{e}_k \end{bmatrix} \begin{bmatrix} d\boldsymbol{x} \\ d\lambda \end{bmatrix} = \begin{bmatrix} \boldsymbol{0} \\ \pm 1 \end{bmatrix} \tag{2.12}$$

The prediction point (denoted by '*') can be obtained by

$$\begin{bmatrix} \boldsymbol{x}^* \\ \lambda^* \end{bmatrix} = \begin{bmatrix} \boldsymbol{x} \\ \lambda \end{bmatrix} + \sigma \begin{bmatrix} d\boldsymbol{x} \\ d\lambda \end{bmatrix} \tag{2.13}$$

Where

$\boldsymbol{J}_{\text{Aug}}$ is the augmented Jacobian matrix;

$\boldsymbol{g}_{\boldsymbol{x}}$ refers to the Jacobian matrix $\partial \boldsymbol{g} / \partial \boldsymbol{x}$;

$\boldsymbol{g}_{\lambda}$ refers to the partial derivative $\partial \boldsymbol{g} / \partial \lambda$;

$\boldsymbol{e}_k$ is an appropriately dimensioned row vector with all elements equal to zero except the $k^{th}$ component, which is equal to one;

$\sigma$ is a scalar designating step size.

The variable relating to the largest component of tangent vector $\boldsymbol{t}$ is chosen to be a continuation parameter. The index $k^{th}$ corresponds to a component of continuation parameter. The proper value of either +1 or -1 on the right side of (2.12) is assigned to the rate of change in a continuation parameter. The corrector process is to determine a power flow solution near a prediction point. The continuation parameter is fixed by an appropriate value $\eta$ for the $k^{th}$ element of $\boldsymbol{Z}$, where $\boldsymbol{Z}=[\mathbf{x}\ \lambda]^{\mathrm{T}}$. The correction step solves the power flow solution from the following:

$$\begin{bmatrix} \boldsymbol{g}(\boldsymbol{Z}) \\ Z_k - \eta \end{bmatrix} = \mathbf{0} \tag{2.14}$$

The predictor-corrector process is shown in the figure below.

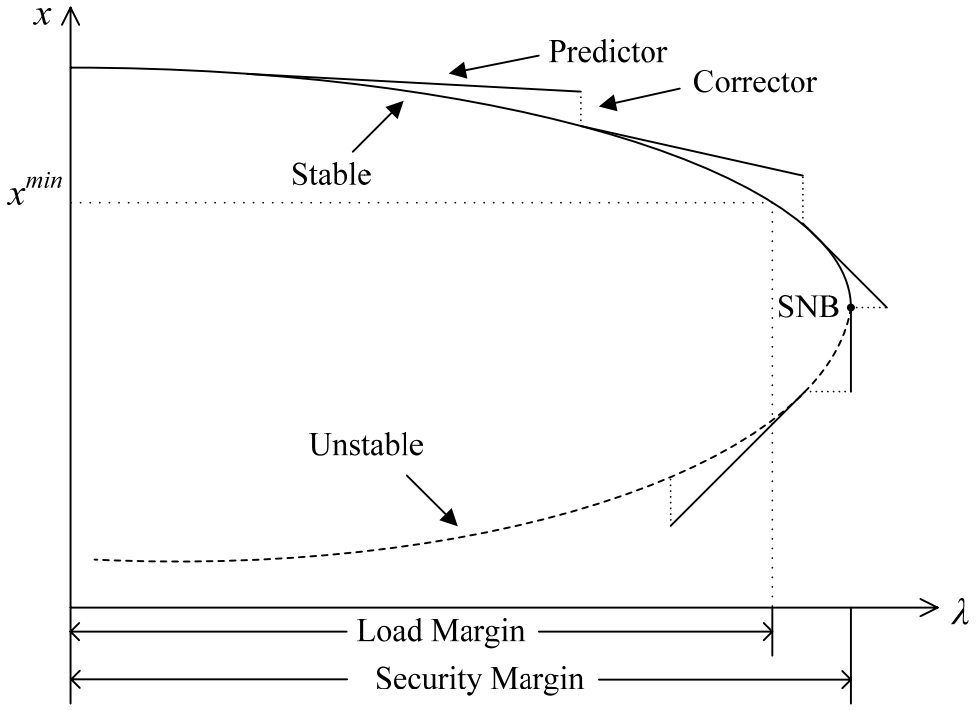


Figure 2.1 Continuation power flow

The CPF curve details the parameter characteristic related to the load increment. From this curve, the load margin can be observed. When the problem considers the steady-state voltage stability limit, the load margin limited by the SNB point is called the security margin. When the parameter limit is taken into account, the load margin is limited by the parameter criteria.

### 2.2.3 Optimal Power Flow

The load margin can be determined by using the optimal power flow method (OPF). The OPF method is to maximize the incremental load parameter $\lambda$ subjected to the power system constraints [6]. This approach incorporates various constraints into the problem. The following is the mathematical formulation of the OPF method

$$\max \quad \lambda \tag{2.15}$$

$$\text{s.t} \quad \boldsymbol{g}(\boldsymbol{x},\lambda) = \mathbf{0} \tag{2.16}$$

$$\boldsymbol{h}(\boldsymbol{x},\lambda) \le \mathbf{0} \tag{2.17}$$

where

$\lambda$ is the load parameter representing the changes of the load in the sink area.

$\boldsymbol{x}$ is the vector of the state variables, including voltage magnitudes of load buses ($\boldsymbol{V}_{pq}$) and voltage phase angles of generator buses and load buses ($\boldsymbol{\delta}_{pv,}\boldsymbol{\delta}_{pq}$).

$\boldsymbol{g}(\boldsymbol{x},\lambda)$ represents the power flow equations

$\boldsymbol{h}(\boldsymbol{x},\lambda)$ represents the inequality constraints which are the operation limits, e.g. the voltage limits, the transmission line limits, the generator limits, etc.

The generation and load are the functions of the load parameter according to (2.8)-(2.10).

## 2.3 Load Margin Determination with FACTS

The flexible AC transmission system or FACTS is the device installed in power system for improvement of power system operations. The FACTS devices can change system parameters, e.g. compensate reactive power at load bus, or change transmission line reactance, etc. In [18], the load margin determination including FACTS devices is proposed. The considered FACTS devices are the static VAr compensator (SVC) and the thyrister controlled series compensator (TCSC).

### 2.3.1 Load Margin Determination with SVC

Static VAr compensator (SVC) is a shunt compensation component which a shunt connected. SVC can generate or absorb the reactive power in order to maintain or control bus voltage at the installed bus. The steady state model of SVC is the reactive power generator, as shown in the figure below.

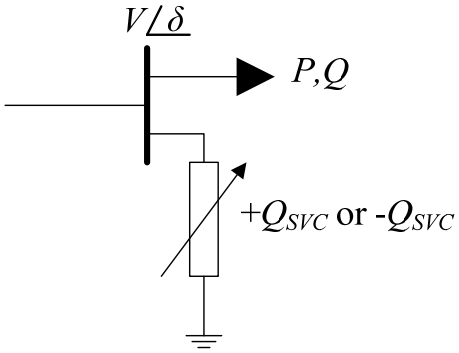


Figure 2.2 Steady state model of SVC

In the power flow equations, SVC is treated as a generator bus supplying reactive power. The load margin of the SVC-installed case can be calculated by the conventional load margin determination, i.e. RPF, CPF, and OPF. When SVC is installed in the system, the risk of nodal voltage violation is reduced, and the load margin of the power transfer is changed.

### 2.3.2 Load Margin Determination with TCSC

Thyrister controlled series compensator (TCSC) consists of a series capacitor bank shunted by thyristor-controlled reactor. TCSC can change the apparent reactance of the installed transmission line. The steady state model of TCSC is the variable reactance on the transmission line, as shown in the figure below.

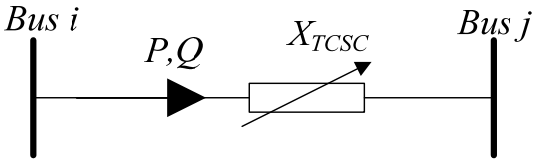


Figure 2.3 Steady state model of TCSC

TCSC reactance ($\boldsymbol{X}_{TCSC}$) affects the transmission line parameter. The change of TCSC reactance leads to the change of system configuration. The load margin can be determined by using new configuration reflected through the bus admittance matrix for the power flow equations. The operational constraints are functions of TCSC reactance. The load margin determination with TCSC can be represented by the following,

$$\max \quad \lambda \tag{2.18}$$

$$\text{s.t} \quad \boldsymbol{g}(\boldsymbol{x}, \lambda, \boldsymbol{X}_{TCSC}) = \boldsymbol{0} \tag{2.19}$$

$$\boldsymbol{h}(\boldsymbol{x}, \lambda, \boldsymbol{X}_{TCSC}) \leq \boldsymbol{0} \tag{2.20}$$

$$\boldsymbol{X}_{TCSC}^{min} \leq \boldsymbol{X}_{TCSC} \leq \boldsymbol{X}_{TCSC}^{max} \tag{2.21}$$

## 2.4 Conclusion

The concept of load margin determination is reviewed in this chapter. The load margin determination is to find a set of feasible load in the specific direction of load change. At the maximum loading point, the load can not increase due to the operational limits or the saddle nod bifurcation. However, the obtained load margin depends on the direction of load change. This phenomenon can be explained by the concepts of security regions in next chapter.

# CHAPTER III

# SECURITY REGION

According to the method of load margin determination, the solution is a maximum loading point under the assumption that the load level increases with the same power factor as the base case. However, the maximum loading point can be varied when the power factor of load increment is changed. A set of maximum loading point arranges as a boundary curve of the security region. This chapter describes about the concept of security regions and the determination of boundary curve.

## 3.1 Classification of Security Region

The regions of power flow solution are bounded by the solvable boundary ($\sum_1$) and the feasible boundary ($\sum_2$) [8], as shown in the figure below. The unsolvable region is the set of points where the power flow equation has no solution. The infeasible region is the set of solvable points, but these points violate at least one operational limit. Finally, the feasible region is the set of solvable points where all system parameters are within their limits. This region is normally desirable for the operation.

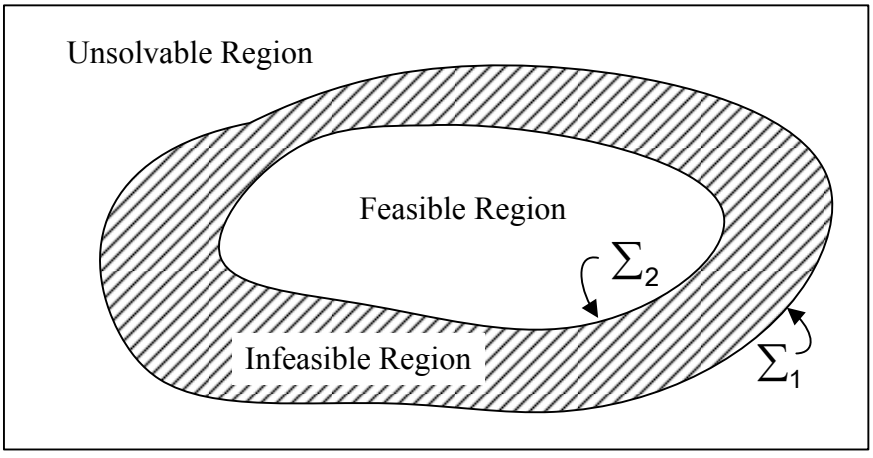


Figure 3.1 Security regions

### 3.2 Boundary Points of Security Region

The boundary points of solvable region are the critical points called “saddle node bifurcation points (SNB)”. The SNB point is not only the power flow solution, but it is also the point, in which the power flow Jacobian is singular. The power flow solution does not exist, when the load level is more than the SNB point. The SNB point varies with the direction of load increment and the changes in power system parameters. The SNB point can be determined by several methods, e.g. the continuation power flow (CPF), the direct method, and the optimization method from the unsolvable case.

#### 3.2.1 CPF Method for Boundary Point of Solvable Region

From the existing loading condition, the CPF method can find the SNB point on a specific direction of load increment. However, different load directions produce different SNB points. A set of SNB points is the boundary of the solvable region, as shown in the figure below.

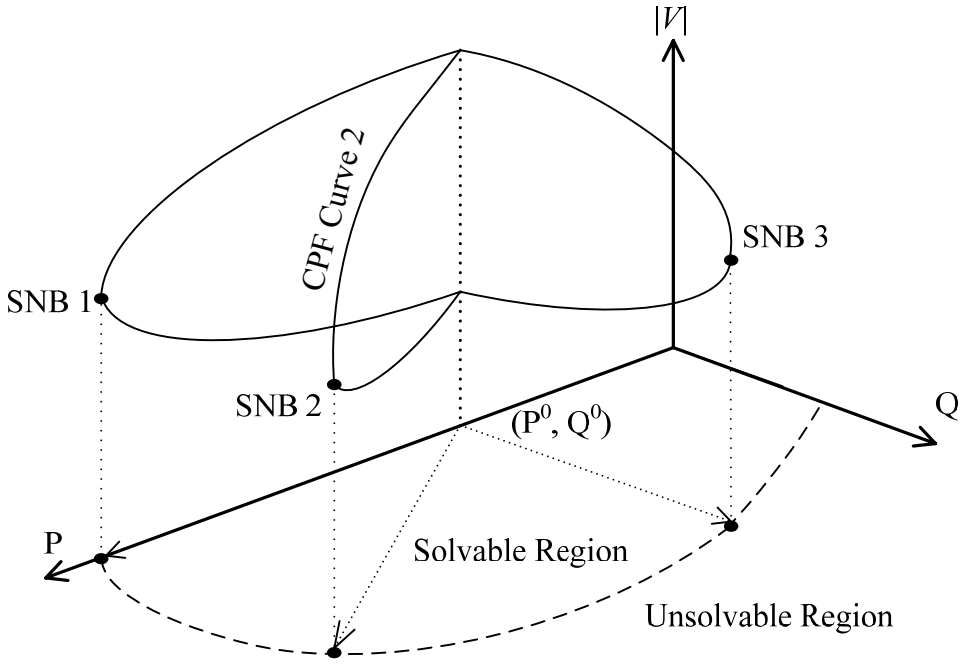


Figure 3.2 CPF curve and solvable boundary curve

### 3.2.2 Direct Method for Boundary Point of Solvable Region

The direct method [16] is to find the SNB point by solving the system of nonlinear equations formulated from the property of SNB point. The SNB point is both the power flow solution and the singular point of Jacobian matrix. The conditions of singular point are the following:

$$\boldsymbol{g}_x(\boldsymbol{x},\boldsymbol{\lambda})\boldsymbol{y} = \boldsymbol{0} \tag{3.1}$$

$$\boldsymbol{y}^T\boldsymbol{y} = 1 \tag{3.2}$$

Where

$\boldsymbol{g}_x$ refers to the power flow Jacobian matrix;

$\boldsymbol{y} \in \mathbb{R}^N$ is the right eigenvector corresponding to the zero eigenvalue of $\boldsymbol{g}_x$;

$\boldsymbol{\lambda} \in \mathbb{R}^p$ is a vector of load parameters with $p$ designated as the number of load parameters.

The SNB point is the point that satisfies the system of nonlinear equations, which is

$$\boldsymbol{\phi}(z) = \begin{bmatrix} \boldsymbol{g} \\ \boldsymbol{g}_x\boldsymbol{y} \\ \boldsymbol{y}^T\boldsymbol{y} - 1 \end{bmatrix} = \boldsymbol{0} \tag{3.3}$$

where $z = \begin{bmatrix} \boldsymbol{x} & \boldsymbol{y} & \boldsymbol{\lambda} \end{bmatrix}^T \in \mathbb{R}^{2N+p}$ and $\boldsymbol{\phi}(z) : \mathbb{R}^{2N+p} \to \mathbb{R}^{2N+1}$. When $p$=1, the system of nonlinear equations in (3.3) has one additional free parameter $\lambda$. The number of equations is $2N$+1 and the number of variables is $2N$+1. The solution of this equation is a SNB point that can be solved by Newton-Raphson method, without creating the CPF curve.

### 3.2.3 OPF Method for Boundary Point of Solvable Region

From the existing loading point, the SNB point corresponds to the maximum load parameter. On the other hand, the SNB point is the nearest power flow solution from the unsolvable point. The optimizations to determine SNB points can be categorized into two

methods, i.e. the optimization method from inside the solvable region [19], and the optimization method from outside the solvable region [8]-[12].

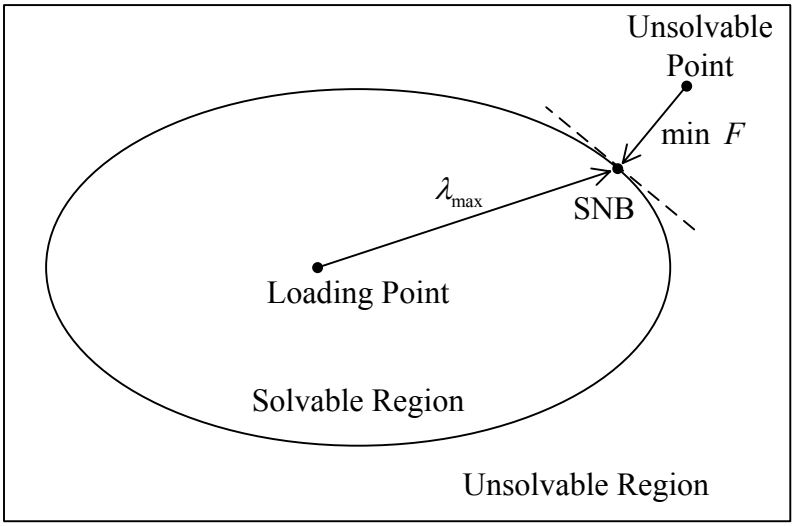


Figure 3.3 Illustration of optimization methods

The optimization method from inside the solvable region is to maximize the load parameter subjected to the power flow algebraic constraints as follows:

$$\max \quad \lambda \tag{3.4}$$

$$s.t. \quad \boldsymbol{g}(\boldsymbol{x},\lambda)=\boldsymbol{0} \tag{3.5}$$

This formulation is proven that the solution is the SNB point [20]. It is equivalent to the CPF method. The SNB point can be obtained without tracing the CPF curve.

The optimization method from outside the solvable region uses the Euclidean distance from the unsolvable point [8]. From the point outside the solvable region ($\boldsymbol{S}^*$), the nearest solvable point can be determined by the unconstrained minimization:

$$\min \quad F(\boldsymbol{x}) = \frac{1}{2}[\boldsymbol{f}(\boldsymbol{x}) - \boldsymbol{S}^*]^T[\boldsymbol{f}(\boldsymbol{x}) - \boldsymbol{S}^*] \tag{3.6}$$

Where

$\boldsymbol{S}^*$ is a vector of unsolvable power injections;

$F(\boldsymbol{x})$: $\mathbb{R}^N \rightarrow \mathbb{R}$ is a cost function, which is one half the square of the power flow mismatch equations.

This minimization problem is proven that the solution is the SNB point when $\boldsymbol{S}^*$ is the unsolvable point. The solution $\boldsymbol{x}$ gives the power injections $\boldsymbol{S}$, which makes the vector $\boldsymbol{S}$-$\boldsymbol{S}^*$ parallel to the normal vector to the surface of solvable region at the point $\boldsymbol{S}$. This concept is useful for the security analysis in order to determine the corrective control actions from the unsolvable case.

### 3.3 Solvable Boundary Tracing Method

Boundary points of solvable region are the points dividing the space of power flow solutions into solvable region and unsolvable region. The boundary point is the power flow solution with a unique property. The power flow Jacobian matrix is singular at the position of boundary point. By this feature, it can determine the boundary curve of solvable region based on the tracing algorithm. The boundary curve determination can be classified into two methods, i.e. the continuation method and the optimization-based method.

#### 3.3.1 Continuation Method

The boundary curve of solvable region consists of a set of SNB points that can be obtained by the tracing process. From the equation (3.3), if the number of free parameters is two ($p$=2), the problem becomes $2N$+2 variables with $2N$+1 equations. Then, the solution is the curve. The continuation method proposed in [13] traces this curve by using the predictor-corrector process. In the prediction step, the method determines a prediction point by moving the existing SNB point $\boldsymbol{z}_k$ along the tangent vector $\boldsymbol{v}_n$ with the step size $\tau$, as shown in the following figure.

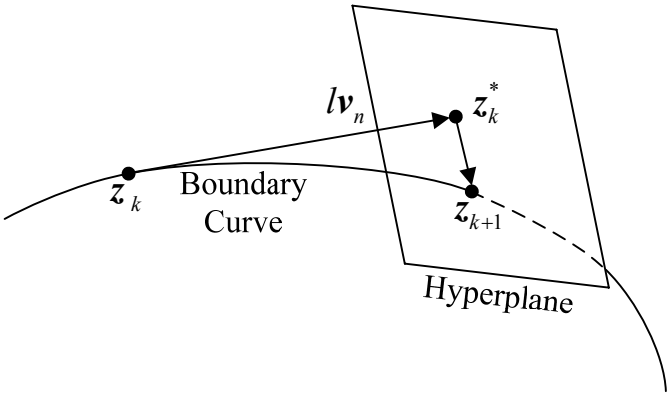


Figure 3.4 Solvable boundary tracing by continuation method

The tangent vector $\boldsymbol{v}$ can be obtained by:

$$\boldsymbol{\phi}_z \mid_{z=z_k} \boldsymbol{v}_k = 0 \tag{3.7}$$

$$\left\| \boldsymbol{v}_k \right\| = 1 \tag{3.8}$$

Where $\boldsymbol{h}_z \in \mathbb{R}^{(2N+1)\times(2N+2)}$ is the Jacobian matrix of (3.3). The prediction $\boldsymbol{z}_k^*$ of next boundary point is

$$\boldsymbol{z}_{\boldsymbol{k}}^* = \boldsymbol{z}_k + l\boldsymbol{v}_k \tag{3.9}$$

However, the tangent vector can be approximated by the previous boundary point $z_{k-1}$ by

$$\boldsymbol{v}_k = \frac{\boldsymbol{z}_k - \boldsymbol{z}_{k-1}}{\left\| \boldsymbol{z}_k - \boldsymbol{z}_{k-1} \right\|} \tag{3.10}$$

The next boundary point is the point on the intersection of the curve and a hyperplane that passes through $\boldsymbol{z}_k^*$ and that is orthogonal to $\boldsymbol{v}_k$. The correction step determines the next boundary point ($z_{k+1}$) by solving the following equations:

$$\boldsymbol{\phi}(\boldsymbol{z}_{k+1}) = \boldsymbol{0} \tag{3.11}$$

$$(\boldsymbol{z}_{k+1} - \boldsymbol{z}_k)^T \boldsymbol{v}_k = l \tag{3.12}$$

### 3.3.2 Optimization-Based Method

According to the solvable boundary curve tracing method in [13], the corrector process is the determination of boundary point by solving the system of nonlinear equations that consist of the power flow equations and the singularity condition of Jacobian matrix. This process can be replaced by the optimization problem. In reference [17], the minimization problem replaces the correction step as the following:

$$\min_{S,x} \ \frac{1}{2}(\boldsymbol{S}-\boldsymbol{S}^*)^T(\boldsymbol{S}-\boldsymbol{S}^*), \tag{3.13}$$

$$\text{s.t.} \quad \boldsymbol{f}(\boldsymbol{x})-\boldsymbol{S}=\boldsymbol{0} \tag{3.14}$$

Where

$\boldsymbol{S}^*$ is the prediction point.

$\boldsymbol{S}$ is the load injection point.

This problem is in the constrained optimization. The objective function is the cost function as same as (3.6), but the power flow equation is treated as the equality constraint, in stead of integrating in the objective function. The meaning of this problem is to find the nearest solution point from the unsolvable point $S^*$.

According to the Kuhn-Tucker necessary condition, the solution of this problem is the singular point of the power flow Jacobian matrix [17]. At this point, the left eigenvector corresponding to the zero eigenvalue is a perpendicular vector of the solvable boundary. This vector is parallel to $\boldsymbol{S}$-$\boldsymbol{S}^*$ and perpendicular to the tangent vector $\boldsymbol{v}$. By this property, the perpendicular vector $\boldsymbol{v}$ is used to predict the next boundary point. The vector $\boldsymbol{v}$ is determined by the following:

$$(\boldsymbol{S}_n-\boldsymbol{S}_n^*)^T\boldsymbol{v}_n=\boldsymbol{0}. \tag{3.15}$$

As the solvable region is not always convex [21], [22], the modified predictor step in [17] determines the next $\boldsymbol{S}^*$ by using the existing $\boldsymbol{S}^*$ to prevent the next $\boldsymbol{S}^*$ from going into the region. As shown in the figure below, on the concave situation (at the point $\boldsymbol{S_2}$) the conventional tracing method defines the tangent vector at the boundary point and predicts the next $\boldsymbol{S}^*$ going into the region as shown by the dotted line. When $\boldsymbol{S}^*$ is inside the

region, the obtained point $\boldsymbol{S}$ equals to $\boldsymbol{S}^*$ because $\boldsymbol{S}^*$ is already solvable. The obtained $\boldsymbol{S}$ is not the boundary point. Accordingly, it will produce the wrong solutions in the next steps of tracing method.

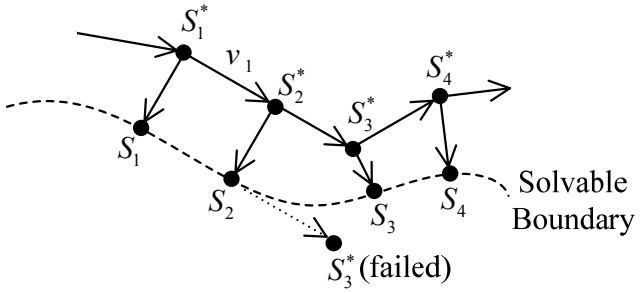


Figure 3.5 Solvable boundary tracing by optimization-based method

### 3.4 Conclusion

According to the concept of security regions, the power flow solution space is bounded by a boundary of solvable region. Most of literatures have studied about the curve of solvable region, and the boundary of solvable region is determined using a property of SNB point, as described in this chapter. However, when the operational limits are taken into account, the desirable space of solutions is bounded to be a feasible region. The feasible region is consistent with a concept of load margin determination. Thus, this dissertation focuses on determining a feasible region of power transfer between source-sink pair. The concept of the proposed method will be discussed in next chapter.

# CHAPTER IV

# CONCEPT OF THE PROPOSED METHOD

The maximum loading point is determined under the assumption that the load of sink area changes with the specific power factor. However, the maximum loading points are different by the existing load condition, especially when the reactive power compensation devices operate. Thus, the determination of load margins in terms of the feasible region will give the overall of the feasible loading conditions. The feasible region is a kind of security regions bounded by operational limits. A curve of security region can be determined by boundary tracing method. However, the literatures related to boundary tracing method [13], [17] focus on the boundary curve of the solvable region which is bounded by the SNB points. The problem in [13] is to determine the power flow solution space for the entire network by using boundary curve tracing method. The problem of the power transfer between a source-sink pair has not been illustrated in terms of feasible regions.

The problem considered in this research is the power transfer between a given source-sink pair. This research develops the boundary tracing method with considering of the operational limits in order to determine the feasible region of power transfer. The determination of the feasible region consists of the method for solving boundary points and the tracing process using vector operations. This work utilizes the optimization based method to determine a solution on the boundary. The advantage of the optimization based method is that the operational limits can be included into the problem.

## 4.1 Problem Consideration

The study of power flow solution space in [13] considers all parameters which can be varied in the system. The study shows that the power flow solution space is very complex, even though the test system is small. The study in [13] provides the concept that the boundary tracing process needs to be implemented on two axes of free parameters. The scenario in this research is the power transfer between a given source-sink pair. Two free parameters considered for this problem are the real and reactive powers at the receiving end. The considered scenarios are:

- The transfer between two buses (one generator and one load bus).

- The transfer between two areas (a group of generators and a group of load buses).

The problem is to determine the loading point on the boundary of the feasible region. The formulation needs to specify the free parameters and the fixed parameter, and then assigns the objective function and constraints. The same concept can utilize to formulate the boundary point determination in the case of the transfer between areas. Finally, the formulation of this scenario can be used as the general form of other scenarios, i.e. the transfer from the area to one bus, the transfer from one generator to the area.

### 4.1.1 Transfer from Source Bus to Sink Bus

For the transfer from the source bus to the sink bus, the source bus supplies the power directly to the sink bus while parameters of other buses are fixed. The loading point considered in this problem consists of the real and reactive power at the sink bus. The boundary curve is plotted on the *P*-*Q* plane of the sink bus. For the conventional load margin determination, the source bus is treated as the slack bus, and the maximum loading point can be determined by the repeated power flow. The load is increased by the specific step until the loading point reaches the limit of system parameters. However, this problem needs to find the boundary loading point from outside the region because the prediction points of the tracing process are the points outside the region, the method to determine the boundary point is based on the distance minimization from the outside of the region. The parameters varying in the system must be treated as free parameters. In this case, the powers at the given source-sink buses must be the free parameters.

### 4.1.2 Transfer from Source Area to Sink Area

The problem formulation of the transfer between areas uses the same concept as the problem of the transfer between buses. The powers at the given source-sink areas are the free parameters. However, the definition of the loading point for this scenario is different. The loading point is a summation of load in the sink area. According to the conventional load margin determination, the loads and generations are assumed to change proportionally by the participation factors. In the optimization problem, the proportional change of loads and generations can be treated as the linear equality constraints.

## 4.2 Concept of Tracing Method

The boundary tracing method in this research is based on the optimization problem. The algorithm is to calculate the sequence of power flow solutions on the boundary of feasible region. The nonlinear programming using in the optimization problem needs an appropriate initial guess of solution. Moreover, the tracing algorithm needs to determine the sequence of prediction point using vector operations.

### 4.2.1 Initial Guess and Prediction Point

The boundary tracing process consists of the predictor and corrector process. The corrector process is to determine the nearest loading point from the particular prediction point. The corrector step is based on the optimization because it can treat the operational limits as the constraints. In order to determine the boundary point of the feasible region, the prediction point used in the optimization problem must be outside the feasible region. The questions are:

- How to choose the prediction points?
- What is the initial guess for the optimization problem?

In the tracing algorithm, the next prediction point can be sequentially determined by using the vector operations from the previous boundary point. Therefore, the previous boundary solution should be the initial guess for the optimization in the next correction step. The following question is how to determine the first initial guess and the first prediction point.

Because the power flow problem is nonconvex, especially when the operational constraints are taken into account [21], [22], the initial guess is very important for the optimal power flow problem. In this case, the initial guess of the minimization should not be far from the solution on the boundary curve. According to the load margin determination, the maximum loading point corresponds to the boundary point of the feasible region. Thus, the first initial guess for the tracing method could be the solution of the maximum loading point determined by the conventional load margin determination. This work chooses the repeated power flow method to determine the solution on the boundary, and then treats the solution of the maximum loading point as the first initial guess for the tracing algorithm. Moreover, the first prediction point can be also determined by increasing the maximum loading point with the appropriated step.

### 4.2.2 Tracing Algorithm

After obtaining the first prediction point, the method to trace the boundary points must be developed. The tracing algorithm consists of:

- The prediction step is to determine the next prediction point by using the vector operations
- The correction step by using the minimization problem to determine the boundary point.

The minimization used in the corrector process can determine the boundary point correctly when the prediction point is outside the boundary. Thus, the tracing algorithm must prevent the prediction point for going into the boundary. The property of the minimization using the cost function is that the vector from the prediction point to the solution point is perpendicular to the surface of the solvable region [8], [17].

When the operational limits are taken into account, it does not guarantee that the vector from the prediction point to the solution point is perpendicular to the surface of the feasible region. Nevertheless, this vector is still pointing to the inner of the region, its perpendicular vector is a good approximation for determining the next prediction point. But, the next prediction point is not guaranteed that it does not go into the feasible region. Thus, the algorithm needs to check the position of the prediction point and re-adjust the position to be outside the feasible region. The position of the prediction point can be checked by the cost function which is the objective function of the minimization problem. When the prediction is inside the region, the obtained solution makes the cost function being zero. In the opposite way, the obtained solution makes the cost function being a positive value when the prediction point is outside the region. If the prediction point is inside the region, the position of the prediction point should be changed automatically by using an appropriated direction as shown in the figure below.

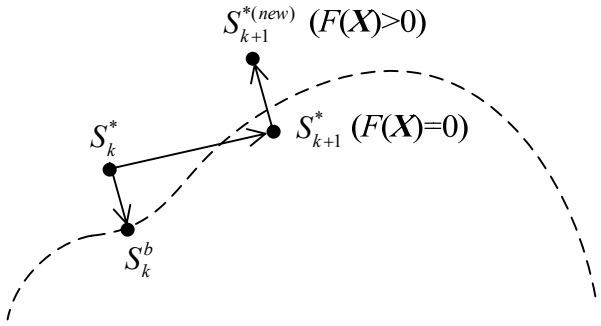


Figure 4.1 New Prediction Point Determination

The gap between the prediction point and the surface of the feasible region also affected the tracing result, as illustrated in Figure 4.2. The tracing result might lose some details when the gap is too wide. Moreover, a prediction point is possible to diverge from the boundary when the tracing process moves through the arc of the region. Thus, in the tracing process, the algorithm should adjust the gap between the prediction point and the boundary.

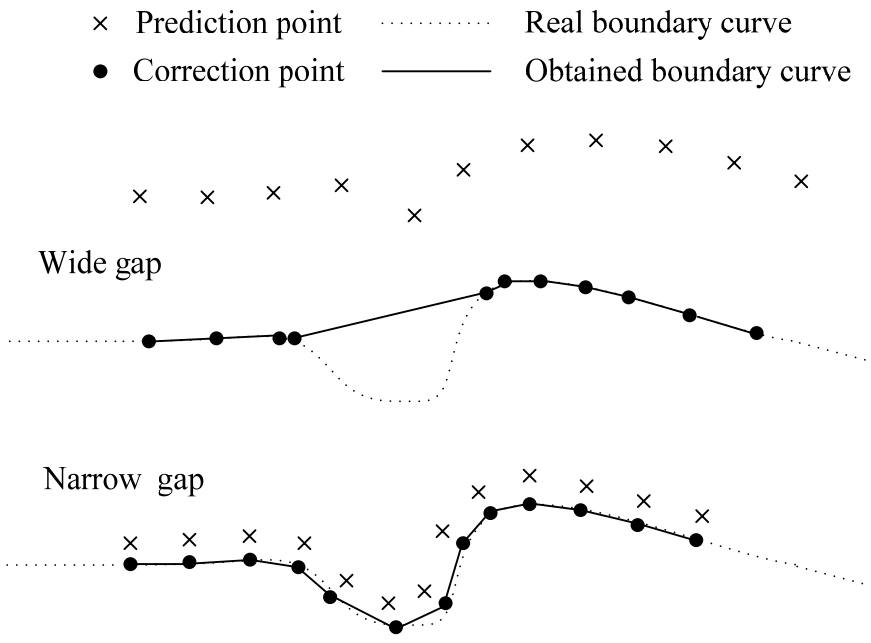


Figure 4.2 Tracing results between wide gap and narrow gap

## 4.3 Conclusion

The concept of proposed method is described in this chapter. A boundary point of feasible region should be determined by using the minimization problem because the

device limits can be treated as the problem constraints. This chapter also provided the concept of tracing algorithm such as, initial guess determination, prediction step, and correction step of the algorithm, etc. However, the details of proposed method will be shown in the next chapter.

# CHAPTER V

# BOUNDARY POINT DETERMINATION

This chapter formulates the optimization problem in order to determine the boundary points of the feasible region. The formulation includes the assignment of unknown variables, the objective function, and constraints. The problems considered in this chapter are: the power transfer from a source bus to a sink bus, and the power transfer from a source area to a sink area. The boundary points of the feasible region correspond to the maximum loading point of a given source-sink pair in the power system. For the boundary tracing process, the boundary points are determined from the prediction points which are outside the feasible region. In each step of the boundary tracing process, the problem must find the nearest feasible loading point from the prediction point. Thus, the formulation of this problem is the distance minimization subjected to the power flow constraints and the operational constraints.

## 5.1 Bus Variables

In power flow analysis, bus variables consist of voltage angle ($\delta$), voltage magnitude ($V$), power demand ($P_d$, $Q_d$), and power generation ($P_g$, $Q_g$), as shown in the figure below.

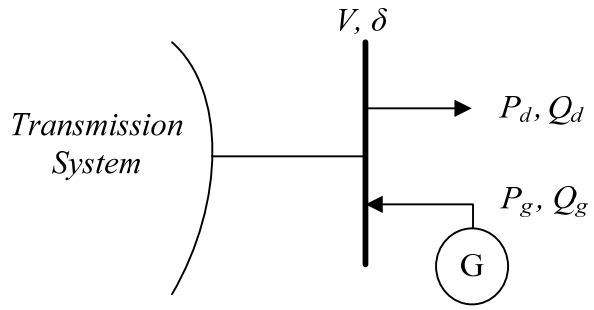


Figure 5.1 Bus variables

The free and fixed variables can be classified by the system devices. For a reference bus, voltage angle is fixed to be a reference angle of other buses. For the generator bus, voltage magnitudes are fixed because the generators can regulate the nodal voltage at their installed buses. Nevertheless, the problem with the source-sink pair causes a

different number of free variables. The classification of free variables can be summarized in the table below.

Table 5.1 Free and fixed variables.

| Devices | Mode | Free Variables | Fixed Variables |
|---|---|---|---|
| Reference Bus | Normal | $P_g$, $Q_g$ | $\delta$, $V$, $P_d$, $Q_d$ |
| | Source | $P_g$, $Q_g$ | $\delta$, $V$, $P_d$, $Q_d$ |
| | Sink | $P_g$, $Q_g$, $Pd$, $Qd$ | $\delta$, $V$ |
| | Source and Sink | $P_g$, $Q_g$, $Pd$, $Qd$ | $\delta$, $V$ |
| Generator Bus | Normal | $\delta$, $Q_g$ | $V$, $P_g$, $P_d$, $Q_d$ |
| | Source | $\delta$, $P_g$, $Q_g$ | $V$, $P_d$, $Q_d$ |
| | Sink | $\delta$, $Q_g$, $P_d$, $Q_d$ | $V$, $P_g$ |
| | Source and Sink | $\delta$, $P_g$, $Q_g$, $P_d$, $Q_d$ | $V$ |
| Load Bus | Normal | $\delta$, $V$ | $P_d$, $Q_d$ |
| | Source | $N/A$ | $N/A$ |
| | Sink | $\delta$, $V$, $P_d$, $Q_d$ | - |
| | Source and Sink | $N/A$ | $N/A$ |
| Synchronous Condenser or SVC (Generator Bus without $P_g$) | Normal | $\delta$, $Q_g$ | $V$, $P_d$, $Q_d$ |
| | Source | $N/A$ | $N/A$ |
| | Sink | $\delta$, $Q_g$, $P_d$, $Q_d$ | $V$ |
| | Source and Sink | $N/A$ | $N/A$ |

According to the table, generator bus and reference bus are possible to be both source bus and sink bus. But, load bus and synchronous condenser bus are not possible to be source bus because these buses can not supply real power. It obviously shows that a number of free variables depend on the bus type and the mode of operation. By using this concept, we can develop the system of unknowns for the power transfer between source-sink pair.

## 5.2 Formulation for Transfer between Two Buses

The power transfer between two buses consists of one source bus and one sink bus, as shown in the figure below. The loading point of the sink bus is the target for the problem. The feasible region of the loading points will be plotted on the plane between the real and reactive power of the sink bus.

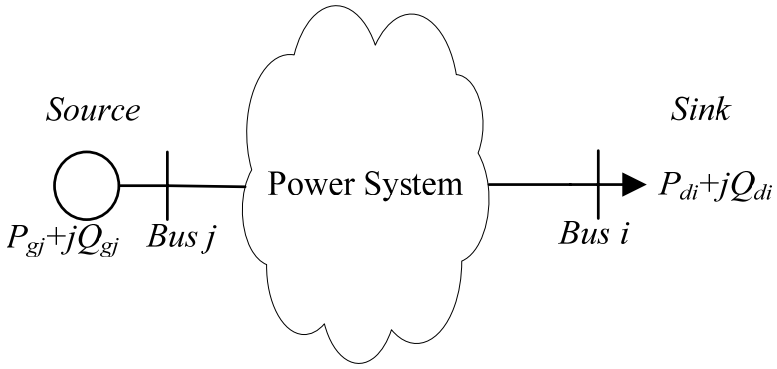


Figure 5.2 Transfer between two buses

### 5.2.1 Unknown Variables of Transfer between Two Buses

The calculation of the load margin is based on the power flow problem. The condition in every step of load increment must satisfy the power flow equations. The maximum loading point relates to the boundary of the feasible region. Therefore, the basic power flow variables are also the unknowns for this problem. The power flow variables consist of:

- The voltage phase angle of load buses and the generator buses designated by the vectors $\boldsymbol{\delta}_{pv}$ and $\boldsymbol{\delta}_{pq}$, respectively;
- The voltage magnitudes of load buses designated by the vector $\boldsymbol{V}_{pq}$.

In this problem, the power at the source bus and the sink bus are unknowns. The variables of the given source-sink buses consist of:

- The real power generation at the source bus $j$ designated by $P_{gj}$ ;
- The reactive power generation at the source bus $j$ designated by $Q_{gj}$;
- The real power demand at the sink bus $i$ designated by $P_{di}$;
- The reactive power demand at the sink bus $i$ designated by $Q_{di}$.

In the power flow problem, the reactive powers at the generator buses are calculated after obtaining the power flow solution. Thus, the reactive powers of all generators (including synchronous condensers and SVC) are also the unknowns designated by the vector $\boldsymbol{Q}_G$, where

$$\boldsymbol{Q}_G = [Q_{ref}\ \boldsymbol{Q}_{pv}]^T \tag{5.1}$$

The subscripts "*ref*" and "*pv*" correspond to the reference bus and the generator bus, respectively. The reactive power of source bus $Q_g$ is a member of $\boldsymbol{Q}_G$ components. Thus, the vector of unknown variables ($\boldsymbol{X}$) for this problem can be summarized as the following,

$$\boldsymbol{X} = [\boldsymbol{\delta}_{pv}\ \boldsymbol{\delta}_{pq}\ \boldsymbol{V}_{pq}\ P_{gj}\ \boldsymbol{Q}_G\ P_{di}\ Q_{di}]^T \tag{5.2}$$

### 5.2.2 Optimization Problem of Transfer between Two Buses

In the predictor-corrector process, the correction process corrects the prediction point to be the solution of the problem. The prediction point is the infeasible point of the problem. The proposed method needs to determine solutions on the boundary of the feasible region by using the optimization problem because the operational limits can be included into the problem as the constraints. Let the point $S^* = P_{di}^* + jQ_{di}^*$ be the loading point outside the feasible region. In this case, we consider one load bus and try to plot the contour of feasible region within two-dimensional space between $P_{di}$ and $Q_{di}$. Therefore, power injections on other load buses are not taken into account. The objective function for determining the boundary point of feasible region is function represented the distance between the point $S^*$ and the unknown boundary point $S^b = P_{di} + jQ_{di}$ as the following:

$$F(\boldsymbol{X}) = \frac{1}{2}\left\{(P_{di} - P_{di}^*)^2 + (Q_{di} - Q_{di}^*)^2\right\} \tag{5.3}$$

The objective function is in terms of one half the square of the power mismatch equations which is similar to the cost function in [8]-[12].

The solution ($\boldsymbol{X}$) has to satisfy power flow equations and all equipments must operate within their limits. Thus, the constraints of this problem consist of:

- The power flow equations:

$$\boldsymbol{g}(\boldsymbol{X}) = \mathbf{0} \tag{5.4}$$

Where $g(\boldsymbol{X})$ consists of real and reactive power functions for all buses in the system.

- The load bus voltage limits:

$$\boldsymbol{V}_{pq}^{\min} \le \boldsymbol{V}_{pq} \le \boldsymbol{V}_{pq}^{\max} \tag{5.5}$$

- The source bus limits:

$$P_{gj}^{\min} \le P_{gj} \le P_{gj}^{\max} \tag{5.6}$$

$$Q_{gj}^{\min} \le Q_{gj} \le Q_{gj}^{\max} \tag{5.7}$$

- The transmission line limits:

$$\boldsymbol{T}(\boldsymbol{X}) \le \boldsymbol{S}_T \tag{5.8}$$

Where

$\boldsymbol{T}(\boldsymbol{X})$ is a function of the transmission line flows;

$\boldsymbol{S}_T$ is a vector of the transmission line limits;

- Let the load demand be a negative value, and the generation be a positive value. Thus, the load is always negative for the realistic case, that is:

$$P_{di} \le 0 \tag{5.9}$$

The boundary point can be determined by minimizing (5.3) subjected to the constraints (5.4)-(5.9). The physical meaning of this minimization is to find the nearest point $S$ from the particular point $S^*$. When $S^*$ is outside the feasible region, the nearest point $S$ is the boundary point of the feasible region and the solution gives a positive value of the

objective function. On the other hand, the solution point $S$ equals to $S^*$ when $S^*$ is inside the feasible region. In this case, the solution is not the boundary point, and the solution gives the zero value of the objective function. Thus, the point $S^*$ must be always outside the feasible region, in the boundary tracing process.

### 5.3 Formulation for Transfer between Two Areas

In the figure below, the source area consists of $m$ generators, and the sink area consists of $n$ buses.

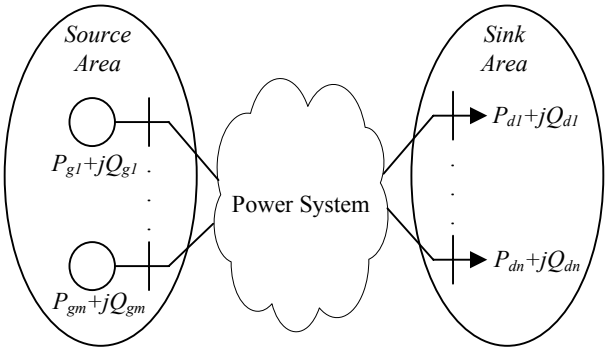


Figure 5.3 Transfer between two areas

In this case, the loading point inside the feasible region can be represented by a summation of sink bus loads as the following:

$$S = P_d + jQ_d = \sum_{i=1}^{n} P_{di} + j\sum_{i=1}^{n} Q_{di} \tag{5.10}$$

Where

$P_d$ is a summation of real powers in the sink area;

$Q_d$ is a summation of reactive powers in the sink area.

#### 5.3.1 Unknown Variables of Transfer between Two Areas

The unknowns for this problem are similar to the case of the transfer between two buses. The basic unknowns are the power flow variables consisting of the voltage magnitudes and the voltage angles ($\boldsymbol{V}_{pq}$, $\boldsymbol{\delta}_{pv}$, and $\boldsymbol{\delta}_{pq}$). The power of the source bus and

the sink bus are still the unknowns but these unknowns are in terms of a vector. The vectors of variables consist of:

- The vector of real power generations at the source area designated by $\boldsymbol{P}_g$, where

$$\boldsymbol{P}_g = [\, P_{g1} \ldots P_{gj} \ldots P_{gm} \,]^T \tag{5.11}$$

- The vector of reactive power generations at the source area designated by $\boldsymbol{Q}_g$, where

$$\boldsymbol{Q}_g = [Q_{g1} \ldots\ Q_{gj} \ldots\ Q_{gm}]^T \tag{5.12}$$

- The vector of real power demands at the sink area designated by $\boldsymbol{P}_d$, where

$$\boldsymbol{P}_d = [\, P_{d1} \ldots P_{di} \ldots P_{dn} \,]^T \tag{5.13}$$

- The vector of reactive power demands at the sink area designated by $\boldsymbol{Q}_{di}$, where

$$\boldsymbol{Q}_d = [Q_{d1} \ldots\ Q_{di} \ldots\ Q_{dn}]^T \tag{5.14}$$

However, the variables in (5.12) are the members of $\boldsymbol{Q}_G$ in (5.1). The reactive powers of all generators are still the unknowns for this problem. Therefore, the unknown variables for this problem can be summarized as the following,

$$\boldsymbol{X} = [\boldsymbol{\delta}_{pv}\ \boldsymbol{\delta}_{pq}\ \boldsymbol{V}_{pq}\ \boldsymbol{P}_g\ \boldsymbol{Q}_G\ \boldsymbol{P}_d\ \boldsymbol{Q}_d]^T \tag{5.15}$$

### 5.3.2 Optimization Problem of Transfer between Two Areas

In this problem, the objective function is the function represented the distance on the plane of the total loads in the sink area. In order to determine the boundary point, the problem is to find the nearest loading point from the infeasible loading point $S^*$, as same as the problem of the power transfer between two buses. The minimization for this case is shown as the following:

$$\text{Minimize} \quad F(\boldsymbol{X}) = \frac{1}{2}\left\{\left[(\sum_{i=1}^{n} P_{di}) - P_d^*\right]^2 + \left[(\sum_{i=1}^{n} Q_{di}) - Q_d^*\right]^2\right\} \tag{5.16}$$

$$\text{Subjected to} \quad \boldsymbol{g}(\boldsymbol{X}) = \mathbf{0} \tag{5.17}$$

$$\boldsymbol{V}_{pq}^{\min} \le \mathbf{V}_{pq} \le \boldsymbol{V}_{pq}^{\max} \tag{5.18}$$

$$\boldsymbol{P}_g^{\min} \le \boldsymbol{P}_g \le \boldsymbol{P}_g^{\max} \tag{5.19}$$

$$\boldsymbol{Q}_g^{\min} \le \boldsymbol{Q}_g \le \boldsymbol{Q}_g^{\max} \tag{5.20}$$

$$\boldsymbol{T}(\boldsymbol{X}) \le \boldsymbol{S}_T \tag{5.21}$$

$$\boldsymbol{P}_d \le \mathbf{0} \tag{5.22}$$

In the conventional load margin determination, the load and generation are changed by their characteristic. The source area generations and the sink area loads are forced by the participation factors. This problem also applies the same concept by forcing the source generations and the sink loads by the participation factors. Assume that the real power demand at the bus $k$ is changed by the factor $K_{Pdi}$, where

$$K_{Pdi} = \frac{P_{di}}{\sum_{k=1}^{n} P_{dk}} \tag{5.23}$$

It implies that

$$\begin{aligned} P_{di} &= K_{Pdi} \sum_{k=1}^{n} P_{dk} \\ &= K_{Pdi}(P_{d1} + \ldots + P_{di} + \ldots + P_{dn}) \end{aligned} \tag{5.24}$$

It can be represented by the linear equation as the following,

$$K_{Pdi}P_{d1} + \ldots + (K_{Pdi} - 1)P_{di} + \ldots + K_{Pdi}P_{dn} = 0 \tag{5.25}$$

By the same way, the reactive power demand at the bus $i$ is changed by the factor $K_{Qdi}$, and the real power generation at bus $j$ is change by the factor $K_{Pgj}$. These quantities can be represented by the linear equations as the following:

$$K_{Qdi}Q_{d1}+\ldots+(K_{Qdi}-1)Q_{di}+\ldots+K_{Qdi}Q_{dn}=0 \tag{5.26}$$

$$K_{Pgj}P_{g1}+\ldots+(K_{Pgj}-1)P_{gj}+\ldots+K_{Pgj}P_{gm}=0 \tag{5.27}$$

The equations (5.25)-(5.27) can be rewritten in terms of the matrix equations as the following:

$$(\boldsymbol{A}_{Pd}-\boldsymbol{I}_d)\boldsymbol{P}_d=\boldsymbol{0} \tag{5.28}$$

$$(\boldsymbol{A}_{Qd}-\boldsymbol{I}_d)\boldsymbol{Q}_d=\boldsymbol{0} \tag{5.29}$$

$$(\boldsymbol{A}_{Pg}-\boldsymbol{I}_g)\boldsymbol{P}_g=\boldsymbol{0} \tag{5.30}$$

Where

$\boldsymbol{I}_d$, $\boldsymbol{I}_g$ are the $n$ x $n$ identity matrix and the $m$ x $m$ identity matrix, respectively;

$$\boldsymbol{A}_{Pd}=\left[\boldsymbol{K}_{Pd}\ldots\boldsymbol{K}_{Pd}\right]_{n\times n}=\begin{bmatrix} K_{Pd1} & \cdot & \cdot & \cdot & K_{Pd1} \\ \cdot & \cdot & & & \cdot \\ \cdot & & \cdot & & \cdot \\ \cdot & & & \cdot & \cdot \\ K_{Pdn} & \cdot & \cdot & \cdot & K_{Pdn} \end{bmatrix}_{n\times n}; \tag{5.31}$$

$$\boldsymbol{A}_{Qd}=\left[\boldsymbol{K}_{Qd}\ldots\boldsymbol{K}_{Qd}\right]_{n\times n}=\begin{bmatrix} K_{Qd1} & \cdot & \cdot & \cdot & K_{Qd1} \\ \cdot & \cdot & & & \cdot \\ \cdot & & \cdot & & \cdot \\ \cdot & & & \cdot & \cdot \\ K_{Qdn} & \cdot & \cdot & \cdot & K_{Qdn} \end{bmatrix}_{n\times n}; \tag{5.32}$$

$$\boldsymbol{A}_{Pg}=\left[\boldsymbol{K}_{Pg}\ldots\boldsymbol{K}_{Pg}\right]_{m\times m}=\begin{bmatrix} K_{Pg1} & \cdot & \cdot & \cdot & K_{Pg1} \\ \cdot & \cdot & & & \cdot \\ \cdot & & \cdot & & \cdot \\ \cdot & & & \cdot & \cdot \\ K_{Pgm} & \cdot & \cdot & \cdot & K_{Pgm} \end{bmatrix}_{m\times m}. \tag{5.33}$$

Where

$$\boldsymbol{K}_{Pd} = [K_{Pd1} \ \ldots K_{Pdi} \ \ldots K_{Pdn}]^T \tag{5.34}$$

$$\boldsymbol{K}_{Qd} = [K_{Qd1} \ \ldots K_{Qdi} \ \ldots K_{Qdn}]^T \tag{5.35}$$

$$\boldsymbol{K}_{Pg} = [K_{Pg1} \ \ldots K_{Pgj} \ \ldots K_{Pgm}]^T \tag{5.36}$$

For the problem of the power transfer between areas, the equations (5.28)-(5.30) are the linear equality constraints added into the minimization problem for forcing loads and generations with the participation factors. The solution of this problem gives the loading point on the boundary of the feasible region by (5.10).

## 5.4 Conclusion

This chapter has developed the method to determine a boundary point of feasible region. The unknowns are manipulated by considering the case of transfer between a given source-sink pair. The solution on boundary can be determined by minimizing a distance from a loading point outside the region. The formulation in this chapter is used in a correction step of the boundary tracing algorithm that will be described in the next chapter.

# CHAPTER VI

# BOUNDARY TRACING METHOD

This chapter develops the tracing method to determine a boundary curve of feasible region. The tracing method consists of the predictor-corrector process. The predictor process is to determine a prediction point by using vector operations. The corrector process is to calculate boundary points by using the minimization problem as described in a previous section. A boundary point can be calculated by using the prediction point and the initial guess of unknown variables as inputs for the minimization problem. The way to obtain a sequence of boundary points is described in this chapter.

## 6.1 First Prediction Point and Initial Guess

The minimization problem for determining the boundary point needs to be assigned the prediction point $S^*$ and the initial guess $\boldsymbol{X}^0$ to the problem. The prediction point $S^*$ is in terms of the loading point which leads to the violation of parameters in the power systems. The initial guess $\boldsymbol{X}^0$ should be the power flow solution near the boundary. In this section, these parameters are determined by the method based on the repeated power flow. The concept of the repeated power flow is to increase the loading point at the sink bus (or area) in the steps of $\sigma$ MVA until the violation of system parameters occurs. After that, the solution on the boundary $S^b$ is searched by the bisection method. The obtained solution is the first initial guess of the minimization problem for the boundary tracing process. Then, the first infeasible point $S^*$ is determined by increasing load from the loading point $S^b$ with the same direction $\theta$ as applying in the repeated power flow. The concept of the determination is illustrated in the figure below.

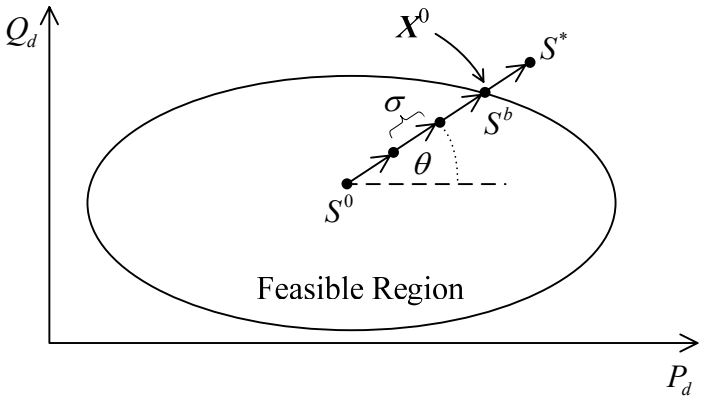


Figure 6.1 Process to determine first infeasible point

### 6.1.1 Repeated Power Flow with Bisection Method

The solution on the boundary point and the first infeasible point can be determined by the repeated power flow as described in the following steps:

1.) Let $k$ be a number corresponding to steps of the load increment, and $\sigma$ be a step size of the load increment. Determine the base case of the system by the power flow.

2.) Define $k$=1 for the first step.

3.) Let $S^0$ be a loading point of the base case, and $\theta$ be an angle corresponding to the direction of load increment. The loading point $S^0$ is calculated by

$$S^0 = P_d^0 + jQ_d^0 = \sum_{i=1}^{n} P_{di}^0 + j\sum_{i=1}^{n} Q_{di}^0 \tag{6.1}$$

The load at sink area (or sink bus) is changed in the following way:

$$\boldsymbol{P}_d^k = \boldsymbol{P}_d^0 + (k\sigma\cos\theta)\boldsymbol{K}_{Pd} \tag{6.2}$$

$$\boldsymbol{Q}_d^k = \boldsymbol{Q}_d^0 + (k\sigma\sin\theta)\boldsymbol{K}_{Qd} \tag{6.3}$$

4.) Determine the power flow solution.

5.) Check the violation of system parameters. If all parameters are still within their limits, then increase the number $k$ by 1 and return to step 3. If there is a violation in the system, then go to the next step.

6.) Let the case A be the case of loading condition without a parameter violation, and the case B be the case of loading condition with parameter violations, where:

- Case A: $\boldsymbol{P}_d^A = \boldsymbol{P}_d^{k-1}$, $\boldsymbol{Q}_d^A = \boldsymbol{Q}_d^{k-1}$, and $S^A = P_d^A + jQ_d^A$
- Case B: $\boldsymbol{P}_d^B = \boldsymbol{P}_d^k$, $\boldsymbol{Q}_d^B = \boldsymbol{Q}_d^k$, and $S^B = P_d^B + jQ_d^B$.

7.) Check the difference between $S^A$ and $S^B$. If $|S^A - S^B|$ is less than a given criterion $\varepsilon$, then go to step 11. If $|S^A - S^B|$ is more than a criterion, then go to the next step.

8.) Let case C be the case of loading condition obtained by:

$$\boldsymbol{P}_d^C = \frac{1}{2}\left(\boldsymbol{P}_d^B - \boldsymbol{P}_d^A\right); \tag{6.4}$$

$$\boldsymbol{Q}_d^C = \frac{1}{2}\left(\boldsymbol{Q}_d^B - \boldsymbol{Q}_d^A\right). \tag{6.5}$$

9.) Determine the power flow solution of the case C.

10.) If all parameters are within their limits, then $\boldsymbol{P}_d^A = \boldsymbol{P}_d^C$ and $\boldsymbol{Q}_d^A = \boldsymbol{Q}_d^C$. If the case C has violations, then $\boldsymbol{P}_d^B = \boldsymbol{P}_d^C$ and $\boldsymbol{Q}_d^B = \boldsymbol{Q}_d^C$. Return to step 7.

11.) Declare the loading point $S^A$ to be the boundary point $S^b$. The obtained solution is treated as an initial guess $\boldsymbol{X}^0$ of the minimization problem in the tracing process.

12.) Determine an infeasible loading point $S^*$ with a step $\mu$ as the following,

$$S^* = S^b + \mu \frac{(S^b - S^0)}{\left|S^b - S^0\right|} \tag{6.6}$$

The repeated power flow with the bisection method can be illustrated as the flow chart below.

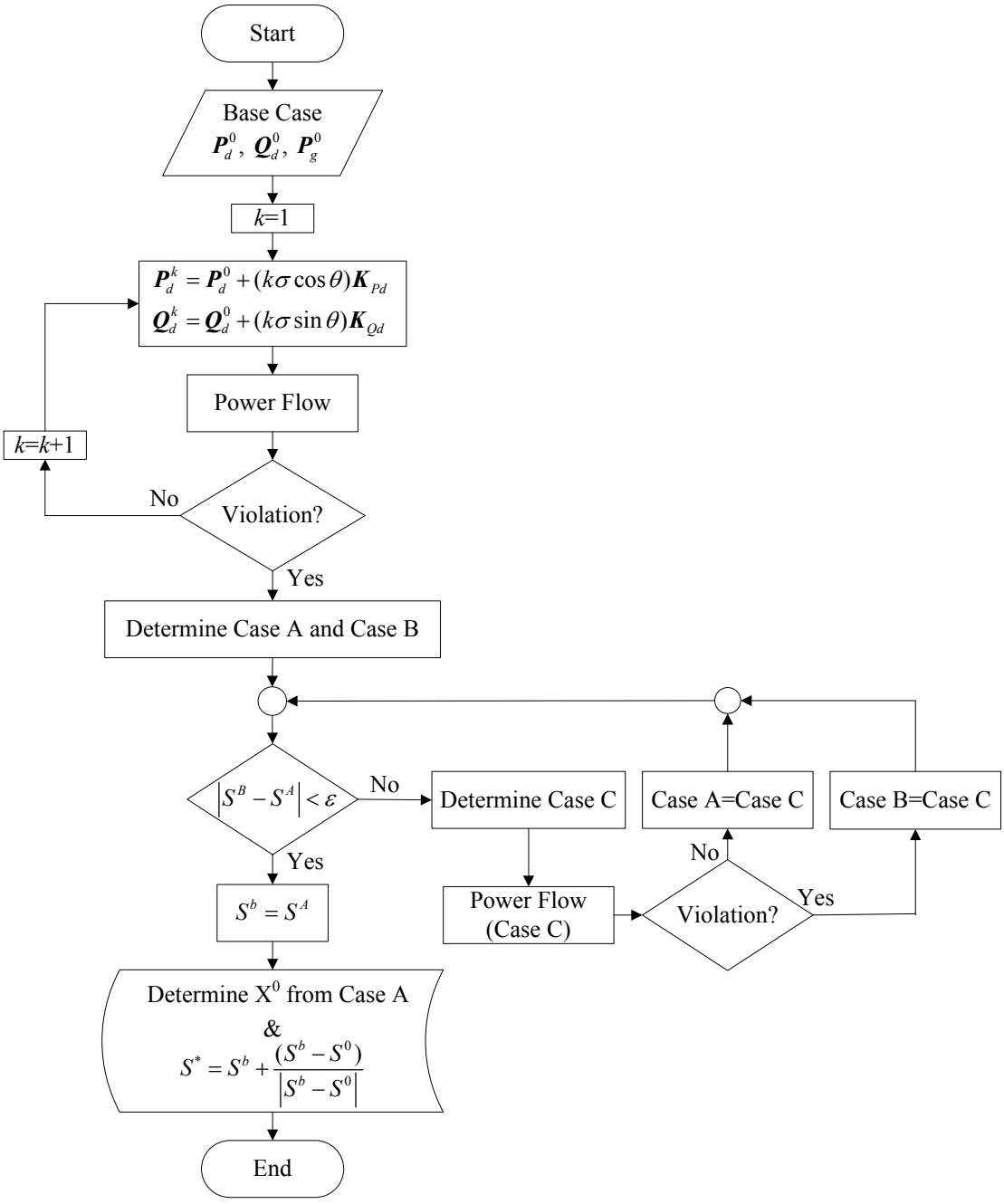


Figure 6.2 Repeated power flow with bisection method

For the case of the power transfer between two buses, a source bus is treated as a slack bus for the power flow in steps 4 and 8. However, for the case of power transfer between areas, a group of generators in the source area must supply the increasing load corresponding to the generator participation factor.

### 6.1.2 Power Flow with Group of Slack Buses

For the power transfer between areas, the load and generation must satisfy participation factors $\boldsymbol{K}_{Pd}$, $\boldsymbol{K}_{Qd}$, and $\boldsymbol{K}_{Pg}$. In the power flow, the load participation factors specify the sink area load as in (6.2) and (6.3). However, the source area generators have to share the power supplying to the sink area by the generator participation factor $\boldsymbol{K}_{Pg}$. In this work, we treat one generator on the source area as a slack bus. After increasing the load in sink area, the slack bus power increased from the base case will be share to other generator in source area, and then repeat the power flow by the same way until the slack bus power does not change. The implementation steps are as the following:

1.) Treat one generator as a slack bus. Let $P_{g1}$ be the slack bus power. Determine the base case power flow solution.

2.) Keep data of the slack bus power before running the power flow, denoted by $P_{g1}^{0}$. And, let $\boldsymbol{P}_{g}^{0}$ be a vector of the source area generations before running the power flow.

3.) Determine the power flow solution.

4.) Check the variation of slack bus power. If $\left|P_{g1}-P_{g1}^{0}\right|<\varepsilon$, then go to step 7. If $\left|P_{g1}-P_{g1}^{0}\right|\geq\varepsilon$, then go to the next step .

5.) The change of slack bus power is shared in the source area by the following way,

$$\boldsymbol{P}_{g}=\boldsymbol{P}_{g}^{0}+(P_{g1}-P_{g1}^{0})\boldsymbol{K}_{pg} \tag{6.7}$$

6.) Treat $P_{g1}^{0}=P_{g1}$, and then return to step 3.

7.) Keep the solution and then the iteration is terminated.

Figure 6.3 shows the flow chart of the process above. By using this method, the generations are followed by generator participation factors. For the transfer between areas, this process can be implemented in steps 4 and 8 of the repeated power flow in the previous section.

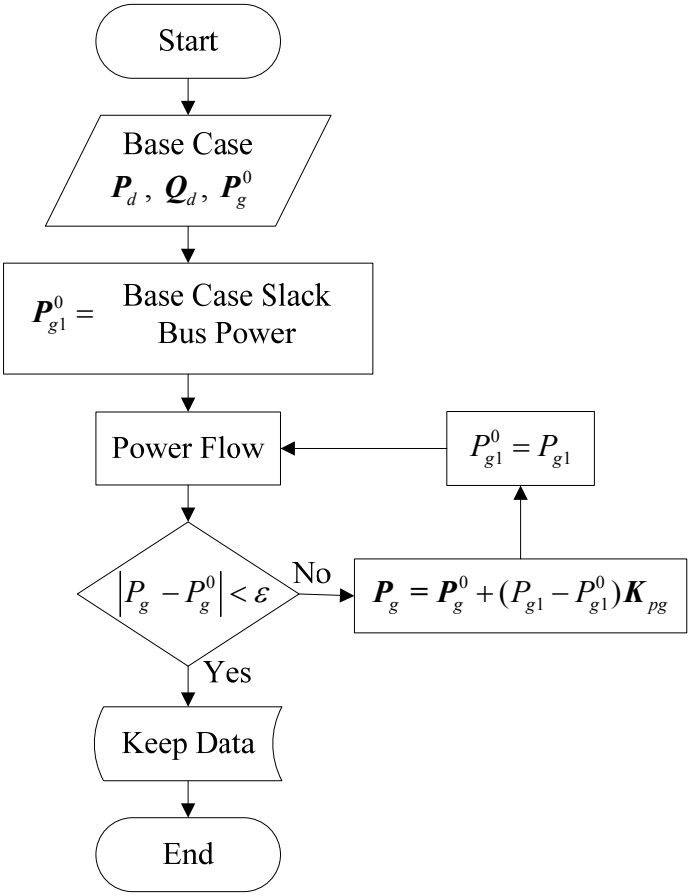


Figure 6.3 Power flow with group of slack buses

## 6.2 Boundary Tracing Method

The tracing method is base on the predictor-corrector process. The correction process uses the minimization problem as formulated in the previous section. The prediction step is developed in order to guarantee that a prediction point will not go into the feasible region. The tracing process begins with the first prediction point $S_1^*$ and the first initial guess $\boldsymbol{X}^0$, which are obtained by using a method in the previous section.

### 6.2.1 Corrector Process

The corrector process utilizes the minimization problem as described in Chapter 5. The inputs of this process are a prediction point $S^*$ and an initial guess $\boldsymbol{X}^0$. The solution $\boldsymbol{X}$ from the minimization can check that a point $S^*$ is inside the feasible region or not. The solution can be categorized into two cases:

- The case of $F(\boldsymbol{X})=0$ implies that a prediction point $S^*$ is inside the feasible region, and the obtained $\boldsymbol{X}$ is not a solution on the boundary curve.
- The case of $F(\boldsymbol{X})>0$ implies that a prediction point $S^*$ is still outside the feasible region, and the obtained $\boldsymbol{X}$ is a solution on the boundary curve.

If the prediction point $S^*$ is inside the region, the process needs to determine a new prediction point by the following way,

$$S_k^{*(new)} = S_k^* + \left[ \frac{(S_{k-1}^* - S_{k-1}^b)}{\left| S_{k-1}^* - S_{k-1}^b \right|} \times \rho \right] \tag{6.8}$$

Where

$S_k^*$ is a prediction point of the corrector step $k$.

$S_k^{*(new)}$ is a new prediction point of the corrector step $k$.

$S_{k-1}^*$ is a prediction point of the previous corrector step.

$S_{k-1}^b$ is a boundary point obtained from the previous corrector step.

$\rho$ is a moving length.

The new prediction point can be found by moving an existing $S_k^*$ in the direction of $S_{k-1}^*$ - $S_{k-1}^*$ with a length $\rho$, as shown in the figure below. If the new prediction point is still inside the region, the same process can be repeated until the prediction point is moved to the outside of region. When the prediction point is outside, the corrector process can properly determine the next boundary point.

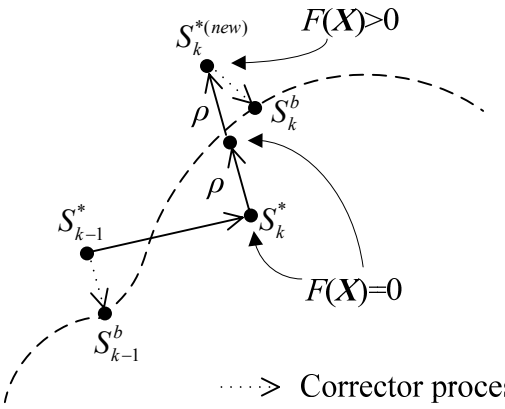


Figure 6.4 Process to determine new prediction point

### 6.2.2 Predictor Process

The predictor process is to predict the next boundary point. The next prediction point can be determined by using a previous prediction point, and the gap between the prediction point and the boundary must be adjusted. Let *d* be the distance parameter for adjusting the gap. For the tracing step *k*, the point $S_k^{*'}$ is determined by the following,

$$S_k^{*'} = S_k^b + \left[ \frac{(S_k^b - S_k^*)}{\left| S_k^b - S_k^* \right|} \times d \right] \tag{6.9}$$

The gap between point $S_k^{*'}$ and the boundary point $S_k^b$ is adjusted by the parameter *d*. The next prediction point can be determined by the following,

$$S_{k+1}^* = S_k^{*'} + l \cdot \Delta S_k^* \tag{6.10}$$

Where *l* is a scalar parameter representing a step size and $\Delta S_k^*$ is a vector representing the direction for determining the next prediction point. The vector $\Delta S_k^*$ is the perpendicular vector of $S_k^b - S_k^*$. Because *S* is in terms of the complex number, the perpendicular vector of $S_k^b - S_k^*$ can be calculated by multiplying the imaginary unit (*j*). Thus, the vector $\Delta S_k^*$ can be determined by the following:

$$\Delta S_k^* = j \times \frac{(S_k^b - S_k^*)}{\left| S_k^b - S_k^* \right|} \tag{6.11}$$

The predictor process with the adjustment of the gap by the parameter *d* is illustrated in the figure below.

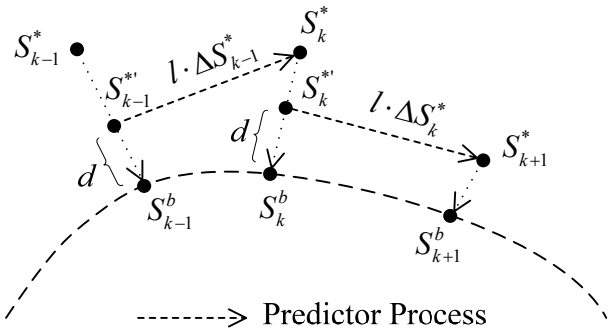


Figure 6.5 Predictor process with gap adjustment

### 6.2.3 Tracing Algorithm

The tracing algorithm can be summarized as the following steps:

1) Determine the first prediction point $S^*_1$ and the first initial guess $\boldsymbol{X}^0_1$ by using the process described in Section 6.1.
2) Let $k$=1 for the first tracing step.
3) Determine the boundary point $S^b_k$ and the solution on the boundary $\boldsymbol{X}_k$ by using the minimization method in Chapter 5.
4) Check that the existing prediction point $S^*_k$ is inside the feasible region or not. If $S^*_k = S^b_k$, then go to the next step. If $S^*_k \neq S^b_k$, then go to step 6.
5) Find a new prediction point $S^{*(new)}_k$ by using the method in Section 6.2.1, and return to the step 3.
6) Check that the contour of feasible region is complete or not. If the contour is not complete, then go to the next step. If the contour is complete, then the tracing process is terminated.
7) The solution of the boundary point $\boldsymbol{X}_k$ is treated as the next initial guess $\boldsymbol{X}^0_{k+1}$ for the minimization problem in order to determine the next boundary point.
8) Determine the next prediction point $S^*_{k+1}$ by using the method in Section 6.2.2.
9) Let $k$=$k$+1 for the next tracing step, and then return to step 3.

The tracing algorithm can be illustrated by the flow chart and the figure below.

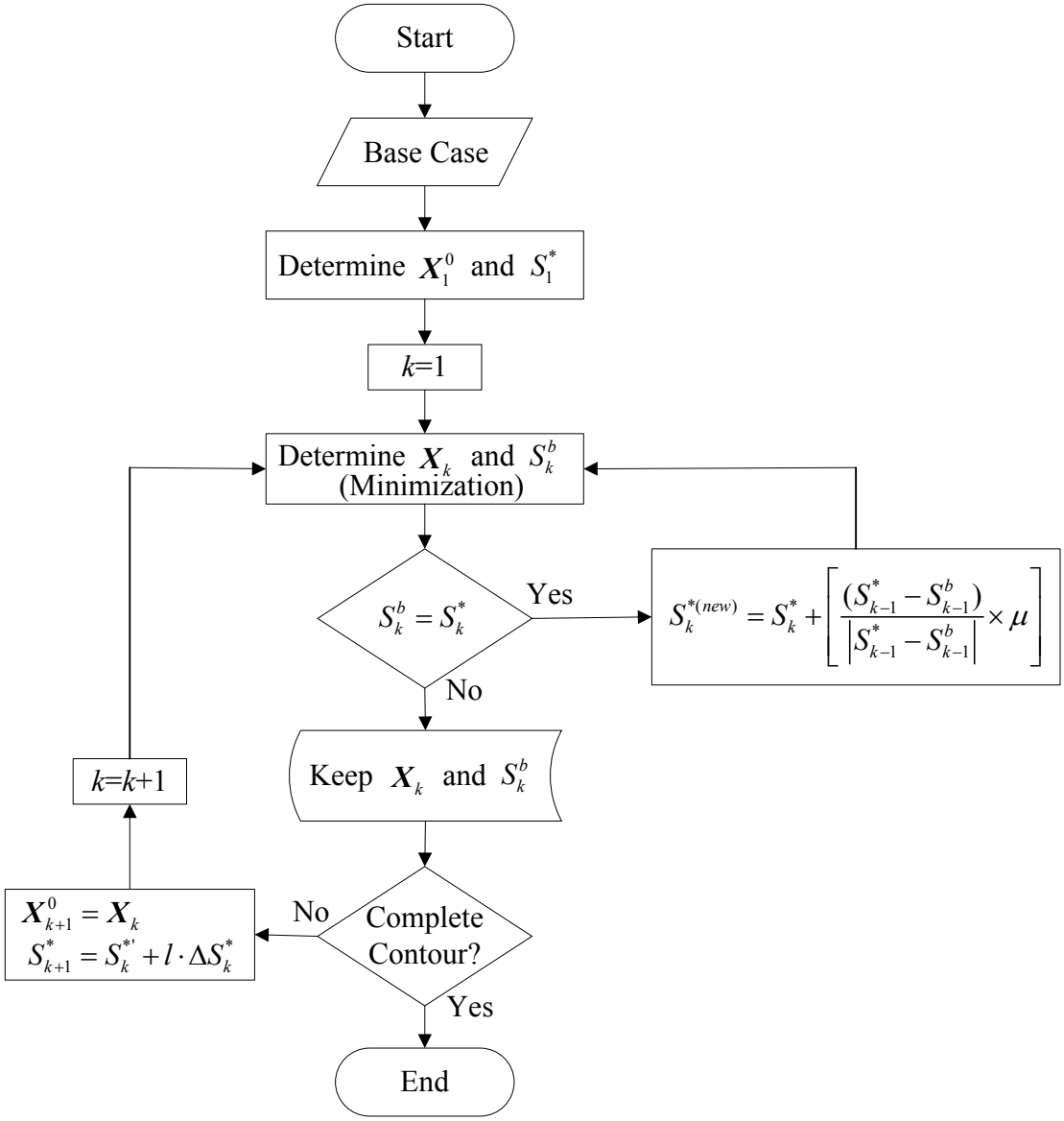


Figure 6.6 Flow chart of tracing algorithm

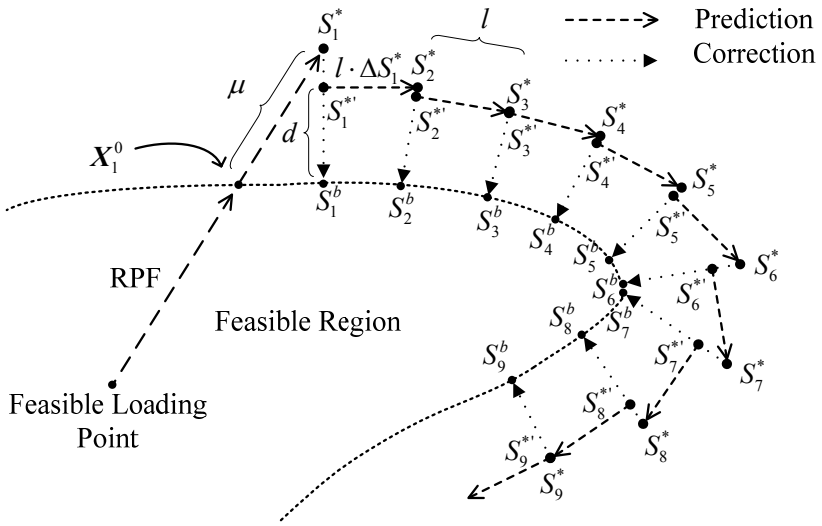


Figure 6.7 Proposed tracing process

### 6.2.4 Modified Algorithm with Real Power Limit Enforcement

The boundary of feasible region consists of solution points with some active constraints. In some cases, an active constraint is real power generation limit. According to the formulation of optimization problem in Chapter 5, the change of real power generations are forced by using participation factors in the linear equality constraints (5.30). The real power generations are changed together until at least one real power generation is active on its limit. However, in practice, when one generator operates at its limit, other generators in source area can continue supplying real power to sink area. By considering this scenario, step 3 of boundary tracing algorithm in Section 6.2.3 can be modified by checking the solution obtained from step 3 of tracing algorithm. If some source buses touch the real power limits, these source buses are removed from a group of source buses. The real power generations of the real power limit buses are fixed. The optimization solution is determined repeatedly until there is no source bus with real power limit or there is only one source bus in source areas. The modified algorithm can be illustrated in the figure below.

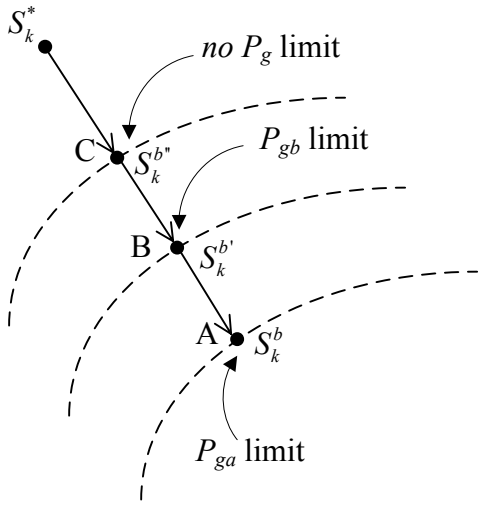


Figure 6.8 Process of modified algorithm with real power enforcement

When the solution at $S_k^b$ has an active real power generation limit at bus *a* ($P_{ga}$), new solution point will be determined by removing bus *a* from a group of source buses. If new solution at $S_k^{b'}$ has an active real power generation limit at bus *b* ($P_{gb}$), the process is repeated again until the obtained solution has no real power generation limit. In this figure, the final boundary point is $S_k^{b''}$.

### 6.3 Closed Area of Feasible Region

The result from the proposed method is a feasible region. The regions are different depended on many factors. The results can be compared by plotting the contours on the *P-Q* plane. The contours might be different in terms of area and position. The position is obviously found by plotting a result in the *P-Q* plane. It details the maximum loading points in many load directions. The area of feasible region is the feasibility of loading points. However, the shape of feasible regions is not a basic geometry shape. It is difficult to compare the area of feasible region by the visualization. Thus, the area of feasible region should be calculated.

The output of tracing process is a set of coordinates on the *P-Q* plane. The area enclosed by feasible region can be found using Green's theorem [23]. Let the curve *C* be the counterclockwise curve along the boundary of region *R* in the *x-y* plane, as shown in the figure below.

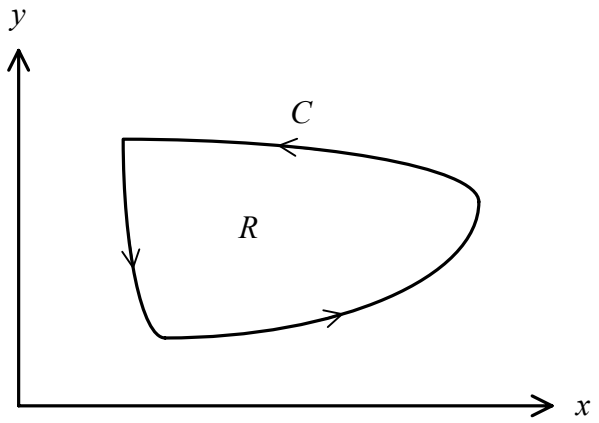


Figure 6.9 Region in *x*-*y* plane

Then, the area of *R* is

$$\text{area} = \frac{1}{2}\oint_C (xdy - ydx), \tag{6.12}$$

When the data of $x$ and $y$ are the coordinates of points around the boundary of *R*, the area of *R* can be found by a numerical approximation [24]. The coordinate of the $k^{th}$ point is denoted by $\{x_k,\ y_k\}$. Segment $i$ connects $\{x_k,\ y_k\}$ and $\{x_{k+1},\ y_{k+1}\}$ for $k$ varying from 1 to the number of data points *N*. The area enclosed by coordinates in the *x*-*y* plane is

$$\text{area} = \frac{1}{2}\sum_{k=1}^{N}\left[\frac{1}{2}(x_{k+1}+x_k)(y_{k+1}-y_k) - \frac{1}{2}(y_{k+1}+y_k)(x_{k+1}-x_k)\right] \tag{6.13}$$

This formula can be applied to output data of the boundary tracing method. The *x*-axis and the *y*-axis are $P_d$ and $Q_d$, respectively. We can find the area of feasible region to compare the feasibility of transfer scenarios by this method.

## 6.4 Conclusion

This chapter has provided the algorithm in order to determine a boundary of feasible region. The proposed boundary tracing method is based on the predictor-corrector process. The minimization in a corrector process needs an unfeasible loading

point as a prediction point of process. Thus, the algorithm of tracing process must prevent the prediction point for going inside the feasible region. The shape of feasible region can be visualized by this proposed method. However, the obtained contour is a feasible region of the considered transfer case. If the system parameters change, the contour of feasible region will be changed. The changes of feasible region affected by system parameters will be discussed in next chapter.

# CHAPTER VII

# EFFECT OF SYSTEM PARAMETERS

According to the conventional load margin determination, the sink area load and the source area generation are assumed to change in a specific direction, while other system parameters are fixed. The load margin can be varied by the change of loading point in sink area, or the variation of system parameters. A feasible region obtained by the boundary tracing method has a same concept of the load margin determination. The obtained region is a set of feasible loading point transferred between a given source-sink pair. The effects of system parameters to feasible regions are classified into two categories: the movement of loading point, and the change of boundary by parameters from the outside of sink area [12].

## 7.1 Movement of Loading Point

The feasible region determined by the proposed algorithm shows a set of available loading points. The change of load at sink bus results in a movement of loading point, and a movement is limited by the boundary. The change of reactive power causes a loading point moving along the reactive power axis. The reactive power can be changed by reactive compensation devices, e.g. capacitor banks, and static VAr compensation devices (SVC), etc. The change of real power also causes a loading point moving along the real power axis. However, in practice, the real power usually changes together with the reactive power. The movements of loading point can be illustrated in the figure below.

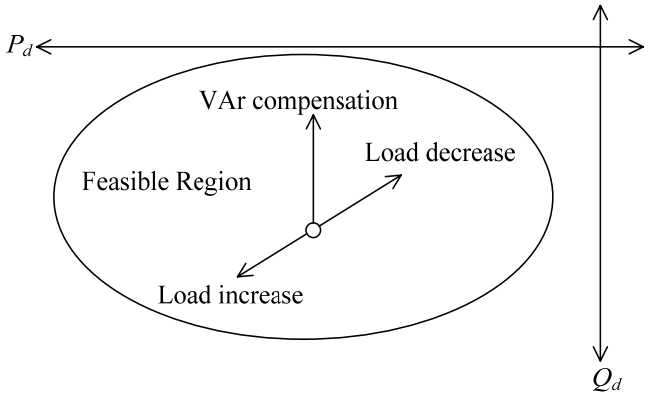


Figure 7.1 Movements of loading point

By using the feasible region, the load margin monitoring can be enhanced, as the example in Figure 7.2. When the loading point of base case is assumed to be point *a*, the maximum loading point is the point *A*. However, the loading point can be compensated by the reactive power device. When the loading point moves to point *b*, the load can increase to point *c* with the same power factor as base case. The loading point can be compensated again to move to point *d*. Finally, the loading point can be operated at point *B*, which has more real power than point *A*. These are the advantages of feasible region visualization in term of the enhancement of load monitoring.

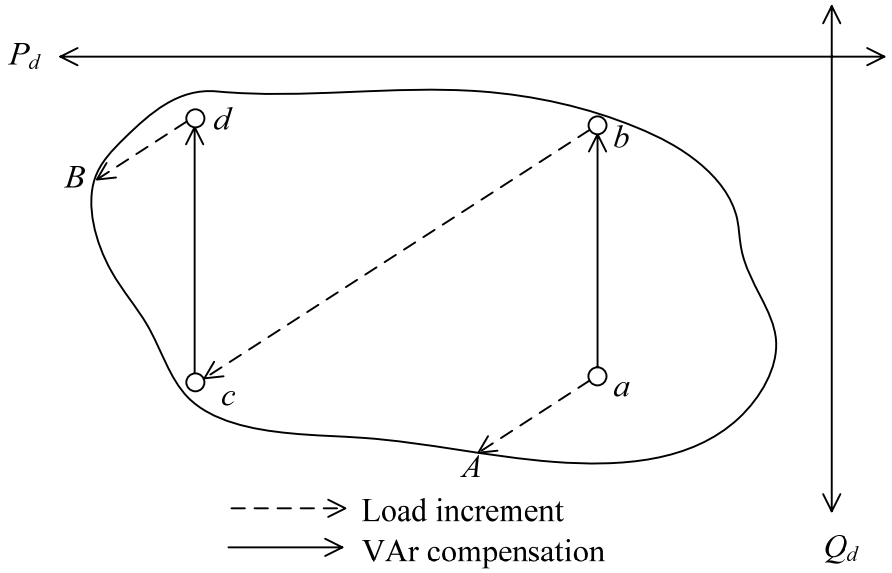


Figure 7.2 Movements of loading point by reactive power compensation

## 7.2 Change of Boundary

The feasible region on the *P*-*Q* plane is a set of feasible loading points of sink area. The varied load in sink area causes the loading point to move over inside the feasible region. Nevertheless, the shape of the feasible boundary is changeable by system parameters.

The loading point always changes by the electricity demand, and it can be controlled by control actions from operators. When an undesirable situation occurs due to a heavy load, the loading point is possibly away from the feasible region. The system operator can bring the system back to normal condition using control actions such as reactive power compensation or load shedding. In sink area, the control actions result in

the loading point moving over the feasible region, as mentioned in previous section. On the other hand, if the control actions are operated on the buses outside sink area, the feasible region of sink area will be reshaped, as shown in Figure 7.3. Beside the control actions at the load side, the feasible region can be reshaped by other control parameters, e.g. generator voltages, and FACTS parameters, etc.

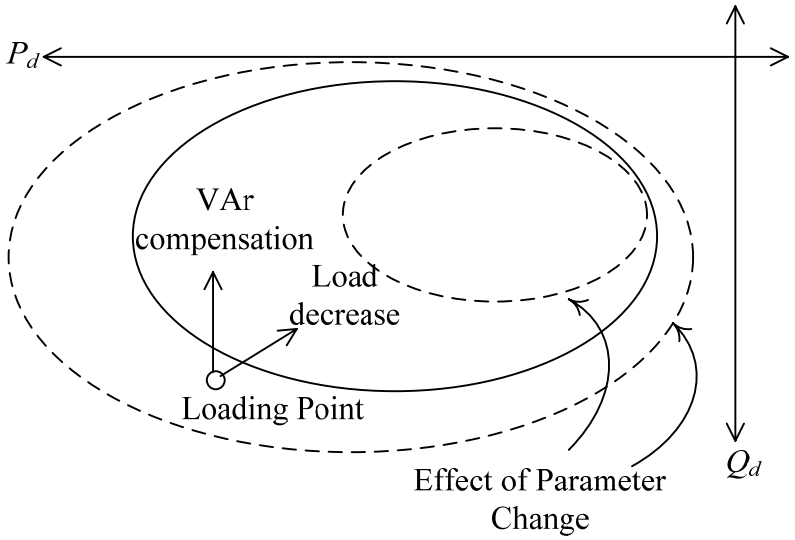


Figure 7.3 Effects of parameter changes to feasible region

### 7.3 Outermost Boundary

The boundary of power flow solution space is multi-dimensional, nonconvex, and varied by a large number of variables [21], [22] Comparing to the proposed boundary curve, the curve obtained by the tracing method is plotted on the two-dimensional plane. The shape of region can be changed by the variation of control parameters. The idea of boundary change can be illustrated in Figure 7.4. The control parameters are assumed to be the z-axis. The multi-dimensional solution space is represented by the three-dimensional object. The x-axis and y-axis are the real and reactive power of the sink area, respectively. When control parameters are fixed with their settings, the boundary curve obtained by the tracing method is like the cut section of the space at that setting. For example, the feasible region is the region *A* when the control parameters are set by the setting point *A*, and the feasible region is the region *B* when the control parameters are set by the setting point *B*. Moreover, when control parameters are free to vary, the cut section

also varies. But, the cut section does not expand over the outermost boundary. The outermost boundary is like the projection of the solution space on the x-y plane. By the manipulation of free variables, the various kinds of outermost boundary can be determined.

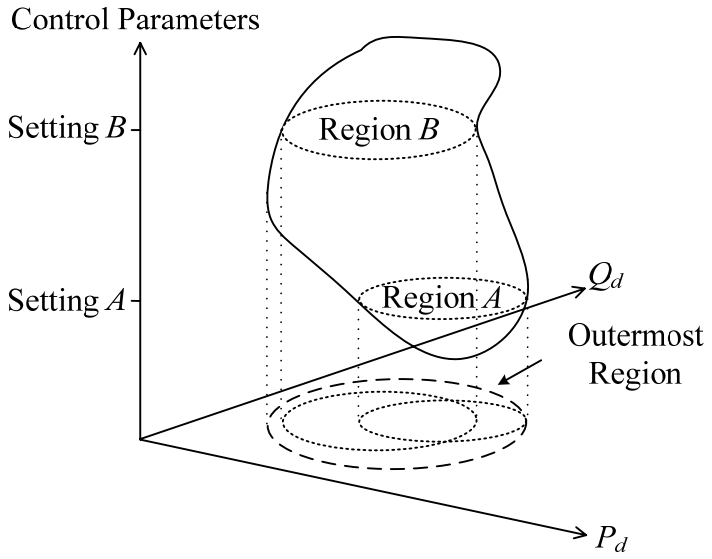


Figure 7.4 Illustration of solution space by using three-dimensional space

### 7.3.1 Outermost Boundary by Generator Voltages

According to the conventional power flow, the load margin determination, or even the proposed feasible region determination, the generator voltages are fixed before solving the solution. The change of generator voltage settings can affect the power flow solution, the load margin, and the shape of feasible region. The inappropriate voltage setting might cause the violation of bus voltages. The voltage settings can lead the shape of feasible region to be different. The outermost boundary affected by generator voltages can be determined by using the proposed tracing algorithm, but the minimization problem for the correction step has to be modified. The minimization problem needs to treat generator voltages as free variables and the inequality constraints of generator voltages must be added into the problem.

Let $\boldsymbol{V}_g$ be a vector of generator voltages which are adjustable for the considered scenario,

$$\boldsymbol{V}_g = [V_{g1} \ \ldots \ V_{gc}]^T \tag{7.1}$$

Where *c* is a number of considered generators. In this case, the considered generators are the generators needed to study the effects of voltage settings, these generator could be the source area generators. These generator voltages are the additional unknown variables for the minimization problem, the free variables can be summarized as the following:

- For the power transfer from source bus *j* to sink bus *i*, a vector of free variables is

$$\boldsymbol{X} = [\boldsymbol{\delta}_{pv} \ \boldsymbol{\delta}_{pq} \ \boldsymbol{V}_{pq} \ P_{gj} \ \boldsymbol{Q}_G \ P_{di} \ Q_{di} \ \boldsymbol{V}_g]^T \tag{7.2}$$

- For the power transfer between source-sink areas, a vector of free variables is

$$\boldsymbol{X} = [\boldsymbol{\delta}_{pv} \ \boldsymbol{\delta}_{pq} \ \boldsymbol{V}_{pq} \ \boldsymbol{P}_g \ \boldsymbol{Q}_G \ \boldsymbol{P}_d \ \boldsymbol{Q}_d \ \boldsymbol{V}_g]^T \tag{7.3}$$

The boundary point can be determined by the minimization problems (5.16)-(5.22), (5.28)-(5.30) with the additional inequality constraint of the generator voltages as the following,

$$\boldsymbol{V}_g^{\min} \le \boldsymbol{V}_g \le \boldsymbol{V}_g^{\max} \tag{7.4}$$

### 7.3.2 Outermost Boundary by FACTS Devices

The FACTS devices considered in this research are SVC and TCSC. For the outermost boundary affected by FACTS, some parameters from FACTS must be treated as free variables. In order to define free variables, the characteristic of each device should be taken into account.

For SVC, this device can regulate a nodal voltage at the installed bus by supplying reactive power. SVC behaves like a reactive power generator. But it can not supply the real power to the system. In the power flow analysis, the SVC-installed bus is set to be a generator bus (PV bus). As same as the generator voltage, a change of SVC voltage setting produces a different feasible region. If SVC voltages are set to be free, a result obtained by the boundary tracing method will be an outermost boundary affected

by SVC. Let $\boldsymbol{V}_{SVC}$ be a vector of nodal voltages at the SVC-installed buses. A vector of free variables for outermost boundary affected by SVC is

$$\boldsymbol{X} = [\boldsymbol{\delta}_{pv}\ \boldsymbol{\delta}_{pq}\ \boldsymbol{V}_{pq}\ \boldsymbol{P}_{g}\ \boldsymbol{Q}_{G}\ \boldsymbol{P}_{d}\ \boldsymbol{Q}_{d}\ \boldsymbol{V}_{SVC}]^{T} \tag{7.4}$$

In this case, the additional inequality constraint for the optimization is

$$\boldsymbol{V}_{SVC}^{\min} \le \boldsymbol{V}_{SVC} \le \boldsymbol{V}_{SVC}^{\max} \tag{7.5}$$

For TCSC, a setting point of TCSC affects the configuration of transmission system. TCSC acts like an adjustable reactance device installed on a transmission line. In the power flow analysis, TCSC will change the configuration of admittance matrix or $Y_{bus}$. A different configuration leads to a different power flow solution. Thus, TCSC also changed the shape of feasible region. With the concept of outermost boundary in this research, the outermost boundary by TCSC parameters can be determined by assigning the free variables as the following,

$$\boldsymbol{X} = [\boldsymbol{\delta}_{pv}\ \boldsymbol{\delta}_{pq}\ \boldsymbol{V}_{pq}\ \boldsymbol{P}_{g}\ \boldsymbol{Q}_{G}\ \boldsymbol{P}_{d}\ \boldsymbol{Q}_{d}\ \boldsymbol{X}_{TCSC}]^{T} \tag{7.6}$$

And, the additional inequality constraint for the optimization is

$$\boldsymbol{X}_{TCSC}^{min} \le \boldsymbol{X}_{TCSC} \le \boldsymbol{X}_{TCSC}^{max} \tag{7.7}$$

The outermost boundary affected by FACTS can be visualized by the proposed tracing algorithm with the optimization problem (5.16)-(5.22), (5.28)-(5.30) and additional constraints (7.5) and (7.7) for cases of SVC and TCSC, respectively.

### 7.3.3 First Prediction Point and Initial Guess

For the tracing process of feasible region, the repeated power flow can determine the maximum loading point which is the boundary point of feasible region. The loading point moved from the maximum loading point can be treated as the first prediction point for the boundary tracing process. However, this loading point is possible to be inside the

outermost boundary affected by additional free parameters. Thus, the process to obtain the first prediction point needs to be modified as shown in the following figure,

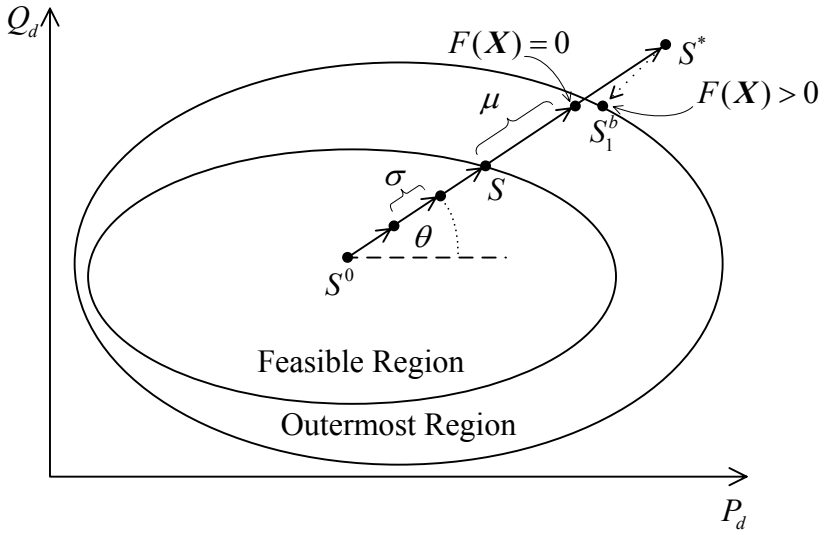


Figure 7.5 First prediction point determination for outermost boundary tracing process

The way to determine the first prediction point $S^*$ for the outermost boundary problem can be summarized as the following steps:

1.) From the loading point $S^0$, determine the boundary point of feasible region $S$ by using the repeated power flow.

2.) Treat the solution $\boldsymbol{X}$ at the loading point $S$ as the initial guess for the minimization problem.

3.) Move the loading point in the same direction with the step $\mu$ in order to obtain the prediction point $S^*$.

4.) Solve the minimal distance $F(\boldsymbol{X})$ from the prediction point $S^*$ subjected to the operational constraints of the outermost boundary problem.

5.) If the obtained solution $\boldsymbol{X}$ gives $F(\boldsymbol{X})=0$, then keep the solution $\boldsymbol{X}$ to be the initial guess for the next round and move the loading point $S^*$ with $\mu$. Return to step 4.

6.) Repeat moving $S^*$ by the step $\mu$ until the obtained solution gives $F(\boldsymbol{X})>0$. The obtained solution is the first solution on the boundary of the outermost region.

After obtaining the first boundary point, the outermost boundary can be determined by using the predictor-corrector process in Chapter 6. The obtained boundary points contain the solution of generator voltages which can be utilized as the guideline of voltage control scheme

## 7.4 Conclusion

This chapter shows the concept of outermost boundary affected by control parameters. A method to determine the outermost boundary is proposed in this chapter based on the free parameter manipulation. The proposed boundary tracing method can be also used for determining this outermost boundary. However, the shape of feasible region can be changed by other factors in the system, e.g. the contingency, and the reactive power enforcement that will be shown in next chapters.

# CHAPTER VIII

# TOTAL TRANSFER CAPABILITY REGION

In the modern deregulated environment, transactions in the power market concentrate on the transfer capability from the source area to the sink area. According to the definition of the available transfer capability (ATC) by the North American Electric Reliability Council (NERC) [3], ATC is an amount of capability able to transfer between areas determined by the total transfer capability less the summation of the appropriate margins. The ATC has the key component called the total transfer capability (TTC). The method to determine the TTC is based on the load margin determination. The TTC calculation applies these methods to obtain the load margin in many contingency cases and declare the smallest one as TTC [6]. This chapter applies the concept of TTC to the feasible region and then develops the method to determine a new security region called total transfer capability region or TTCR.

## 8.1 Total Transfer Capability

TTC is the available power transfer between source-sink pair. The TTC calculation is to determine the maximum loading point for each contingency (including the base case) and then select the smallest one as TTC [5]-[7], that is,

$$TTC = \min(MLP_1, \ ..., \ MLP_k) \tag{8.1}$$

Where $MLP_i$ is maximum loading point of case *i*. *MLP* can be determined by the conventional load margin calculation.

## 8.2 Relationship of TTC and Feasible Regions

According to security regions, a maximum loading point from load margin determination is on the boundary of feasible region. TTC is similar to the load margin, but the contingencies are taken into account in the determination process. The contingency such as transmission line outage leads to the changes of system parameters and the transfer capability. In terms of feasible region, the feasible region would be

reshaped or moved when system parameters change, that is, one case of contingency has an individual contour of feasible region. As shown in Figure 8.1, the conventional TTC determination is to find the nearest MLP on the considered direction. In this case, $MLP_B$ is declare as TTC because this point is the nearest from the loading point. TTC can be selected from another case depends on the load direction. An intersection of feasible regions from different cases corresponds to TTC. This intersection region is a novel region. In this research, this region is called the total transfer capability region (TTCR).

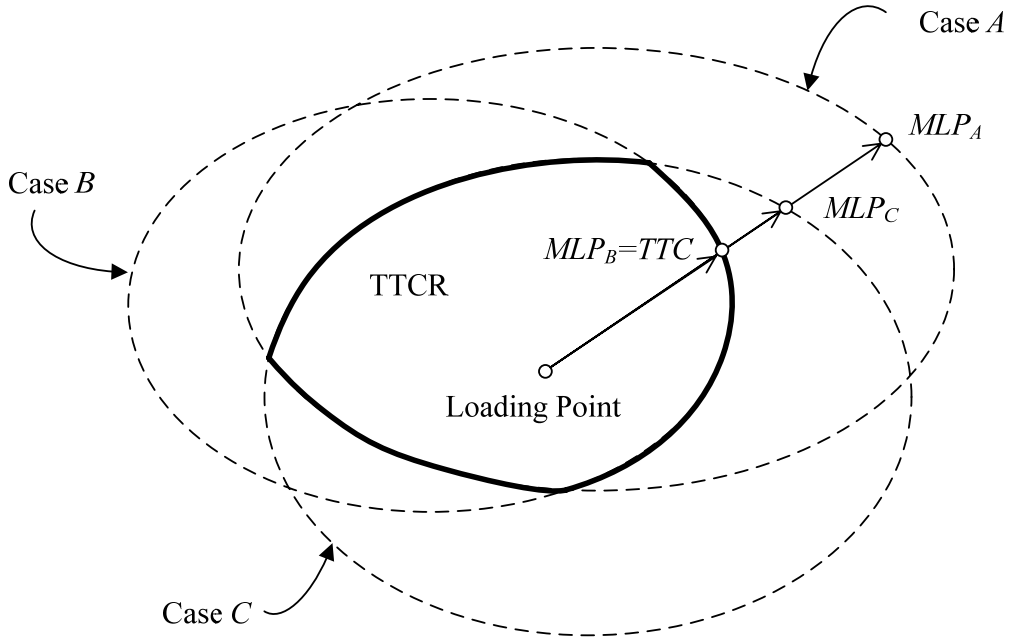


Figure 8.1 Relationship of TTC and feasible regions

TTCR is a security region bounded by system parameter limits and contingencies. The size of TTCR can be equal or less than the size of base case feasible region. Because TTCR is an intersection of feasible regions from several cases of contingency, TTCR is a subset of feasible region as shown in Figure 8.2. The TTCR ensures that the power flow solution is obtainable, feasible, and survivable for the contingencies.

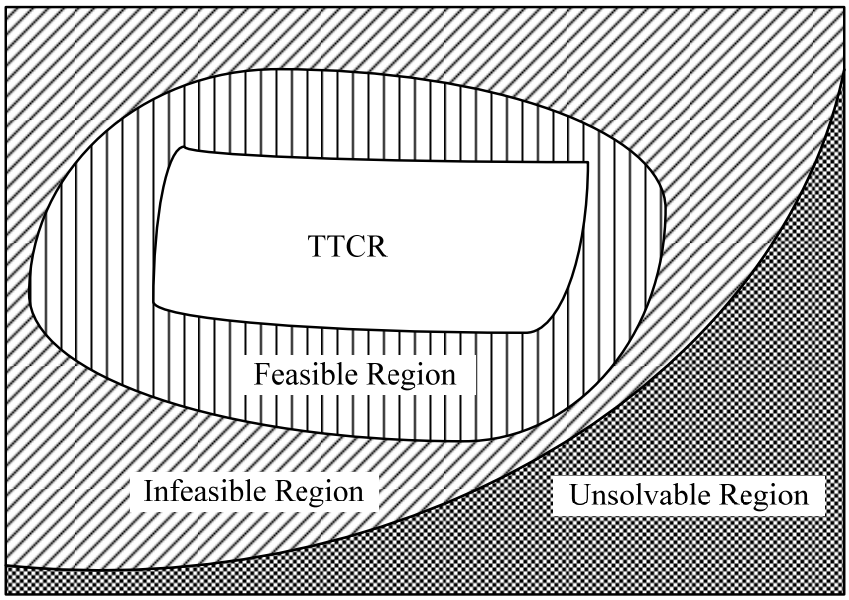


Figure 8.2 TTCR and conventional security regions

## 8.3 Boundary Point of TTCR

As well as TTC determination, a boundary point of TTCR is selected from candidates which are boundary points from a base case and contingencies. Figure 8.3 compares calculation processes of the TTC calculation and the boundary point determination in the boundary tracing method. The determination process of the conventional TTC calculation is to find the nearest point from an existing loading point $S^0$. The TTC candidates come from boundary points of feasible regions in many cases. In this figure, a boundary point from contingency 2 is the nearest from $S^0$, it is declared as TTC at the point $TTC_B$. For the boundary tracing method, each boundary point is calculated by the prediction point $S^*$ which is in the outside of feasible region. Therefore, the farthest boundary point, among contingency cases, is declared as TTC. In this figure, the point $TTC_A$ is selected to be a boundary point of TTCR. The TTCR boundary point is determined by this concept in this research.

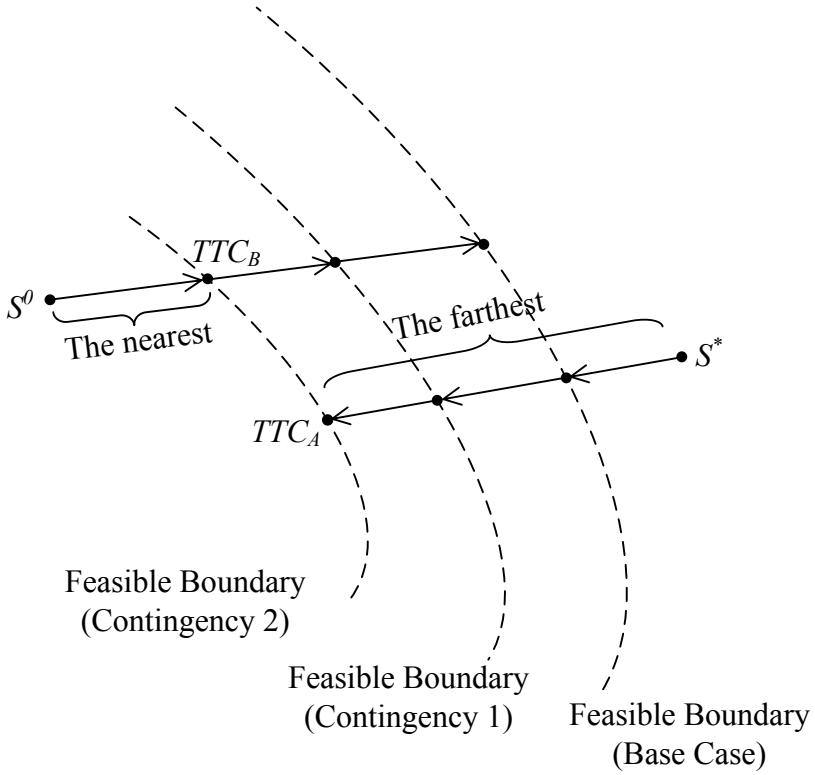


Figure 8.3 Calculation processes of conventional TTC calculation and boundary point determination by boundary tracing method

.

**8.4 Modified Boundary Tracing Process for TTCR**

For determining the boundary point of TTCR, the minimization of TTCR problem is still as same as the formulation in Chapter 5. However, for TTCR problem, the algorithm to select the TTCR boundary point must be developed. The distance from $S^*$ to a boundary point of feasible region can be checked by the objective function (5.16) because this function directly varies by a distance from $S^*$ to the boundary of feasible region. The process to determine a boundary point of TTCR can be described by the following steps:

1.) From a prediction point $S^*$, determine a boundary point of feasible region corresponding to the base case by the optimization problem (5.16)-(5.22) and (5.28)-(5.30). The outputs of this process are a solution ($\boldsymbol{X}$) and a loading point on boundary ($S$).

2.) By the same $S^*$, determine a boundary point of feasible region corresponding to contingency case by the same optimization problem.

3.) Compare results using the obtained objective value $F(\boldsymbol{X})$. The boundary point corresponding to the case which has the largest value of $F(\boldsymbol{X})$ is declared as the boundary point of TTCR.

4.) Come back to step 2 and continue the process until all considered contingency cases have be done. The end of process gives the boundary point of TTCR.

An example of above process is illustrated in the figure below. The requirement of prediction point $S^*$ is that $S^*$ must be in the outside of TTCR. In this figure, the prediction point $S_A^*$ is in the outside of TTCR. The farthest distance of boundary points belongs to the boundary point from contingency 2 ($S_{A2}$). However, the point $S^*$ is not necessary to be in the outside of feasible regions for all cases. As shown in this figure, the prediction point $S_B^*$ is inside the feasible regions of the base case and contingency 1, but this point is outside the feasible region of contingency 2. For the solution using this prediction point, the objective function is zero for the base case and contingency 1 ($F(\boldsymbol{X}_{B0}) = F(\boldsymbol{X}_{B1}) = 0$). But, the objective function is a positive number for contingency 2. The solution from contingency 2 is selected to be a boundary point of TTCR. The conclusion is that the prediction point must be unfeasible for one case at least. If the loading point $S$ is feasible for all cases, it implies that this point is inside TTCR.

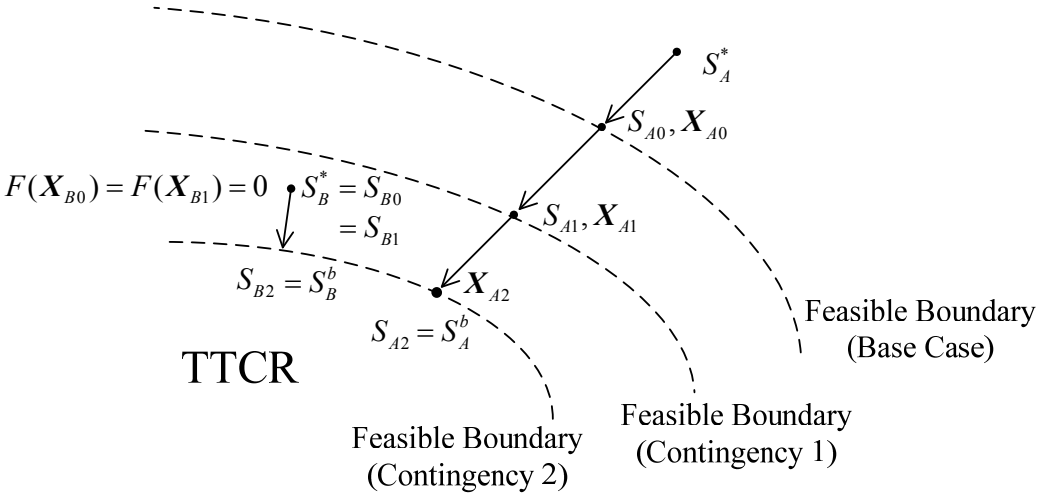


Figure 8.4 Determination of TTCR boundary point

In the beginning of tracing algorithm, the process needs to determine a prediction point and an initial guess. For TTCR, the first initial guess can be determined using the conventional TTC methods, i.e. RPF, CPF, and OPF. The obtained solution is a boundary point of TTCR which can be treated as the first initial guess of the boundary tracing process. The first prediction point is determined by increasing load from this point with the same load increment direction. The contour of TTCR can be determined by using the proposed tracing algorithm in section 6.2.3 with replacing step 3 by the process in this section.

## 8.5 Conclusion

The concept of TTC can be applied to the boundary tracing method, and another kind of security region is proposed in this chapter. The TTC region (TTCR) is defined. In terms of security regions, TTCR is an intersection set of feasible regions corresponding to contingencies. TTCR is able to determine by the modified tracing algorithm in order to select the innermost boundary point.

# CHAPTER IX

# EFFECT OF RACTIVE POWER LIMIT

In the load margin determination, when the system reaches the generator reactive power limit, the generator will lose the ability to maintain voltage levels. However, the load can continue increasing with a deviation of generator voltage. In term of feasible region, some parts of region limited by reactive powers can be expanded with the same way. Thus, this chapter focuses on the generator reactive power limit and modifies the boundary tracing algorithm in order to determine the feasible region with the effect of reactive power limit.

## 9.1 Reactive Power Limits in Power Flow Equations

In power flow studies, the system of power flow equations consists of real and reactive power mismatch functions. The power flow calculation is to determine a solution point that satisfies all nonlinear equations of the problem. In the system, one function belongs to one bus. If the power system has $n$ buses, there are $n$ nonlinear equations. However, the number of nonlinear equations is reduced in order to keep the number of unknowns equaling to the number of equations. The known variables of power flow problem are real powers at load buses ($\boldsymbol{P}_d$), reactive powers at load buses ($\boldsymbol{Q}_d$), and real powers at generator buses ($\boldsymbol{P}_g$). The problem needs to determine the unknowns, i.e. load bus voltage magnitudes ($\boldsymbol{V}$), bus voltage angles ($\boldsymbol{\delta}$) that satisfy all equations. The generator reactive powers ($\boldsymbol{Q}_g$) are not specified. Therefore, the power mismatch equations of generator buses are ignored. However, the generator reactive powers are calculated after receiving the solution. For the obtained power flow solution, it is possible that there are some violations of generator reactive power.

When the generator reactive power limit is out of range, the corresponding generator bus (PV) is converted to a load bus (PQ), as shown in Figure 9.1. The reactive power $Q_g$ is fixed and the bus voltage magnitude ($V_g$) is free. The real power $P_g$ and voltage angle $\delta$ are still free variables. By this new configuration, the power flow solution is repeatedly obtained. If any reactive power limit is violated again, new solution can be determined by the same way.

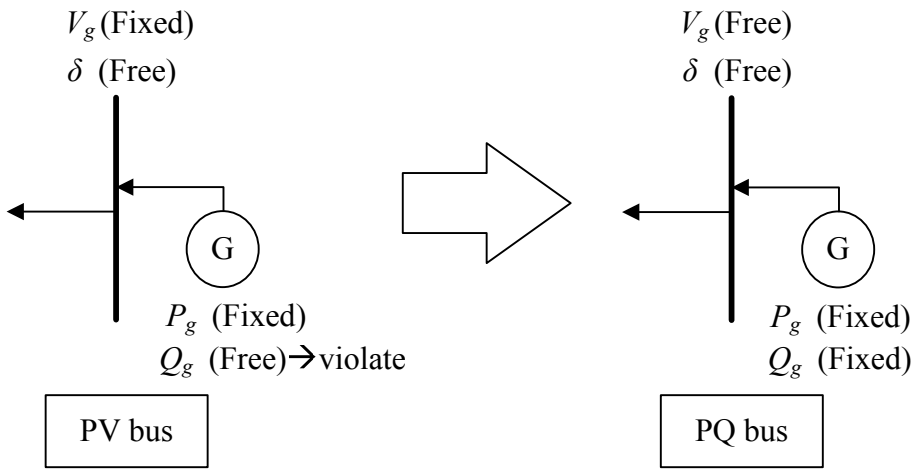


Figure 9.1 Conversion of bus type when generator reactive power is violated

## 9.2 Reactive Power Limits in Load Margin Determination

The determination of load margin is based on calculating the power flow solution. In RPF and CPF methods, power flow solutions are repeatedly determined under the load increment scenario. If the reactive power limit $Q_g$ is not taken into account, the load increment is stopped when the solution reaches some reactive power limits. As illustrated in Figure 9.2, the load parameter $\lambda$ represents an incremental load. The generator voltage $V_g^0$ is held as long as $Q_g$ is within its limit. The maximum load is limited by $\lambda_A$ due to the $Q_g$ limit. At this point, the corresponding generator has not enough capacity to supply the reactive power. However, with fixing the generator reactive power at its limit, the load can be increased with a deviation of voltage from $V_g^0$, until reaching another parameter limit such as a voltage limit $V_g^{\min}$ in this figure. The load margin can be extended by this approach.

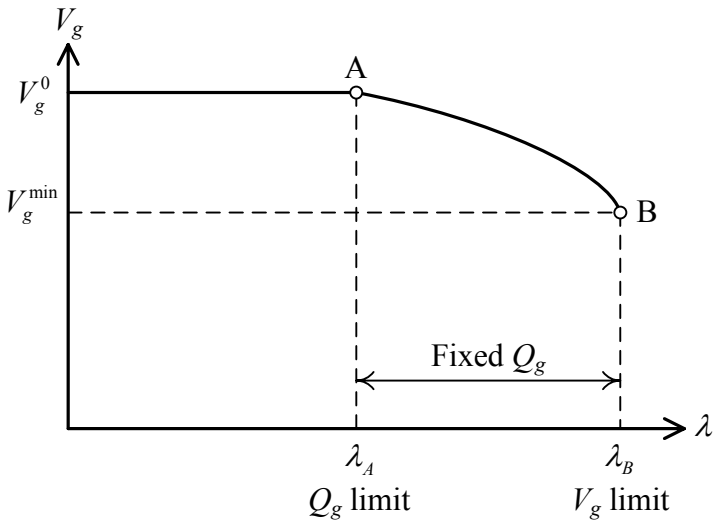


Figure 9.2 Load increment characteristic with generator reactive power enforcement

### 9.3 Influence of Generator Reactive Power Limits to Feasible Region

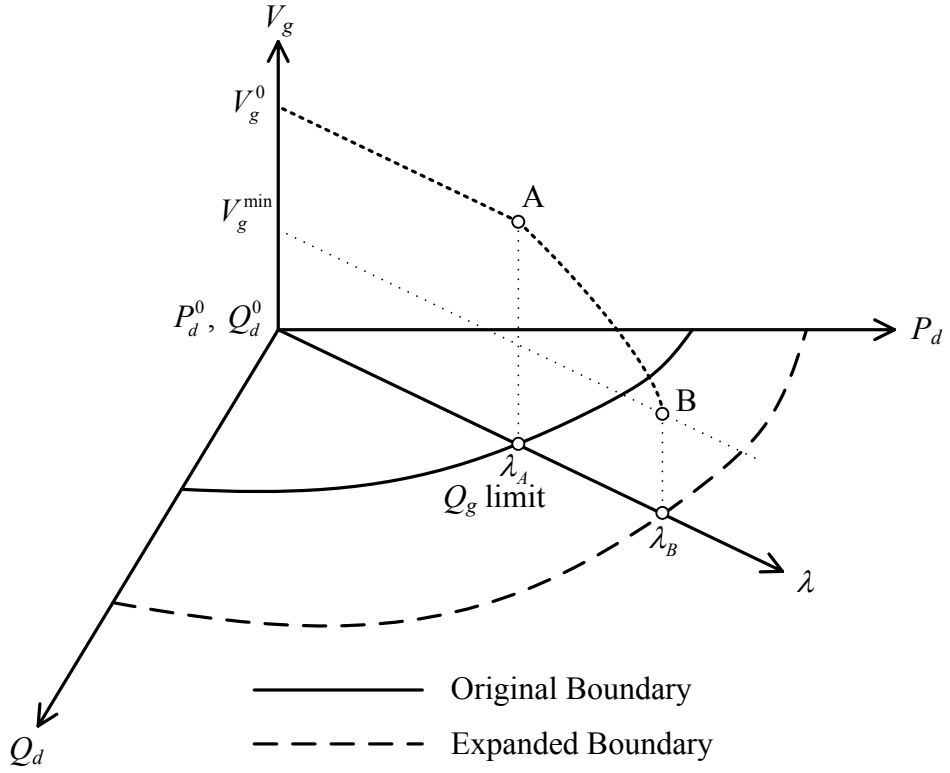


Figure 9.3 Expansion of feasible region by reactive power enforcement

After the load increment touches a reactive power limit, the reactive power enforcement allows the load to increase with a deviation of nodal voltage. In the security

region viewpoint, a solution limited by reactive powers is on a boundary of feasible region. However, if the enforcement of reactive powers is considered, the load margin can be expanded to another boundary point. Figure 9.3 shows the expansion of feasible region compared with the characteristic curve of generator voltage. The load is limited by a generator reactive power at point $\lambda_A$ that is a boundary point on the original feasible region. When the reactive power is enforced, the load can be increased to $\lambda_B$, this point is on the expanded region. In the operation, the loading point between an original region and an expanded region is still feasible. Thus, in this research, the boundary tracing method should be able to determine boundary points of this expanded region.

## 9.4 Feasible Region with Reactive Power Enforcement

The formulation of proposed boundary tracing method is based on solving the power flow equations on the edge of feasible region. Therefore, we can check reactive power limits from a solution point on the boundary. As same as the power flow calculation, if any generators reach their reactive power limits, we can determine another boundary point by manipulating variables on the corresponding bus. The reactive power limit bus is converted to a load bus. The nodal voltage magnitude is set to be free, and the reactive power is set to be fixed. In the correction step (step 3 in Section 6.2.3), the boundary tracing algorithm is modified by the following steps:

1.) From the prediction point $S^*$, determine a boundary point by using the minimization problem in Chapter 5.

2.) Check the solutions $\boldsymbol{X}$, if there is a reactive power limit at bus $i$ ($\boldsymbol{Q}_{gi} = \boldsymbol{Q}_{gi}^{\max}$ or $\boldsymbol{Q}_{gi} = \boldsymbol{Q}_{gi}^{\min}$), fix the reactive power $Q_{gi}$ at its limit, free the generator bus voltage $V_{gi}$, and then come back to step 1. In this case, $\boldsymbol{X}$ is converted from (5.15) to $\boldsymbol{X}'$, as in the following,

$$\boldsymbol{X}' = [\boldsymbol{\delta}_{pv}' \ \boldsymbol{\delta}_{pq}' \ \boldsymbol{V}_{pq}' \ \boldsymbol{P}_g \ \boldsymbol{Q}_G' \ \boldsymbol{P}_d \ \boldsymbol{Q}_d]^T \tag{9.1}$$

Where

$\boldsymbol{V}'_{pq} = [\boldsymbol{V}_{pq}\ V_{gi}]^T$ is a converted vector of bus voltages.

$\boldsymbol{Q}'_{\boldsymbol{G}}$ is a vector of generator reactive power which is deleted $\boldsymbol{Q}_{gi}$ from a member.

A voltage angle $\delta_i$ is moved from $\boldsymbol{\delta}_{pv}$ to $\boldsymbol{\delta}_{pq}$. These vectors are converted to $\boldsymbol{\delta}'_{pv}$ and $\boldsymbol{\delta}'_{pq}$, respectively.

3.) If there is no reactive power limit bus, the last solution of $\boldsymbol{X}'$ is the boundary solution of feasible region influenced by reactive power limits. And the loading point $S^{b'}$ is a boundary point of the expanded feasible region.

4.) Set a vector of free variables back to an original vector, and continue tracing a new boundary. The process of determining a new boundary point is illustrated in the figure below.

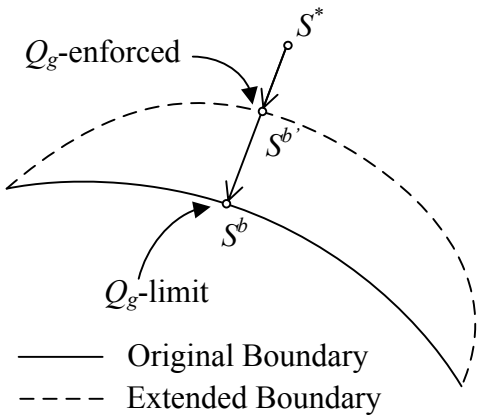


Figure 9.4 Modified process to determine an extend boundary point

## 9.5 Conclusion

The reactive power enforcement in the power flow calculation leads to an expansion of load margin. As same as the feasible region, the region can be expanded when the reactive power is taken to account. The boundary tracing method is modified in order to handle this problem. The expansion of boundary point can be determined u variable conversion on the reactive power limit bus.

# CHAPTER X

# NUMERICAL RESULTS: BOUNDARY TRACING METHOD

In this chapter, the proposed boundary tracing method is illustrated with test systems. This chapter uses the two-bus test system and the six-bus test system. The feasible region of several transfer scenarios are determined by using the proposed boundary tracing method in order to monitor the load margin in terms of feasible region.

## 10.1 Power Transfer from Source Bus to Sink Bus

The proposed boundary tracing method is illustrated in this section by the two-bus system and the six-bus system. The illustration compares the feasible region to the solvable region, and then checks the obtained boundary curve by determining the maximum loading point in several directions.

### 10.1.1 Bus-to-Bus Transfer with Two-Bus System

The numerical example in [13] illustrates the boundary of solvable region by using the continuation method on the two-bus test system. The system consists of the generator bus and the load bus as shown in the figure below. In this case, $V_1 = X = 1.0$ pu.

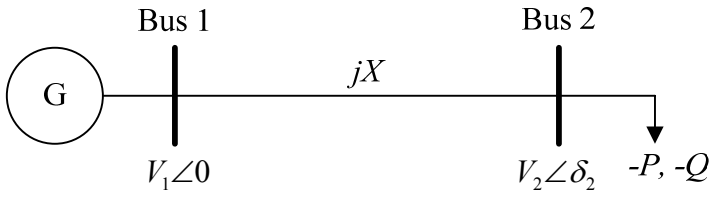


Figure 10.1 Two-bus system

In the simulation, it would be noted that the load is represented by a negative value and the generation is represented by a positive value. In order to determine the boundary of feasible region, the simulation in this section assigns the devices limits into the system. The criterion of bus voltage is 0.95-1.05 pu. The criteria of generator capacity are 0-2 MW and $\pm 2$ MVAr. The load injection is forced not to be positive because the load bus

can not generate a real power. By the power flow, we found that the load injection $-0.2 + j0.0$ MVA at bus 2 is a feasible point. This point is selected to be an existing loading point for the simulation.

From an existing loading point, the simulation finds the first initial point and the first prediction point by using the repeated power flow. The repeated power flow increases the load with a step $\sigma$ = 0.1 MW on a direction of fixed power factor. The first initial point is the solution on the boundary at the loading point equals to -0.296+*j*0.0 MVA. The first prediction point is determined by changing the loading point by -0.2+*j*0.0 MVA. Then, the first prediction point is $-0.496 + j0.0$ MVA.

The boundary is traced by using the proposed tracing algorithm. The test defines a step size *l* and a gap *d* equal to 0.05 pu. The region contour is plotted on a plane of apparent power injections. The x-axis and y-axis are real and reactive power injections of bus 2, respectively. The tracing result is shown in the figure below.

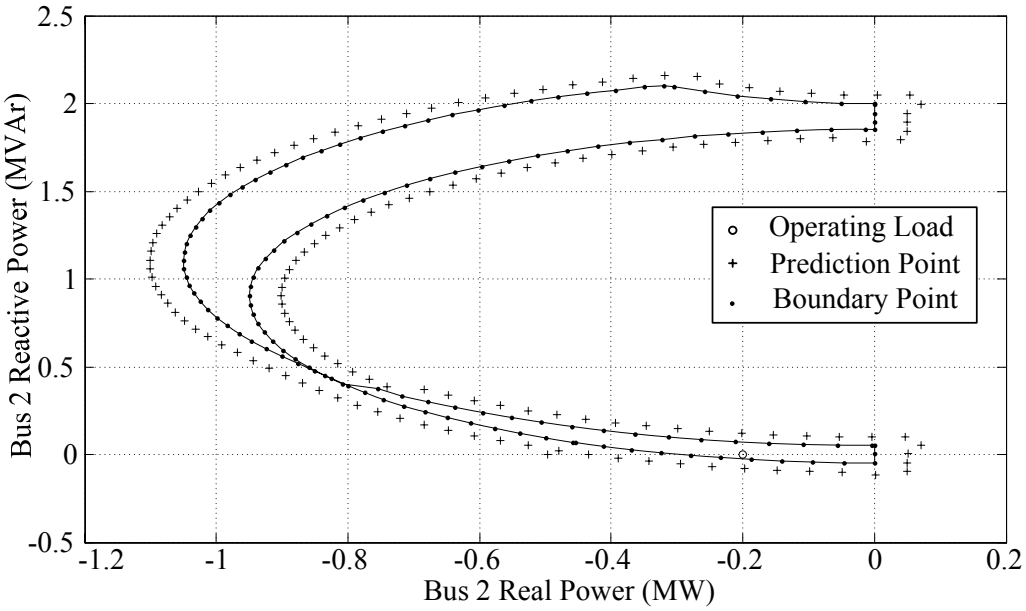


Figure 10.2 Illustration of boundary tracing process

It can be observed that an existing loading point is inside the region. In order to compare a result with maximum loading points, the load injection $-0.8 + j1.5$ MVA is selected to be another base case. From two existing loading points, the maximum loading points are determined by the repeated power flow method. The simulation changes the

load in several directions around the existing operating point, and then compares the result to the obtained boundary, as shown in the figures below.

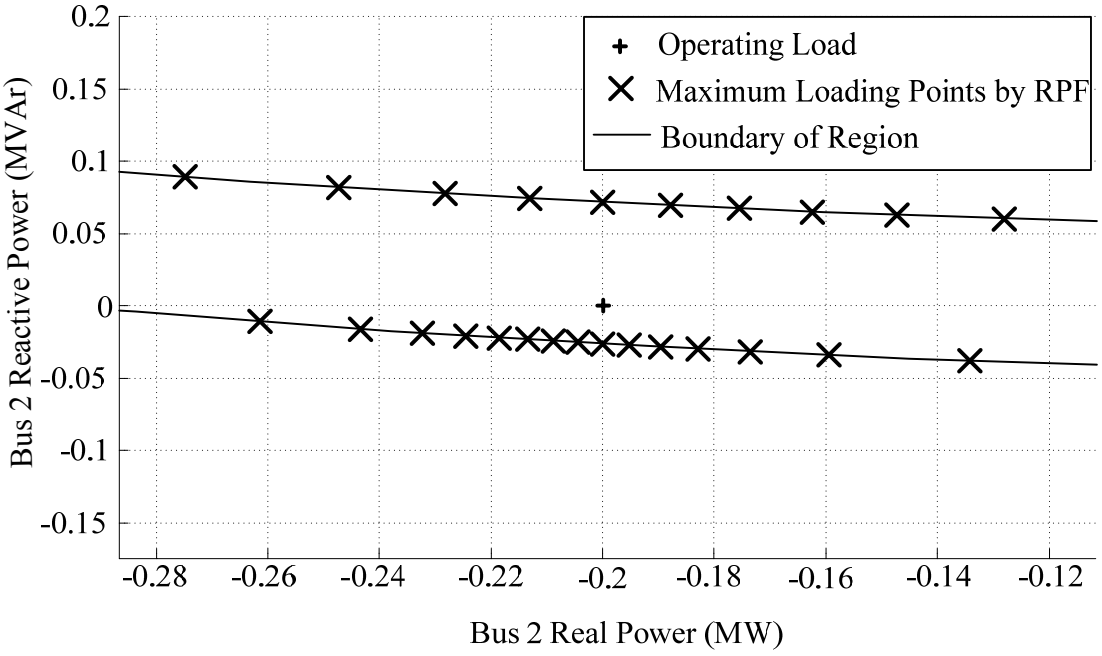


Figure 10.3 Maximum loading points from the base case of -0.2+*j*0.0 MVA

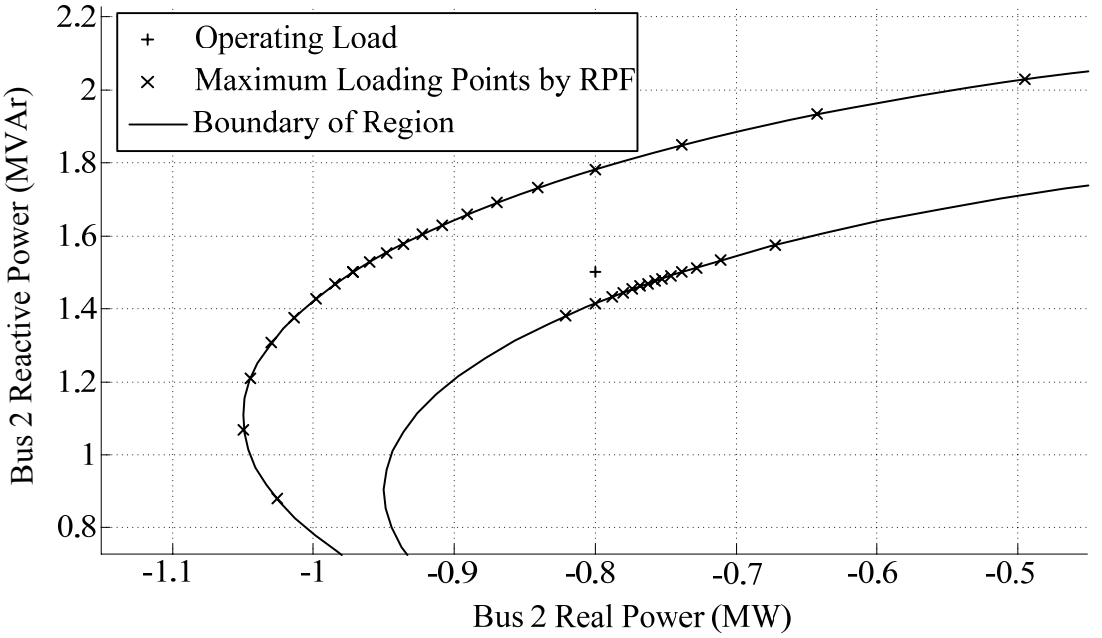


Figure10.4 Maximum loading points from the base case of -0.8+*j*1.5 MVA

The results show that the obtained maximum loading points lie on a region boundary. A region obtained from the proposed tracing algorithm has a boundary which is a curve of the maximum loading point from several load directions. This region is bounded by device limits considered in the problem. These limits are the practical constraints for the power system operation. The figure below compares the obtained region to the solvable region. This solvable region has been determined in [13]. A curve of solvable region is determined by using the proposed tracing algorithm, but the minimization problem is formulated without device limits. It can be observed that the region bounded by the device limits is smaller than the solvable region. This region is called the feasible region in many literatures [8]-[12]. However, the test system in this section is a very simple system. The proposed tracing algorithm needs to be tested on the larger system in order to study the effects of system parameters to the feasible region.

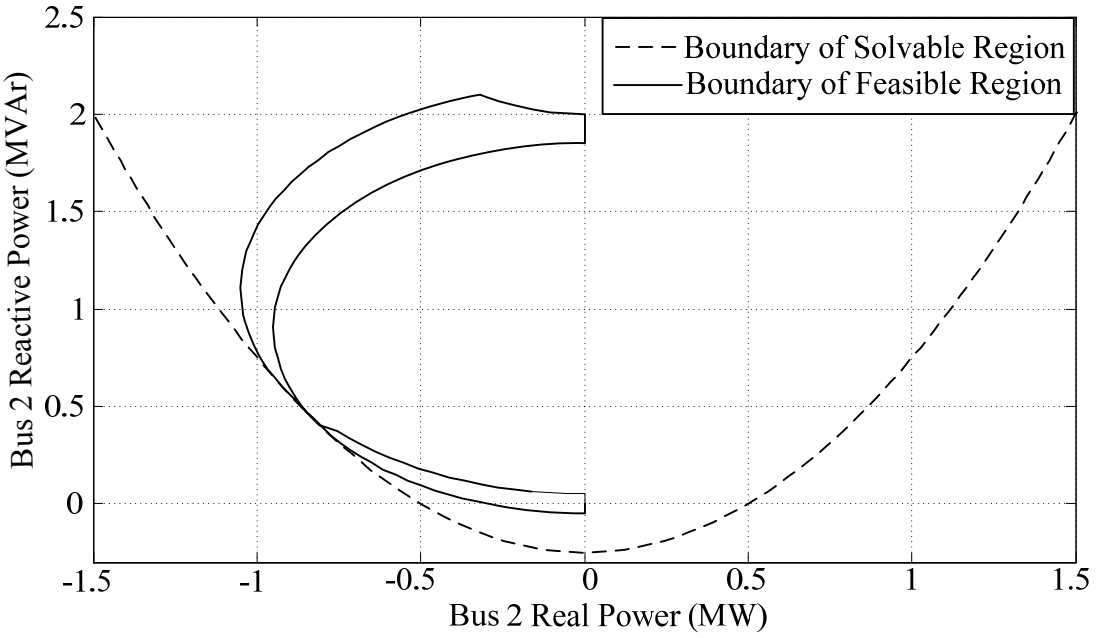


Figure 10.5 Feasible region and solvable region of two-bus system

### 10.1.2 Bus-to-Bus Transfer with Six-Bus System

This section implements the boundary tracing method using six-bus system [25]. The information of the system is in Appendix. The first test scenario is the power transfer from bus 1 to bus 4. The real and reactive powers at bus 4 are the observed variables.

From the base case, the loading point is -70-*j*70 MVA. By the repeated power flow with the steps $\sigma=\mu=1$ MVA, the first prediction point is $-74.6 - j74.6$ MVA, and the first initial guess is the solution at -73.9-j73.9 MVA. The tracing process uses a gap $d$= 0.1 MVA and a step size $l$=1 MVA. A result of tracing process is illustrated in a figure below. The obtained region is compared to 36 maximum loading points.

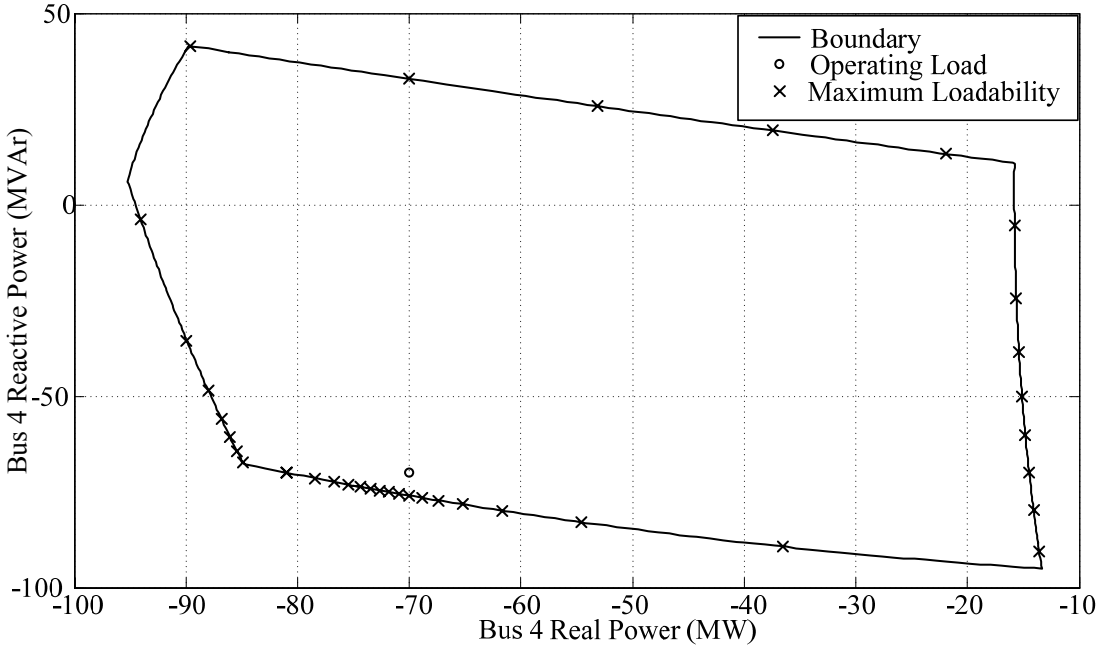


Figure 10.6 Maximum loading points and feasible region of bus-to-bus transfer (Source: Bus 1 / Sink: Bus 4)

This result shows that the maximum loading points calculated by the repeated power flow are located on the obtained feasible boundary. By using the proposed method, the feasible region of several scenarios can be determined. When bus 4 is the sink bus, the feasible regions of receiving the power from each source bus are shown in the figure below.

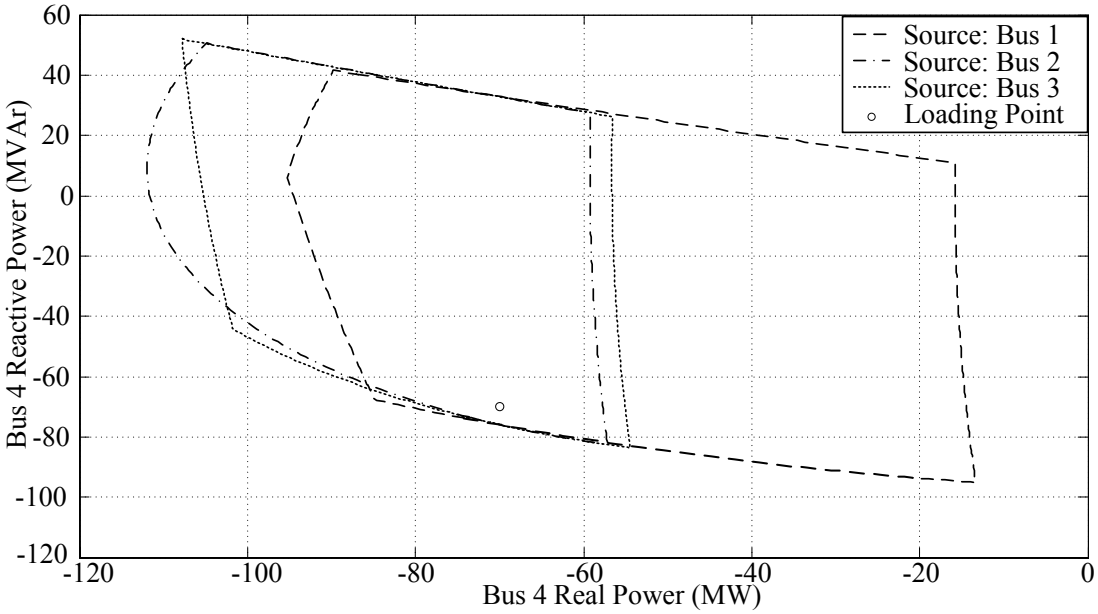


Figure 10.7 Feasible region of bus 4 (6-bus system)

When bus 5 is the sink bus, the feasible regions are determined and illustrated in the figure below.

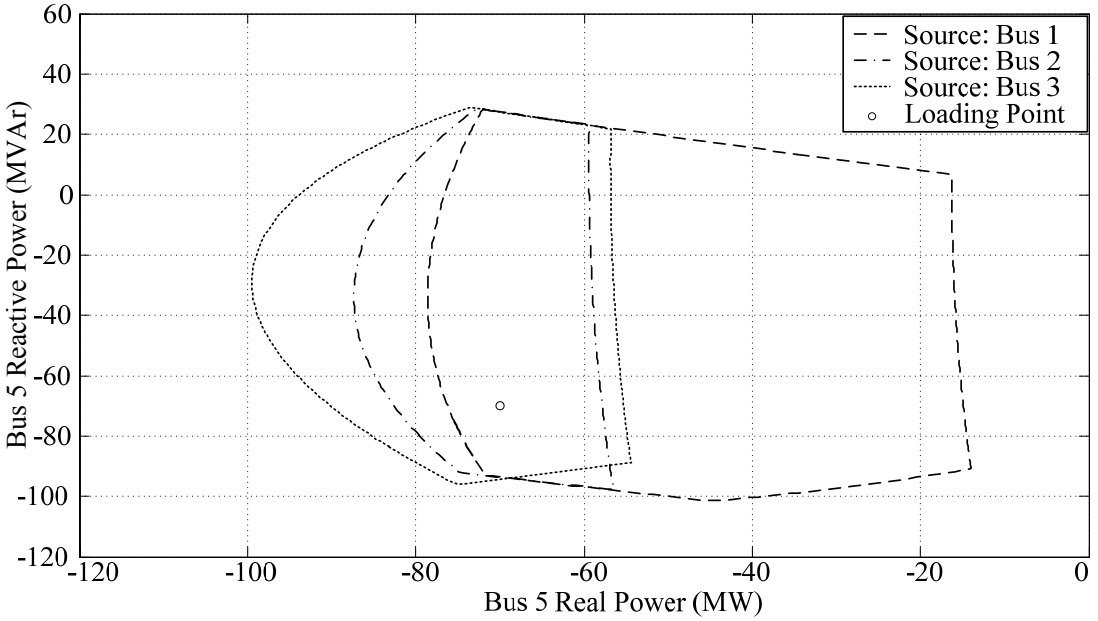


Figure 10.8 Feasible region of bus 5 (6-bus system)

When bus 6 is the sink bus, the feasible regions are determined and illustrated in the figure below.

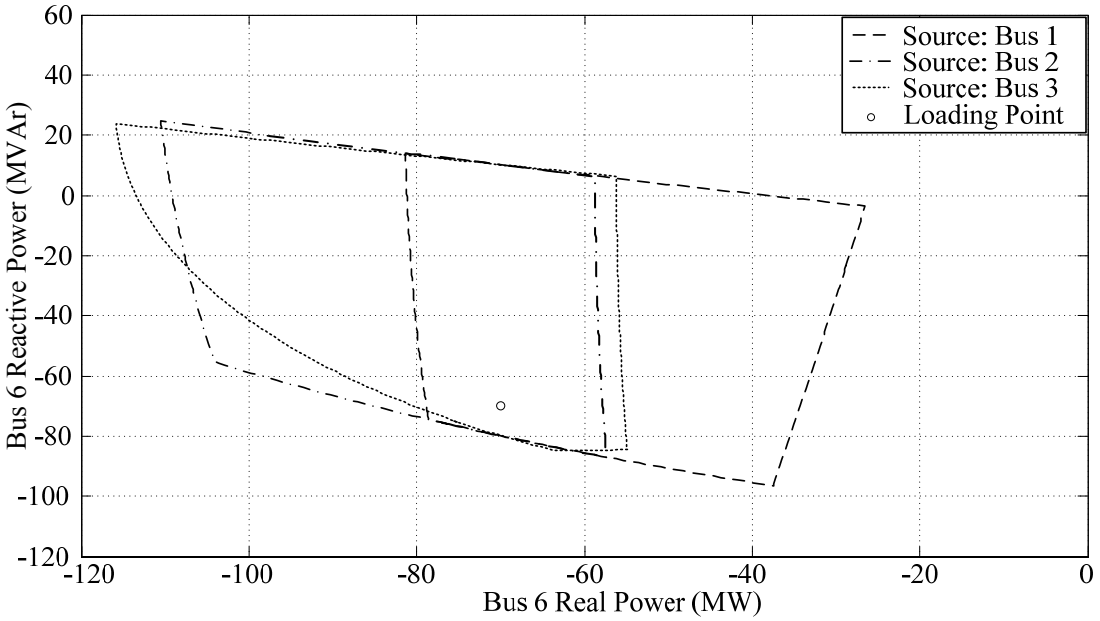


Figure 10.9 Feasible region of bus 6 (6-bus system)

The computational times and areas of the obtained feasible regions are in the table below.

Table 10.1 Information of feasible regions for bus-to-bus transfer (6-bus system)

| Case | Source Bus | Sink Bus | Maximum Load (MW) | Area (MW x MVAr) | Time (sec) | Points | Time/ Point (sec) |
|---|---|---|---|---|---|---|---|
| 1 | 1 | 4 | 95.20 | **8,238** | 43.67 | 378 | 0.116 |
| 2 | 2 | 4 | **111.95** | 5,112 | 37.43 | 320 | 0.117 |
| 3 | 3 | 4 | 107.78 | 5,124 | 39.05 | 330 | 0.118 |
| 4 | 1 | 5 | 78.60 | **6,983** | 39.83 | 344 | 0.116 |
| 5 | 2 | 5 | 87.37 | 2,932 | 32.16 | 282 | 0.114 |
| 6 | 3 | 5 | **99.50** | 4,274 | 33.59 | 292 | 0.115 |
| 7 | 1 | 6 | 81.35 | **4,490** | 32.17 | 290 | 0.111 |
| 8 | 2 | 6 | 110.50 | 4,242 | 33.07 | 290 | 0.114 |
| 9 | 3 | 6 | **115.86** | 4,289 | 33.71 | 291 | 0.116 |

The results show that the feasible regions is different depending on a given source-sink bus. The differences are in terms of the shape and the size of the region. For each sink bus, the maximum loads belong to cases 2, 5, and 9. And the maximum closed areas belong to cases 1, 4, and 7. The area shows the feasibility of each transfer case. The calculation time depends on a number of solution points. The average time is 0.11 second/point, approximately. The proposed method can properly determine the feasible

regions of the power transfer between two buses. The obtained boundary corresponds to the maximum loading points obtained by the repeated power flow.

### 10.2 Area-to-Area Transfer with Six-Bus System

This section considers the power transfer between areas.The test is illustrated on the six-bus test system. In the first transfer scenario, a given source area consists of bus 1 and bus 2, a given sink area consists of bus 4 and bus 5. The base case load is -140-$j$140 MVA. By the repeated power flow with the steps $\sigma$=$\mu$=1 MVA, the first prediction point is -147.4 - $j$147.4 MVA, and the first initial guess is the solution at -146.7 - $j$146.7 MVA. The tracing process uses a gap $d$= 0.1 MVA and a step size $l$=5 MVA. The obtained boundary is compared to 36 maximum loading points obtained by the repeated power flow, as shown in the figure below.

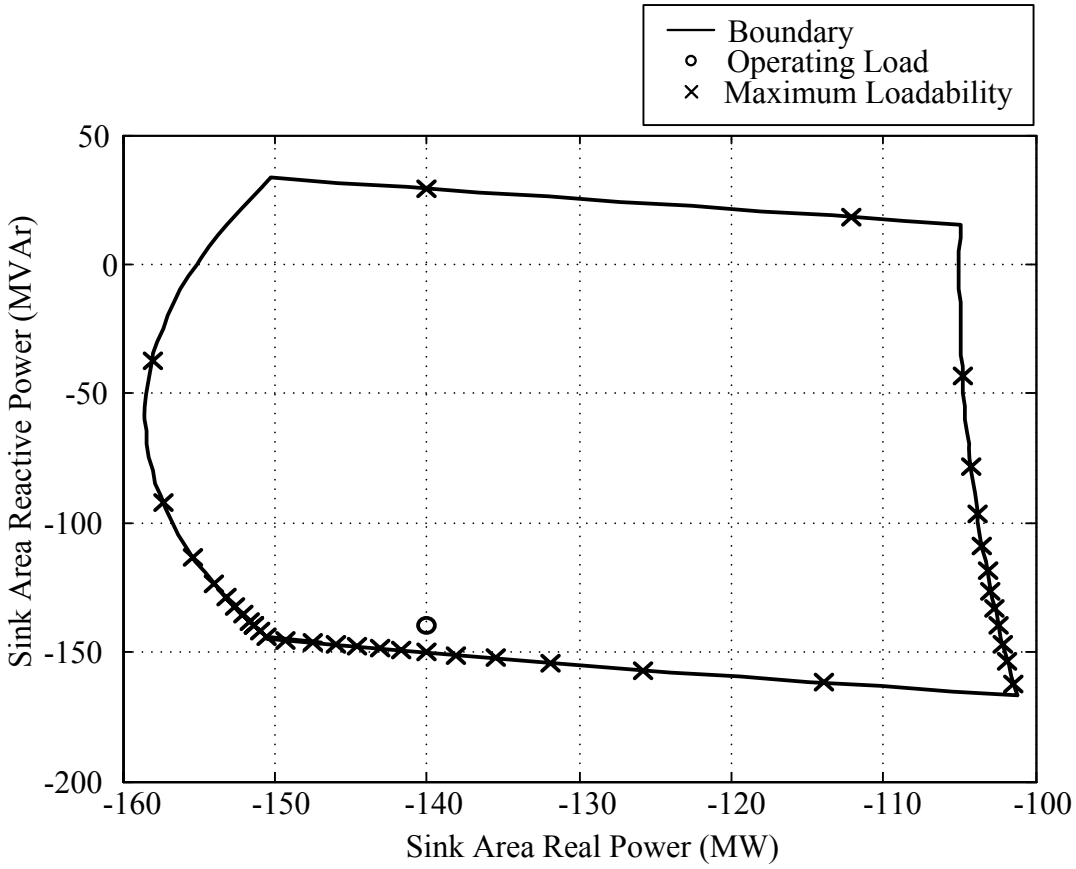


Figure 10.10 Feasible region of power and maximum loading points of area-to-area transfer (Source: Bus 1, Bus 2 / Sink: Bus 4, Bus 5)

With the different source-sink pairs, the feasible regions can be compared as in Figure 10.11-10.13. The computational time of the tracing process is in Table 10.2.

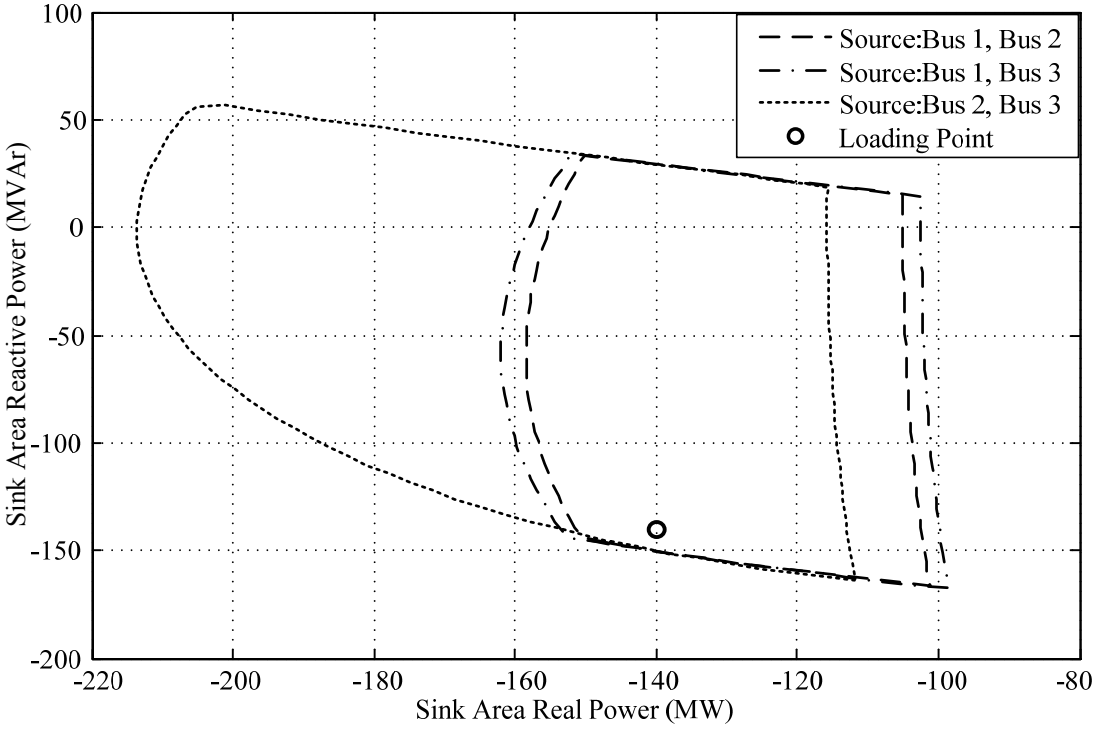


Figure 10.11 Feasible regions of sink area consisting of bus 4 and bus 5 (6-bus system)

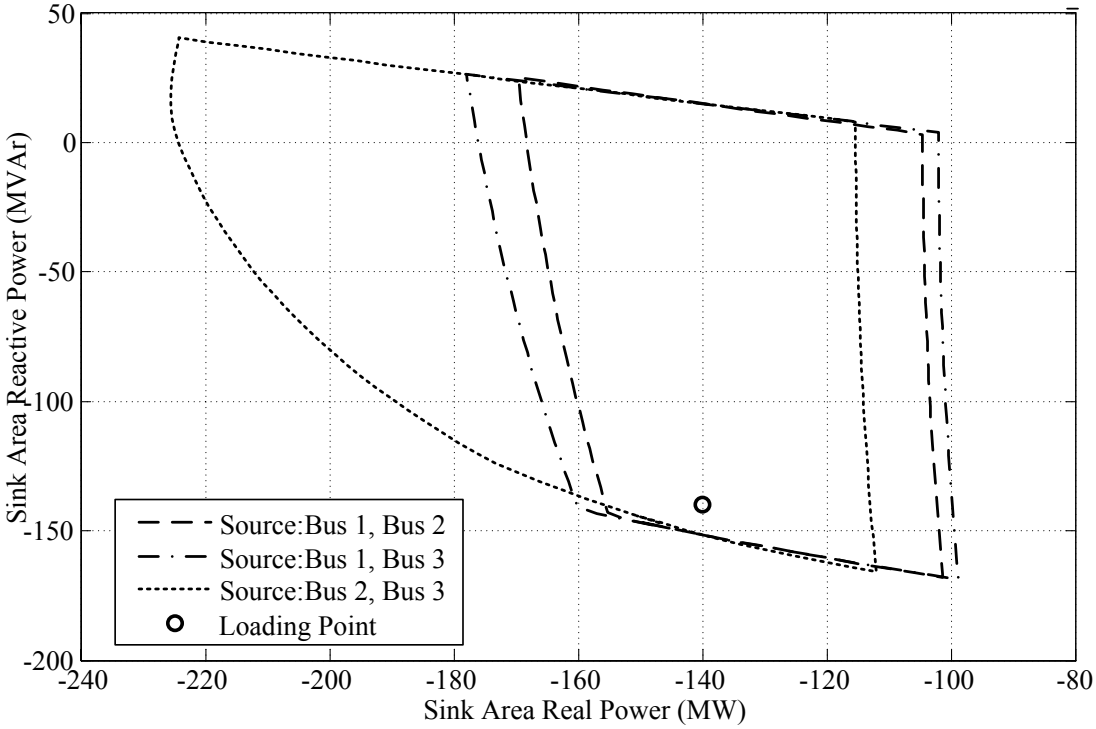


Figure 10.12 Feasible regions of sink area consisting of bus 4 and bus 6 (6-bus system)

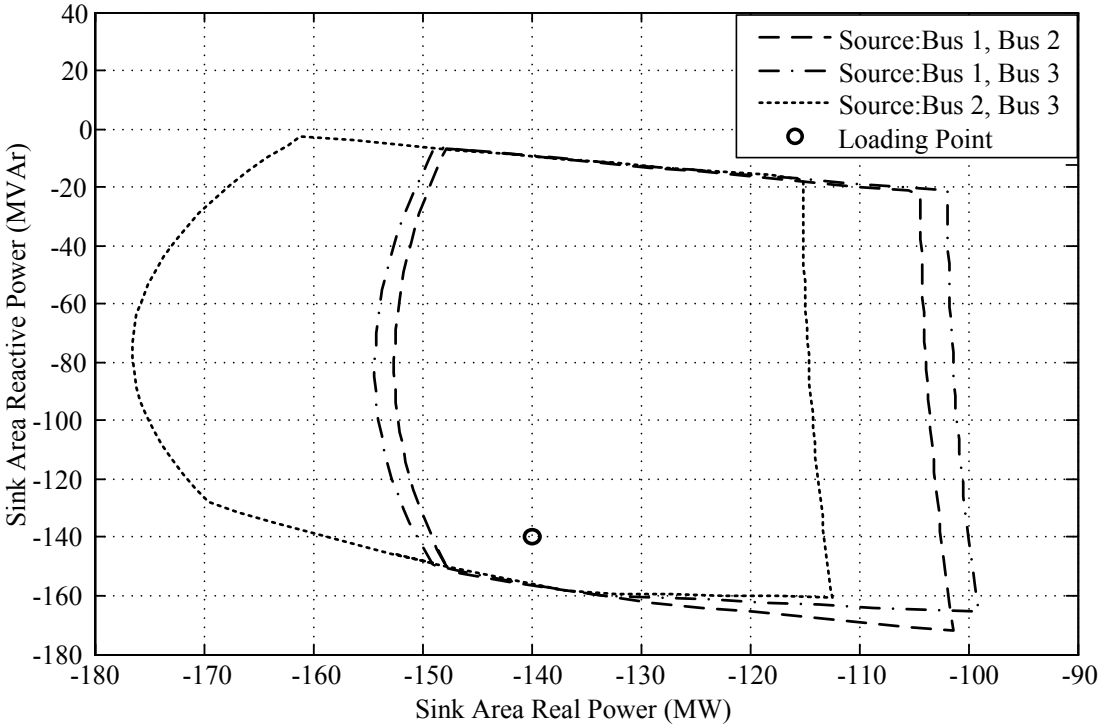


Figure 10.13 Feasible regions of sink area consisting of bus 5 and bus 6 (6-bus system)

Table 10.2 Information of feasible regions for area-to-area transfer (6-bus system)

| Case | Source Bus | Sink Bus | Maximum Load (MW) | Area (MW x MVAr) | Time (sec) | Points | Time/ Point (sec) |
|---|---|---|---|---|---|---|---|
| 1 | 1, 2 | 4, 5 | 158.49 | 9,335 | 13.63 | 96 | 0.142 |
| 2 | 1, 3 | 4, 5 | 161.99 | 10,334 | 13.75 | 98 | 0.140 |
| 3 | 2, 3 | 4, 5 | **213.60** | **15,679** | 17.21 | 111 | 0.155 |
| 4 | 1, 2 | 4, 6 | 169.65 | 10,028 | 14.07 | 97 | 0.145 |
| 5 | 1, 3 | 4, 6 | 177.97 | 11,584 | 15.02 | 100 | 0.150 |
| 6 | 2, 3 | 4, 6 | **225.52** | **15,263** | 16.55 | 111 | 0.149 |
| 7 | 1, 2 | 5, 6 | 152.52 | 7,047 | 11.84 | 82 | 0.144 |
| 8 | 1, 3 | 5, 6 | 154.32 | 7,526 | 11.43 | 80 | 0.143 |
| 9 | 2, 3 | 5, 6 | **176.51** | **8,230** | 12.77 | 81 | 0.158 |

From the results, the source area consisting of bus 2 and bus 3 gives the maximum loading point and the maximum area for every case in this table. The average computational time is 0.14-0.16 second/point, approximately. The proposed tracing algorithm can determines several feasible regions from several transfer scenarios transfer.

The obtained feasible region is under the assumption that the load and generation are proportionally changed by the participation factors. The obtained boundary is checked by the results of maximum loading points obtained from the repeated power flow. By using this tool, the operators can compare capabilities of power transfer scenarios in terms of feasible regions.

### 10.3 Boundary Tracing Method with IEEE 24-Bus System

This section applies the boundary tracing method on IEEE 24-bus system [26]. The information of the system is in Appendix. This system consists of 4 areas with 10 generators and 1 synchronous condenser. For the base case, five generators in area 4 are operating at full capacities. The generators are available in area 1, area 2, and area 3. The first simulation considers the load in area 1. By using the boundary tracing method with a gap $d$= 1 MVA and a step size $l$=10 MVA, a feasible region of the power transfer from area 2 is shown in the figure below. There is one generator in area 2. Therefore, this scenario is equivalent to the power transfer from source bus to sink area.

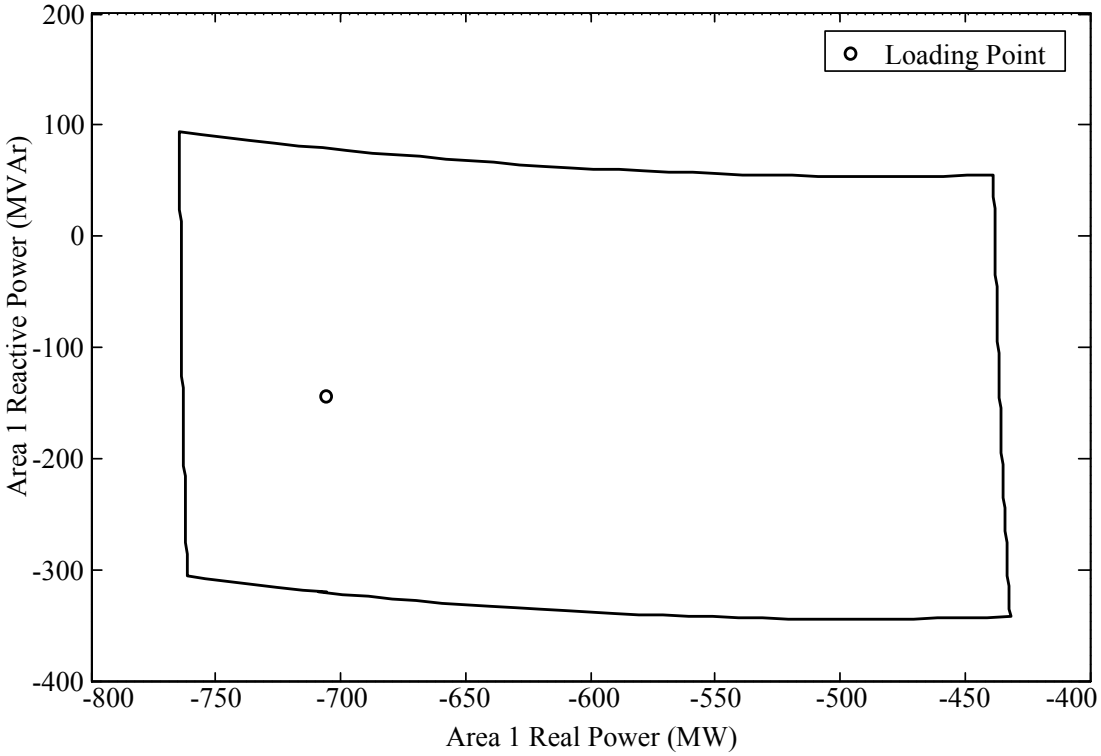


Figure 10.14 Feasible region of power transfer from area 2 to area 1 (IEEE 24-bus system)

When area 1 receives the power from area 3, the corresponding feasible regions are shown in the figure below. Area 3 consists of two generators and one synchronous condenser on bus 13, bus 23, and bus 14, respectively. The simulation must define bus 13 and bus 23 as source buses. The obtained feasible region is represented by a solid line. The operating load of area 3 is on the region boundary because area 3 has a generator on bus 23 operating at full capacity. However, area 3 still has one available generator on bus 13. The boundary tracing method should be modified using the real power enforcement in Section 6.2.4. The real power-limit generator will be removed from a list of source buses, and then determine a boundary point again. The feasible region obtained by this modified algorithm is shown as a dashed line in the figure below.

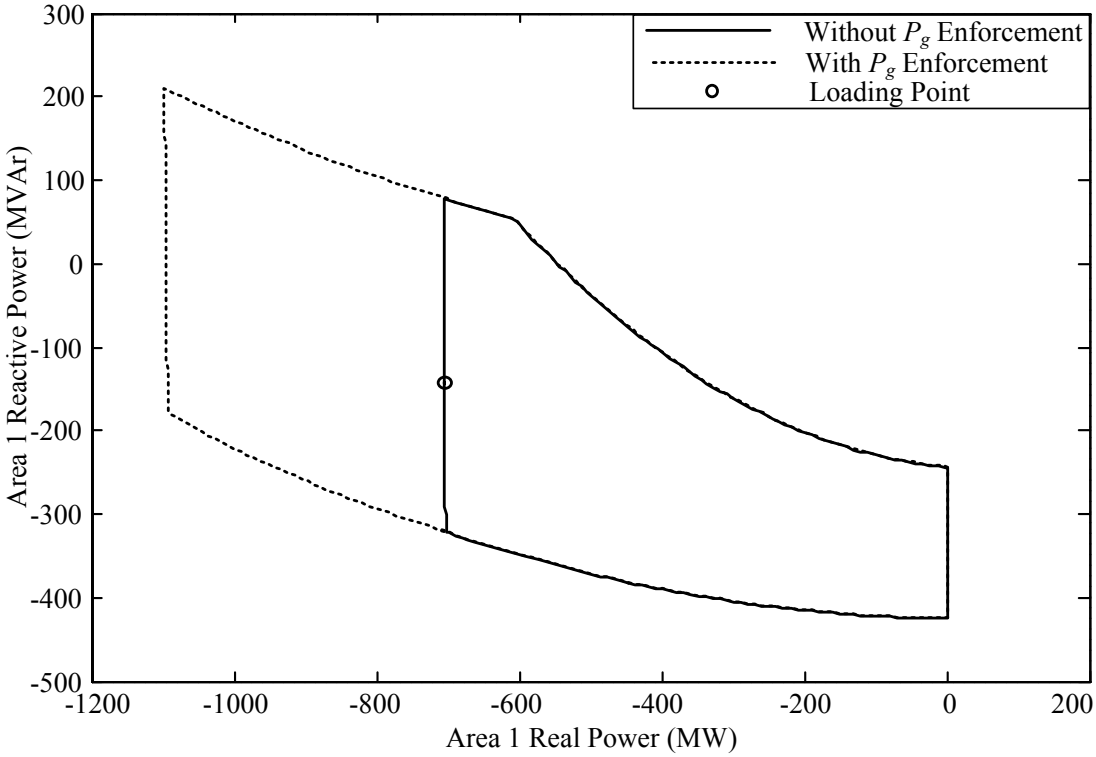


Figure 10.15 Feasible regions of power transfer from area 3 to area 1 (IEEE 24-bus system)

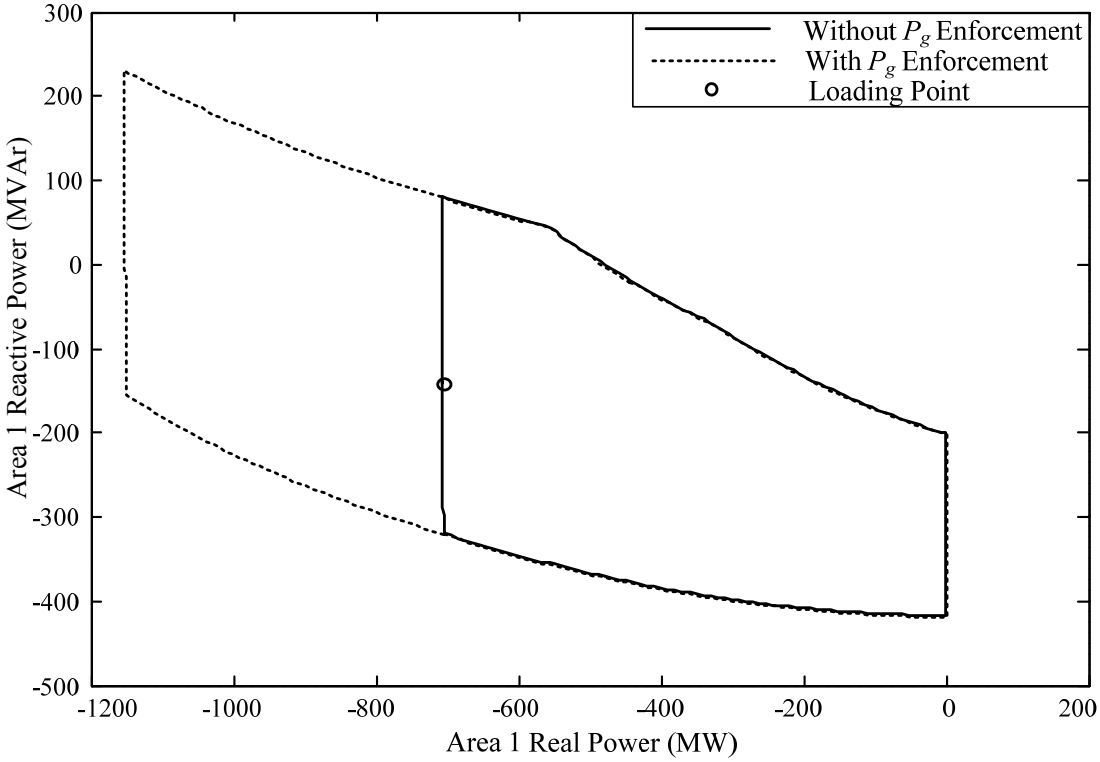


Figure 10.16 Feasible regions of power transfer from area 2, 3 to area 1 (IEEE 24-bus system)

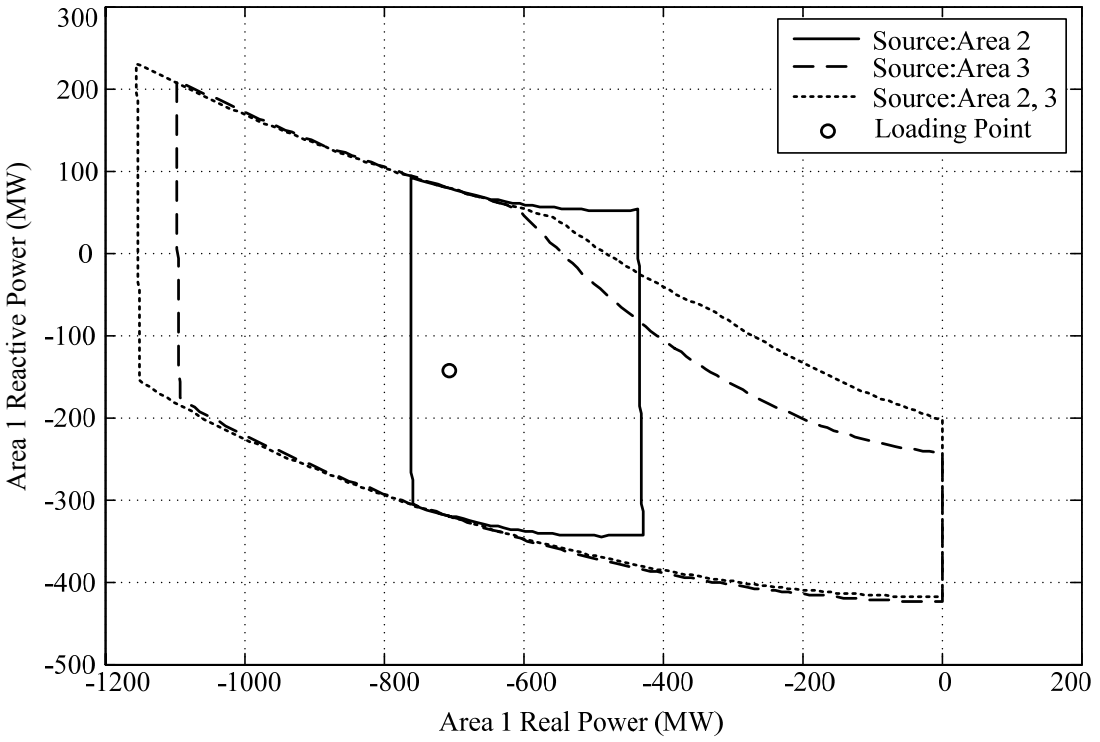


Figure 10.17 Feasible regions of area 1 (IEEE 24-bus system)

When area 1 receives the power from generators in area 2 and area 3, the corresponding feasible regions are shown in Figure 10.16. As same as the previous scenario, an operating load of area 1 is on the boundary due to a generator with full capacity in area 3. The feasible region is obtained again by the modified tracing algorithm with the real power enforcement. A new feasible region is illustrated as a dashed line in the same figure. The feasible regions of area 1 with three cases of source area are illustrated in Figure 10.17. And, the information of feasible regions is shown in Table 10.3. Between cases 1 and 2, the maximum load and maximum closed area belong to case 2, in which area 1 receives the power from area 3. For case 3 that the source area combines with area 2 and area 3, the closed area of feasible region is increased 15.4%, and the maximum load is increased by 5.2% from case 2, approximately.

Table 10.3 Information of feasible regions for area 1 (IEEE 24-bus system)

| Case | Source Area | Sink Area | Maximum Load (MW) | Closed Area (MW x MVAr) | Time (sec) | Points | Time/ Point (sec) |
|---|---|---|---|---|---|---|---|
| 1 | 2 | 1 | 764 | 130,696 | 71.04 | 150 | 0.474 |
| 2 | 3 | 1 | 1,097 | 351,329 | 240.87 | 294 | 0.819 |
| 3 | 2,3 | 1 | 1,154 | 405,446 | 320.57 | 307 | 1.044 |

The next simulation treats area 2 as a sink area. The first scenario is the power transfer from area 1 to area 2. Two generators in area 1 are equally operating at 172 MW with 192 MW capacities. These generators will touch their limit at the same time with generator participation factors. The option of real power generation enforcement is not necessary. The result of feasible region is shown in Figure 10.18.

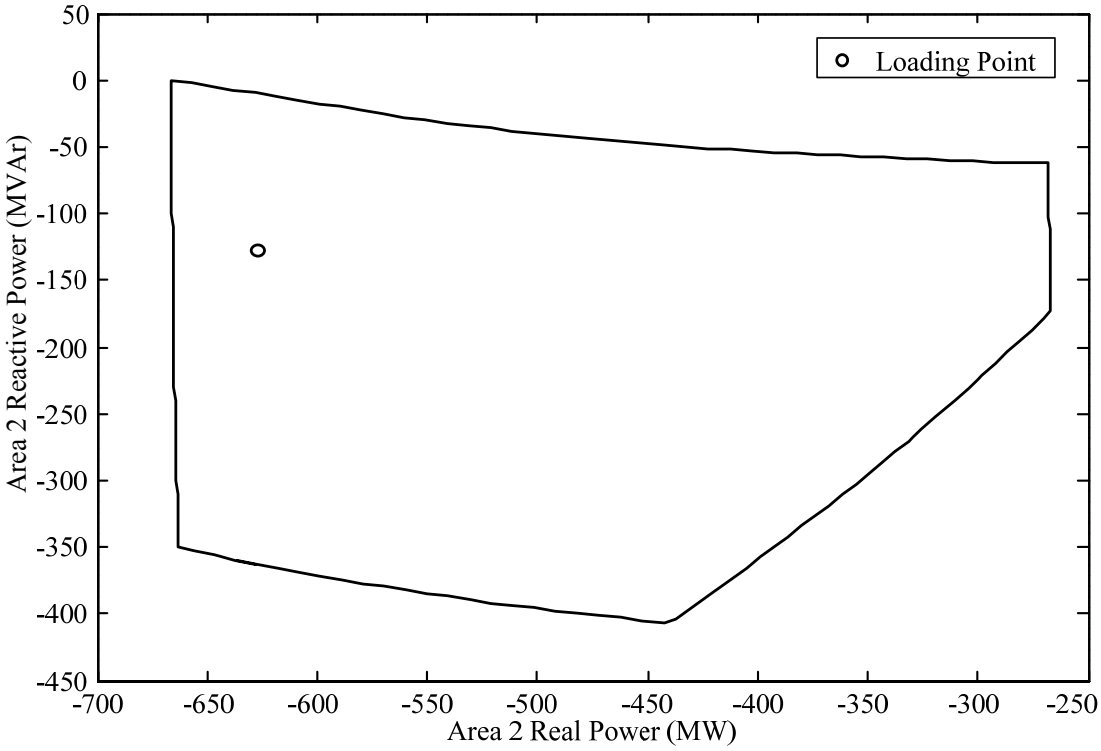


Figure 10.18 Feasible region of power transfer from area 1 to area 2

(IEEE 24-bus system)

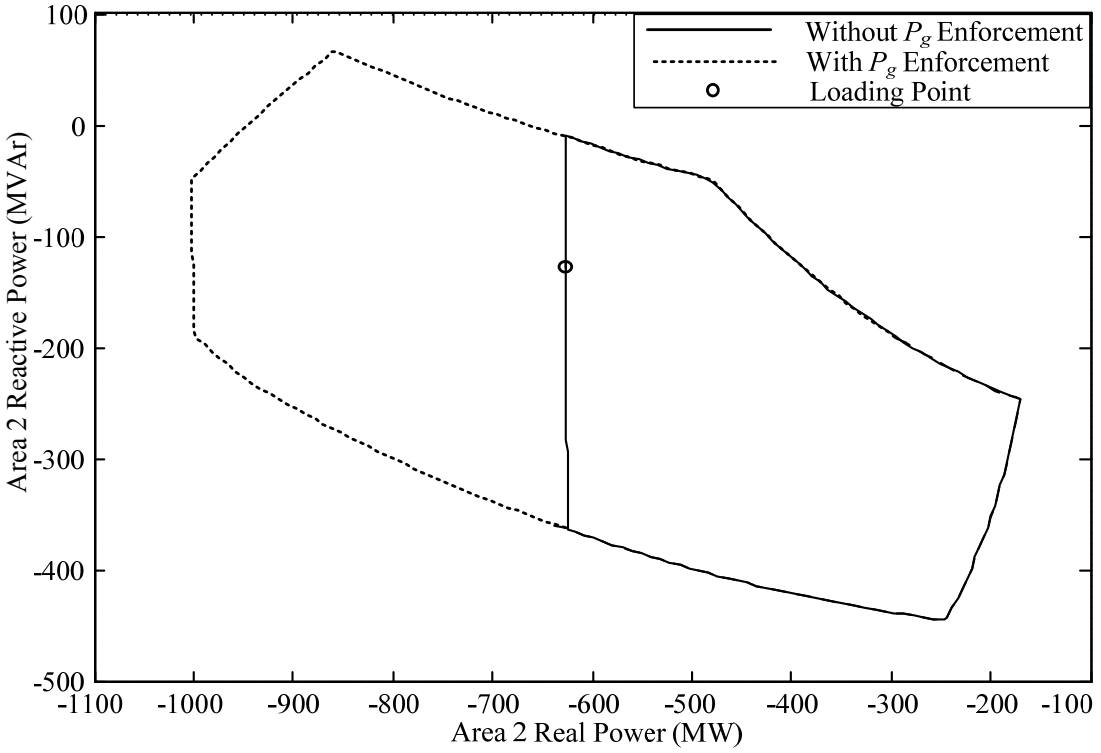


Figure 10.19 Feasible regions of power transfer from area 3 to area 2

(IEEE 24-bus system)

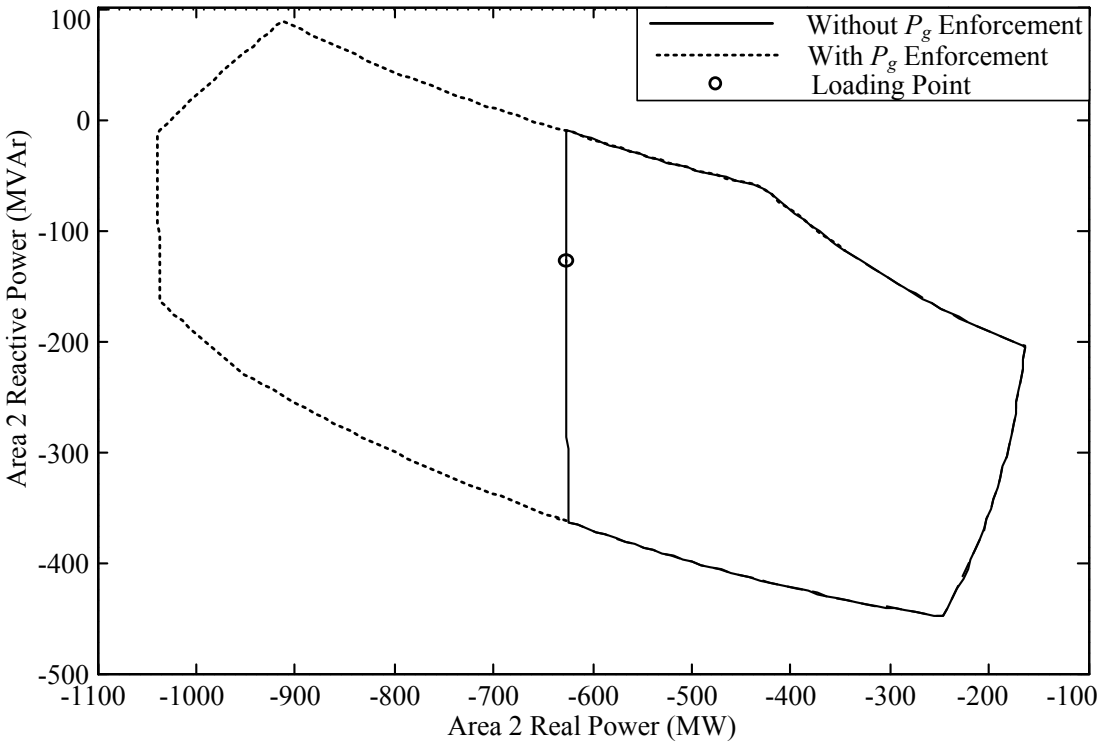


Figure 10.20 Feasible regions of power transfer from area 1,3 to area 2 (IEEE 24-bus system)

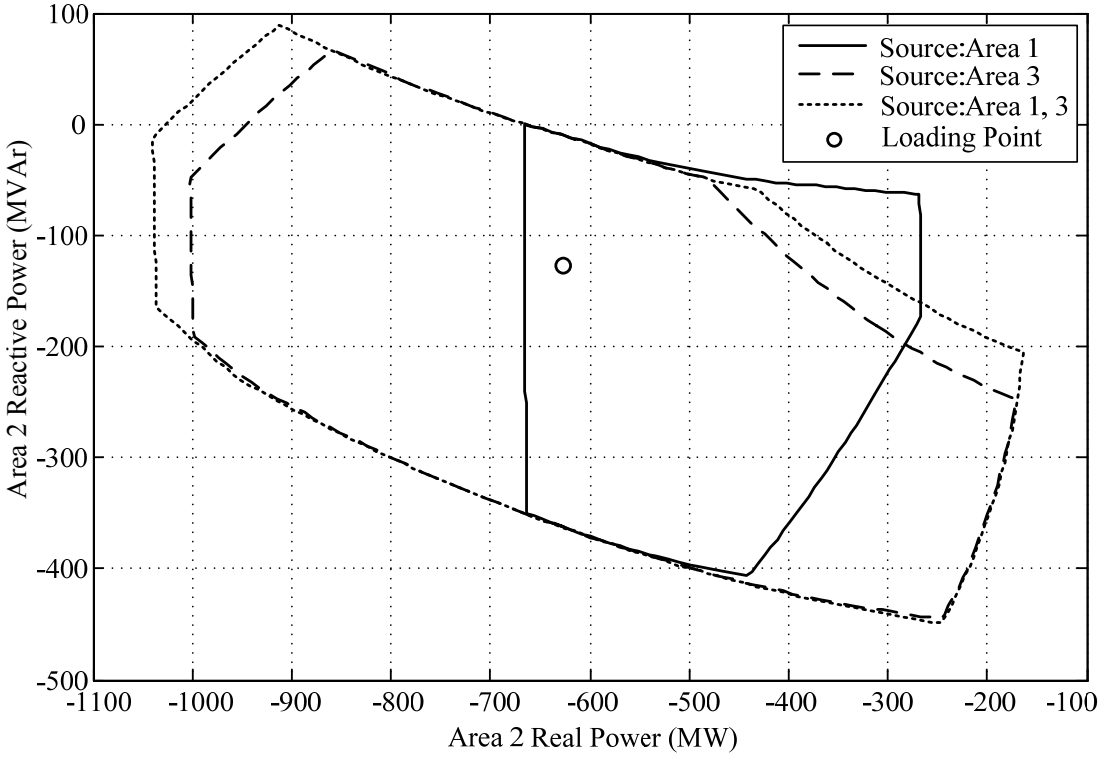


Figure 10.21 Feasible regions of area 2 (IEEE 24-bus system)

When area 2 receives the power from area 3, the obtained feasible regions are shown in Figure 10.19. And, the case of power transfer from area 1, 3 to area 2 is shown in Figure 10.20. The feasible regions of area 2 obtained from three cases of source area is illustrated in Figure 10.21. The information of these feasible regions is shown in Table 10.4. The feasibility observed by the closed area and the maximum load of case 2 are better than case 1. If the load at area 2 receives the power form both area 1 and area 3, the maximum load and the feasibility can be improved. However, the improvement is not too much. The improvements from case 2 are 1.6% of the maximum load and 11.2% of the feasibility, approximately.

Table 10.4 Information of feasible regions for area 2 (IEEE 24-bus system)

| Case | Source Area | Sink Area | Maximum Load (MW) | Area (MW x MVAr) | Time (sec) | Points | Time/ Point (sec) |
|---|---|---|---|---|---|---|---|
| 1 | 1 | 2 | 666 | 121,262 | 80.09 | 143 | 0.560 |
| 2 | 3 | 2 | 1,002 | 244,165 | 179.44 | 215 | 0.835 |
| 3 | 1,3 | 2 | 1,039 | 271,474 | 244.26 | 227 | 1.076 |

The test results illustrate the modified algorithm when a generator in source area touches the real power limit. Other generators in source area are still available. By the modified algorithm, the feasible region can be expanded until all generators in source area are not available to supply the real power. The modified algorithm needs to repeat the minimization in the correction step, and it impacts the computational time. The comparison of computational time is shown in the table below. It can be obviously seen that the average computational time of the modified algorithm ($P_g$ enforcement) is more than the unmodified algorithm.

Table 10.5 Computational time of tracing process with/without real power enforcement (IEEE 24-bus system)

| Source Area | Sink Area | without $P_g$ Enforcement | | | With $P_g$ Enforcement | | |
|---|---|---|---|---|---|---|---|
| | | Time (sec) | Points | Time/ Point (sec) | Time (sec) | Points | Time/ Point (sec) |
| 3 | 1 | 107.50 | 213 | 0.505 | 240.87 | 294 | 0.819 |
| 2,3 | 1 | 106.96 | 213 | 0.502 | 320.57 | 307 | 1.044 |
| 3 | 2 | 74.93 | 151 | 0.496 | 179.44 | 215 | 0.835 |
| 1,3 | 2 | 76.10 | 154 | 0.494 | 244.26 | 227 | 1.076 |

## 10.4 Conclusion

In order to show the robustness of the proposed algorithm, this chapter implements the boundary tracing method with three test systems and many cases of source-sink pair. The boundary tracing method can properly determine the contour of feasible regions. The feasible regions are checked with the maximum loading points obtained from the conventional repeated power flow. The shape of feasible regions show the feasibility of loading points and the maximum real power of sink area can be observed.

# CHAPTER XI

# NUMERICAL RESULTS: EFFECT OF SYSTEM PARAMETERS

The proposed boundary tracing can be implemented as a tool for observing a feasible region of the corresponding transfer scenario. An existing loading point is represented by a point inside the obtained region. In sink area, the variation of load causes the loading point moving inside the region. However, the variation of other parameters can change a region shape. This section will implement the boundary tracing method to study movements of loading point and variations of feasible region.

## 11.1 Movement of Loading Point

According to test results of the six-bus system, the illustration in Figure 11.1 shows the feasible region of the power transfer from bus 3 to bus 6. The existing loading point is -70-*j*70 MVA. The movements of loading point are demonstrated in three directions. The load increment with a constant power factor is limited by the loading point A. The reactive load compensation is limited by the point B. And finally, the load decrement with a constant power factor is limited by the point C.

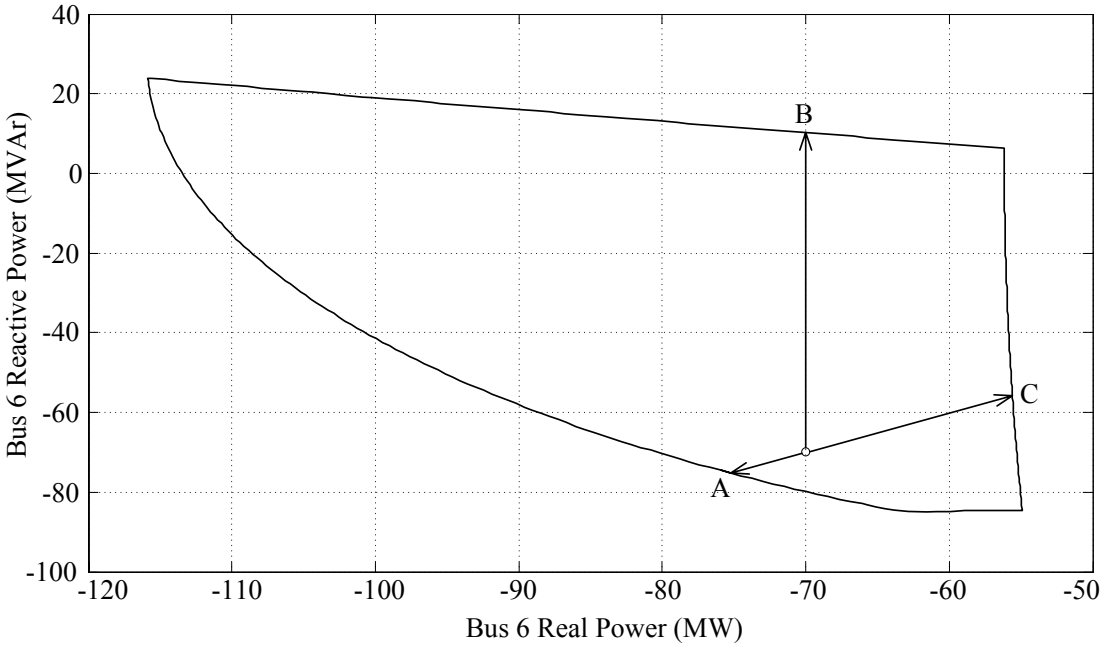

Figure 11.1 Feasible region of power transfer from bus 3 to bus 6 and movement of loading point (6-bus system)

In order to observe the potential of loading point, three feasible regions of bus 6 corresponding to three source buses are illustrated in the figure below.

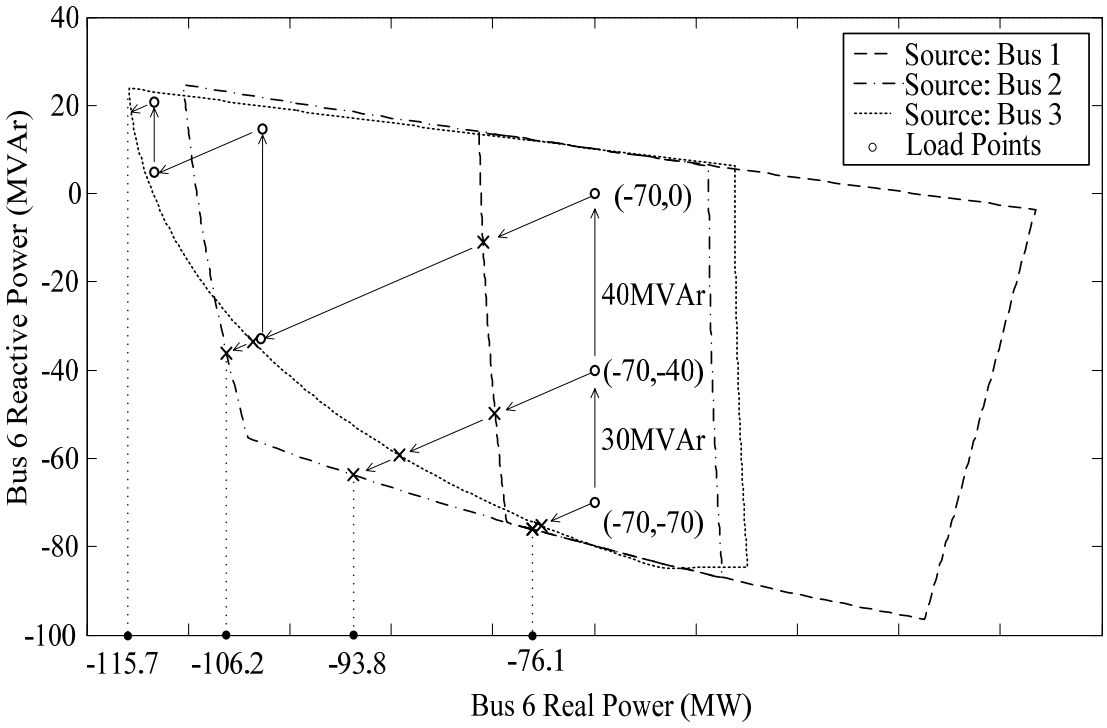


Figure 11.2 Visualization of load margins of bus 6 with several transfer scenarios (6-bus system)

According to a result, from the existing loading point -70-*j*70 MVA, the real power can increase to 76.1 MW when receiving power from bus 1 or bus 2. If the existing loading point is compensated 30 MVAr by the reactive power devices, the real power is able to increase to 93.8 MW when receiving power from bus 2. Furthermore, if the loading point is additionally compensated by 40 MVAr, the real power loading point can operate at 106.2 MW when receiving power from bus 2.

From the shape of regions, the potential of bus 6 for receiving load is up to 115.7 MW when receiving power from bus 3. However, the loading point at that real power level is difficult to operate because the shape of feasible region is unfavorable for controlling the loading point to that position.

## 11.2 Change of Boundary by Control Actions

According to the concept of security regions mentioned in [8]-[12], when the operating point is driven away from the feasible region, a control strategy must pull the system back to a feasible condition. The control action can be operated in two ways, either by pushing an operating point back into the feasible region or by enlarging the feasible region. The feasible region in this research is under the transfer scenario between a source-sink pair. The control actions in sink area directly cause an operating point moving over on the *P-Q* plane. On the other hand, the control actions at other buses result in resizing the feasible region. This section will illustrate the effect of control actions. Two control actions in this illustration are the reactive load compensation (usually capacitor banks), and the load shedding.

The test is implemented on the six-bus system by treating all generator buses as source buses (bus 1, bus 2, and bus 3). The feasible region of each load bus is determined by using the boundary tracing method. In this section, the generator participation factors are ignored by implementing the minimization problem without a constraint (5.30). Three feasible regions corresponding to bus 4, bus 5 and bus 6 are shown in the figure below.

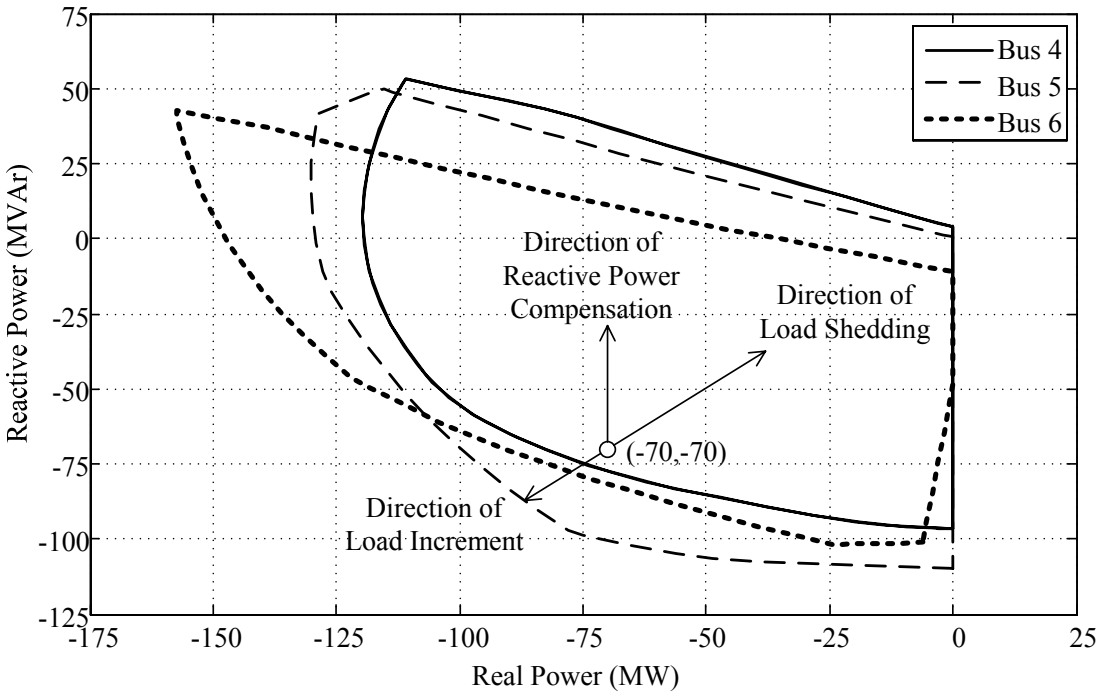


Figure 11.3 Feasible regions of three load buses (6-bus system)

The directions of control actions at sink bus are shown in this figure. The results can be observed that:

- For bus 6, the point (0, 0) is outside the feasible region, the load shedding on bus 6 is therefore unavailable.
- Bus 4 has the largest margin for the reactive power compensation.

The control action limits for each bus can be observed using the feasible region corresponding to the sink bus. However, if the controls acts in other load buses in the system, it results in the shape of feasible region changing. In the figure below, the capacitor banks are assumed to force the operating point to be 0 MVAr for bus 4 and bus 5, alternately. The feasible region of bus 6 is observed. It can be seen that the lower part of the feasible region shifts down and the operation of bus 5 leads to the maximum load margin of bus 6.

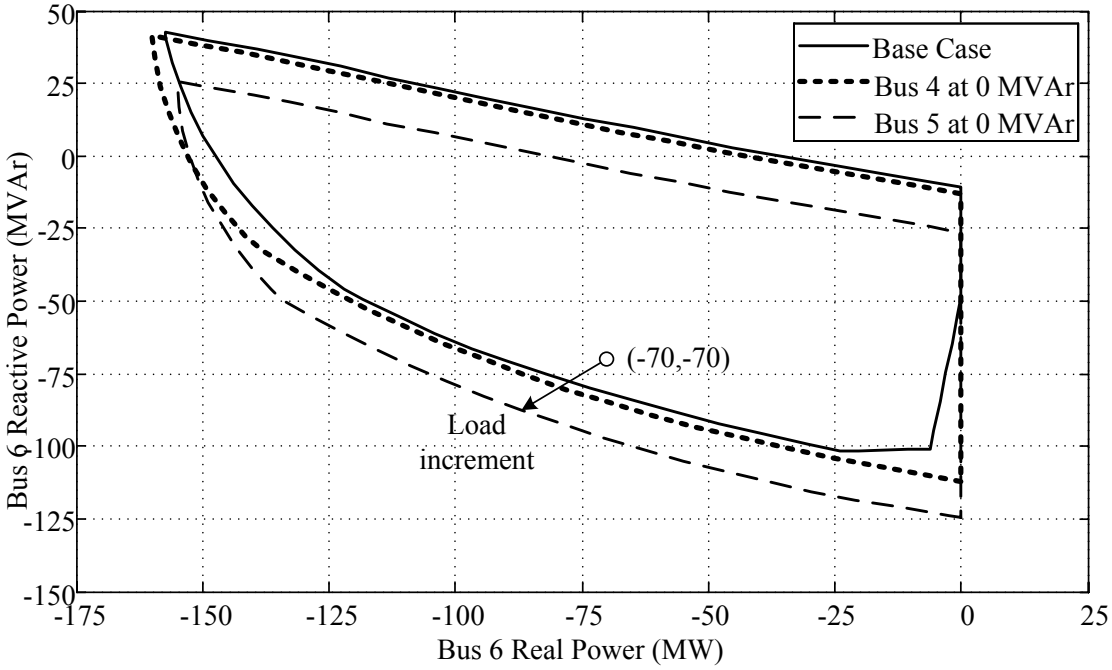


Figure 11.4 Changes of feasible region by reactive power compensation (6-bus system)

For the load shedding, the figure below compares three feasible regions of bus 6 in the cases of: base load, load shedding at bus 4, and load shedding at bus 5, respectively. The result shows that the load shedding can improve the load margin in the

load increment direction, but the obtained region is smaller than that of the base case. Especially for the load shedding of bus 5, the upper part of region significantly decreases. This implies that the operation of capacitor banks at this condition will bring about an unfeasible situation. Furthermore, the right part of region also decreases because of the minimal limit of generators. The operating load of bus 6 can not be less than 60 MW, approximately.

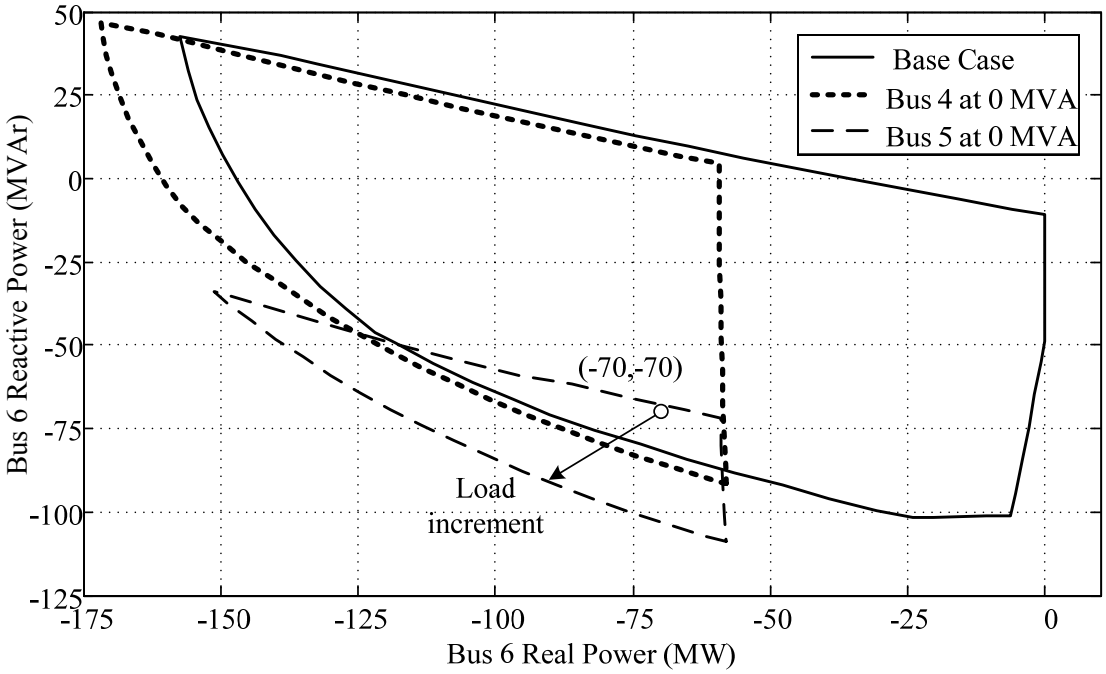


Figure 11.5 Change of feasible region by load shedding (6-bus system)

### 11.3 Outermost Boundary Affected by Generator Voltages

The setting of generator voltage also affects the boundary of the feasible region. In the boundary tracing process, the generator voltage is fixed as a constant. The proposed boundary tracing method can visualize several feasible regions varied by the generator voltage, as illustrated in Figure 11.6. The feasible regions are obtained by using the boundary tracing method on the six-bus test system. The result compares the boundaries obtained from different cases of generator voltage setting. The scenario is the power transfer from bus 3 to bus 6. In this simulation, the generator voltage at bus 3 is set to be 1.07, 1.03, and 1.01 pu., three contours are represented by the dashed line, the dash-dot line, and the dotted line, respectively. It can be observed that the obtained boundaries are different.

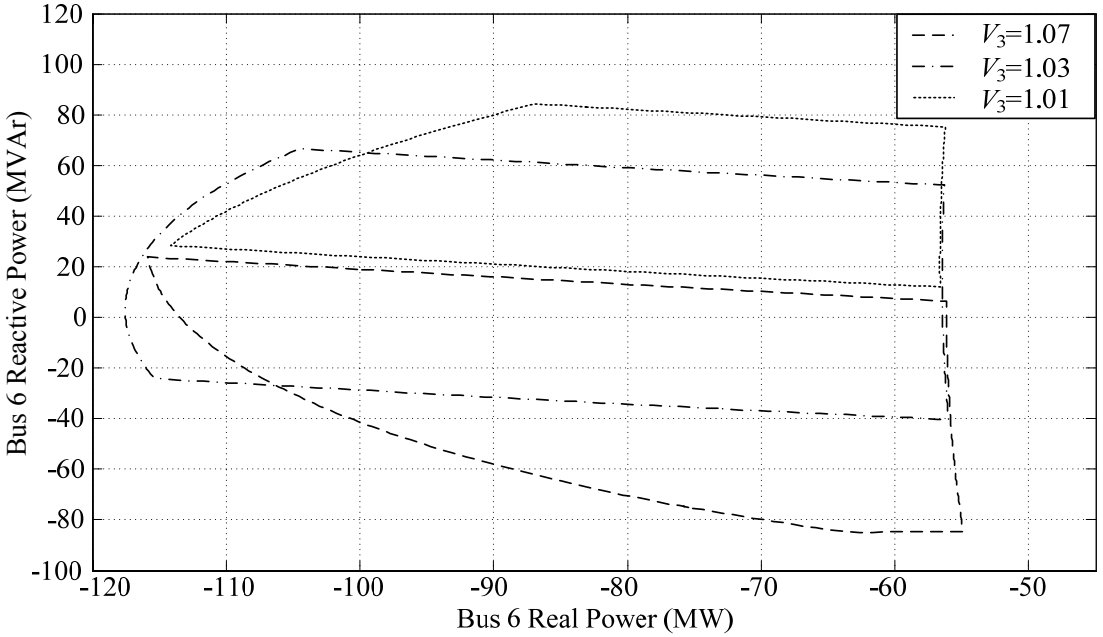


Figure 11.6 Feasible regions of power transfer from bus 3 to bus 6 with different generator voltage settings (6-bus system)

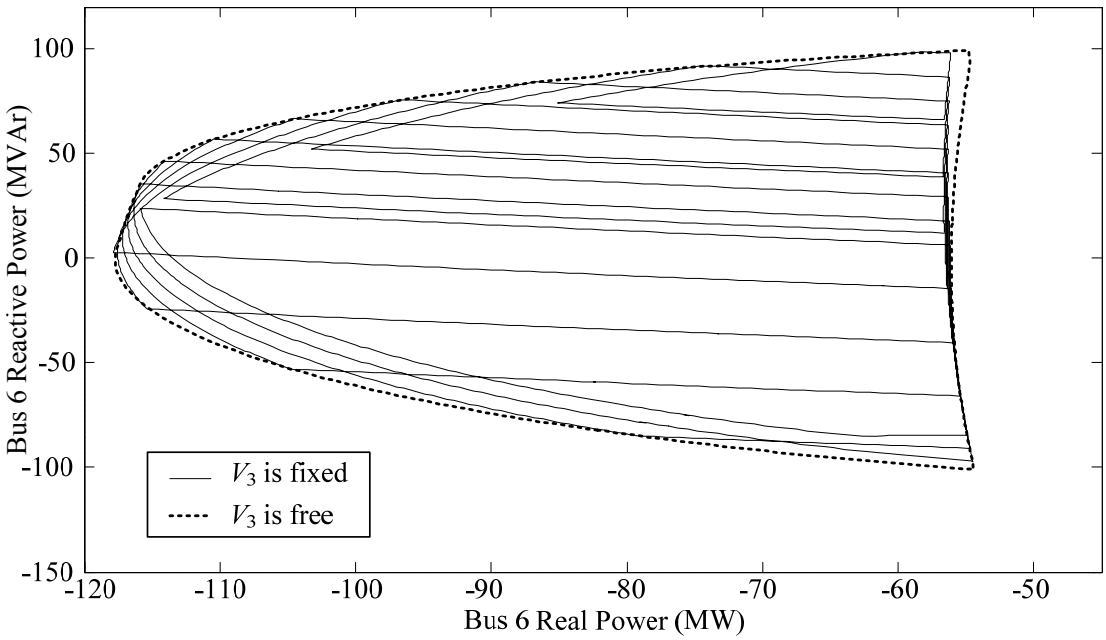


Figure 11.7 Outermost region of power transfer from bus 3 to bus 6 comparing to feasible regions of several generator voltage settings (6-bus system)

When the generator voltage at bus 3 is set to be free, the outermost boundary affected by the generator voltage is determined by the method in Chapter 7. The

outermost boundary is compared to the feasible regions from several cases of generator voltage settings, as shown in Figure 11.7. The dashed line represents the outermost boundary when a generator voltage at bus 3 ($V_3$) is free to vary. The computational time of this contour is 63.67 seconds with 459 solution points (0.139 second/point). The solid lines represent 9 feasible regions from 9 settings of $V_3$( 0.99, 1.00, …,1,07 pu.). The result shows that the obtained outermost boundary covers all regions represented by solid lines.

Considering the same scenario of power transfer, Figure 11.8 shows the outermost region and the feasible region of base case with $V_3$=1.07 pu. The solution from the boundary point of outermost region can be used as the guideline for improving the load margin. At the point *A* of outermost boundary, the solution gives that $V_3$=1.05 pu. When we set the generator voltage at bus 3 equals to 1.05 pu, the feasible region obtained again by the proposed method is illustrated as the dashed line. The boundary of feasible region with new voltage setting is expanded to the point A. The load margin in that direction is improved up to 82 MW.

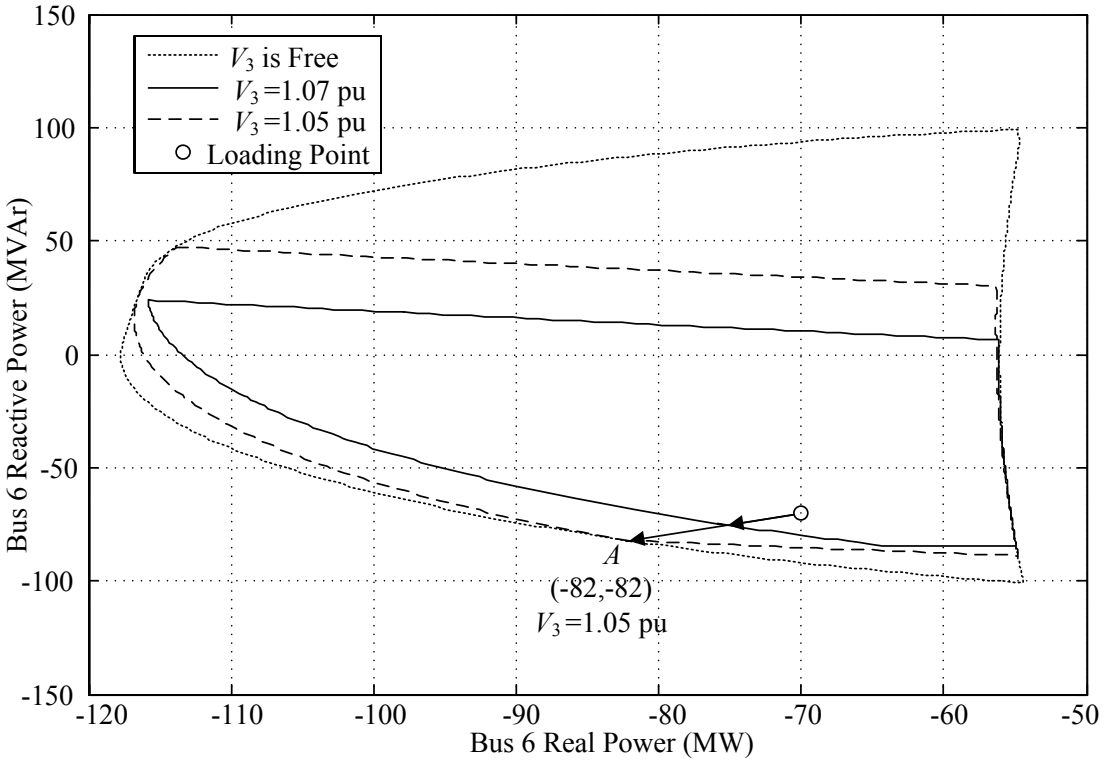


Figure 11.8 Utilization of outermost boundary for case of power transfer from bus 3 to bus 6 (6-bus system)

Figure 11.9 shows the outermost boundary affected by generator voltages for the case of power transfer between areas. The given source area consists of generators at bus 2 and bus 3. The given sink area consists of bus 5 and bus 6. The outermost region of loading points at sink area is represented by the solid line. The boundary tracing process of the outermost region spends 30.93 seconds with 141 solution points (0.219 second/point). At point A, the solution of generator voltages at bus 2 and bus 3 are 1.05 pu and 1.06 pu, respectively. By setting the generator voltages with these values ($V_2$=1.05, $V_3$=1.06), the obtained boundary is represented by the dotted line. The region is compared to the feasible region of the base case represented by the dashed line ($V_2$=1.05, $V_3$=1.07). The boundary of feasible region corresponding to new voltage setting (voltage setting 2) is expanded to the point A, and then it makes the maximum loading point in this direction increasing to 155 MW.

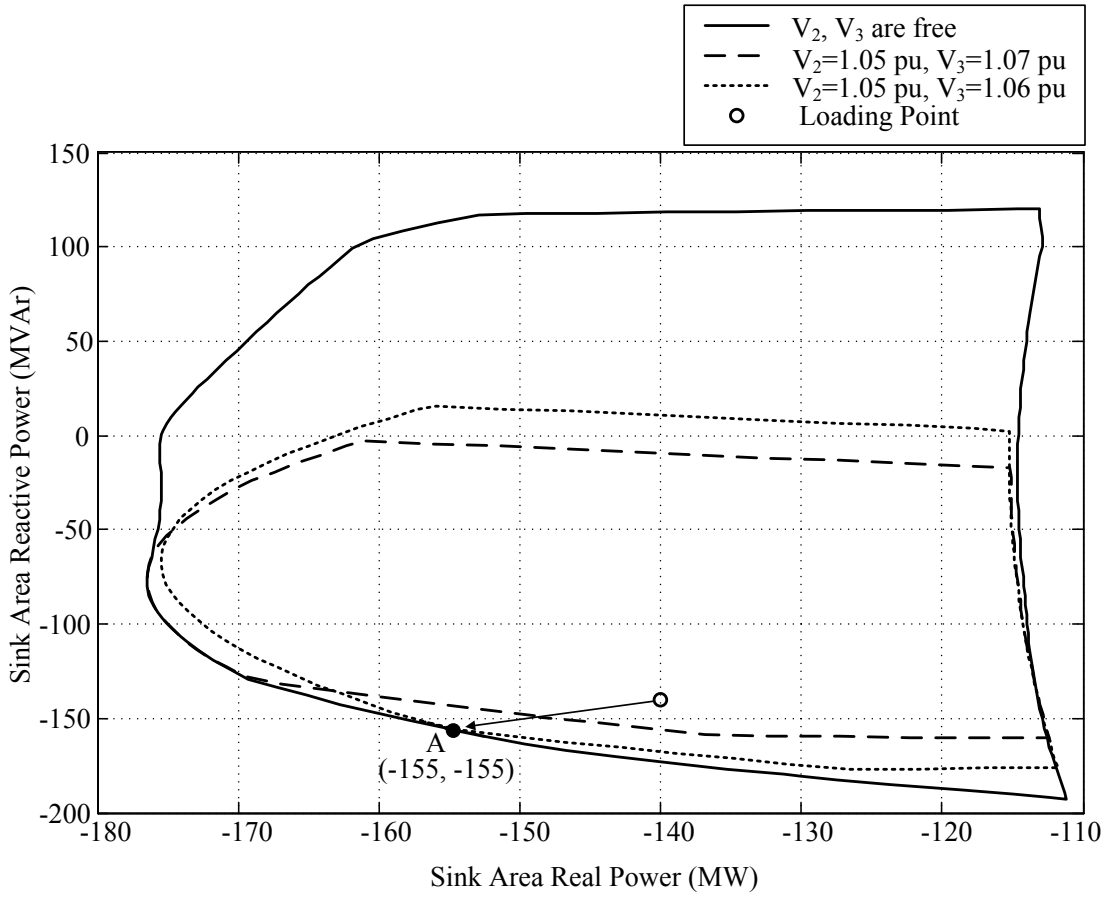


Figure 11.9 Utilization of outermost boundary for power transfer between areas (Source: Bus 2, Bus 3/ sink: Bus 5, Bus6)

## 11.4 Outermost Boundary Affected by FACTs Devices

The FACTS devices are installed in order to control some parameters in power systems. The FACTS devices illustrated in this section are SVC and TCSC. The boundary tracing method determines the outermost boundary affected by FACTS using the 6-bus test system.

### 11.4.1 Outermost Boundary Affected by SVC

In this simulation, a source area consists of bus 1, bus 2 and bus 3, a sink bus is bus 5. Assume that two SVCs are installed at bus 4 and bus 6, the capacity of installed SVC is ± 50 MVAr. According to Section 7.3.2, the outermost boundary point can be determined by treating a voltage magnitude at the SVC-installed bus as a free variable. The obtained outermost boundary is checked by several cases of SVC voltage setting. The result is shown in the figure below.

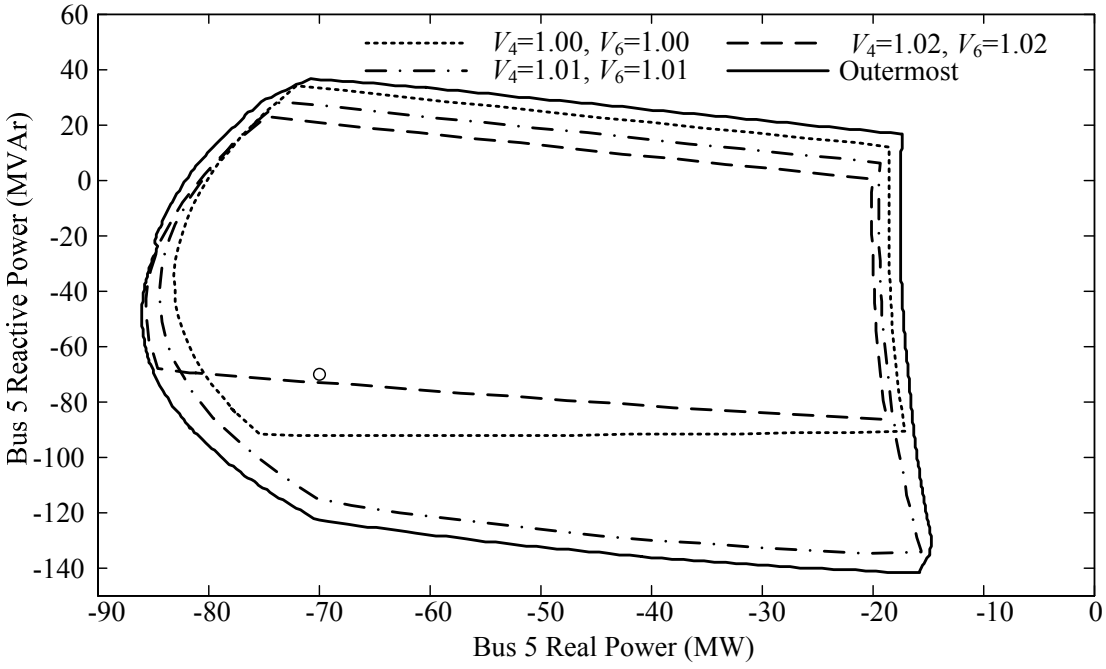


Figure 11.10 Outermost region comparing to feasible regions of several SVC voltage settings (Source: Bus 1, Bus 2, Bus 3/ Sink: Bus 5)

The result can confirm the performance of proposed method for the outermost boundary problem. Three contours of different SVC voltages are compared to the outermost

boundary affected by SVC. It is obviously seen that the outermost boundary covers all three contour.

With the same SVC capacity, the following test compares the outermost boundary by SVC installed in many cases. The outermost feasible regions affected by SVC are shown in the figure below.

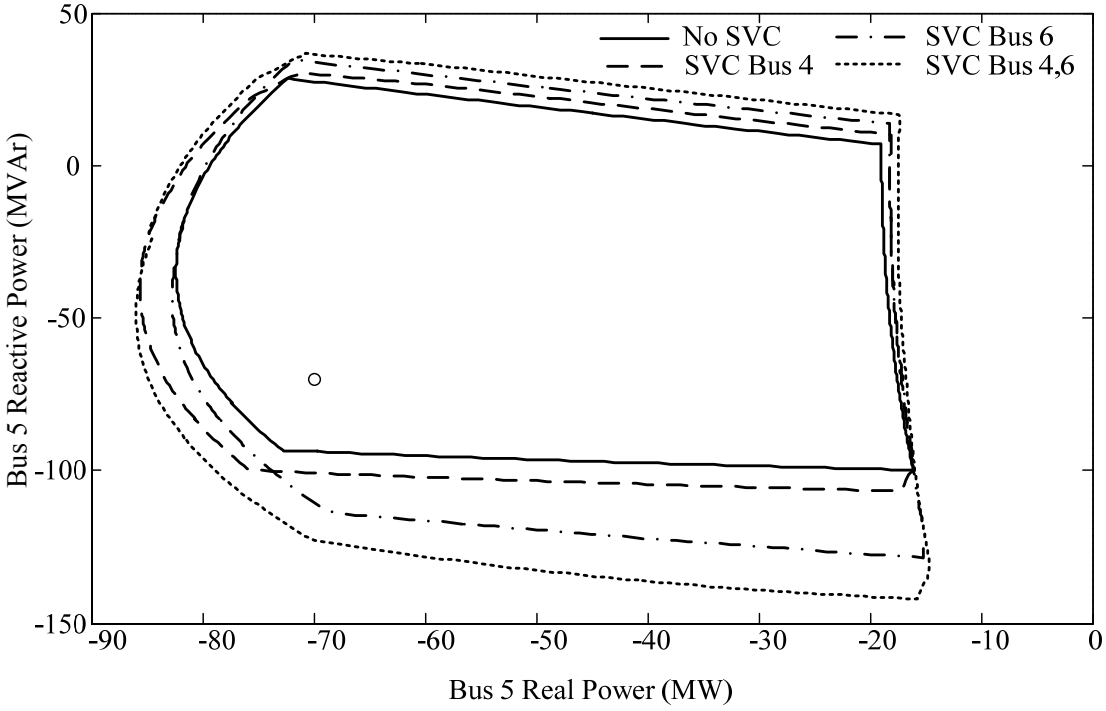


Figure 11.11 Outermost regions affected by SVC installation
(Source: Bus 1, Bus 2, Bus 3/ Sink: Bus 5)

Table 11.1 Area and computational Time for outermost regions affected by SVC

| Case | SVC Bus | Maximum Load (MW) | Area (MW x MVAr) | Time (Sec) | Points | Time/Point (sec) |
|---|---|---|---|---|---|---|
| Base Case | - | 82.38 | 7,026 | 42.87 | 349 | 0.123 |
| SVC01 | 4 | **85.63** | 8,049 | 59.51 | 370 | 0.161 |
| SVC02 | 6 | 82.73 | **8,933** | 63.72 | 410 | 0.155 |
| SVC03 | 4, 6 | **85.97** | **10,386** | 84.15 | 441 | 0.191 |

The information of obtained regions is in the table above. Considering one SVC installation, the result shows that the maximum load 85.63 MW belongs to the case of SVC installed at bus 4. The case of SVC installed at both bus 4 and bus 6 results in a slight increase of maximum load and the feasibility increases by 3.9% and 16.3% from

the case of SVC installed at bus 6, respectively. The average computational times are about 0.1-0.2 second, approximately.

### 11.4.2 Outermost Boundary Affected by TCSC

With the six-bus test system, two TCSCs are assumed to be installed in the transmission system at branch 2 and branch 3. The range of TCSC reactance is $\pm 0.05$ pu. In this simulation, the source area consists of buses 1-3, and the sink area consists of buses 4-6. The outermost boundary can be determined by the proposed method with freeing the TCSC reactance. The obtained outermost boundary is compared to feasible regions from several TCSC settings. Let $X_{TCSC2}$ and $X_{TCSC3}$ be an operating TCSC reactance on branch 2 and branch 3, respectively. The setting points of TCSC in this test are:

- Setting 1: $X_{TCSC2}$=0 pu, $X_{TCSC3}$=0 pu
- Setting 2: $X_{TCSC2}$=0.05 pu, $X_{TCSC3}$=0.05 pu
- Setting 3: $X_{TCSC2}$=-0.05 pu, $X_{TCSC3}$=-0.05 pu
- Setting 4: $X_{TCSC2}$=-0.05 pu, $X_{TCSC3}$=0.05 pu
- Setting 5: $X_{TCSC2}$=0.05 pu, $X_{TCSC3}$=-0.05 pu
- Setting 6: $X_{TCSC2}$=-0.018 pu, $X_{TCSC3}$=0.05 pu

In the figure below, an outermost region affected by TCSC and feasible regions with several setting points of TCSC are compared.

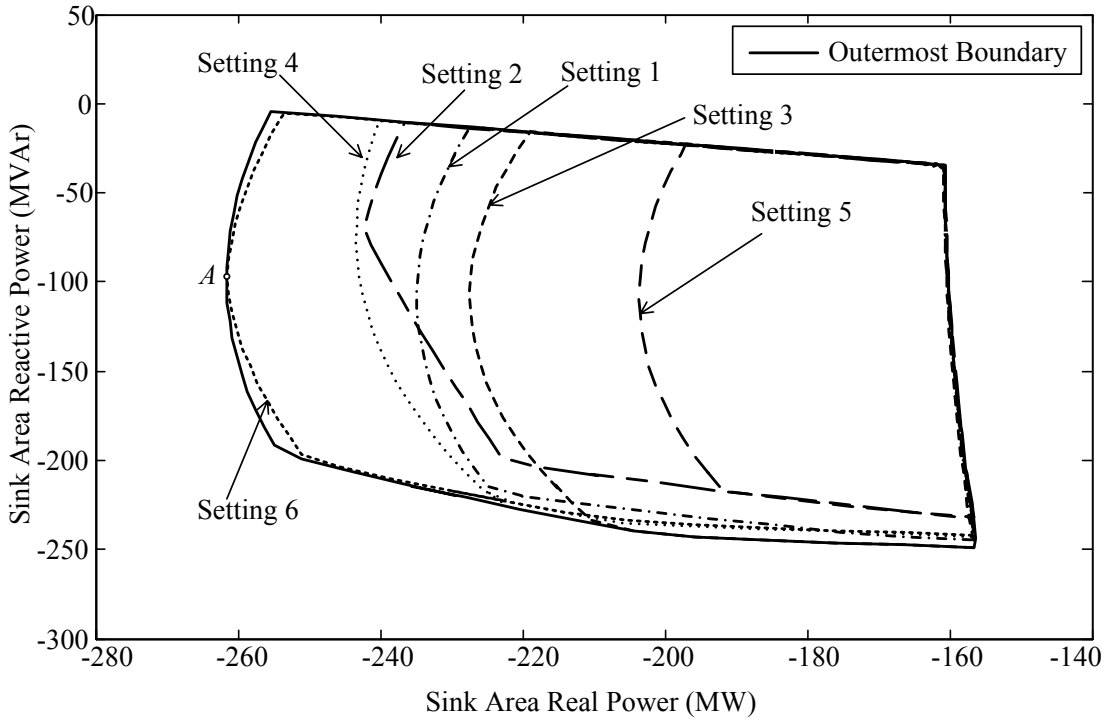


Figure 11.12 Outermost region and feasible regions from several TCSC settings (Source: Bus 1, Bus 2, Bus 3/ Sink: Bus 4, Bus 5, Bus 6)

The result confirms that feasible regions from several cases of TCSC settings are inside the obtained outermost region. For setting 1 to setting 5, the setting points are randomly selected. For setting 6, the setting point is determined by using the solution of the outermost boundary at point *A*. The result shows that using TCSC setting 6 can expand the feasible region to point *A*.

The next simulation is to find the location of TCSC by assuming that TCSC with $\pm 0.05$ pu of reactance will be installed into the system. Several outermost regions affected by TCSC are determined in order to compare the performance of TCSC in each location. Three examples of outermost regions are shown in the figure below. It can be seen that the different locations of TCSC installation leads to the different shapes of outermost regions.

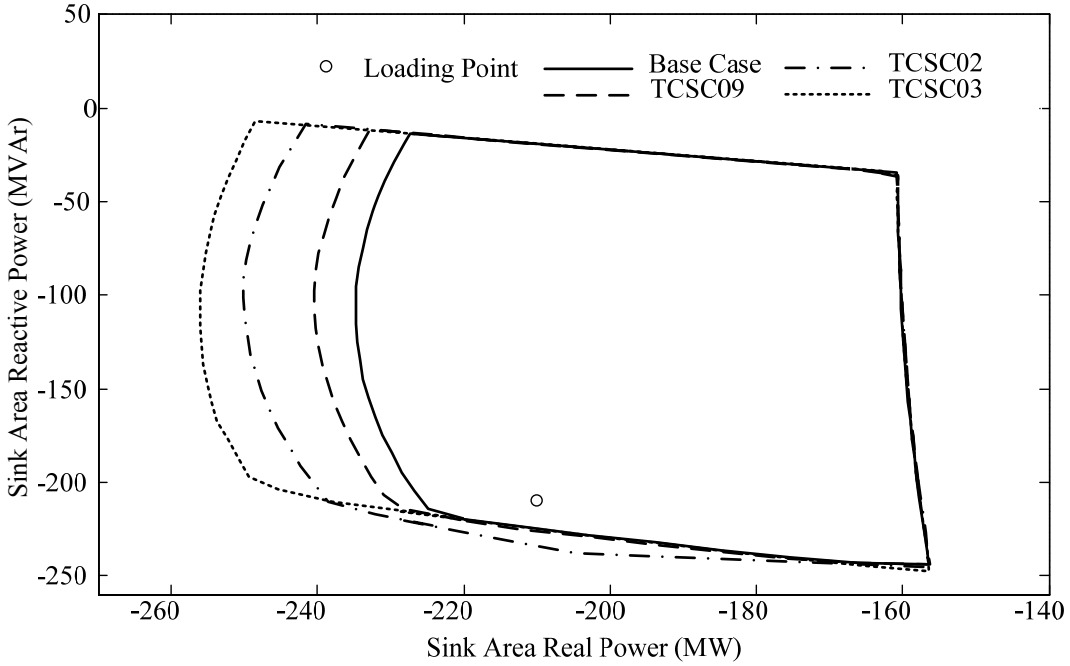


Figure 11.13 Outermost regions affected by TCSC installation

(Source: Bus 1, Bus 2, Bus 3/ Sink: Bus 4, Bus 5, Bus 6)

All details of the obtained outermost regions are shown in the table below. The six-bus system consists of 11 branches (transmission lines). Each location of TCSC gives a different performance. The largest maximum load and the largest area belong to the case of TCSC installed at branch 3. According to this case, the maximum load increases from the base case by 9.1%, and the closed area of region increased from the base case by 29.1%.

Table 11.2 Area and computational Time for outermost regions affected by TCSC

| Case | TCSC Branch | Maximum Load (MW) | Area (MW x MVAr) | Time (sec) | Points | Time/Point (sec) |
|---|---|---|---|---|---|---|
| Base Case | - | 234.81 | 15,044 | 11.33 | 59 | 0.192 |
| TCSC01 | 1 | 240.45 | 16,204 | 14.85 | 59 | 0.252 |
| TCSC02 | 2 | 250.13 | 18,478 | 44.88 | 62 | 0.724 |
| TCSC03 | 3 | **256.10** | **19,423** | 48.15 | 65 | 0.741 |
| TCSC04 | 4 | 234.92 | 15,097 | 15.84 | 60 | 0.264 |
| TCSC05 | 5 | 238.38 | 16,057 | 29.47 | 60 | 0.491 |
| TCSC06 | 6 | 238.65 | 16,038 | 14.08 | 61 | 0.231 |
| TCSC07 | 7 | 238.31 | 16,373 | 14.10 | 62 | 0.227 |
| TCSC08 | 8 | 237.55 | 15,804 | 14.12 | 61 | 0.232 |
| TCSC09 | 9 | 235.36 | 16,098 | 19.67 | 62 | 0.317 |
| TCSC10 | 10 | 235.30 | 15,170 | 10.36 | 59 | 0.176 |
| TCSC11 | 11 | 234.81 | 15,169 | 13.59 | 59 | 0.230 |

## 11.5 Conclusion

The concept of outermost region is illustrated by the six-bus test system in this chapter. The results show that several parameters, such as, generator voltage, SVC voltage, and TCSC reactance are able to impact the shape of feasible region and the outermost boundary affected by these parameter can be determined by the proposed tracing method. The outermost boundary gives information of the improvement of feasible region, and a solution on outermost boundary can be used as a guideline in order to improve the performance of the system.

# CHAPTER XII

# NUMERICAL RESULTS: TTCR

According to the concept of total transfer capability (TTC), this research studies about the security region corresponding to the concept of TTC and defines the intersection of feasible regions from several contingencies as the total transfer capability region (TTCR). This chapter will implement the method to determine the boundary curve of TTCR with the test systems.

## 12.1. TTCR with Six-Bus System

This section illustrates the proposed method to determine TTCR boundaries for several cases. The considered contingencies for this simulation are the outages of transmission lines 4, 10, and 11 connecting bus 2 to bus 3, bus 4 to bus 5, and bus 5 to bus 6, respectively. The tests in this section are classified into the bus-to-bus transfer and the area-to-area transfer.

### 12.1.1 TTCR of Bus-to-Bus Transfer (Six-Bus System)

For the first scenario of bus-to-bus transfer, bus 3 and bus 4 are chosen as a source bus and a sink bus, respectively. The feasible regions of base case and given contingencies are determined by the boundary tracing method. Then, a boundary of TTCR is determined by the proposed method in Chapter 8 using a gap $d$=0.1 MVA and a step size $l$=1 MVA. The obtained regions are shown in the figure below. The result shows that the obtained boundary of TTCR represented by a solid line is an intersection of feasible regions from considered contingencies and base case. A boundary of TTCR is checked by 36 maximum loading points of TTC. It obviously shows that all maximum loading points are on the obtained boundary.

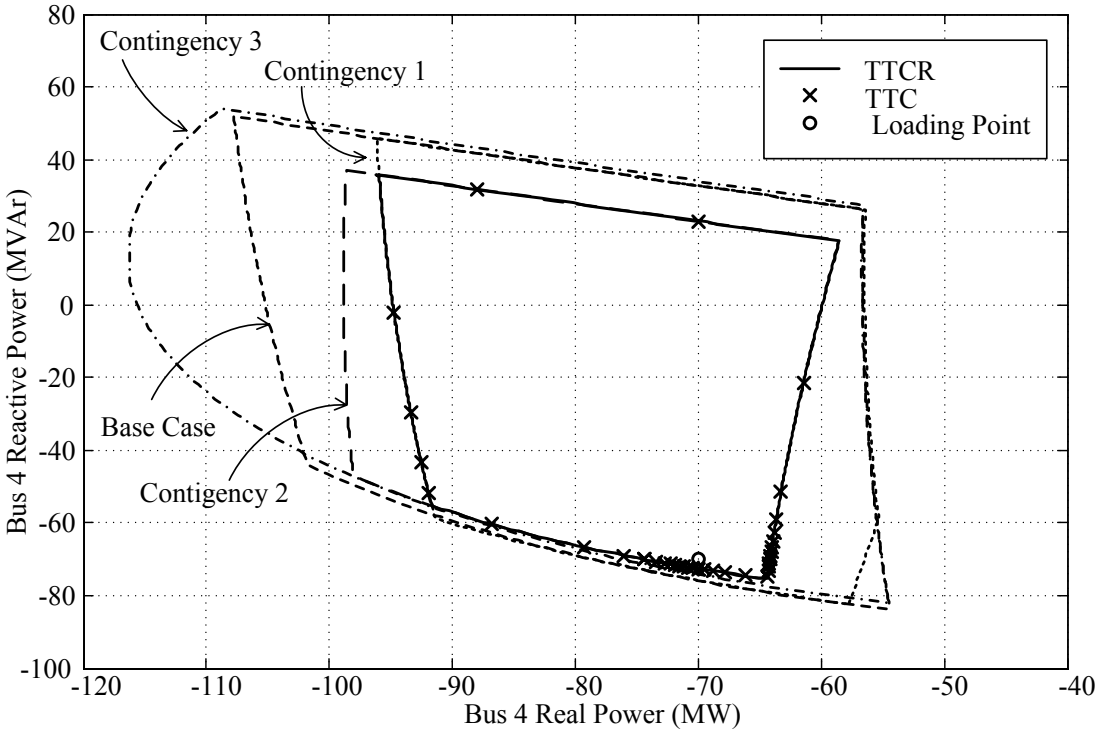


Figure 12.1 TTCR compared to feasible regions and TTC

(Source: Bus 3 / Sink: Bus 4)

The table below shows the computational time of each contour. For the base case and contingencies, a total computational time of four contours is 164.33 second. The computational time of TTCR is 137.23 second. A determination of TTCR spends the time less than determinations of all corresponding cases about 16.5% for this simulation. However, the average calculation time of TTCR is 0.52 second/point more than the average time of other cases because a correction step in boundary tracing process of TTCR needs to calculate all candidates of boundary point from each case.

Table 12.1 Computational time of boundary tracing process (bus 3 to bus 4)

| Case | Time (sec) | Points | Time/Point(sec) |
|---|---|---|---|
| Base Case | 44.08 | 330 | 0.134 |
| Contingency 1 | 39.38 | 303 | 0.130 |
| Contingency 2 | 34.89 | 271 | 0.129 |
| Contingency 3 | 45.98 | 334 | 0.138 |
| **Total** | **164.33** | | |
| **TTCR** | **137.23** | 264 | 0.520 |

The results of TTCR from other transfer scenarios are illustrated in the following figures.

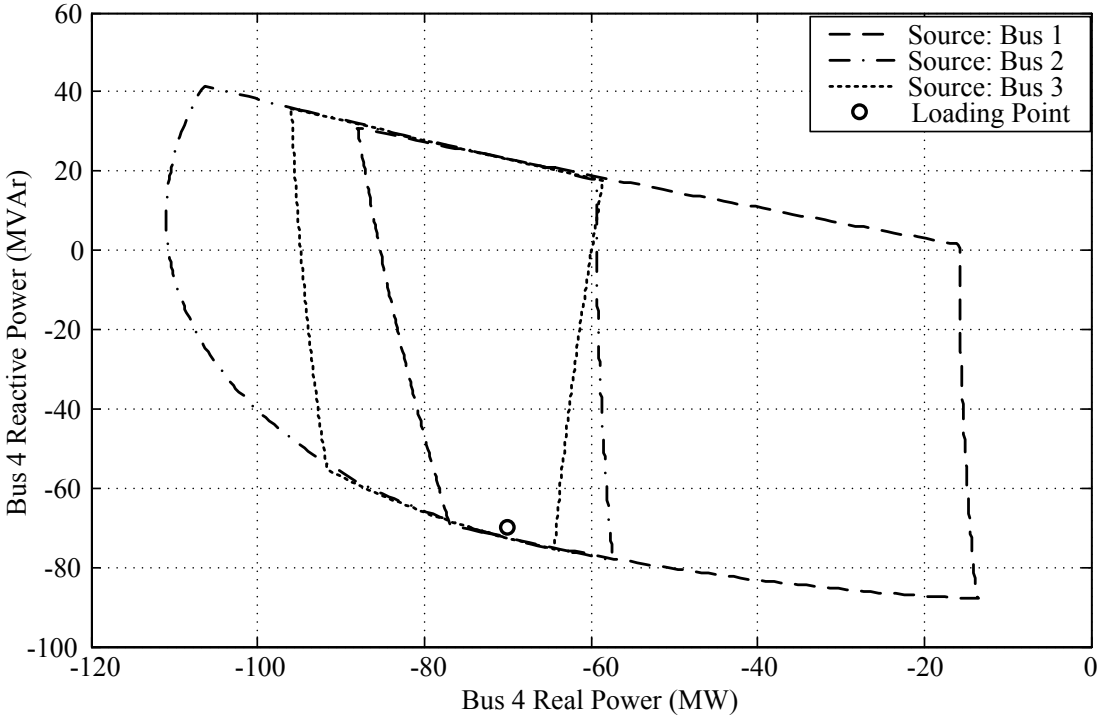


Figure 12.2 TTCR of bus 4 (6-bus system)

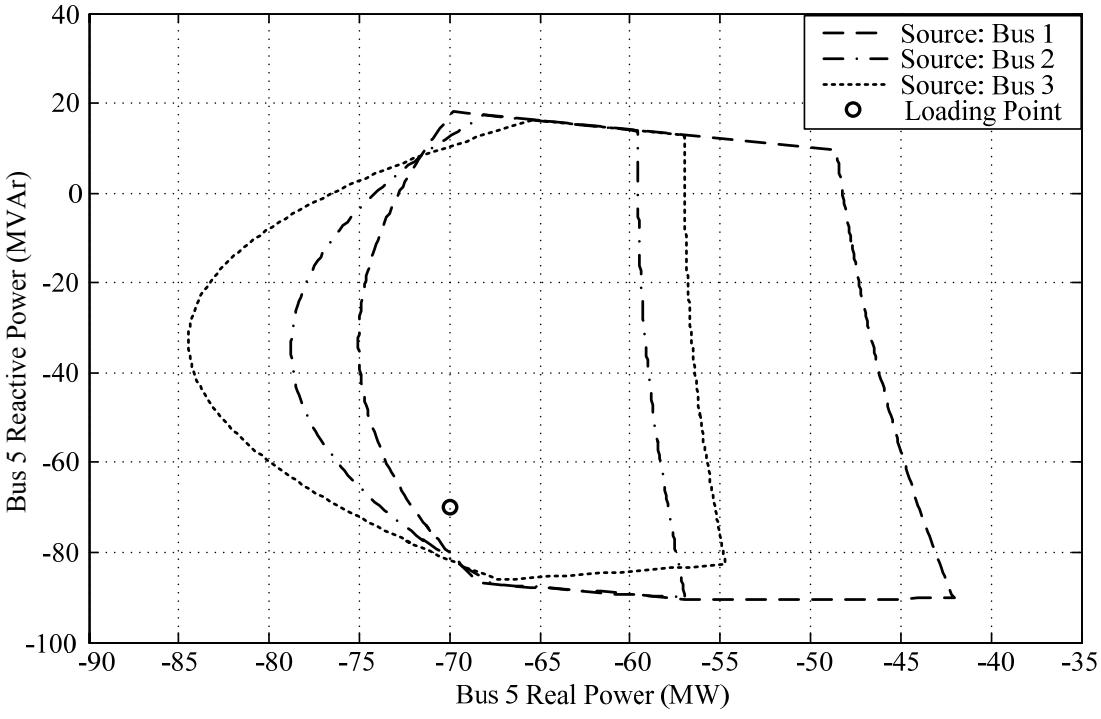


Figure 12.3 TTCR of bus 5 (6-bus system)

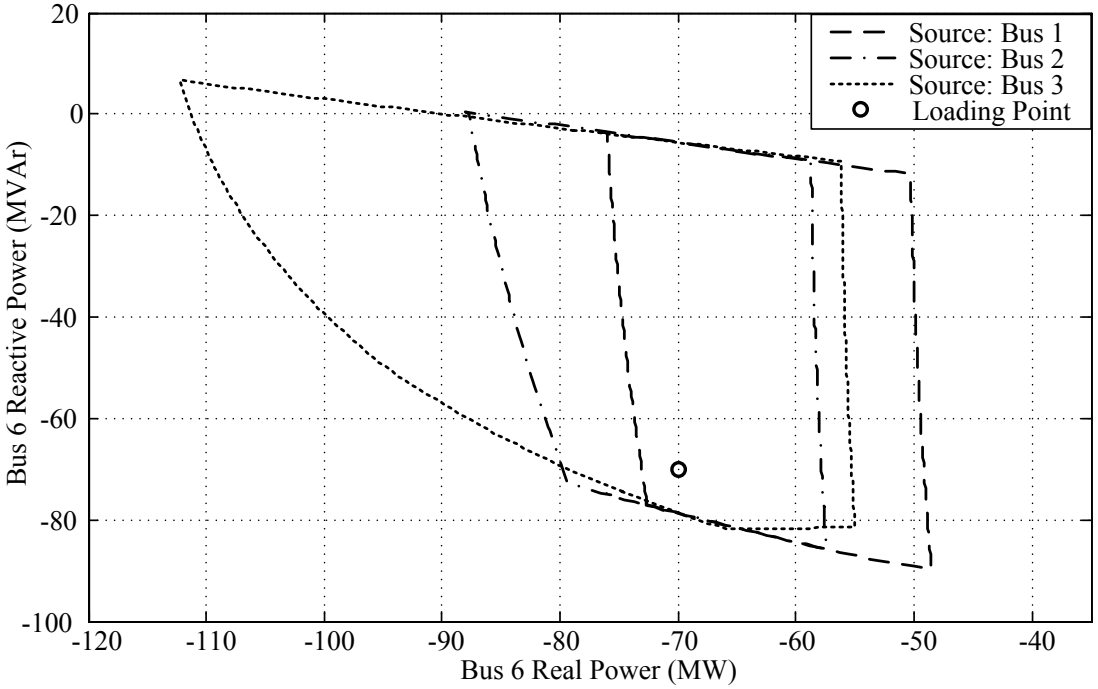


Figure 12.4 TTCR of bus 6 (6-bus system)

The information of all contours is shown in the table below. For bus 4, the largest maximum load is 110.97 MW by receiving the power form bus 2, and the highest feasibility belongs to a case of receiving the power from bus 1. For bus 5, the largest maximum load is 84.47 MW by receiving the power from bus 3, and the highest feasibility belongs to a case of receiving the power from bus 1. For bus 6, the largest maximum load and the highest feasibility belong to a case of receiving the power from bus 3. The average computational time is about 0.5 second/ point.

Table 12.2 Information of obtained TTCR (bus-to-bus)

| Case | Source Bus | Sink Bus | Maximum Load (MW) | Area (MW x MVAr) | Time (sec) | Points | Time/ Point (sec) |
|---|---|---|---|---|---|---|---|
| 1 | 1 | 4 | 88.01 | **6,389** | 177.28 | 339 | 0.523 |
| 2 | 2 | 4 | **110.97** | 4,455 | 145.35 | 294 | 0.494 |
| 3 | 3 | 4 | 96.22 | 3,036 | 137.23 | 264 | 0.520 |
| 4 | 1 | 5 | 75.05 | **2,801** | 132.10 | 259 | 0.510 |
| 5 | 2 | 5 | 78.77 | 1,706 | 117.23 | 236 | 0.497 |
| 6 | 3 | 5 | **84.47** | 2,245 | 123.55 | 232 | 0.533 |
| 7 | 1 | 6 | 76.42 | 1,875 | 116.80 | 210 | 0.556 |
| 8 | 2 | 6 | 88.07 | 1,883 | 104.17 | 211 | 0.494 |
| 9 | 3 | 6 | **112.22** | **3,193** | 121.39 | 248 | 0.489 |

### 12.1.2 TTCR of Area-to-Area Transfer (Six-Bus System)

This section considers the problem of power transfer between areas. The first scenario defines a source area consisting of bus 1 and bus 2, a sink area consisting of bus 4 and bus 6. With the same contingencies as the previous section, the boundary of TTCR is determined with a gap $d$=1 MVA, and a step size $l$=2 MVA. The result of TTCR is illustrated in the figure below with four feasible regions from cases of contingencies and base case. In the figure, the obtained TTCR is an intersection of all considered cases. The maximum loading points of TTC obtained by the conventional repeated power flow are also shown in this figure. It can be observed that all maximum loading points are on the boundary of TTCR.

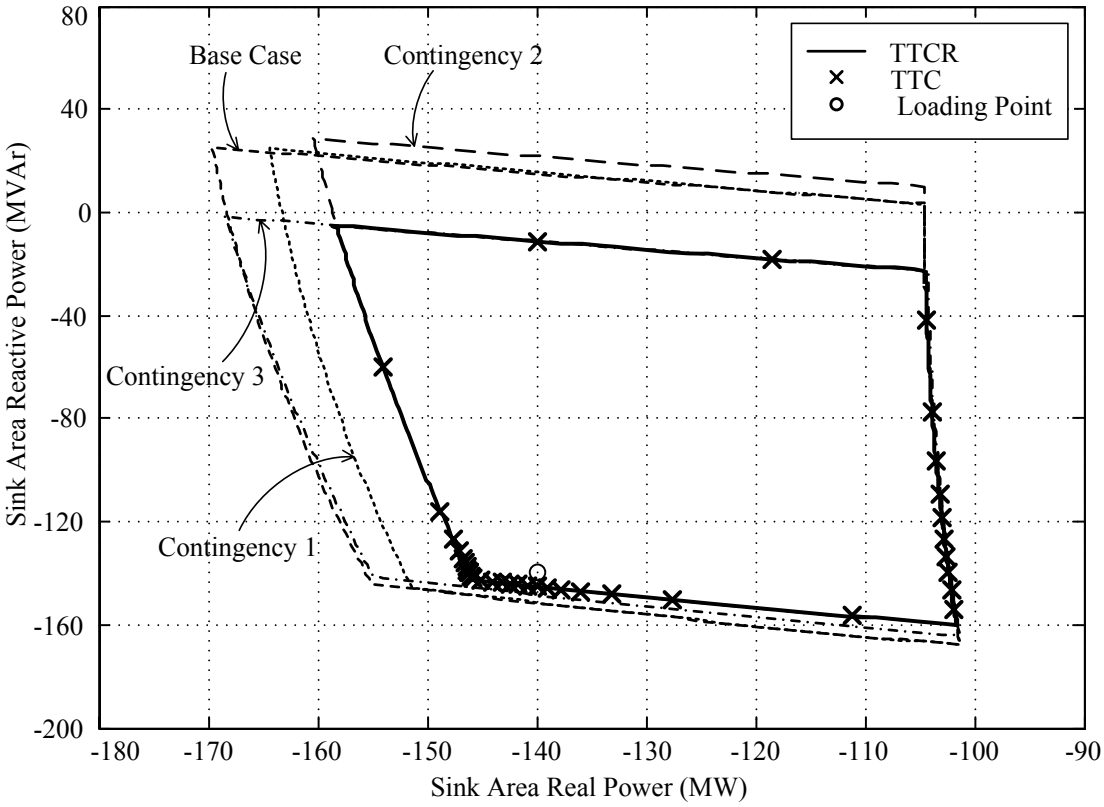


Figure 12.5 TTCR compared to feasible regions and TTC

(Source: Bus 1, Bus 2 / Sink: Bus 4, Bus 6)

The computational time is shown in the table below. A result is resemble to a result in the previous section. The computational time of TTCR boundary tracing is about 10.3% less than the total computational time of all contingencies and base case. The TTCR boundary tracing spends more average computational time per solution point than the ordinary feasible region tracing.

Table 12.3 Computational time of boundary tracing process (bus 1, 2 to bus 4, 5)

| Case | Time (sec) | Points | Time/Point (sec) |
|---|---|---|---|
| Base Case | 29.90 | 238 | 0.126 |
| Contingency 1 | 29.44 | 233 | 0.126 |
| Contingency 2 | 28.37 | 228 | 0.124 |
| Contingency 3 | 28.29 | 207 | 0.137 |
| **Total** | **116.00** | | |
| **TTCR** | **104.05** | 193 | 0.539 |

The following figures show several results of TTCR from many cases of source-sink pair.

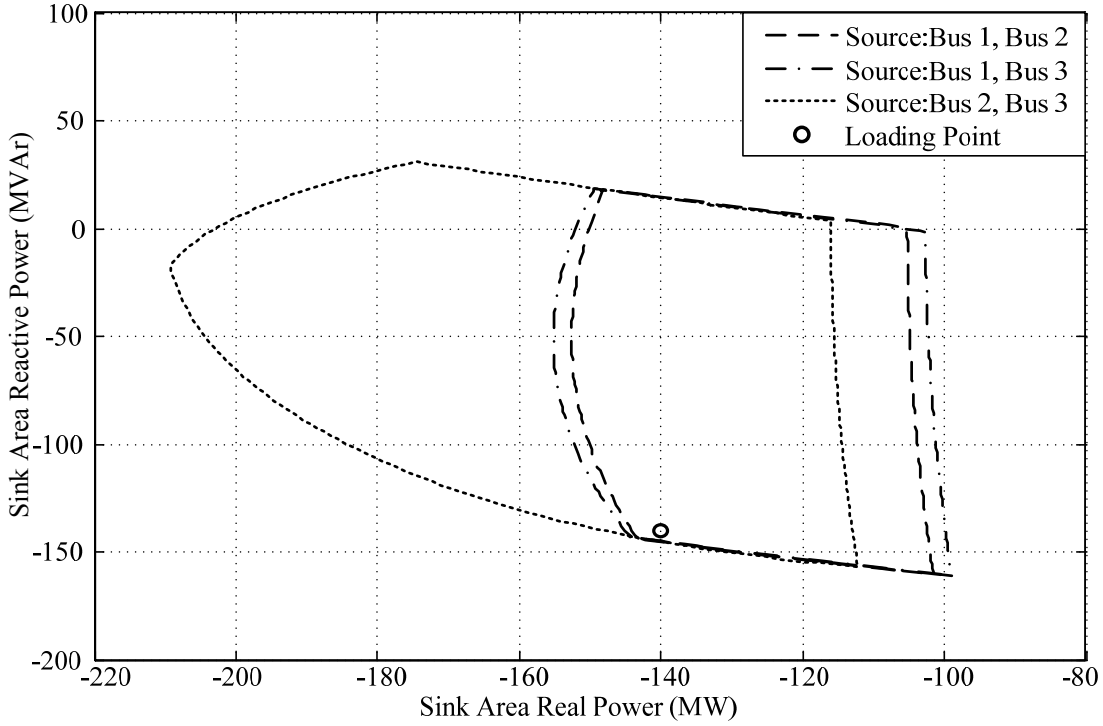


Figure 12.6 TTCR of sink area consisting of bus 4 and bus 5 (6-bus system)

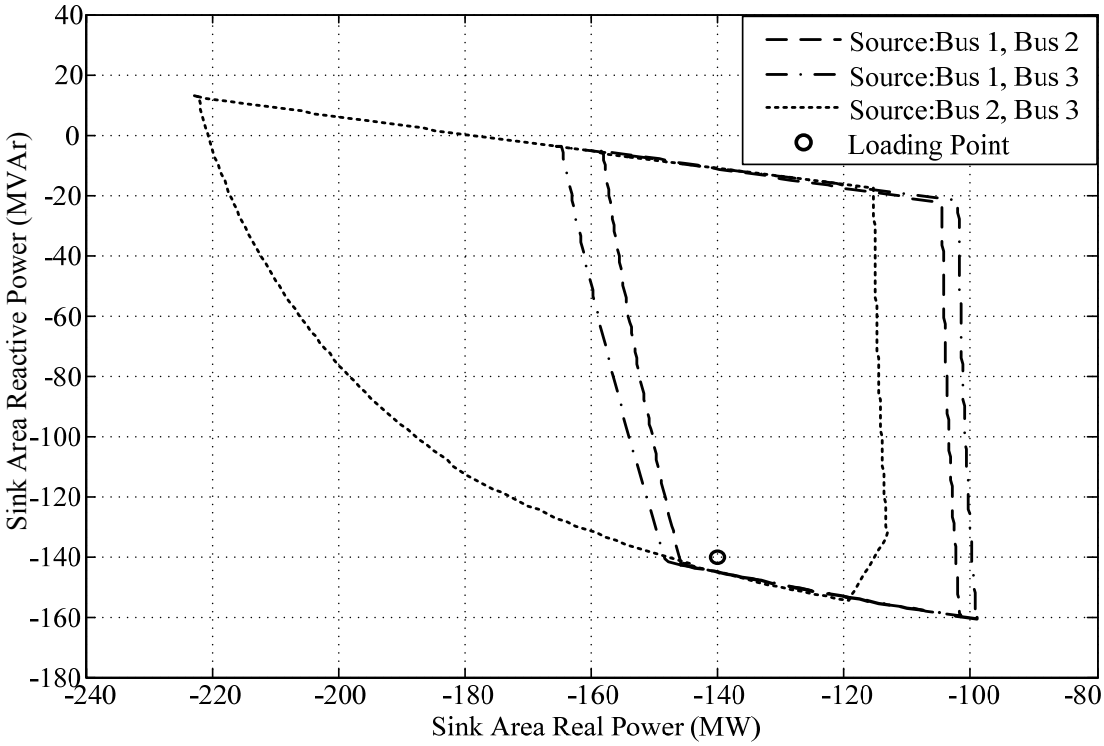


Figure 12.7 TTCR of sink area consisting of bus 4 and bus 6 (6-bus system)

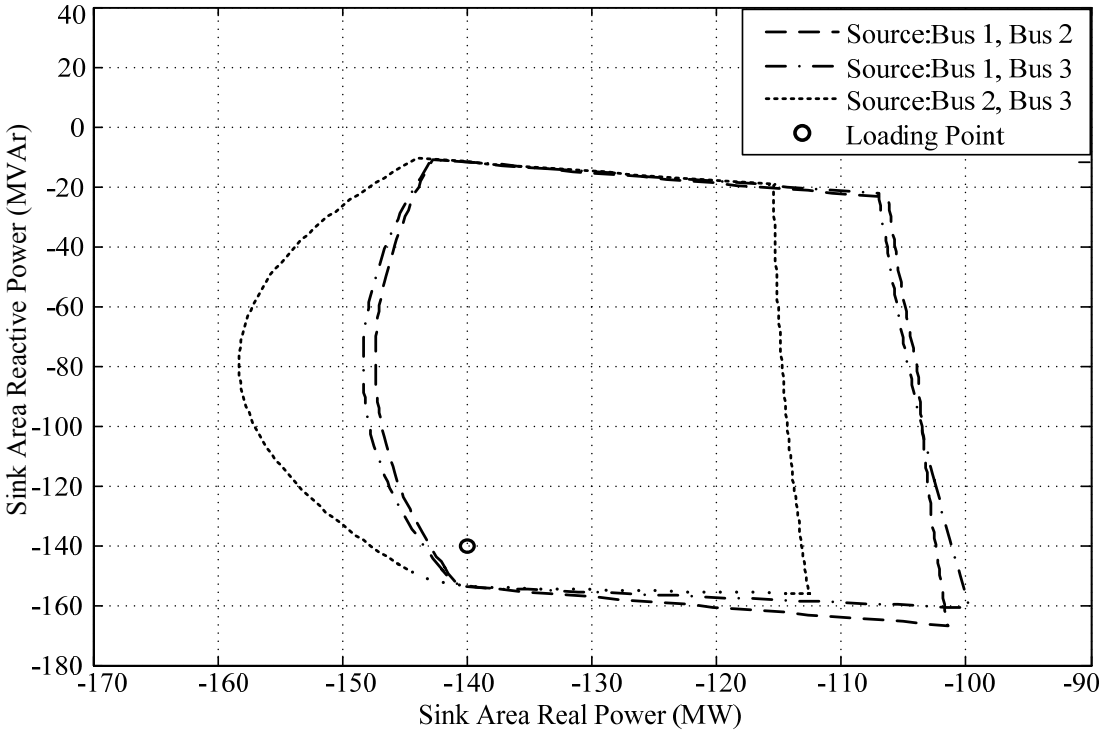


Figure 12.8 TTCR of sink area consisting of bus 5 and bus 6 (6-bus system)

The information of all feasible regions is shown in the table below. The largest maximum loading points belong to case 3, case 6 and case 9. The highest feasibility belongs to case 3, case 6, and case 8. The average computational time is around 0.5 second/point.

Table 12.4 Information of obtained TTCR (area-to-area)

| Case | Source Bus | Sink Bus | Maximum Load (MW) | Area (MW x MVAr) | Time (sec) | Points | Time/ Point (sec) |
|---|---|---|---|---|---|---|---|
| 1 | 1, 2 | 4, 5 | 152.63 | 7,397 | 114.09 | 211 | 0.541 |
| 2 | 1, 3 | 4, 5 | 155.20 | 8,136 | 128.87 | 214 | 0.602 |
| 3 | 2, 3 | 4, 5 | **209.26** | **12,652** | 124.01 | 237 | 0.523 |
| 4 | 1, 2 | 4, 6 | 158.67 | 6,637 | 104.05 | 193 | 0.539 |
| 5 | 1, 3 | 4, 6 | 165.53 | 7,620 | 111.30 | 203 | 0.548 |
| 6 | 2, 3 | 4, 6 | **222.98** | **11,550** | 127.75 | 233 | 0.548 |
| 7 | 1, 2 | 5, 6 | 147.36 | 5,914 | 111.22 | 186 | 0.598 |
| 8 | 1, 3 | 5, 6 | 148.37 | **5,932** | 112.61 | 184 | 0.612 |
| 9 | 2, 3 | 5, 6 | **158.28** | 5,460 | 88.38 | 176 | 0.502 |

## 12.2 TTCR with IEEE 24-Bus Test System

In this section, the TTCR boundary tracing method is implemented on IEEE 24-bus system. The considered contingencies in this simulation are line outages on branch 2, 21, 22, and 5. For the power transfer from area 3 to area 2, feasible regions of contingencies and base case are shown in Figure 12.9. An intersection of feasible regions is TTCR. By using the proposed TTCR boundary tracing method with a gap $d$=1 MVA and a step size $l$=10 MVA, a boundary of TTCR is determined, and the information of computational time is shown in Table 12.5.

Table 12.5 Computational time of boundary tracing process (area 3 to area 2)

| Case | Time (sec) | Points | Time/Point (sec) |
|---|---|---|---|
| Base Case | 182.04 | 214 | 0.851 |
| Contingency 1 | 175.45 | 210 | 0.835 |
| Contingency 2 | 160.94 | 208 | 0.774 |
| Contingency 3 | 184.03 | 222 | 0.829 |
| Contingency 4 | 79.40 | 133 | 0.597 |
| **Total** | **781.86** | | |
| **TTCR** | **423.28** | 132 | 3.207 |

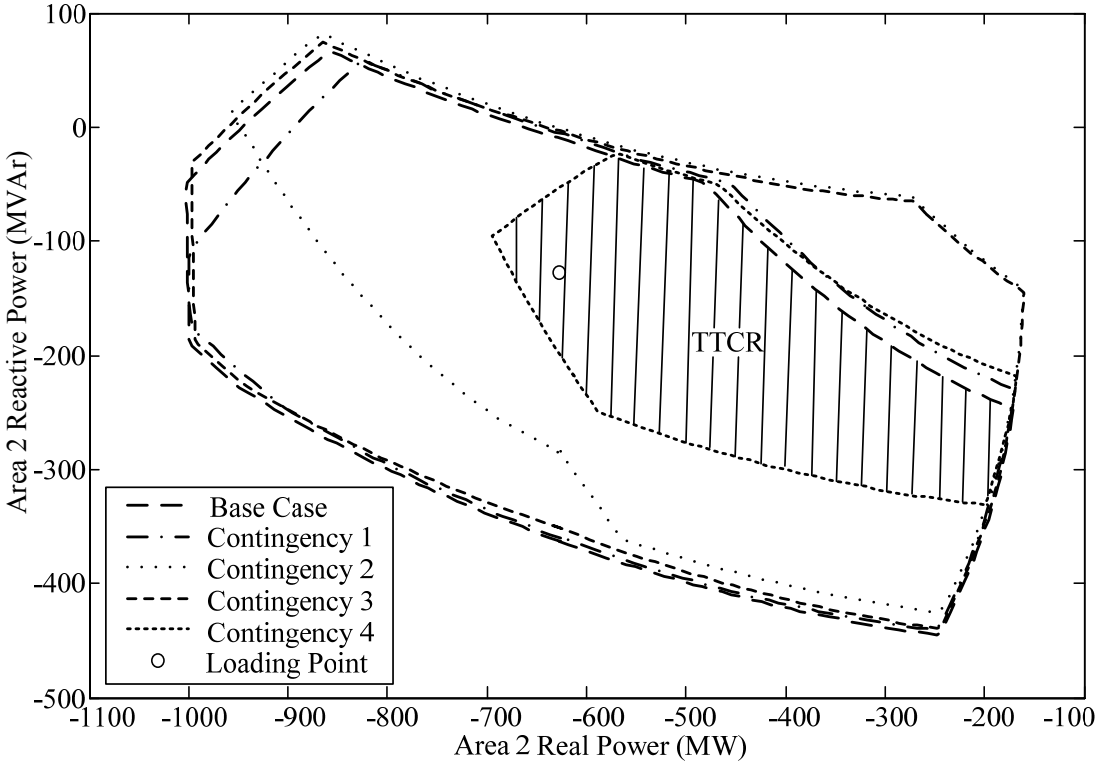


Figure 12.9 Feasible regions of power transfer from area 3 to area 2 with contingencies (IEEE-24 bus system)

The total computational time of all cases of feasible regions is 781.86 second, and the computational time of TTCR tracing process is less than the total time about 6 minute (358 second).

The next simulation will show differences between feasible region and TTCR with several transfer scenarios. The first test treats area 1 as a sink area. For each source-sink pair, the contour of TTCR from several cases is compared to the base case feasible region, as shown in the following figures.

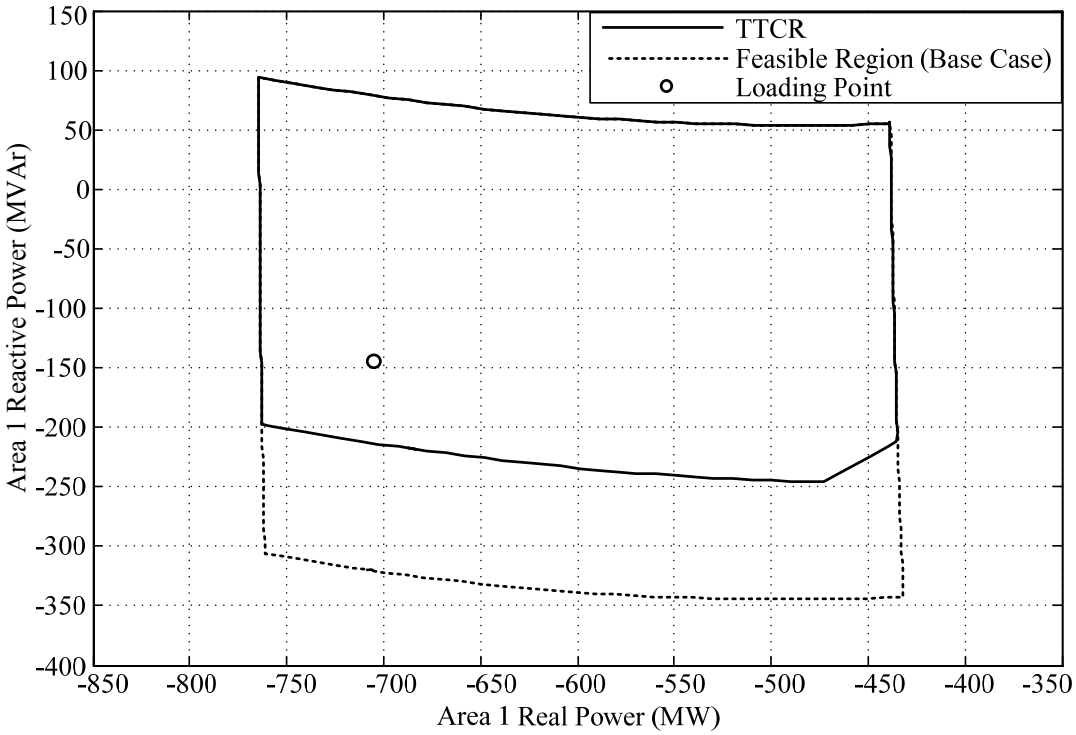


Figure 12.10 TTCR and feasible region of power transfer from area 2 to area 1 (IEEE-24 bus system)

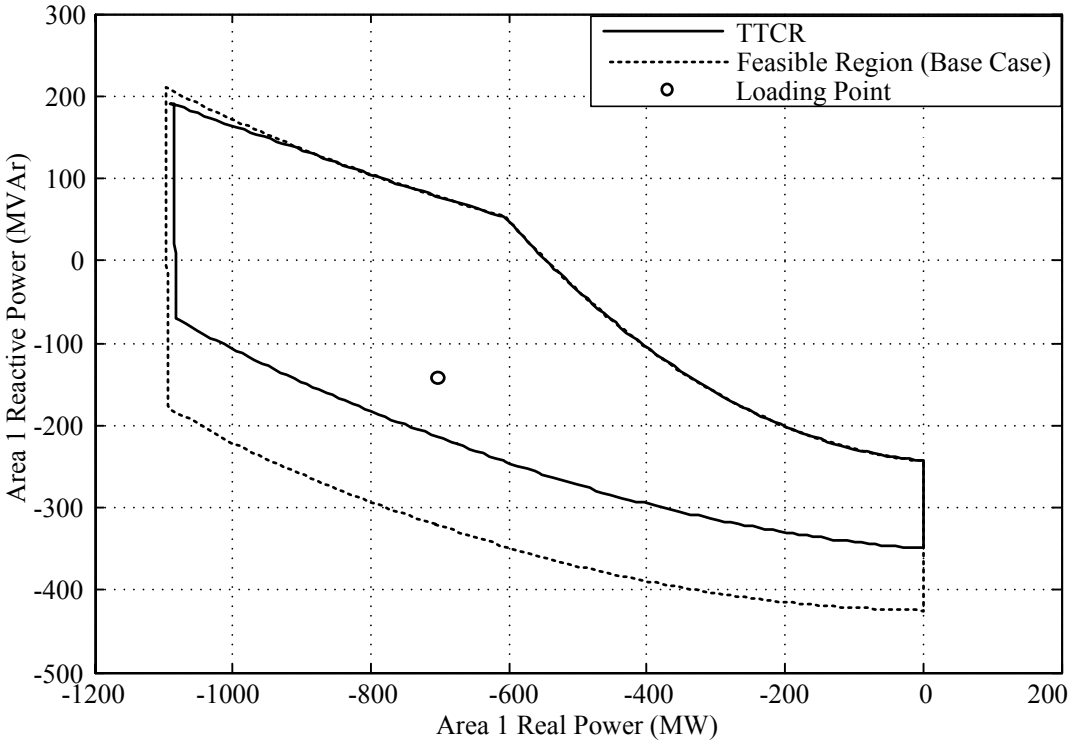


Figure 12.11 TTCR and feasible region of power transfer from area 3 to area 1 (IEEE-24 bus system)

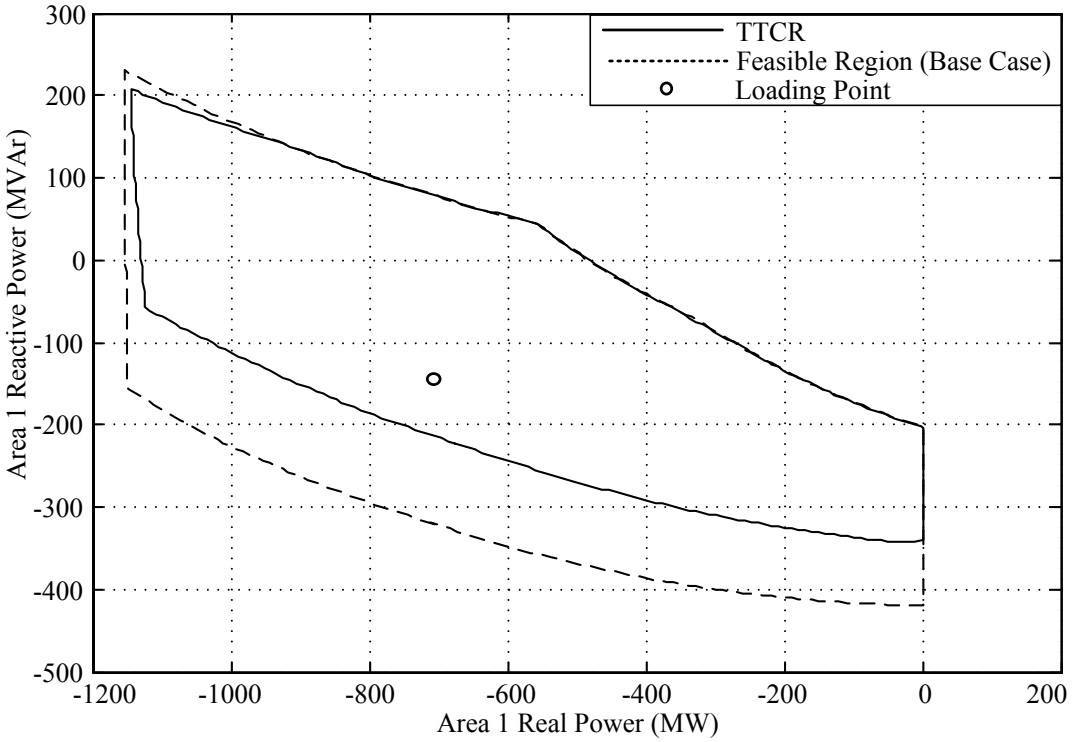


Figure 12.12 TTCR and feasible region of power transfer from area 2, 3 to area 1 (IEEE-24 bus)

The obtained TTCR contours of area 1 are compared in the figure below.

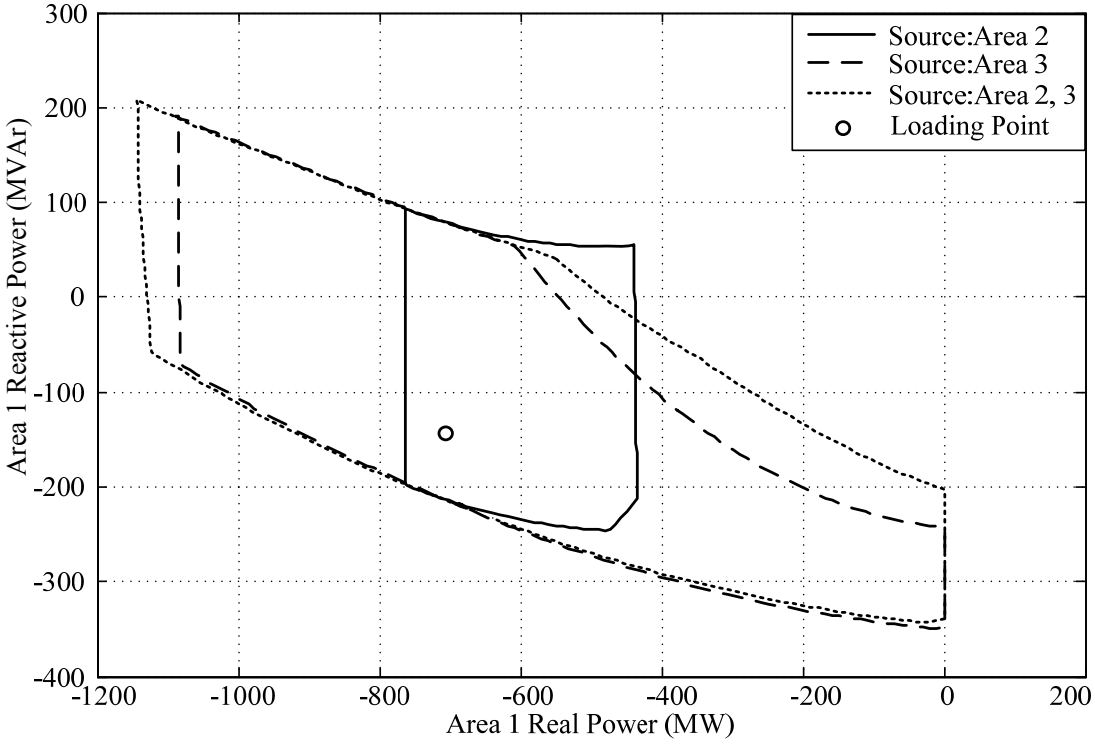


Figure 12.13 TTCR of area 1 (IEEE 24-bus system)

By the same way, the next simulation considers the load in area 2. The contours of TTCR from several cases are compared to the base case feasible regions, as shown in Figure 12.14-12.16. The contours of TTCR are compared in Figure 12.17. And, the information of all power transfer cases is shown in Table 12.6.

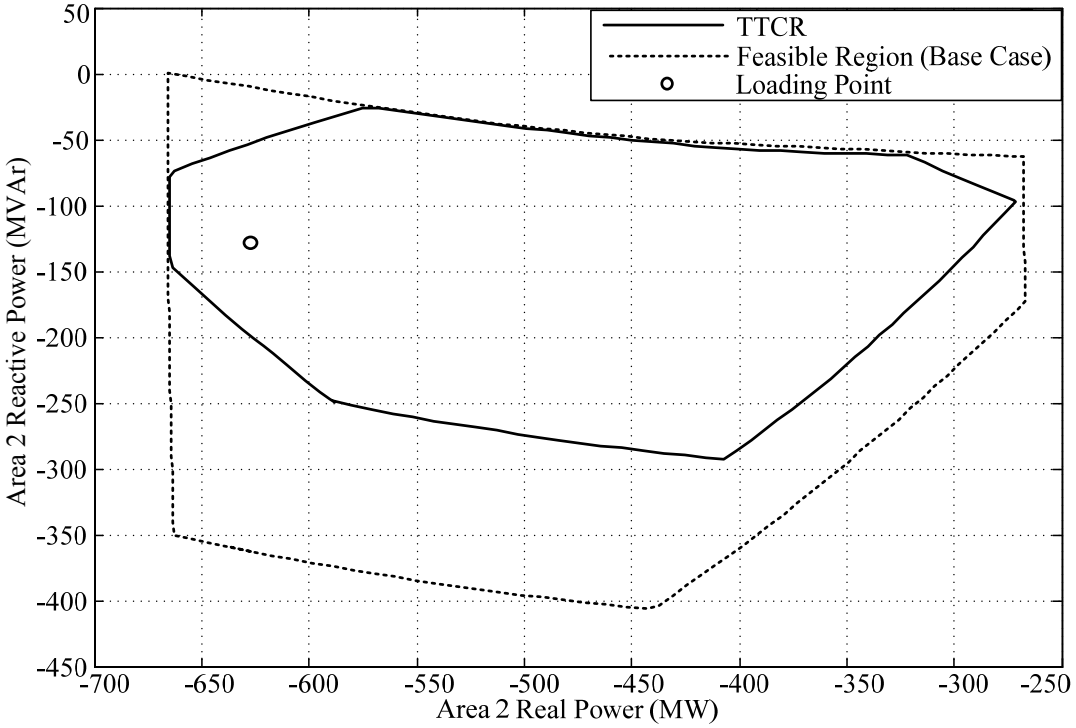


Figure 12.14 TTCR and feasible region of power transfer from area 1 to area 2 (IEEE-24 bus system)

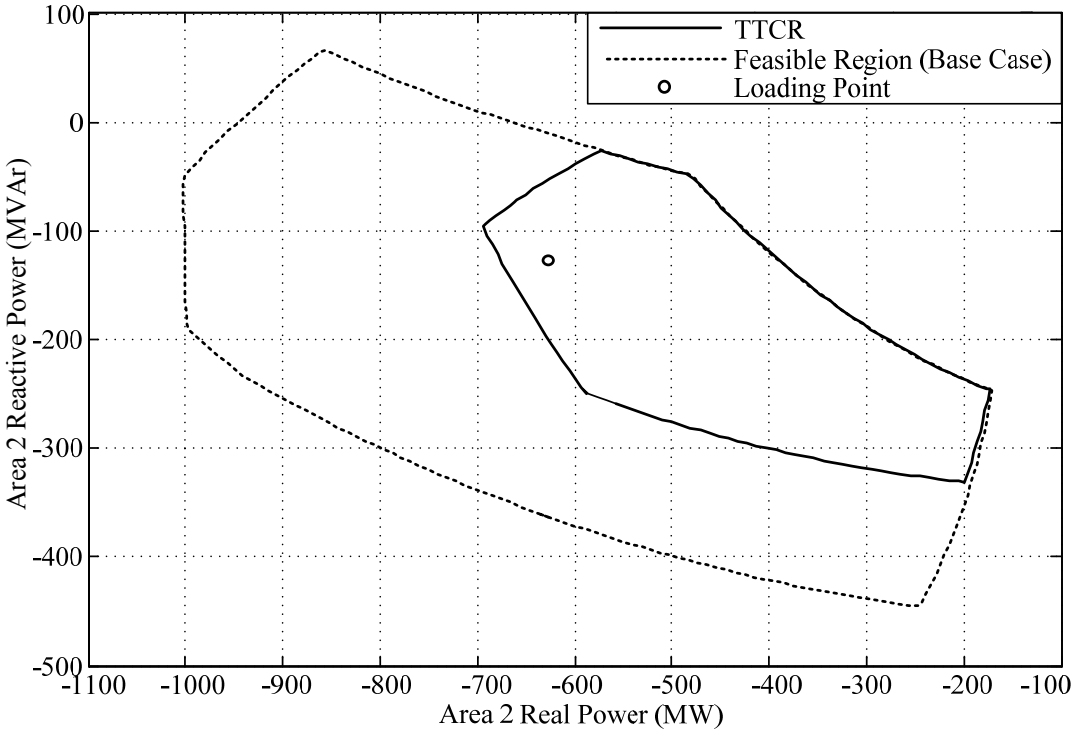


Figure 12.15 TTCR and feasible region of power transfer from area 3 to area 2 (IEEE-24 bus system)

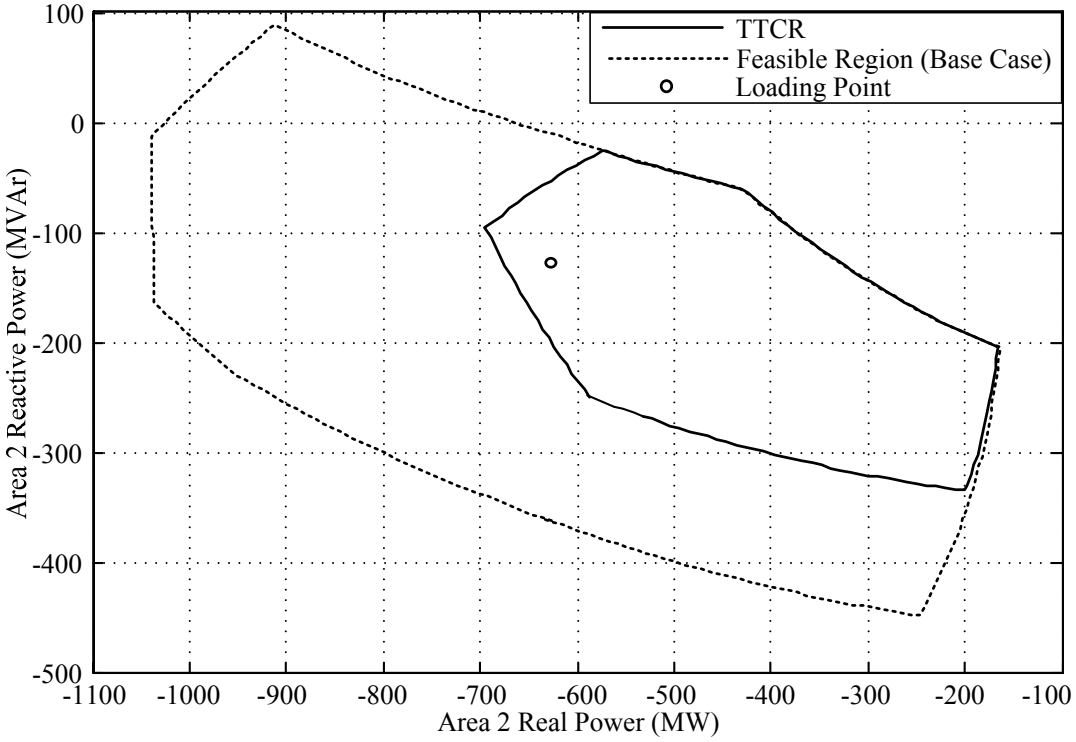


Figure 12.16 TTCR and feasible region of power transfer from area 1, 3 to area 2 (IEEE-24 bus system)

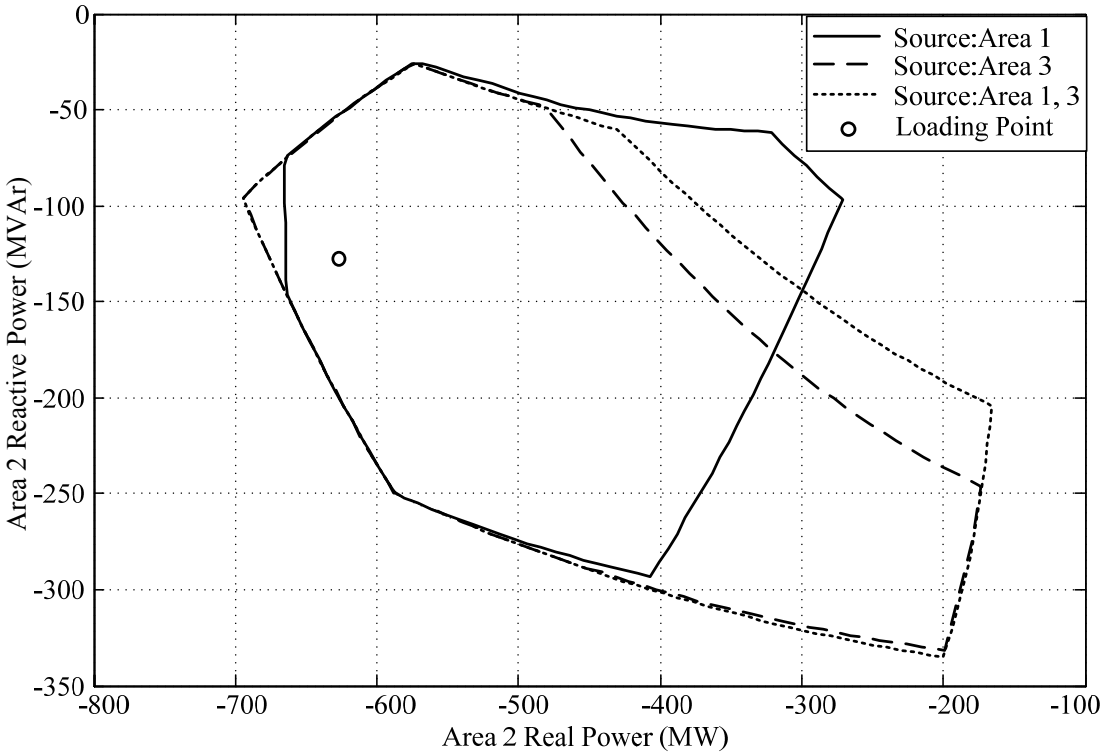


Figure 12.17 TTCR of area 2 (IEEE 24-bus system)

Table 12.6 TTCR information (IEEE 24-bus system)

| Case | Source Area | Sink Area | Maximum Load (MW) | Closed Area (MW x MVAr) | Time (sec) | Points | Time/ Point (sec) |
|---|---|---|---|---|---|---|---|
| 1 | 2 | 1 | 764 | 95,974 | 325.80 | 128 | 2.545 |
| 2 | 3 | 1 | 1,089 | 238,633 | 1198.42 | 272 | 4.406 |
| 3 | 2,3 | 1 | 1,145 | 284,421 | 1525.18 | 282 | 5.408 |
| 4 | 1 | 2 | 665 | 71,641 | 296.90 | 108 | 2.749 |
| 5 | 3 | 2 | 694 | 81,505 | 423.28 | 132 | 3.207 |
| 6 | 1,3 | 2 | 695 | 94,152 | 456.49 | 135 | 3.381 |

For area 1, the maximum load is not too much affected from contingencies. On the other hand, the maximum load of area 2 is decreased from the base case due to the considered contingencies. For the obtained TTCR, the maximum load of area 1 and area 2 belong to the case of receiving load from area 3. The additional source area in case 3 leads to an increment of maximum load and an increment of feasibility about 5% and 19.2% from case 2, respectively. The additional source area in case 6 does not give more available real power, but give more feasibility about 15.5% from case 5.

## 12.3 Conclusion

The illustration of TTCR boundary tracing is done in this chapter. The result in this chapter shows that the obtained TTCR is an intersection of all considered contingency cases (including base case). Morover, in order to show the robustness of the proposed TTCR boundary tracing method, many contours of TTCR from several cases of source-sink pair are determined using two test systems, i.e. six-bus test system, and IEEE 24-bus test system. The result also shows that the proposed TTCR boundary tracing method can be properly determined. The obtained TTCR can be used as the information for system operators.

# CHAPTER XIII

# NUMERICAL RESULTS: REACTIVE POWER ENFORCEMENT

This chapter illustrates the proposed boundary tracing method when the reactive power limit is enforced. The reactive power enforcement leads to an expansion of load feasible region due to an allowance of voltage variation at the generator side when reaching reactive power limits. The modified algorithm with reactive power enforcement is implemented on the six-bus test system and the IEEE 24-bus test system in this chapter.

## 13.1 Reactive Power Enforcement with Six-Bus Test System

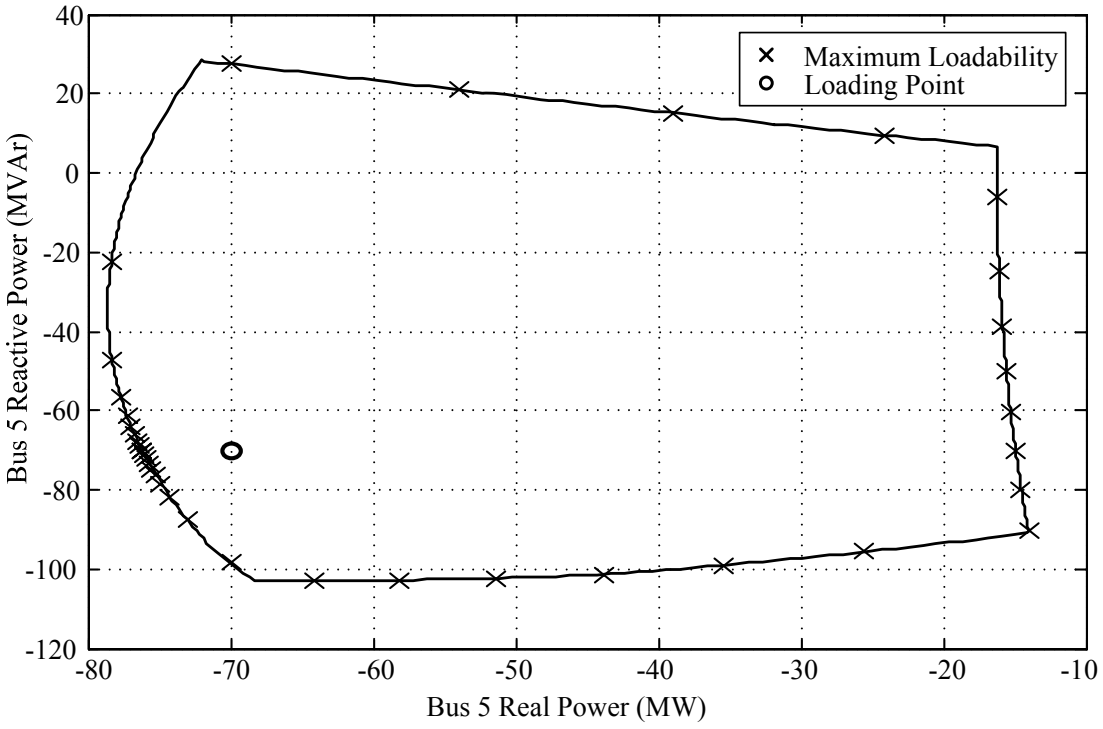


Figure 13.1 Feasible region of power transfer from bus 1 to bus 5 and maximum loading points with reactive power limit enforcement (6-bus system)

According to results from the six-bus system, the reactive power limits are active for the bus-to-bus transfer scenarios of bus 1 to bus 5, bus 2 to bus 5, bus 3 to bus 5, and bus 3 to bus 6. For this simulation, the boundary tracing algorithm is implemented with the reactive power enforcement, as described in Chapter 9. A gap and a step size for this

test are set to be 0.1 MVA and 1 MVA, respectively. In Figure 13.1, a result of power transfer from bus 1 to bus 5 is checked by 36 maximum loading points obtained by RPF which is also run using the reactive power enforcement in every steps of power flow calculation. A result shows that an obtained boundary is consistent with maximum loading points from RPF.

In order to show differences of result for with and without reactive power enforcement, two feasible regions traced by the normal mode and the reactive power enforcement mode are compared. For the power transfer from bus 1 to bus 5, the modified tracing algorithm with reactive power enforcement spends 54.2 second in order to determine 350 boundary points. An average time per point is 0.15 second/point. An obtained feasible region is compared to the feasible region obtained by the normal algorithm, as shown in the figure below.

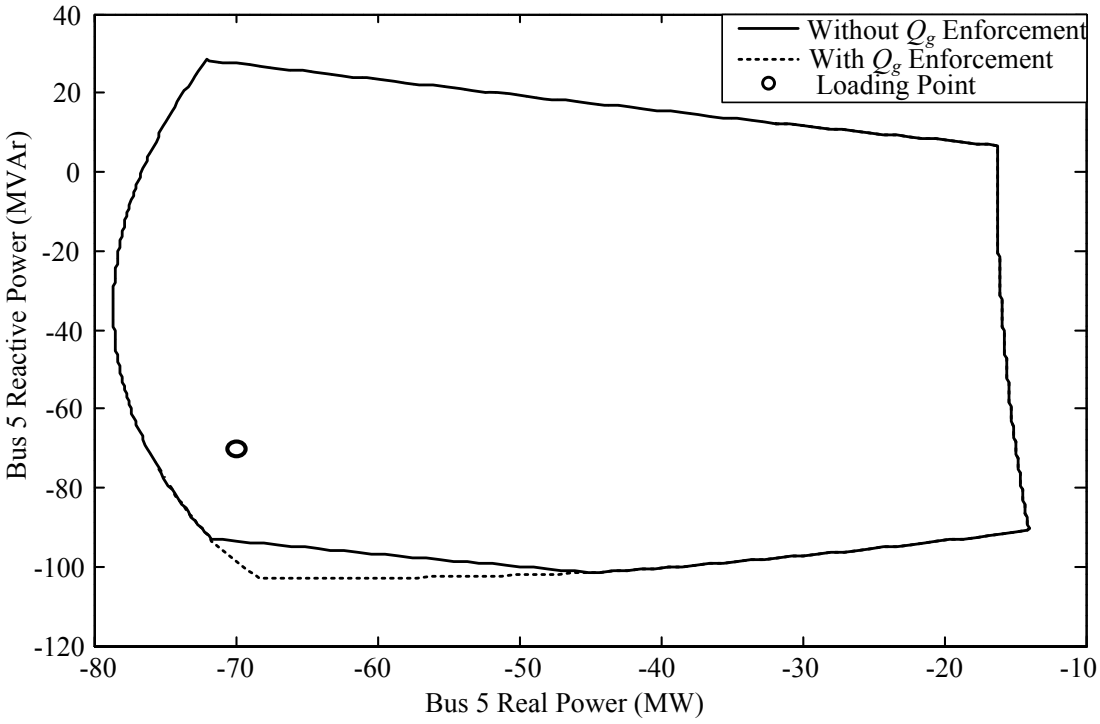


Figure 13.2 Feasible region of power transfer from bus 1 to bus 5 with reactive power enforcement (6-bus system)

For the power transfer from bus 2 to bus 5, the modified tracing algorithm with reactive power enforcement spends 47.78 second for determining 304 boundary points. An average time per point is 0.16 second/point. An obtained feasible region is compared to the feasible region without reactive power enforcement, as shown in the figure below.

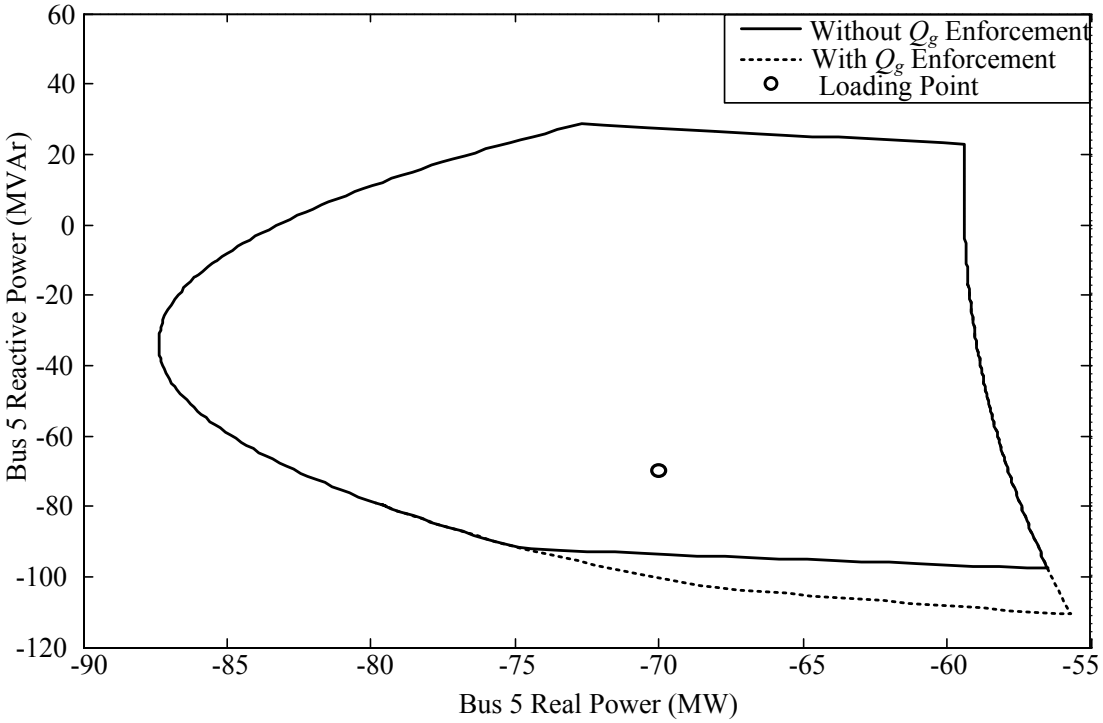


Figure 13.3 Feasible region of power transfer from bus 2 to bus 5 with reactive power enforcement (6-bus system)

For the power transfer from bus 3 to bus 5, the modified tracing algorithm with reactive power enforcement spends 50.67 second for determining 317 boundary points. An average time per point is 0.16 second/point. An obtained feasible region is compared to the feasible region without reactive power enforcement, as shown in Figure 13.4.

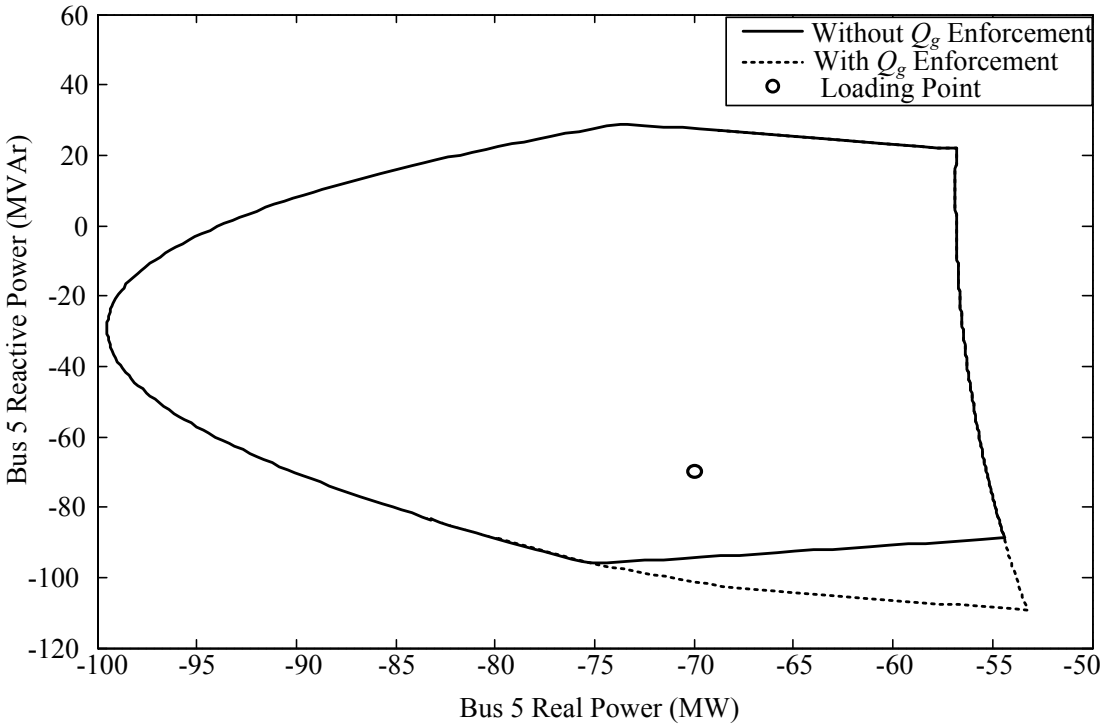


Figure 13.4 Feasible region of power transfer from bus 3 to bus 5 with reactive power enforcement (6-bus system)

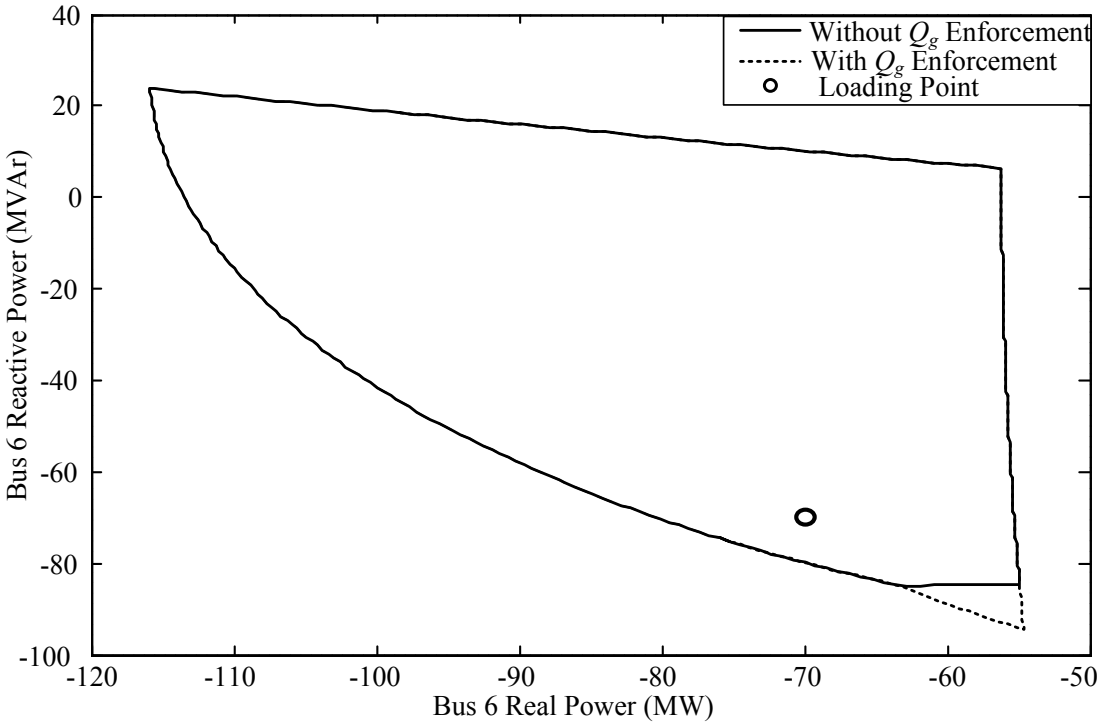


Figure 13.5 Feasible region of power transfer from bus 3 to bus 6 with reactive power enforcement (6-bus system)

For the power transfer from bus 3 to bus 6, the modified tracing algorithm with reactive power enforcement spends 43.94 second for determining 305 boundary points. An average time per point is 0.14 second/point. An obtained feasible region is shown in Figure 13.5.The results show that load feasible regions are expanded with the mode of reactive power enforcement. The expansions are different due to the transfer scenarios.

By the same way, the area-to-area transfer scenarios are also illustrated with the reactive power enforcement. The area-to-area power transfer scenarios with reactive power limits are illustrated in this simulation using the modified tracing process with a gap $d$=0.1 MVA and a step size $l$=5 MVA. When source area consists of bus 1, bus 3, and sink area consists of bus 5, bus 6, a feasible region of this scenario is obtained by the modified tracing algorithm. In Figure 13.6, an obtained feasible region with reactive power enforcement is checked with maximum loading points obtained by RPF method. A boundary is also consistent with maximum loading points.

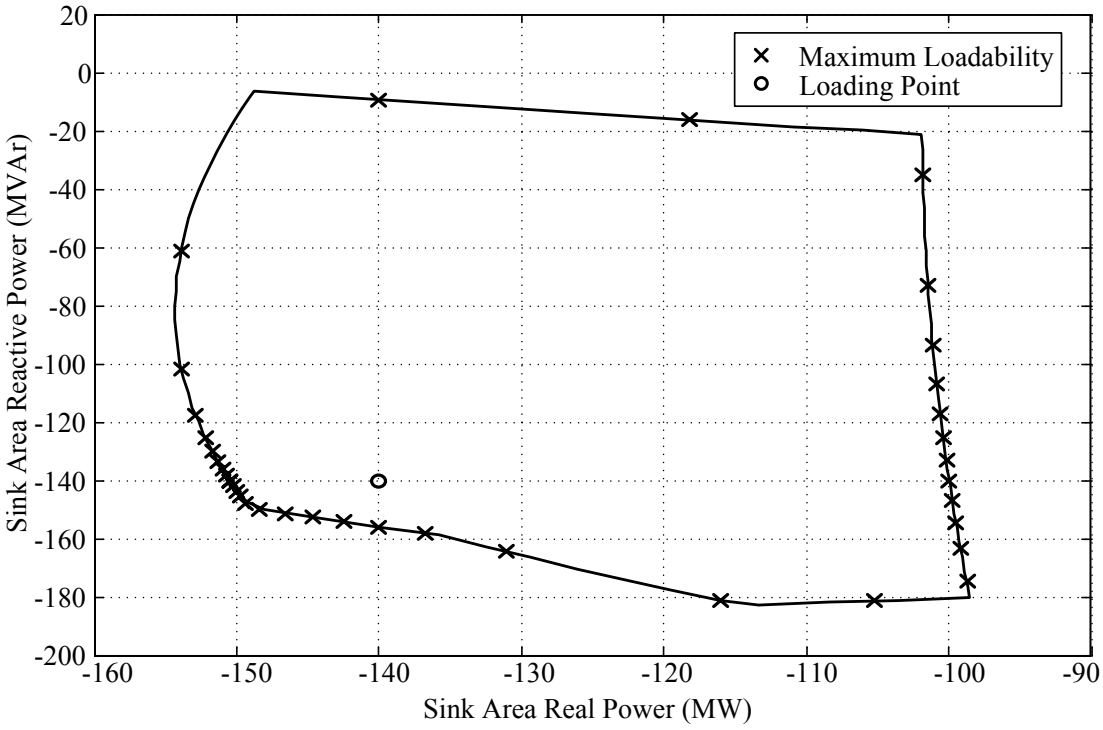


Figure 13.6 Feasible region and maximum loading points with reactive power limit enforcement (Source: Bus 1, Bus 3/ Sink: Bus 5, Bus 6/ 6-bus system)

A feasible region from the same scenario is compared to a feasible region obtained without reactive power enforcement, as shown in the figure below. The modified tracing process spends 16.55 second for 86 boundary points. The average time is 0.19 second/point.

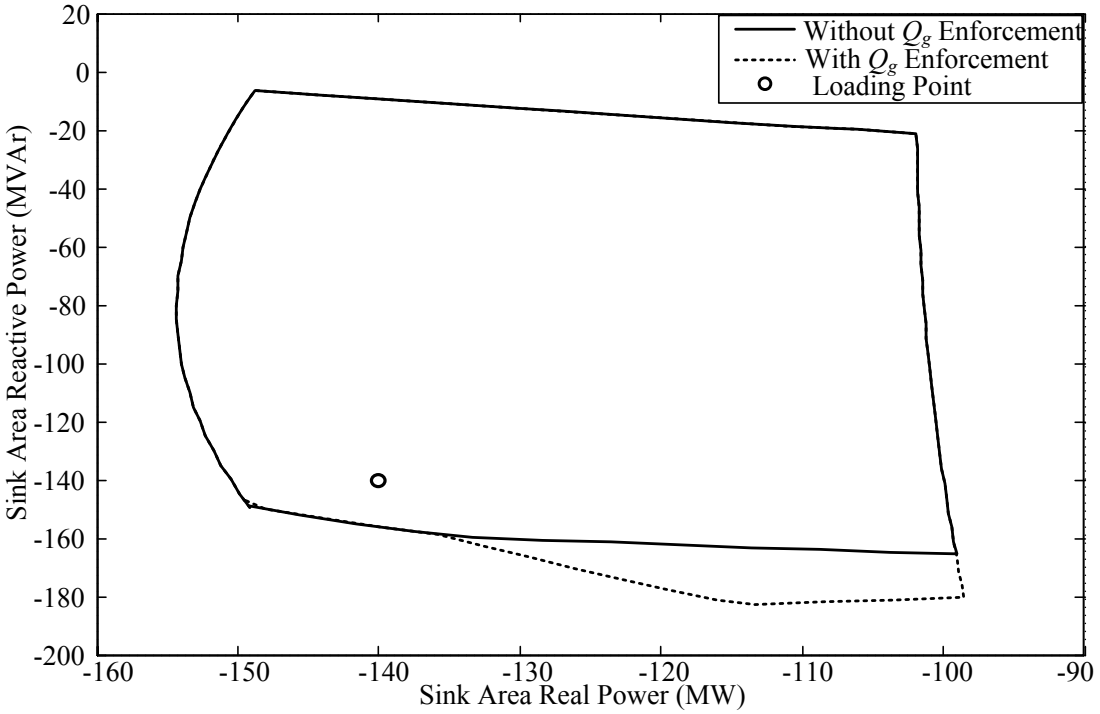


Figure 13.7 Feasible region with reactive power enforcement (Source: Bus 1, Bus 3/ Sink: Bus 5, Bus 6/6-bus system)

When source area consists of bus 1, bus 2 and sink area consists of bus 5, bus 6, the results of normal algorithm and modified algorithm are shown in Figure 13.8. The modified tracing process spends 15.28 second for 85 boundary points, the average time is 0.18 second/point.

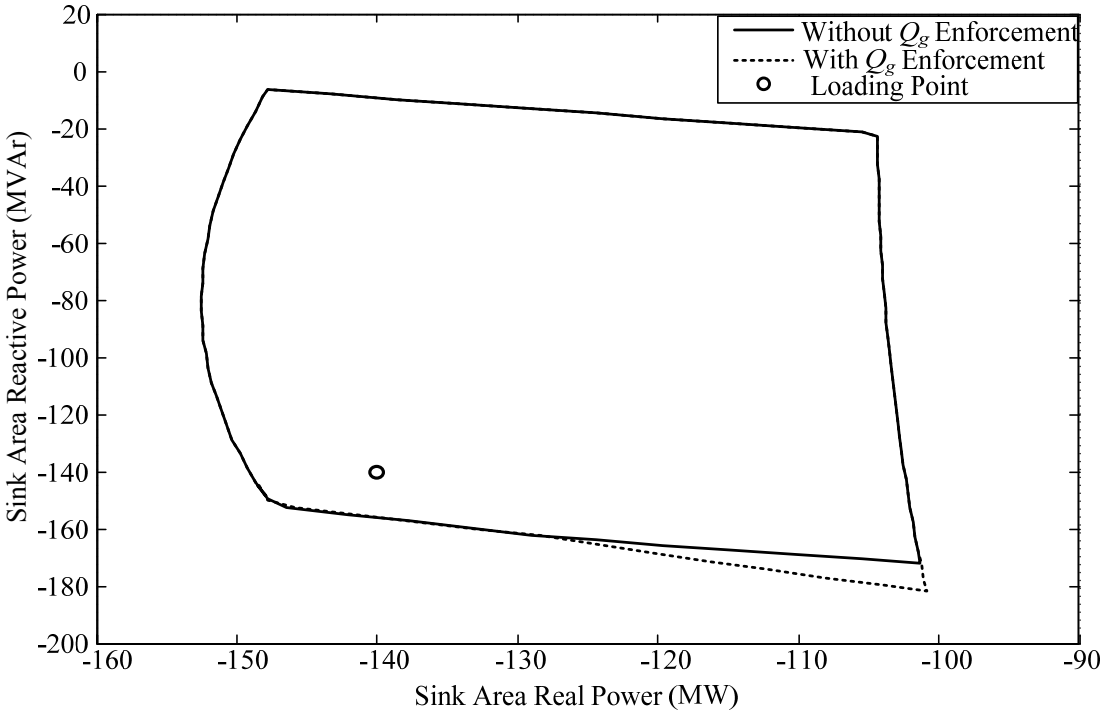


Figure 13.8 Feasible region with reactive power enforcement (Source: Bus 1, Bus 2/ Sink: Bus 5, Bus 6/ 6-bus system)

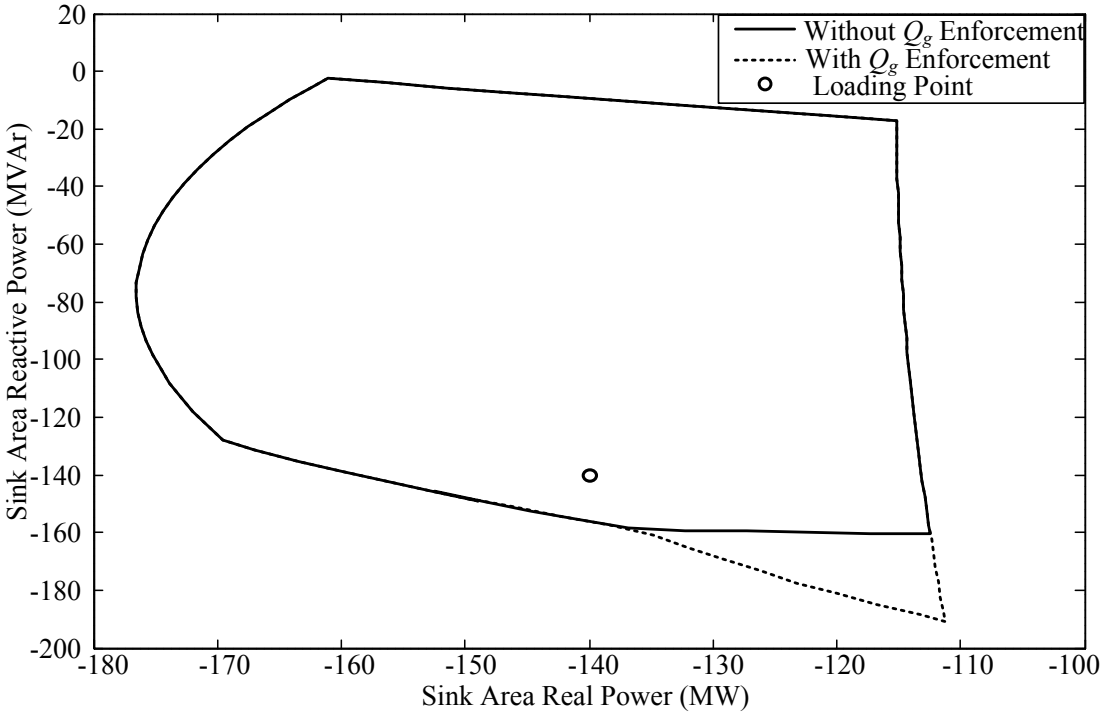


Figure 13.9 Feasible region with reactive power enforcement (Source: Bus 2, Bus 3/ Sink: Bus 5, Bus 6/6-bus system)

When source area consists of bus 2, bus 3 and sink area consists of bus 5, bus 6. The effect of reactive power enforcement is shown in Figure 13.9. The modified tracing process with reactive power enforcement spends 19.12 second for 90 boundary points, the average is 0.21 second/point.

Table 13.1 Comparison of closed area and computational time for feasible regions with reactive power enforcement (6-bus system)

| Source Bus | Sink Bus | Closed Area (MW*MVAr) | | | Computational Time (second/point) | | |
|---|---|---|---|---|---|---|---|
| | | Un-Enforced $Q_g$ | Enforced $Q_g$ | % Increase | Un-Enforced $Q_g$ | Enforced $Q_g$ | % Increase |
| 1 | 5 | 6,983 | 7,107 | 1.78 | 0.116 | 0.155 | 33.81 |
| 2 | 5 | 2,932 | 3,094 | 5.52 | 0.114 | 0.157 | 37.83 |
| 3 | 5 | 4,274 | 4,518 | 5.72 | 0.115 | 0.160 | 38.95 |
| 3 | 6 | 4,289 | 4,332 | 1.02 | 0.116 | 0.141 | 21.53 |
| 1, 2 | 5, 6 | 7,047 | 7,184 | 1.94 | 0.144 | 0.180 | 24.43 |
| 1, 3 | 5, 6 | 7,526 | 8,017 | 6.52 | 0.143 | 0.192 | 34.72 |
| 2, 3 | 5, 6 | 8,230 | 8,617 | 4.71 | 0.158 | 0.212 | 34.75 |

Table 13.1 shows differences between normal feasible regions and feasible regions with reactive power enforcement, for every transfer scenarios in this section. The reactive power enforcement leads to the expansion of feasible region. The area of feasible region is increases depending on considered transfer scenario. The modified algorithm spends more computational time than the normal algorithm about 20-37% for this simulation.

## 13.2 Reactive Power Enforcement with IEEE 24-Bus Test System

In this section, the modified boundary tracing algorithm with reactive power enforcement is implemented using the IEEE 24-bus system. The feasible regions of area 1 and area 2 with reactive power enforcement are determined and compared to the feasible regions obtained from the algorithm without reactive power enforcement. The tracing process uses a gap $d$=1 MVA and a step size $l$=10 MVA. The first case considers the power transfer from area 2 to area 1. The tracing process with reactive power enforcement spends 171 second for 161 boundary points, which is 1.07 second/point. An obtained feasible region is compared to a normal feasible region, as shown in the figure below.

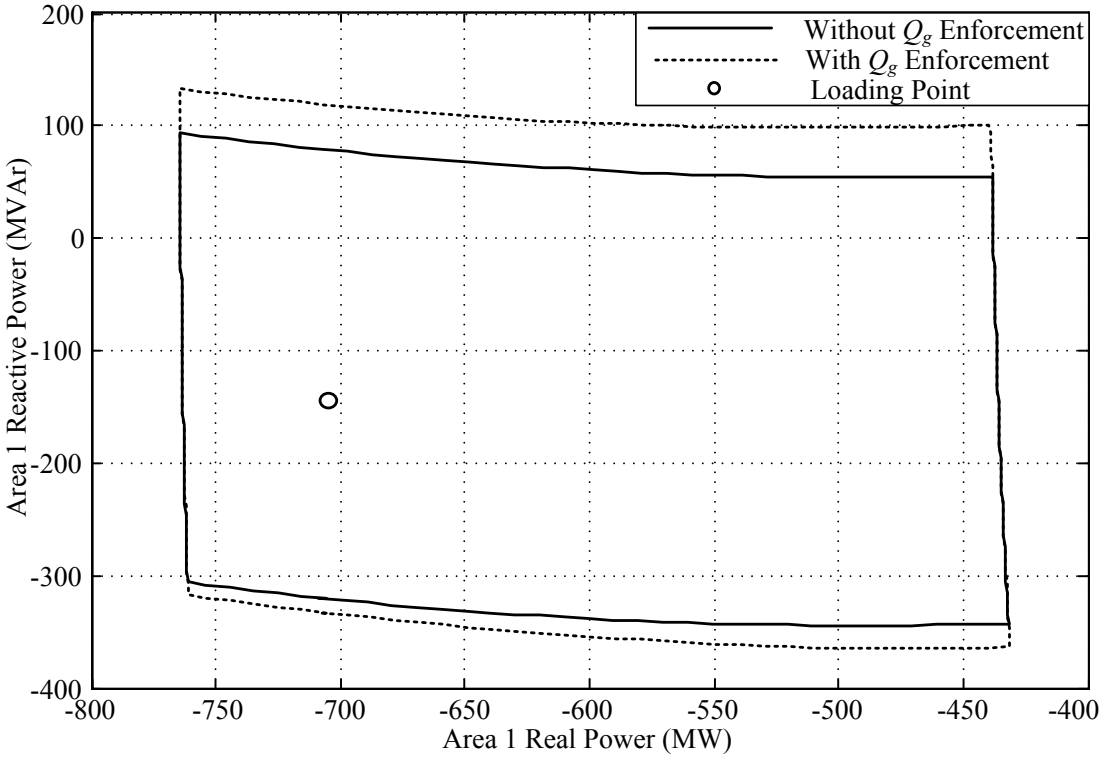


Figure 13.10 Feasible regions of power transfer from area 2 to area 1 with reactive power enforcement (IEEE 24-bus system)

For the case of power transfer from area 3 to area 1, the modified tracing algorithm spends 666 second for 319 boundary points, the average is 2.09 second/point. The final scenario is a sink area 1 receiving the power from a combined source area consisting of area 2 and area 3. The computational time is 753 second for 330 boundary points, the average time is 2.28 second/point. The obtained feasible regions are compared to the feasible regions without reactive power enforcement, as shown in Figure 13.11 and 13.12, respectively.

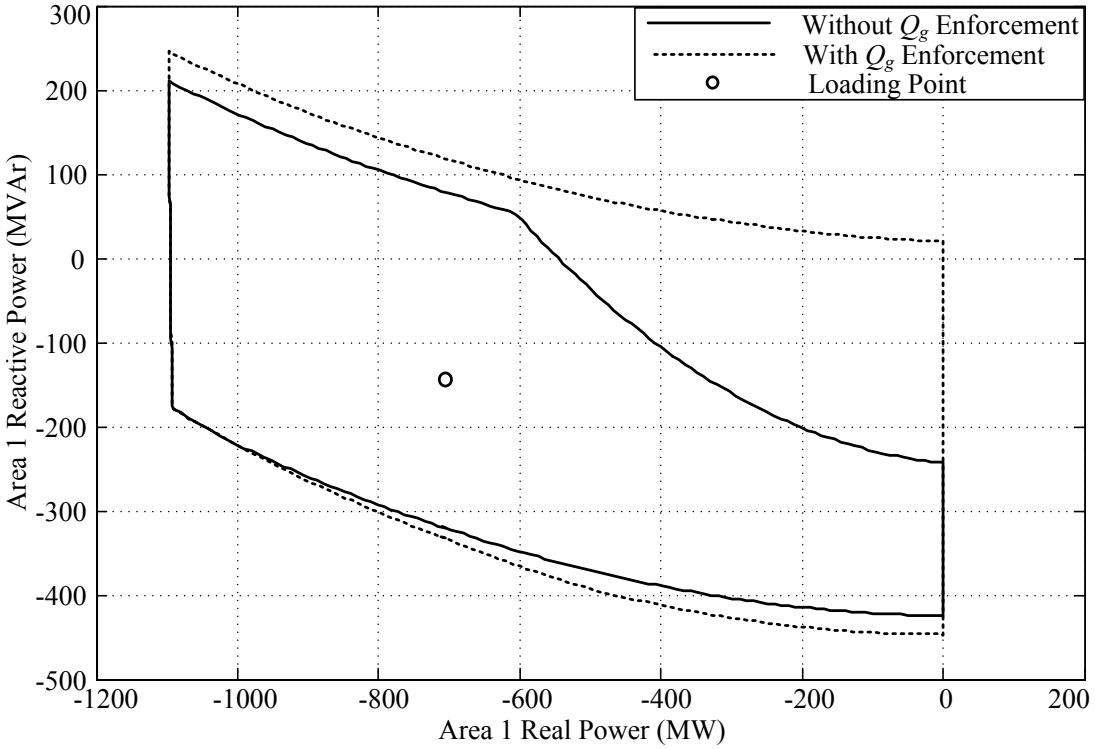


Figure 13.11 Feasible regions of power transfer from area 3 to area 1 with reactive power enforcement (IEEE 24-bus system)

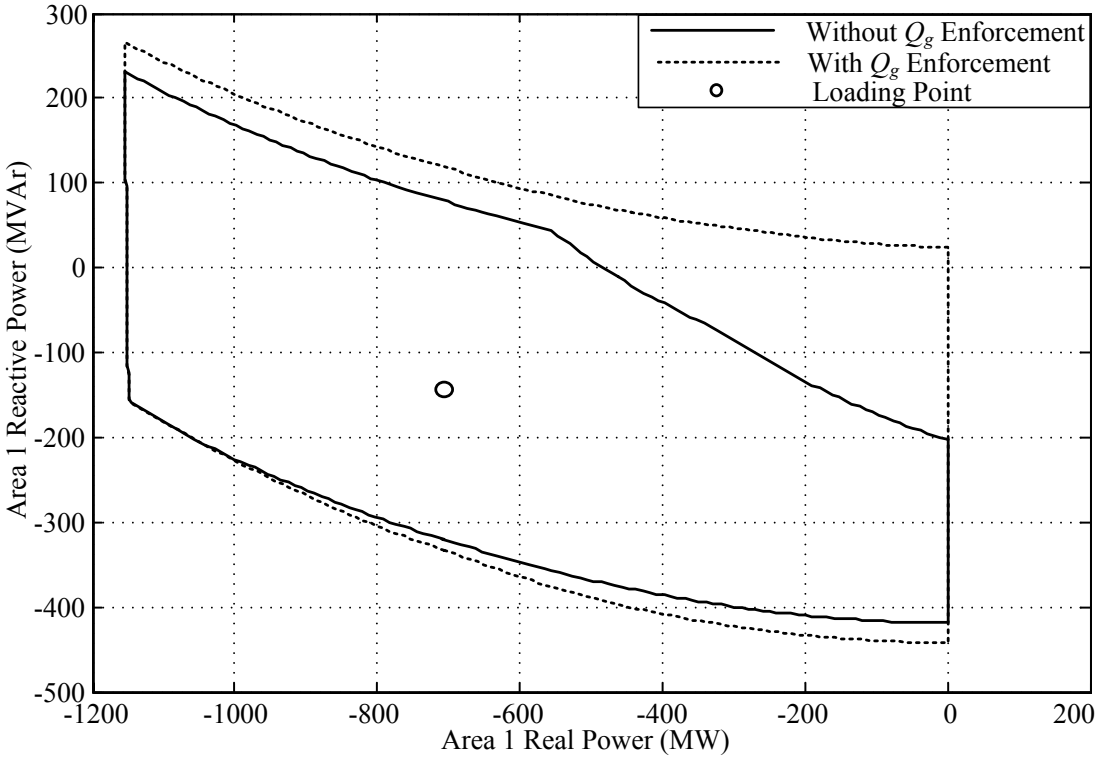


Figure 13.12 Feasible regions of power transfer from area 2, 3 to area 1 with reactive power enforcement (IEEE 24-bus system)

The next simulation treats area 2 as a sink area, and determines the feasible regions with reactive power limit enforcement. The tracing algorithm also uses a gap $d$=1 MVA and a step size $l$=10 MVA. The first scenario is the power transfer from area 1 to area 2. The modified tracing process spends 136 second for 150 boundary points, the average time is 0.91 second/point. The obtained region is compared to the normal feasible region, as shown in the figure below.

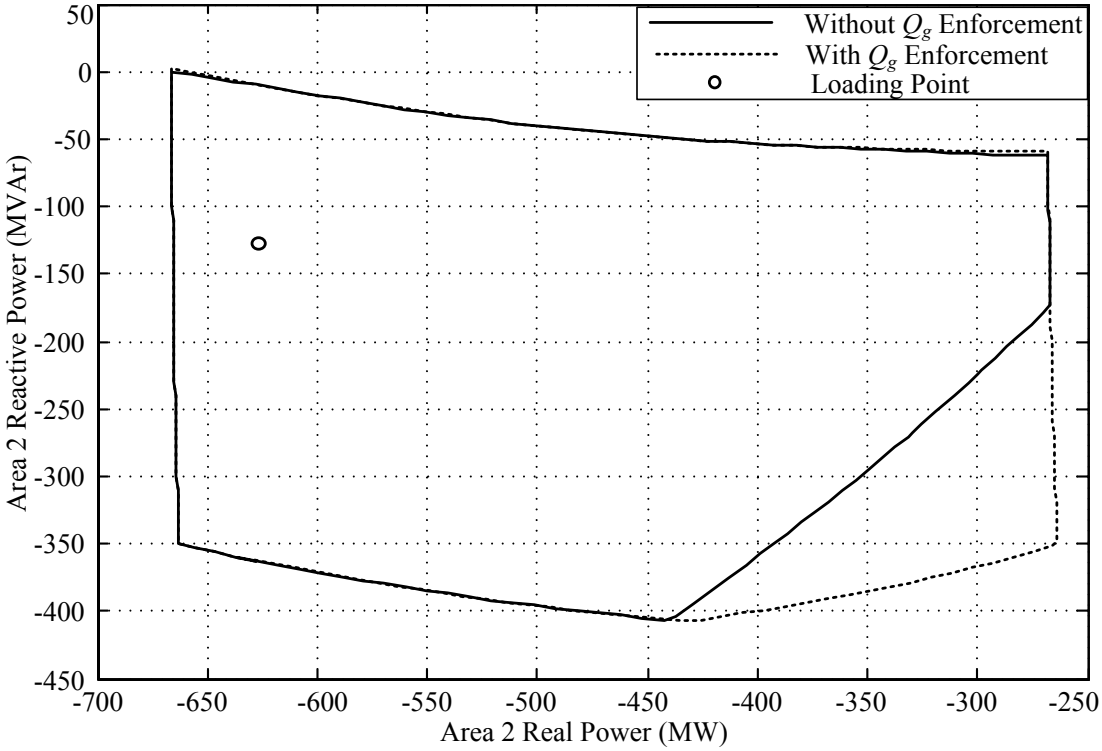


Figure 13.13 Feasible regions of power transfer from area 1 to area 2 with reactive power enforcement (IEEE 24-bus system)

When area 3 is a source area, the modified tracing process with reactive power enforcement spend 235 second for 227 boundary points, the average time is 1.04 second/point. The result is shown in Figure 13.14. Finally, when area 2 and area 3 supply power to area 2, the feasible region with reactive power enforcement is shown in Figure 13.15. The computational time is 302 second for 236 boundary points, the average time is 1.28 second/point.

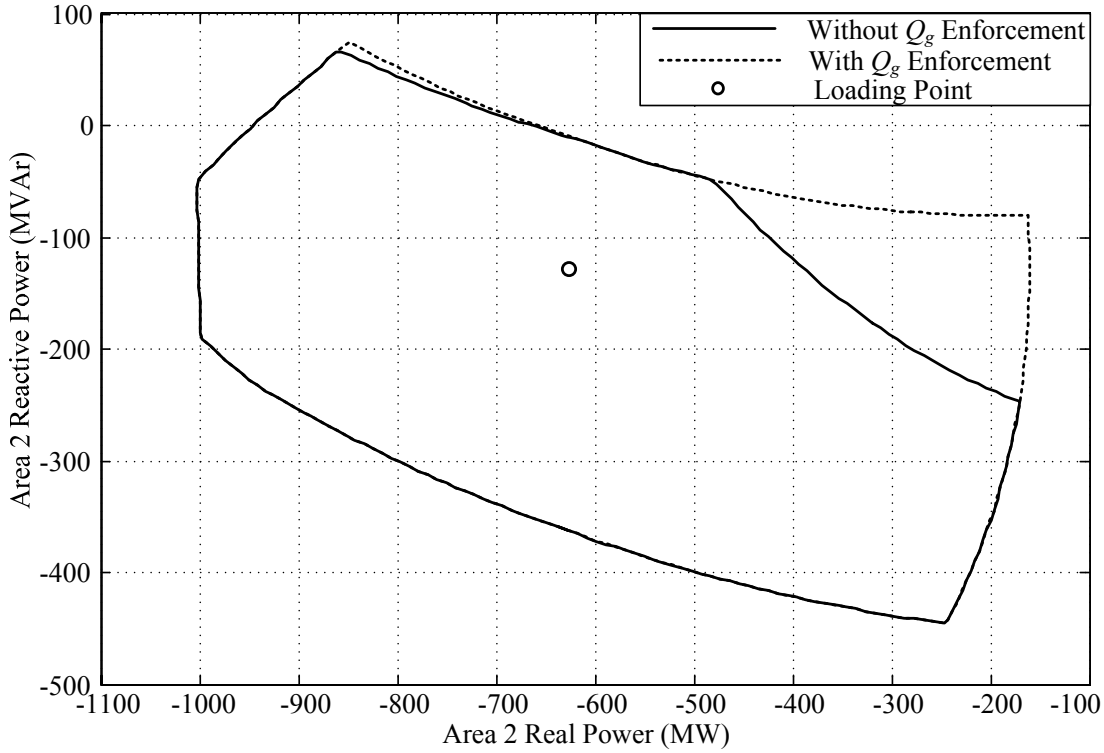


Figure 13.14 Feasible regions of power transfer from area 3 to area 2 with reactive power enforcement (IEEE 24-bus system)

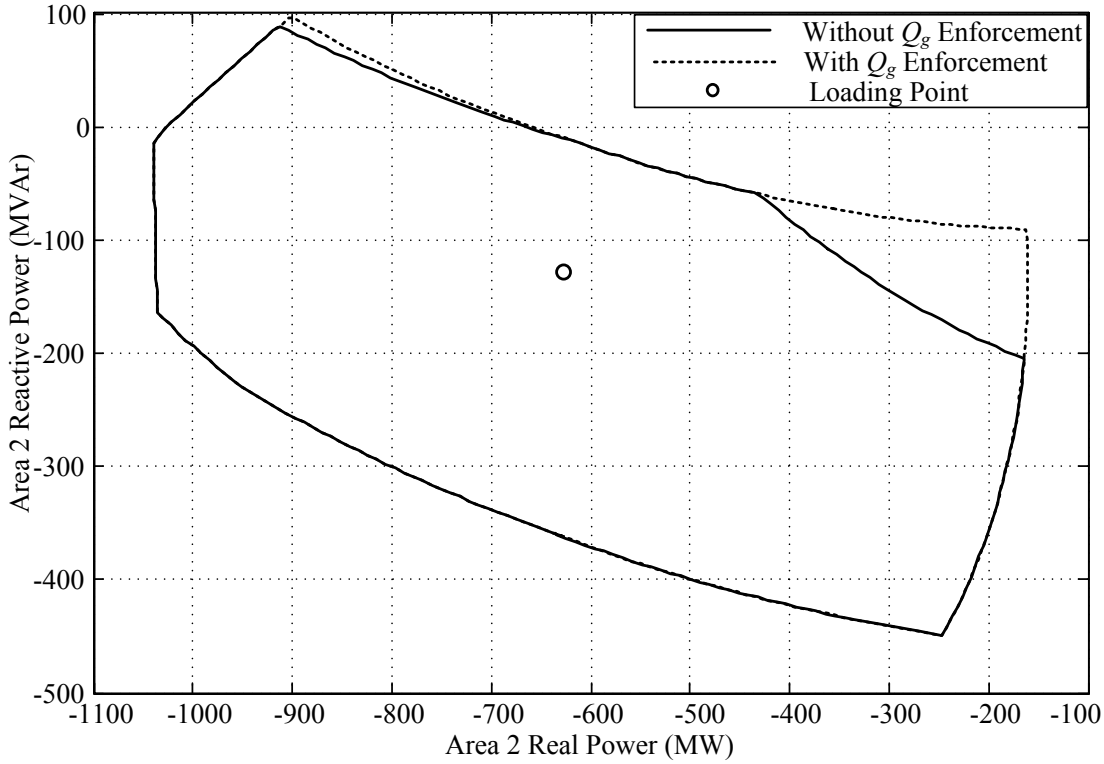


Figure 13.15 Feasible regions of power transfer from area 1, 3 to area 2 with reactive power enforcement (IEEE 24-bus)

Table 13.2 Comparison of closed area and computational time for feasible regions with reactive power enforcement (IEEE 24-bus)

| Source Area | Sink Area | Closed Area (MW*MVAr) | | | Computational Time (second/point) | | |
|---|---|---|---|---|---|---|---|
| | | Un-Enforced $Q_g$ | Enforced $Q_g$ | % Increase | Un-Enforced $Q_g$ | Enforced $Q_g$ | % Increase |
| 2 | 1 | 130,696 | 149,773 | 14.60 | 0.474 | 1.065 | 124.90 |
| 3 | 1 | 351,329 | 499,203 | 42.09 | 0.819 | 2.087 | 154.77 |
| 2,3 | 1 | 405,446 | 523,569 | 29.13 | 1.044 | 2.283 | 118.68 |
| 1 | 2 | 121,262 | 136,884 | 12.88 | 0.560 | 0.910 | 62.58 |
| 3 | 2 | 244,165 | 275,679 | 12.91 | 0.835 | 1.036 | 24.08 |
| 1,3 | 2 | 271,474 | 290,116 | 6.87 | 1.076 | 1.280 | 18.94 |

The results are compared in Table 13.2, it obviously seen that the computational time of boundary tracing process with reactive power enforcement increases from the normal tracing algorithm very much because when the tracing process is passing through the reactive power limits curve, the process needs to calculate minimization problem in many times before sending a boundary point. Thus, when the system reaches reactive power limits in many parts of boundary curve, there is more computational burden for the boundary tracing process. For the case of load in area 1, it can be observed that the reactive power limits are active on the upper and the lower of the region, therefore the process needs to spend more computational time.

## 13.3 Conclusion

The effect of reactive power limits can be taken into account for the conventional method, i.e. power flow, and load margin determination. When the reactive power limits are reached, generators are able to supply load with generator voltage variation. It leads to the expansion of load margin. As same as the feasible region, the feasible region can be expanded by the reactive power limit enforcement. This chapter illustrates the modified boundary tracing algorithm on the six-bus test system and the IEEE 24-bus test system. The results show the performance of the proposed method with the reactive power limit issue. The proposed method can properly determine the feasible region expanded by reactive power enforcement.

# CHAPTER XIV

# NUMERICAL RESULTS: THAILAND POWER SYSTEM

From previous chapters, the proposed boundary tracing method is illustrated on three test systems, i.e. two-bus system, six-bus system, and IEEE 24-bus system. The illustrations check the obtained boundary curves with many solutions obtained by the conventional method. Moreover, the proposed method is tested in many cases of source-sink pair in order to show the robustness of the method. In this chapter, the proposed boundary tracing method is applied to the Thailand power system. The load feasible regions of many cases of source-sink pair will be compared.

## 14.1 System Topology

The test system for this chapter is the Thailand power system. The system data is converted to a format of MATPOWER simulation program [27]. The converted data consists of 313 buses and 678 transmission lines. The Thailand electrical power system is divided into 7 areas: 1.) Bangkok area, 2.) Northeast area, 3.) South area, 4.) North area, 5.) Central area, 6.) East area, and 7.) West area. By using the proposed boundary tracing method, the load feasible regions of many cases of power transfer will be determined. The target load areas for the simulation are Bangkok area, East area, and South area. The information of Thailand power system is in Appendix.

## 14.2 Load Feasible Regions of Bangkok Thailand

The case study for this section is the Bangkok area load. The simulation treats Bangkok area as sink area, and then determines the load feasible regions from many cases of source area. The loading condition in this simulation is the peak load. The boundary tracing process is implemented with a gap $d$=1 MVA and a step size $l$=50 MVA. The enforcements of real power limit and reactive power limit are set to be enable for this simulation. The obtained feasible regions are compared in Figure 14.1, and the information of results is shown in Table 14.1.

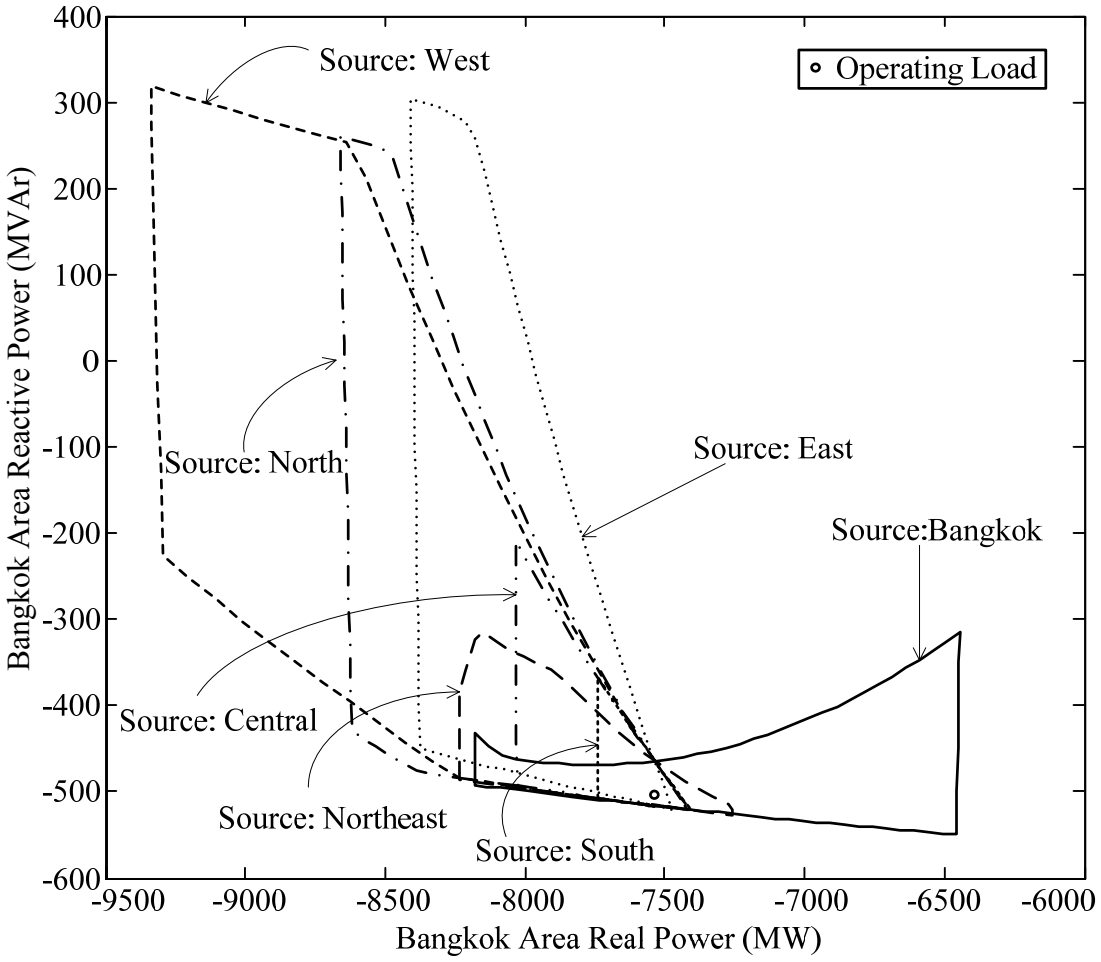


Figure 14.1 Load feasible regions of Bangkok area

Table 14.1 Information of feasible regions for Bangkok area

| Source Area | Sink Area | Maximum Load (MW) | Closed Area (MW x MVAr) | Time (sec) | Points | Time/ Point (sec) |
|---|---|---|---|---|---|---|
| Bangkok | Bangkok | 8,177 | 163,275 | 4,359 | 79 | 55.18 |
| Northeast | Bangkok | 8,237 | 94,045 | 16,901 | 47 | 359.59 |
| South | Bangkok | 7,740 | 22,937 | 2,802 | 21 | 133.45 |
| North | Bangkok | 8,661 | 435,695 | 11,517 | 72 | 159.95 |
| Central | Bangkok | 8,034 | 83,616 | 2,329 | 36 | 64.69 |
| East | Bangkok | 8,408 | 397,886 | 6,733 | 63 | 106.88 |
| West | Bangkok | 9,337 | 782,295 | 12,966 | 51 | 254.24 |

This simulation takes more computational time than the simulations on the smaller systems in previous chapters. However, the result obviously shows the total picture of loading condition with different source areas. The feasible regions are different depending on the source area. The result shows that receiving the power from West area gives the

highest real power supply to this sink area, and South area has the lowest potential for supplying the power to this sink area. West area can supply Bangkok area up to 9,337 MW from the base case load 7,536 MW (1,801 MW available). The highest feasibility, observed by the closed area of feasible regions, also belongs to a case of receiving the power from West area.

### 14.3 Load Feasible Regions of Eastern Thailand

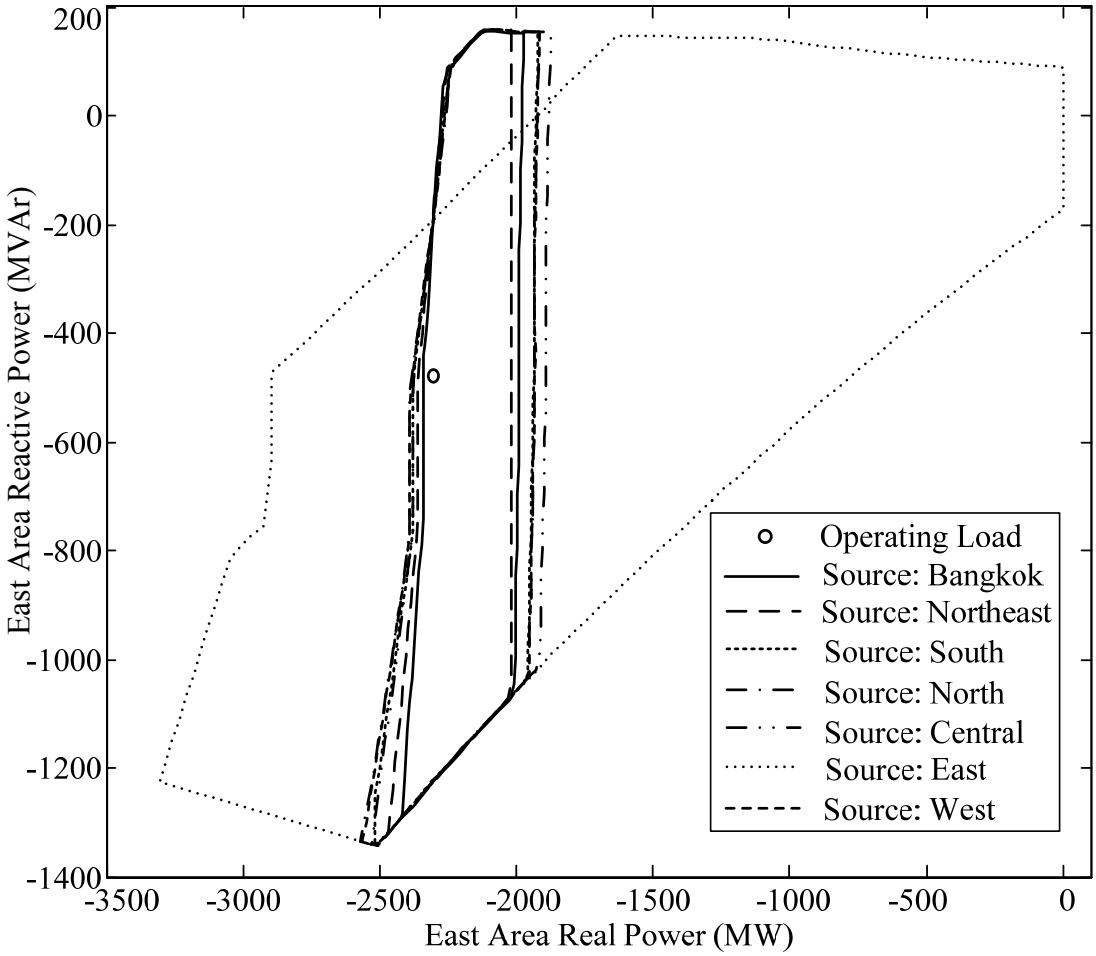


Figure 14.2 Load feasible regions of East area

This section considers the loads of Eastern Thailand. The simulation treats East area as sink area, and then determines the load feasible regions from many cases of source area, as same as the simulation in the previous section. The boundary tracing process is implemented with a gap $d$=1 MVA and a step size $l$=50 MVA. The obtained feasible regions are compared in Figure 14.2. It can be obviously seen that most of feasible regions are very similar except a feasible region of East area supplying power for itself.

For showing differences of these regions, the result is zoomed in and illustrated in Figure 14.3. And, the information of feasible regions is shown in Table 14.2.

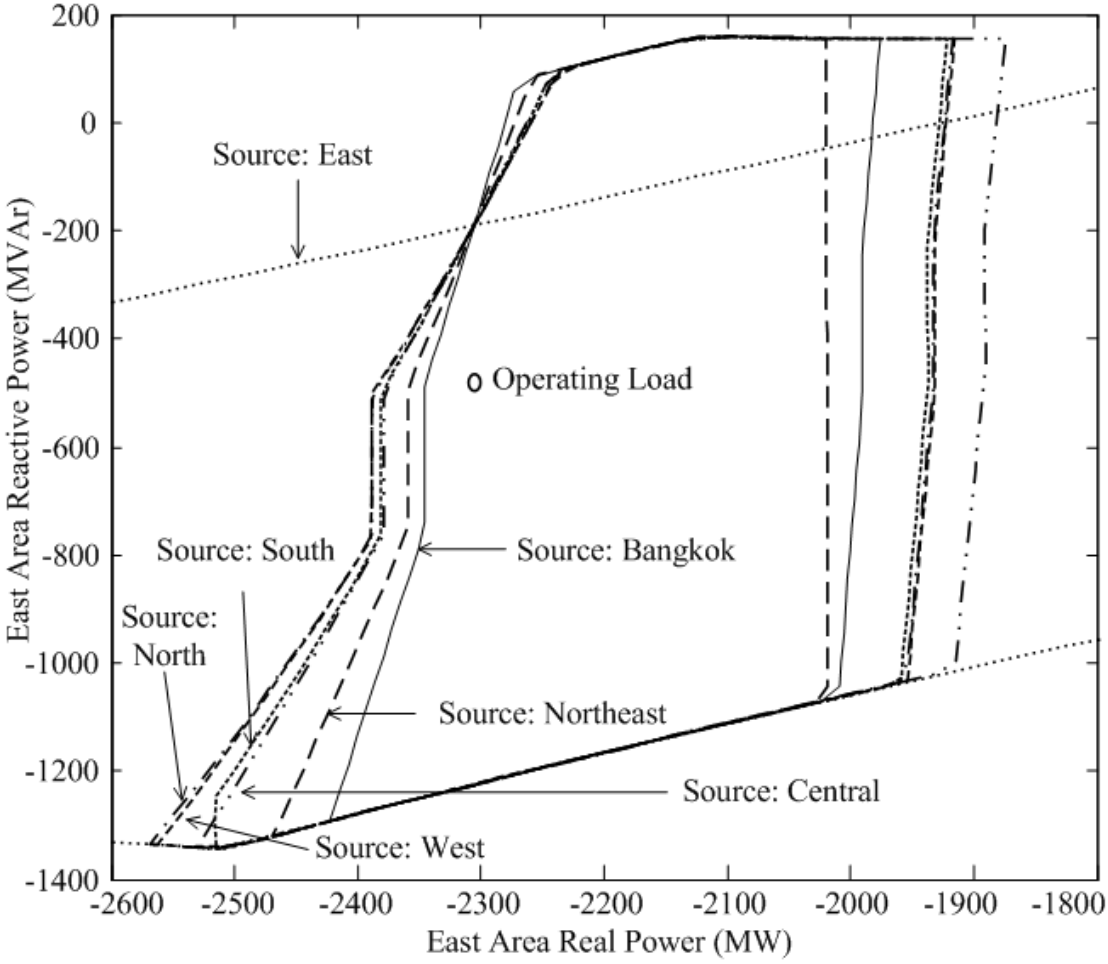


Figure 14.3 Load feasible regions of East area (zoom in)

Table 14.2 Information of feasible regions for East area

| Source Area | Sink Area | Maximum Load (MW) | Closed Area (MW x MVAr) | Time (sec) | Points | Time/ Point (sec) |
|---|---|---|---|---|---|---|
| Bangkok | East | 2,423 | 447,234 | 28,998 | 72 | 402.75 |
| Northeast | East | 2,469 | 433,914 | 29,729 | 72 | 412.90 |
| South | East | 2,516 | 558,793 | 23,792 | 77 | 308.98 |
| North | East | 2,569 | 576,293 | 34,321 | 77 | 445.73 |
| Central | East | 2,531 | 609,410 | 30,729 | 78 | 393.96 |
| East | East | 3,307 | 2,423,466 | 56,725 | 159 | 356.76 |
| West | East | 2,563 | 576,783 | 35,473 | 78 | 454.78 |

The result shows that the best feasibility of operating load in East area belongs to a case of receiving the power from generators in this area. East area can supply itself up to 3,307 MW and other areas can supply East area not more than 2,569 MW. In this case, the operating load in East area is 2,305 MW. It implies that the available transfer capabilities from other areas are not more than 264 MW. On the other hand, the best available transfer capability of this sink area is 1,002 MW by receiving the power to its area.

### 14.4 Load Feasible Regions of Southern Thailand

This section considers the loads of Southern Thailand. The boundary tracing process is implemented with a gap $d$=1 MVA and a step size $l$=10 MVA. The obtained feasible regions are compared in Figure 14.4. For this sink area, the obtained load feasible regions are very similar. The figure is zoomed in, as shown in Figure 14.5. And, the information of each region is shown in Table 14.3.

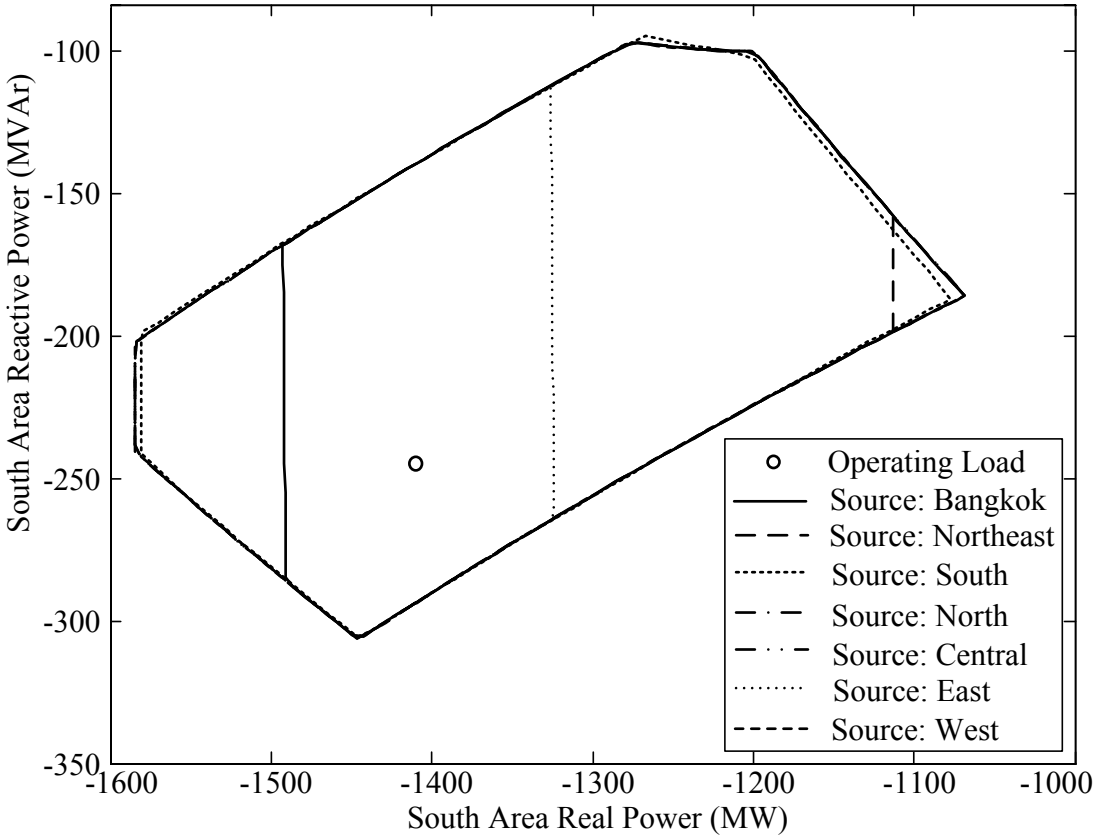


Figure 14.4 Load feasible regions of South area

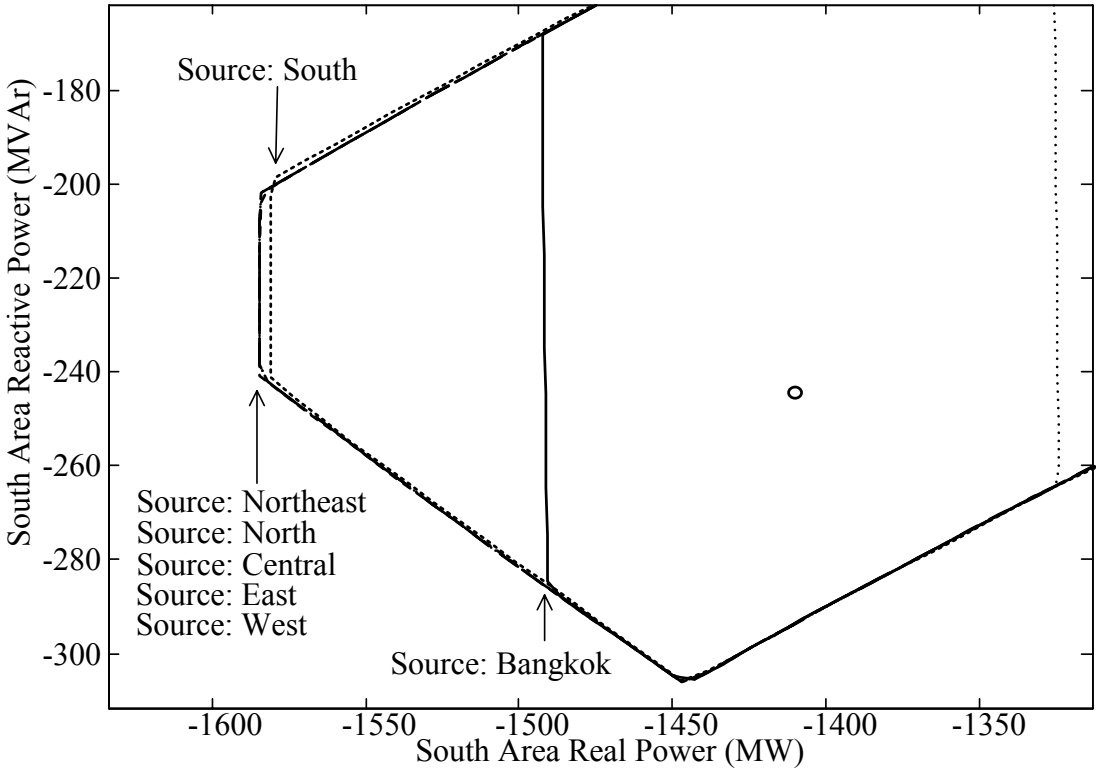


Figure 14.5 Feasible regions of South area (zoom in)

Table 14.3 Information of feasible regions for South area

| Source Area | Sink Area | Maximum Load (MW) | Closed Area (MW x MVAr) | Time (sec) | Points | Time/ Point (sec) |
|---|---|---|---|---|---|---|
| Bangkok | South | 1,493 | 50,792 | 6,817 | 106 | 64.31 |
| Northeast | South | 1,585 | 57,184 | 13,283 | 113 | 117.55 |
| South | South | 1,581 | 57,385 | 8,803 | 116 | 75.89 |
| North | South | 1,585 | 58,092 | 7,677 | 119 | 64.51 |
| Central | South | 1,585 | 58,092 | 8,672 | 119 | 72.87 |
| East | South | 1,585 | 32,134 | 3,528 | 79 | 44.65 |
| West | South | 1,585 | 58,093 | 9,778 | 119 | 82.16 |

The operating load of South area is 1410 MW. For the cases of receiving the power from Northeast area, North area, Central area, East area, and West area, the maximum load of these feasible regions is 1,585 MW that is 175 MW available for this sink area. By receiving the power from its area, the maximum load is 1,581 MW slightly smaller than previous cases. On the other hand, the smallest real power available belongs to a case of receiving the power from Bangkok area. A case of receiving the power from East area is the least feasibility for this test. In addition, the computational time of this test is less than

the previous tests because the feasible regions of these source-sink pairs are mostly bounded by voltage limits. In the boundary tracing process with reactive power enforcement, a boundary point with voltage limits does not need to repeat solving minimization. Then, the computational burden is less due to this reason.

## 14.5 Conclusion

The illustration in this chapter shows the load feasible regions of three areas for the Thailand power system. For Bangkok area, the shapes of feasible regions are various depending on source areas. Comparing to East area and South area, Bangkok area has a good potential to receive the power from other areas. For East area, the load feasibility is good when receiving the power from generators in its area. Finally, the feasibility of load in South is quite limited; the load feasible regions of many cases are bounded by bus voltage constraints.

# CHAPTER XV

# CONCLUSION

All chapters in this dissertation provide the concept of load feasible region determination and the numerical results. In this chapter, the advantage and disadvantage of the proposed method is summarized. In addition, the some details about the further developments of the boundary tracing method are discussed.

## 15.1 Dissertation Summary

This research focuses on visualizing a set of loading points by developing the method to determine a boundary of feasible region. The formulation considers feasible loading points of power transfer between a given source-sink pair which do not violate the operational limits. The proposed boundary tracing method utilized a predictor-corrector process in order to determine a sequence of boundary points. The predictor process is to find the next prediction point by using vector operations, while the corrector process is to determine a boundary point by calculating the minimal distance from an existing prediction point to a boundary of feasible region. The result of process is a contour of the feasible region. The shape of feasible region shows the limitation of load changes in several directions. This dissertation also studies the changes of feasible region due to the changes of system parameters. The concept of outermost boundary is described in this dissertation. Based on the manipulation of free variables, the outermost region affected by control parameters can be determined using the boundary tracing method. This concept is applied in order to determine the outermost boundary affected by generator voltage settings and FACTs device parameters.

In addition, this dissertation also develops the method to visualize the various kinds of feasible region. Using the concept of total transfer capability (TTC), the total transfer capability region or TTCR is proposed in this dissertation. TTCR is an intersection of feasible regions from many contingency cases. Using the concept of reactive power limit enforcement from the conventional power flow, the reactive power enforcement is taken into account to the proposed method. The feasible region expanded by reactive power limit enforcement can be determined by the modified tracing process.

The numerical results in this dissertation show the robustness of the proposed boundary tracing method with four test systems and several source-sink pairs. The obtained boundary curves are consistent to maximum loading points determined by the conventional method.

## 15.2 Advantage and Disadvantage

The advantage of the proposed method is that the available load can be visualized in term of a feasible region. Comparing to the conventional methods, the power flow is a tool for solving the condition of power system, i.e. nodal voltage, and transmission line flows. The output of power flow calculation is a point in power flow solution space. The conventional method for determining load margin such as RPF, CPF, and OPF are tools for determining a set of available loading points in a fixed load increment direction. The output of these methods is a load margin which is a line in the power flow solution space. The proposed method gives more information than the conventional methods. The output of proposed method is the load feasible region that is a plane in the power flow solution space. The load feasible region shows load margins in all directions of load changes on the *P*-*Q* plane.

The visualization of feasible region allows system operators knowing about the real potential of load in the target sink area, while the conventional load margin determination just gives a maximum real power in a specific direction. The loading point can be moved to the higher real power level with suitable reactive power compensation. Sometimes, the loading point is difficult to move to the higher real power level due to a shape of feasible region. Visualizing the shape of feasible region is useful to define the operation scheme.

In addition, the outermost boundary defined in this dissertation can give the information of parameter settings in order to improve the performance of considered transfer scenario. And, the outermost boundary shows the expansion of feasible region due to the parameter setting, e.g. generator voltage setting, and FACTS parameter setting, etc. The potential of sink area load affected by considered parameters can be observed.

Although, the output of this method gives more information than the output of conventional load margin determination, but more information comes with more computational burden, especially when the method is applied to the large-scale power system. This is the disadvantage of the proposed method. The method takes much

computational burden because the tracing process needs to solve minimization problem in many times. However, for the large-scale power system, this method can be used for the off-line planning.

### 15.3 Further Works

This dissertation develops the boundary tracing method as a new tool for power system analysis, and shows the examples of utilization. However, this work does not focus into the details of analysis. The further work can apply the proposed boundary tracing method to several problems of power systems. The information of feasible region, i.e. closed area, range of real power, range of reactive power, can be used as the indices for comparing the planning scheme or the operational scheme. Moreover, the computational time is an aspect that can be improved. The computational time would be improved by using the advance optimization technique in the further works.

# REFERENCES


[1] Ajjarapu, V., and Christy, C. The continuation power flow: a tool for steady state voltage stability analysis. IEEE Transactions on Power Systems 7, 1 (February 1992): 416-423.

[2] Chiang, H. D.; Flueck, A. J.; Shah, K. S.; and Balu, N. CPFLOW: A practical tool for tracing power system steady-state stationary behavior due to load and generation variations. IEEE Transactions on Power Systems 10, 2 (May 1995): 623-634.

[3] Available Transfer Capability Definitions and Determination[Online]. NERC, 1996. Available from: http://www.nerc.com/~filez/atcwg.html [2006, June 17]

[4] Khairuddin, A. B.; Ahmed, S. S.; Mustafa, M. W.; Zin, A. A. M.; and Ahmad, H. A Novel Method for ATC Computations in a Large-Scale Power System. IEEE Transactions on Power Systems 19, 2 (May 2004): 1150-1158.

[5] Ou, Y., and Sigh, C. Assessment of Available Transfer Capability and Margins. IEEE Transactions on Power Systems 17, 2 (May 2002): 463-468.

[6] Li, W.; Wang, P.; and Guo, Z. Determination of optimal total transfer capability using a probabilistic approach. IEEE Transactions on Power Systems 21, 2 (May 2006): 862-868.

[7] Min, L., and Abur, A. Total transfer capability computation for multi-area power systems. IEEE Transactions on Power Systems 21, 3 (August 2006): 1141-1147l

[8] Overbye, T. J. A power flow measure for unsolvable cases. IEEE Transactions on Power Systems 9, 3 (August 1994): 1359-1365.

[9] Overbye, T. J. Computation of a practical method to restore power flow solvability. IEEE Transactions on Power Systems 10, 1 (February 1995): 280-287.

[10] Singh, S. N., and Srivastava, S. C. Corrective action planning to achieve a feasible optimal power flow solution. IEE Proceedings Generation, Transmission and Distribution 142, 6, (November 1995): 576-582.

[11] Granville, S.; Mello, J. C. O.; and Melo, A. C. G. Application of interior point methods to power flow unsolvability. IEEE Transaction on Power Systems 11, 2 (May 1996): 1096-1103.

[12] Conceicao, A. G. C., and Castro, C. A. A new approach to defining corrective control actions in case of infeasible operating situations. IEEE Porto Power Tech Conference (September 2001).

[13] Hiskens, I. A., and Davy, R. J. Exploring the power flow solution space boundary. IEEE Transactions on Power Systems 16, 3, (August 2001): 389-395.

[14] Canizares C. A., and Avarado, F. L. Point of collapse and continuation methods for large AC/DC systems. IEEE Transactions on Power Systems 8, 1, (February 1993): 1-8.

[15] Makarov, Y. V.; Hill, D. J.; and Dong, Z. Y. Computation of bifurcation boundaries for power systems: a new Δ-plane method. IEEE Transaction on Circuits and Systems 47, 4, (April 2000): 536-544.

[16] Ajjarapu, V. Computational techniques for voltage stability assessment and control New York: Springer, 2006.

[17] Yu, Y.; Li, P.; Jia, H.; Lee, S. T.; and Zhang, P. Computation of boundary of power flow feasible region with hybrid method. in Power Systems Conference and Exposition, 137-143. New York : IEEE PES, 2004.

[18] Ou, Y., and Singh, C. Improvement of Total Transfer Capability Using TCSC and SVC. IEEE Power Engineering Society Summer Meeting 2 (2001): 944-948.

[19] Canizares, C. A. Calculating optimal system parameters to maximize the distance to saddle-node bifurcations. IEEE Transactions on Circuits and Systems-I: Fundamental Theory and Applications 45, 3 (March 1998): 225-237.

[20] Avalos, R. J.; Canizares, C. A.; Milano, F.; and Conejo, A. J. Equivalency of continuation and optimization methods to determine saddle-node and limit-induced bifurcation in power systems. IEEE Transactions on Circuits and Systems 56, 1 (January 2009): 210-223.

[21] Lesieutre, B. C., and Hiskens, I. A. Convexity of the set of feasible injections and revenue adequacy in FTR markets. IEEE Transactions on Power Systems 20, 4 (November 2005): 1790-1798.

[22] Makarov, Y. V.; Dong, Z. Y.; and Hill, D. J. On convexity of power flow feasibility boundary. IEEE Transactions on Power Systems 23, 2 (May pp. 811-813.

[23] Weissten, E. W. Green's theorem[Online]. MathWorld, Available from: http://mathworld.wolfram.com/GreensTheorem.html [2011, July 25]

[24] Edward, D. H. Finding Areas with the Gauss-Green Formula[Online]. Available from: http://www.ma.iup.edu/projects/CalcDEMma/Green/ Green.html [2011, January 19]

[25] Wood, A. J., and Wollenberg, B. F. Power generation operation and control New York: John Willey & Sons, 1996.

[26] Reliability Test System Task Force. The IEEE reliability test system-1996. IEEE Transactions on Power System 14, 3 (1999): 1010-1020.

[27] Zimmerman, D.; Murillo-Sánchez, C.E.; and Gan, D. MATPOWER[Online]. PSERC. Available from: http://www.pserc.cornell.edu/matpower/ [2011, July 25]

# APPENDIX

# APPENDIX

# DATA OF TEST SYSTEMS

## A.1 Data of 6-Bus Test System

The 6-bus test system consists of 3 generators, 3 load buses, and 11 transmission lines, as shown in the figure below. The information of the 6-bus test system is shown in Table A.1-A.2.

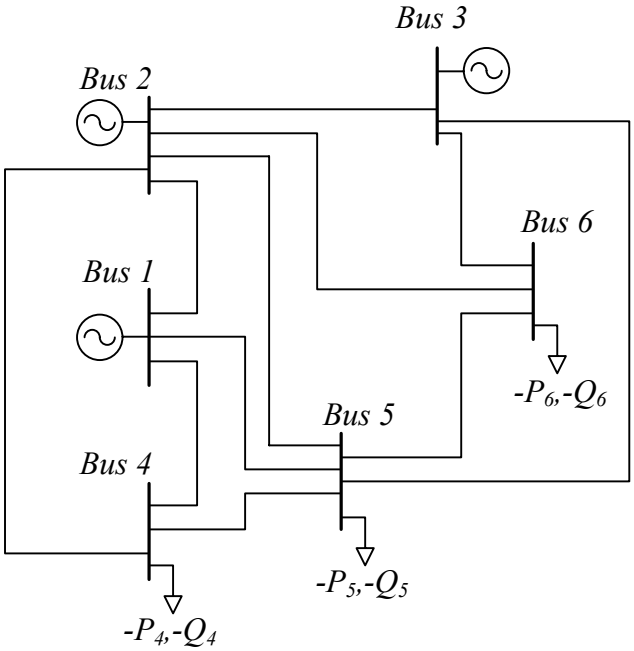


Figure A.1 Six-bus test system

Table A.1 Bus and generator data of 6-bus test system

| Bus | Bus type | Voltage (pu) | *P* (pu) | *Q* (pu) | $P_{gen}$ min (pu) | $P_{gen}$ max (pu) | $Q_{gen}$ min (pu) | $Q_{gen}$ max (pu) | Voltage limit (pu) |
|---|---|---|---|---|---|---|---|---|---|
| 1 | Slack | 1.05 | - | - | 0.5 | 2 | -1 | 1 | 0.95-1.05 |
| 2 | Gen | 1.05 | 0.5 | - | 0.375 | 1.5 | -1 | 1 | 0.95-1.05 |
| 3 | Gen | 1.07 | 0.6 | - | 0.45 | 1.8 | -1 | 1 | 0.97-1.07 |
| 4 | Load | - | -0.7 | -0.7 | - | - | - | - | 0.95-1.05 |
| 5 | Load | - | -0.7 | -0.7 | - | - | - | - | 0.95-1.05 |
| 6 | Load | - | -0.7 | -0.7 | - | - | - | - | 0.95-1.05 |

Table A.2 Transmission line data of 6-bus test system

| Line | From Bus | To Bus | Resistance (pu) | Reactance (pu) | Line Charging Susceptance (pu) | Line limit (pu) |
|---|---|---|---|---|---|---|
| 1 | 1 | 2 | 0.1 | 0.2 | 0.02 | 0.4 |
| 2 | 1 | 4 | 0.05 | 0.2 | 0.02 | 0.6 |
| 3 | 1 | 5 | 0.08 | 0.3 | 0.03 | 0.4 |
| 4 | 2 | 3 | 0.05 | 0.25 | 0.03 | 0.4 |
| 5 | 2 | 4 | 0.05 | 0.1 | 0.01 | 0.6 |
| 6 | 2 | 5 | 0.1 | 0.3 | 0.02 | 0.3 |
| 7 | 2 | 6 | 0.07 | 0.2 | 0.025 | 0.9 |
| 8 | 3 | 5 | 0.12 | 0.26 | 0.025 | 0.7 |
| 9 | 3 | 6 | 0.02 | 0.1 | 0.01 | 0.8 |
| 10 | 4 | 5 | 0.2 | 0.4 | 0.04 | 0.2 |
| 11 | 5 | 6 | 0.1 | 0.3 | 0.03 | 0.4 |

## A.2 Data of IEEE 24-Bus System

The IEEE 24-bus test system [22] consists of 10 generators, 1 synchronous condenser, and 38 transmission lines, as shown in the figure below. The information of this test system is shown in Table A.3-A.5.

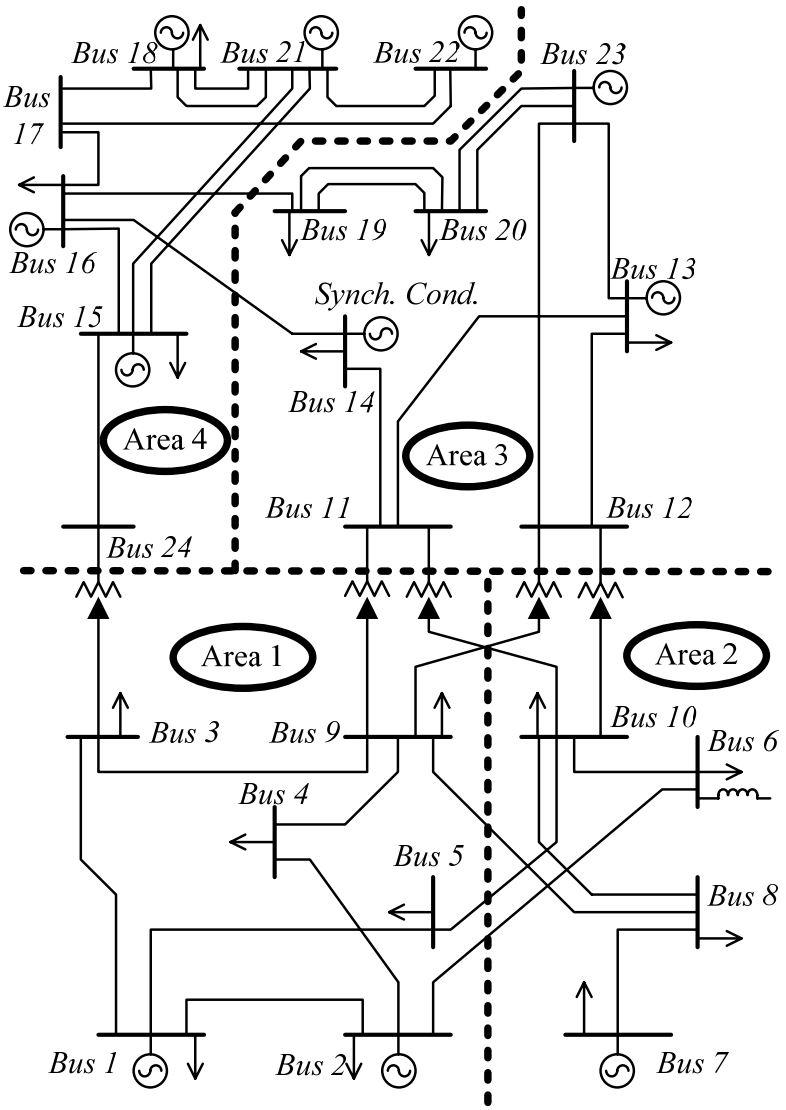


Figure A.2 IEEE 24-bus test system

Table A.3 Bus data of IEEE 24-bus test system

| Bus | Bus Type | $P_d$ | $Q_d$ | $G_s$ | $B_s$ | Area | kV | $V^{max}$ | $V^{min}$ |
|---|---|---|---|---|---|---|---|---|---|
| 1 | 2 | 108 | 22 | 0 | 0 | 1 | 138 | 1.05 | 0.95 |
| 2 | 2 | 97 | 20 | 0 | 0 | 1 | 138 | 1.05 | 0.95 |
| 3 | 1 | 180 | 37 | 0 | 0 | 1 | 138 | 1.05 | 0.95 |
| 4 | 1 | 74 | 15 | 0 | 0 | 1 | 138 | 1.05 | 0.95 |
| 5 | 1 | 71 | 14 | 0 | 0 | 1 | 138 | 1.05 | 0.95 |
| 6 | 1 | 136 | 28 | 0 | -100 | 2 | 138 | 1.05 | 0.95 |
| 7 | 2 | 125 | 25 | 0 | 0 | 2 | 138 | 1.05 | 0.95 |
| 8 | 1 | 171 | 35 | 0 | 0 | 2 | 138 | 1.05 | 0.95 |
| 9 | 1 | 175 | 36 | 0 | 0 | 1 | 138 | 1.05 | 0.95 |
| 10 | 1 | 195 | 40 | 0 | 0 | 2 | 138 | 1.05 | 0.95 |
| 11 | 1 | 0 | 0 | 0 | 0 | 3 | 230 | 1.05 | 0.95 |
| 12 | 1 | 0 | 0 | 0 | 0 | 3 | 230 | 1.05 | 0.95 |
| 13 | 3 | 265 | 54 | 0 | 0 | 3 | 230 | 1.05 | 0.95 |
| 14 | 2 | 194 | 39 | 0 | 0 | 3 | 230 | 1.05 | 0.95 |
| 15 | 2 | 317 | 64 | 0 | 0 | 4 | 230 | 1.05 | 0.95 |
| 16 | 2 | 100 | 20 | 0 | 0 | 4 | 230 | 1.05 | 0.95 |
| 17 | 1 | 0 | 0 | 0 | 0 | 4 | 230 | 1.05 | 0.95 |
| 18 | 2 | 333 | 68 | 0 | 0 | 4 | 230 | 1.05 | 0.95 |
| 19 | 1 | 181 | 37 | 0 | 0 | 3 | 230 | 1.05 | 0.95 |
| 20 | 1 | 128 | 26 | 0 | 0 | 3 | 230 | 1.05 | 0.95 |
| 21 | 2 | 0 | 0 | 0 | 0 | 4 | 230 | 1.05 | 0.95 |
| 22 | 2 | 0 | 0 | 0 | 0 | 4 | 230 | 1.05 | 0.95 |
| 23 | 2 | 0 | 0 | 0 | 0 | 3 | 230 | 1.05 | 0.95 |
| 24 | 1 | 0 | 0 | 0 | 0 | 4 | 230 | 1.05 | 0.95 |

Table A.4 Generator data of IEEE 24-bus test system

| Gen | Bus | $P_g$ | $Q_g^{max}$ | $Q_g^{min}$ | Vg | Base | $P_g^{max}$ | $P_g^{min}$ |
|---|---|---|---|---|---|---|---|---|
| 1 | 1 | 172 | 80 | -50 | 1.035 | 100 | 192 | 0 |
| 2 | 2 | 172 | 80 | -50 | 1.035 | 100 | 192 | 0 |
| 3 | 7 | 240 | 180 | 0 | 1.025 | 100 | 300 | 0 |
| 4 | 13 | 187.25 | 240 | 0 | 1.02 | 100 | 591 | 0 |
| 5 | 14 | 0 | 200 | -50 | 0.98 | 100 | 0 | 0 |
| 6 | 15 | 215 | 110 | -50 | 1.014 | 100 | 215 | 0 |
| 7 | 16 | 155 | 80 | -50 | 1.017 | 100 | 155 | 0 |
| 8 | 18 | 400 | 200 | -50 | 1.05 | 100 | 400 | 0 |
| 9 | 21 | 400 | 200 | -50 | 1.05 | 100 | 400 | 0 |
| 10 | 22 | 300 | 96 | -60 | 1.05 | 100 | 300 | 0 |
| 11 | 23 | 660 | 310 | -125 | 1.05 | 100 | 660 | 0 |

Table A.5 Transmission line data of IEEE 24-bus test system

| Line | From Bus | To Bus | *r* | *x* | *b* | Rating | Ratio |
|---|---|---|---|---|---|---|---|
| 1 | 1 | 2 | 0.0026 | 0.0139 | 0.4611 | 250 | 0 |
| 2 | 1 | 3 | 0.0546 | 0.2112 | 0.0572 | 208 | 0 |
| 3 | 1 | 5 | 0.0218 | 0.0845 | 0.0229 | 208 | 0 |
| 4 | 2 | 4 | 0.0328 | 0.1267 | 0.0343 | 208 | 0 |
| 5 | 2 | 6 | 0.0497 | 0.192 | 0.052 | 208 | 0 |
| 6 | 3 | 9 | 0.0308 | 0.119 | 0.0322 | 208 | 0 |
| 7 | 3 | 24 | 0.0023 | 0.0839 | 0 | 510 | 1.03 |
| 8 | 4 | 9 | 0.0268 | 0.1037 | 0.0281 | 208 | 0 |
| 9 | 5 | 10 | 0.0228 | 0.0883 | 0.0239 | 208 | 0 |
| 10 | 6 | 10 | 0.0139 | 0.0605 | 2.459 | 193 | 0 |
| 11 | 7 | 8 | 0.0159 | 0.0614 | 0.0166 | 208 | 0 |
| 12 | 8 | 9 | 0.0427 | 0.1651 | 0.0447 | 208 | 0 |
| 13 | 8 | 10 | 0.0427 | 0.1651 | 0.0447 | 208 | 0 |
| 14 | 9 | 11 | 0.0023 | 0.0839 | 0 | 510 | 1.03 |
| 15 | 9 | 12 | 0.0023 | 0.0839 | 0 | 510 | 1.03 |
| 16 | 10 | 11 | 0.0023 | 0.0839 | 0 | 510 | 1.02 |
| 17 | 10 | 12 | 0.0023 | 0.0839 | 0 | 510 | 1.02 |
| 18 | 11 | 13 | 0.0061 | 0.0476 | 0.0999 | 600 | 0 |
| 19 | 11 | 14 | 0.0054 | 0.0418 | 0.0879 | 625 | 0 |
| 20 | 12 | 13 | 0.0061 | 0.0476 | 0.0999 | 625 | 0 |
| 21 | 12 | 23 | 0.0124 | 0.0966 | 0.203 | 625 | 0 |
| 22 | 13 | 23 | 0.0111 | 0.0865 | 0.1818 | 625 | 0 |
| 23 | 14 | 16 | 0.005 | 0.0389 | 0.0818 | 625 | 0 |
| 24 | 15 | 16 | 0.0022 | 0.0173 | 0.0364 | 600 | 0 |
| 25 | 15 | 21 | 0.0063 | 0.049 | 0.103 | 600 | 0 |
| 26 | 15 | 21 | 0.0063 | 0.049 | 0.103 | 600 | 0 |
| 27 | 15 | 24 | 0.0067 | 0.0519 | 0.1091 | 600 | 0 |
| 28 | 16 | 17 | 0.0033 | 0.0259 | 0.0545 | 600 | 0 |
| 29 | 16 | 19 | 0.003 | 0.0231 | 0.0485 | 600 | 0 |
| 30 | 17 | 18 | 0.0018 | 0.0144 | 0.0303 | 600 | 0 |
| 31 | 17 | 22 | 0.0135 | 0.1053 | 0.2212 | 600 | 0 |
| 32 | 18 | 21 | 0.0033 | 0.0259 | 0.0545 | 600 | 0 |
| 33 | 18 | 21 | 0.0033 | 0.0259 | 0.0545 | 600 | 0 |
| 34 | 19 | 20 | 0.0051 | 0.0396 | 0.0833 | 600 | 0 |
| 35 | 19 | 20 | 0.0051 | 0.0396 | 0.0833 | 600 | 0 |
| 36 | 20 | 23 | 0.0028 | 0.0216 | 0.0455 | 600 | 0 |
| 37 | 20 | 23 | 0.0028 | 0.0216 | 0.0455 | 600 | 0 |
| 38 | 21 | 22 | 0.0087 | 0.0678 | 0.1424 | 600 | 0 |

## A.3 Data of Thailand Power System

The Thailand power system used in this research consists of 7 areas which are Bangkok (area 1), Northeast (area 2), South (area 3), North (area 4), Central (area 5), East (area 6), and West (area 7). The information of this system is shown in Table A.6-A.8.

Table A.6 Bus data of Thailand power system

| Bus | Type | $P_d$ | $Q_d$ | $G_s$ | $B_s$ | Area | kV | $V^{max}$ | $V^{min}$ |
|---|---|---|---|---|---|---|---|---|---|
| 1 | 1 | 293.85 | -22.00 | 0 | 0 | 1 | 69 | 1.05 | 0.98 |
| 2 | 2 | 250.70 | -11.81 | 0 | 0 | 1 | 69 | 1.063 | 0.993 |
| 3 | 1 | 191.25 | -3.15 | 0 | 0 | 1 | 69 | 1.05 | 0.98 |
| 4 | 1 | 265.85 | 14.28 | 0 | 0 | 1 | 69 | 1.05 | 0.98 |
| 5 | 1 | 232.40 | 2.59 | 0 | 0 | 1 | 69 | 1.05 | 0.98 |
| 6 | 1 | 400.86 | 17.48 | 0 | 0 | 1 | 69 | 1.05 | 0.98 |
| 7 | 1 | 232.40 | 128.58 | 0 | 0 | 1 | 69 | 1.05 | 0.98 |
| 8 | 1 | 273.70 | 27.19 | 0 | 0 | 1 | 69 | 1.05 | 0.98 |
| 9 | 1 | 195.70 | 6.12 | 0 | 0 | 1 | 69 | 1.05 | 0.98 |
| 10 | 1 | 202.10 | 29.40 | 0 | 0 | 1 | 69 | 1.05 | 0.98 |
| 11 | 1 | 293.85 | -7.68 | 0 | 0 | 1 | 69 | 1.05 | 0.98 |
| 12 | 1 | 191.25 | 3.66 | 0 | 0 | 1 | 69 | 1.05 | 0.98 |
| 13 | 1 | 265.85 | 16.60 | 0 | 0 | 1 | 69 | 1.05 | 0.98 |
| 14 | 1 | 232.40 | 10.67 | 0 | 0 | 1 | 69 | 1.05 | 0.98 |
| 15 | 1 | 273.70 | 15.22 | 0 | 0 | 1 | 69 | 1.05 | 0.98 |
| 16 | 1 | 195.70 | -35.09 | 0 | 0 | 1 | 69 | 1.05 | 0.98 |
| 17 | 1 | 358.20 | -17.47 | 0 | 0 | 1 | 115 | 1.05 | 0.98 |
| 18 | 1 | 132.70 | 5.32 | 0 | 0 | 1 | 115 | 1.05 | 0.98 |
| 19 | 1 | 318.10 | 38.65 | 0 | 0 | 1 | 115 | 1.05 | 0.98 |
| 20 | 1 | 189.67 | -6.71 | 0 | 0 | 1 | 115 | 1.05 | 0.98 |
| 21 | 1 | 189.20 | 13.11 | 0 | 0 | 1 | 115 | 1.05 | 0.98 |
| 22 | 1 | 122.00 | -0.60 | 0 | 0 | 1 | 115 | 1.05 | 0.98 |
| 23 | 1 | 319.15 | 69.00 | 0 | 0 | 1 | 115 | 1.05 | 0.98 |
| 24 | 1 | 164.10 | -8.21 | 0 | 0 | 1 | 115 | 1.05 | 0.98 |
| 25 | 1 | 271.00 | 24.03 | 0 | 0 | 1 | 115 | 1.05 | 0.98 |
| 26 | 1 | 219.23 | 53.20 | 0 | 0 | 1 | 115 | 1.05 | 0.98 |
| 27 | 2 | 160.82 | -18.60 | 0 | 0 | 1 | 115 | 1.064 | 0.994 |
| 28 | 1 | 346.10 | 57.51 | 0 | 0 | 1 | 230 | 1.05 | 0.98 |
| 29 | 1 | 61.10 | -33.19 | 0 | 0 | 1 | 230 | 1.05 | 0.98 |
| 30 | 1 | 0.00 | -133.98 | 0 | 0 | 1 | 230 | 1.05 | 0.98 |
| 31 | 1 | 0.00 | 0.00 | 0 | 0 | 1 | 230 | 1.05 | 0.98 |
| 32 | 1 | 296.80 | -21.19 | 0 | 0 | 1 | 230 | 1.05 | 0.98 |
| 33 | 1 | 0.00 | -123.60 | 0 | 0 | 1 | 230 | 1.05 | 0.98 |
| 34 | 1 | 0.00 | -66.99 | 0 | 0 | 1 | 230 | 1.05 | 0.98 |
| 35 | 1 | 0.00 | 0.00 | 0 | 0 | 1 | 230 | 1.05 | 0.98 |
| 36 | 1 | 0.00 | 0.00 | 0 | 0 | 1 | 230 | 1.05 | 0.98 |

Table A.6 Bus data of Thailand power system-continued

| Bus | Type | $P_d$ | $Q_d$ | $G_s$ | $B_s$ | Area | kV | $V^{max}$ | $V^{min}$ |
|---|---|---|---|---|---|---|---|---|---|
| 37 | 1 | 0.00 | 0.00 | 0 | 0 | 1 | 230 | 1.05 | 0.98 |
| 38 | 1 | 0.00 | 0.00 | 0 | 0 | 1 | 230 | 1.05 | 0.98 |
| 39 | 2 | 0.00 | -133.98 | 0 | 0 | 1 | 230 | 1.05 | 0.98 |
| 40 | 1 | 396.30 | 157.47 | 0 | 0 | 1 | 230 | 1.05 | 0.98 |
| 41 | 1 | 0.00 | 0.00 | 0 | 0 | 1 | 230 | 1.05 | 0.98 |
| 42 | 1 | 0.00 | -61.80 | 0 | 0 | 1 | 230 | 1.05 | 0.98 |
| 43 | 1 | 0.00 | 0.00 | 0 | 0 | 1 | 500 | 1.05 | 0.98 |
| 44 | 1 | 0.00 | 0.00 | 0 | 0 | 1 | 500 | 1.05 | 0.98 |
| 45 | 2 | 0.00 | 0.00 | 0 | 0 | 2 | 69 | 1.05 | 0.98 |
| 46 | 1 | 26.21 | -8.20 | 0 | 0 | 2 | 115 | 1.05 | 0.98 |
| 47 | 1 | 22.64 | 3.10 | 0 | 0 | 2 | 115 | 1.05 | 0.98 |
| 48 | 1 | 4.50 | 2.49 | 0 | 0 | 2 | 115 | 1.05 | 0.98 |
| 49 | 1 | 29.95 | 4.01 | 0 | 0 | 2 | 115 | 1.05 | 0.98 |
| 50 | 1 | 15.80 | -0.64 | 0 | 0 | 2 | 115 | 1.05 | 0.98 |
| 51 | 1 | 61.91 | -41.52 | 0 | 0 | 2 | 115 | 1.05 | 0.98 |
| 52 | 1 | 61.99 | 19.16 | 0 | 0 | 2 | 115 | 1.05 | 0.98 |
| 53 | 2 | 0.00 | 0.00 | 0 | 0 | 2 | 115 | 1.05 | 0.98 |
| 54 | 1 | 34.47 | 15.95 | 0 | 0 | 2 | 115 | 1.05 | 0.98 |
| 55 | 1 | 48.41 | 11.18 | 0 | 0 | 2 | 115 | 1.05 | 0.98 |
| 56 | 1 | 14.86 | 8.22 | 0 | 0 | 2 | 115 | 1.05 | 0.98 |
| 57 | 1 | 89.77 | 30.59 | 0 | 0 | 2 | 115 | 1.05 | 0.98 |
| 58 | 1 | 41.42 | 22.92 | 0 | 0 | 2 | 115 | 1.05 | 0.98 |
| 59 | 1 | 65.18 | -6.18 | 0 | 0 | 2 | 115 | 1.05 | 0.98 |
| 60 | 1 | 47.30 | -10.85 | 0 | 0 | 2 | 115 | 1.05 | 0.98 |
| 61 | 1 | 60.77 | -7.71 | 0 | 0 | 2 | 115 | 1.05 | 0.98 |
| 62 | 1 | 50.84 | -6.70 | 0 | 0 | 2 | 115 | 1.05 | 0.98 |
| 63 | 1 | 20.06 | 11.10 | 0 | 0 | 2 | 115 | 1.05 | 0.98 |
| 64 | 1 | 74.35 | -47.07 | 0 | 0 | 2 | 115 | 1.05 | 0.98 |
| 65 | 1 | 155.72 | 33.03 | 0 | 0 | 2 | 115 | 1.05 | 0.98 |
| 66 | 1 | 75.59 | 12.64 | 0 | 0 | 2 | 115 | 1.05 | 0.98 |
| 67 | 1 | 0.00 | 0.00 | 0 | 0 | 2 | 115 | 1.05 | 0.98 |
| 68 | 1 | 4.66 | 2.58 | 0 | 0 | 2 | 115 | 1.05 | 0.98 |
| 69 | 1 | 33.78 | -13.38 | 0 | 0 | 2 | 115 | 1.05 | 0.98 |
| 70 | 1 | 31.43 | -4.60 | 0 | 0 | 2 | 115 | 1.05 | 0.98 |
| 71 | 1 | 58.91 | 20.73 | 0 | 0 | 2 | 115 | 1.05 | 0.98 |
| 72 | 1 | 48.69 | -2.24 | 0 | 0 | 2 | 115 | 1.05 | 0.98 |
| 73 | 2 | 0.00 | 0.00 | 0 | 0 | 2 | 115 | 1.05 | 0.98 |
| 74 | 1 | 76.59 | 1.24 | 0 | 0 | 2 | 115 | 1.05 | 0.98 |
| 75 | 1 | 75.65 | -10.18 | 0 | 0 | 2 | 115 | 1.05 | 0.98 |
| 76 | 1 | 21.63 | 2.60 | 0 | 0 | 2 | 115 | 1.05 | 0.98 |
| 77 | 1 | 23.97 | 0.70 | 0 | 0 | 2 | 115 | 1.05 | 0.98 |
| 78 | 1 | 32.25 | 8.48 | 0 | 0 | 2 | 115 | 1.05 | 0.98 |
| 79 | 1 | 53.26 | 1.54 | 0 | 0 | 2 | 115 | 1.05 | 0.98 |
| 80 | 1 | 19.82 | 10.97 | 0 | 0 | 2 | 115 | 1.05 | 0.98 |
| 81 | 1 | 0.00 | 0.00 | 0 | 0 | 2 | 115 | 1.05 | 0.98 |
| 82 | 1 | 18.09 | 10.01 | 0 | 0 | 2 | 115 | 1.05 | 0.98 |
| 83 | 1 | 93.39 | -15.27 | 0 | 0 | 2 | 115 | 1.05 | 0.98 |

Table A.6 Bus data of Thailand power system-continued

| Bus | Type | $P_d$ | $Q_d$ | $G_s$ | $B_s$ | Area | kV | $V^{max}$ | $V^{min}$ |
|---|---|---|---|---|---|---|---|---|---|
| 84 | 1 | 54.49 | 0.97 | 0 | 0 | 2 | 115 | 1.05 | 0.98 |
| 85 | 2 | 27.88 | 15.43 | 0 | 0 | 2 | 115 | 1.06 | 0.99 |
| 86 | 1 | 36.28 | 7.55 | 0 | 0 | 2 | 115 | 1.05 | 0.98 |
| 87 | 1 | 42.22 | -26.66 | 0 | 0 | 2 | 115 | 1.05 | 0.98 |
| 88 | 1 | 19.11 | 1.21 | 0 | 0 | 2 | 115 | 1.05 | 0.98 |
| 89 | 2 | 0.00 | 0.00 | 0 | 0 | 2 | 115 | 1.05 | 0.98 |
| 90 | 1 | 58.48 | 32.36 | 0 | 0 | 2 | 115 | 1.05 | 0.98 |
| 91 | 1 | 73.52 | 17.98 | 0 | 0 | 2 | 115 | 1.05 | 0.98 |
| 92 | 1 | 53.04 | -13.99 | 0 | 0 | 2 | 115 | 1.05 | 0.98 |
| 93 | 1 | 50.20 | -15.36 | 0 | 0 | 2 | 115 | 1.05 | 0.98 |
| 94 | 1 | 43.25 | -36.77 | 0 | 0 | 2 | 115 | 1.05 | 0.98 |
| 95 | 1 | 0.00 | 0.00 | 0 | 0 | 2 | 230 | 1.05 | 0.98 |
| 96 | 1 | 0.00 | 0.00 | 0 | 0 | 2 | 230 | 1.05 | 0.98 |
| 97 | 1 | 0.00 | 0.00 | 0 | 0 | 2 | 230 | 1.05 | 0.98 |
| 98 | 2 | 0.00 | 0.00 | 0 | 0 | 2 | 230 | 1.05 | 0.98 |
| 99 | 1 | 0.00 | 0.00 | 0 | 0 | 2 | 230 | 1.05 | 0.98 |
| 100 | 1 | 0.00 | 0.00 | 0 | 0 | 2 | 230 | 1.05 | 0.98 |
| 101 | 2 | 0.00 | 0.00 | 0 | 0 | 2 | 230 | 1.05 | 0.98 |
| 102 | 1 | 0.00 | 0.00 | 0 | 0 | 2 | 230 | 1.05 | 0.98 |
| 103 | 1 | 0.00 | 0.00 | 0 | 0 | 2 | 230 | 1.05 | 0.98 |
| 104 | 1 | 0.00 | 0.00 | 0 | 0 | 2 | 230 | 1.05 | 0.98 |
| 105 | 2 | 0.00 | 0.00 | 0 | 0 | 2 | 115 | 1.05 | 0.98 |
| 106 | 1 | 0.00 | 0.00 | 0 | 0 | 2 | 115 | 1.05 | 0.98 |
| 107 | 1 | 0.00 | 0.00 | 0 | 0 | 2 | 115 | 1.05 | 0.98 |
| 108 | 2 | 0.00 | 0.00 | 0 | 0 | 2 | 115 | 1.06 | 0.98 |
| 109 | 2 | 0.00 | 20.60 | 0 | 0 | 2 | 230 | 1.05 | 0.98 |
| 110 | 1 | 0.00 | 0.00 | 0 | 0 | 2 | 230 | 1.05 | 0.98 |
| 111 | 2 | 0.00 | 20.60 | 0 | 0 | 2 | 230 | 1.05 | 0.98 |
| 112 | 1 | 44.42 | 24.58 | 0 | 0 | 3 | 115 | 1.05 | 0.98 |
| 113 | 2 | 10.10 | 5.59 | 0 | 0 | 3 | 115 | 1.05 | 0.98 |
| 114 | 1 | 41.36 | -1.90 | 0 | 0 | 3 | 115 | 1.05 | 0.98 |
| 115 | 1 | 59.65 | 7.00 | 0 | 0 | 3 | 115 | 1.05 | 0.98 |
| 116 | 1 | 150.24 | 16.13 | 0 | 0 | 3 | 115 | 1.05 | 0.98 |
| 117 | 2 | 65.70 | 36.35 | 0 | 0 | 3 | 115 | 1.05 | 0.98 |
| 118 | 1 | 50.86 | 28.14 | 0 | 0 | 3 | 115 | 1.05 | 0.98 |
| 119 | 1 | 84.46 | 6.67 | 0 | 0 | 3 | 115 | 1.05 | 0.98 |
| 120 | 1 | 19.38 | 1.30 | 0 | 0 | 3 | 115 | 1.05 | 0.98 |
| 121 | 1 | 89.87 | 21.15 | 0 | 0 | 3 | 115 | 1.05 | 0.98 |
| 122 | 1 | 29.65 | 1.57 | 0 | 0 | 3 | 115 | 1.05 | 0.98 |
| 123 | 1 | 67.13 | -0.55 | 0 | 0 | 3 | 115 | 1.05 | 0.98 |
| 124 | 1 | 27.62 | -7.05 | 0 | 0 | 3 | 115 | 1.05 | 0.98 |
| 125 | 1 | 39.54 | 21.88 | 0 | 0 | 3 | 115 | 1.05 | 0.98 |
| 126 | 1 | 35.21 | -25.92 | 0 | 0 | 3 | 115 | 1.05 | 0.98 |
| 127 | 1 | 96.11 | 30.48 | 0 | 0 | 3 | 115 | 1.05 | 0.98 |
| 128 | 1 | 35.90 | 19.86 | 0 | 0 | 3 | 115 | 1.05 | 0.98 |
| 129 | 1 | 6.22 | 3.44 | 0 | 0 | 3 | 115 | 1.05 | 0.98 |
| 130 | 1 | 38.27 | -23.95 | 0 | 0 | 3 | 115 | 1.05 | 0.98 |

Table A.6 Bus data of Thailand power system-continued

| Bus | Type | $P_d$ | $Q_d$ | $G_s$ | $B_s$ | Area | kV | $V^{max}$ | $V^{min}$ |
|---|---|---|---|---|---|---|---|---|---|
| 131 | 1 | 29.23 | 9.93 | 0 | 0 | 3 | 115 | 1.05 | 0.98 |
| 132 | 1 | 28.91 | 0.46 | 0 | 0 | 3 | 115 | 1.05 | 0.98 |
| 133 | 1 | 39.19 | -13.19 | 0 | 0 | 3 | 115 | 1.05 | 0.98 |
| 134 | 1 | 71.10 | -3.46 | 0 | 0 | 3 | 115 | 1.05 | 0.98 |
| 135 | 1 | 20.54 | 0.24 | 0 | 0 | 3 | 115 | 1.05 | 0.98 |
| 136 | 1 | 17.62 | 9.75 | 0 | 0 | 3 | 115 | 1.05 | 0.98 |
| 137 | 1 | 22.07 | -6.64 | 0 | 0 | 3 | 115 | 1.05 | 0.98 |
| 138 | 1 | 141.21 | 55.80 | 0 | 0 | 3 | 115 | 1.05 | 0.98 |
| 139 | 1 | 48.49 | 26.83 | 0 | 0 | 3 | 115 | 1.05 | 0.98 |
| 140 | 1 | 0.00 | 0.00 | 0 | 0 | 3 | 115 | 1.05 | 0.98 |
| 141 | 1 | 0.00 | 0.00 | 0 | 0 | 3 | 230 | 1.05 | 0.98 |
| 142 | 2 | 0.00 | 0.00 | 0 | 0 | 3 | 230 | 1.05 | 0.98 |
| 143 | 1 | 0.00 | 0.00 | 0 | 0 | 3 | 230 | 1.05 | 0.98 |
| 144 | 2 | 0.00 | 0.00 | 0 | 0 | 3 | 230 | 1.05 | 0.98 |
| 145 | 1 | 0.00 | 0.00 | 0 | 0 | 3 | 230 | 1.05 | 0.98 |
| 146 | 1 | 0.00 | 0.00 | 0 | 0 | 3 | 230 | 1.05 | 0.98 |
| 147 | 2 | 0.00 | 0.00 | 0 | 0 | 3 | 230 | 1.05 | 0.98 |
| 148 | 2 | 0.00 | 0.00 | 0 | 0 | 3 | 230 | 1.05 | 0.98 |
| 149 | 1 | 0.00 | 0.00 | 0 | 0 | 3 | 230 | 1.05 | 0.98 |
| 150 | 1 | 0.00 | 0.00 | 0 | 0 | 3 | 230 | 1.05 | 0.98 |
| 151 | 1 | 44.24 | 11.91 | 0 | 0 | 4 | 115 | 1.05 | 0.98 |
| 152 | 1 | 3.87 | 2.14 | 0 | 0 | 4 | 115 | 1.05 | 0.98 |
| 153 | 1 | 21.75 | 5.75 | 0 | 0 | 4 | 115 | 1.05 | 0.98 |
| 154 | 1 | 51.03 | -6.95 | 0 | 0 | 4 | 115 | 1.05 | 0.98 |
| 155 | 1 | 70.34 | -16.19 | 0 | 0 | 4 | 115 | 1.05 | 0.98 |
| 156 | 1 | 156.24 | 30.92 | 0 | 0 | 4 | 115 | 1.05 | 0.98 |
| 157 | 1 | 73.44 | 19.87 | 0 | 0 | 4 | 115 | 1.05 | 0.98 |
| 158 | 1 | 37.37 | -7.43 | 0 | 0 | 4 | 115 | 1.05 | 0.98 |
| 159 | 1 | 38.27 | -12.91 | 0 | 0 | 4 | 115 | 1.05 | 0.98 |
| 160 | 1 | 43.78 | 24.22 | 0 | 0 | 4 | 115 | 1.05 | 0.98 |
| 161 | 1 | 65.31 | 26.77 | 0 | 0 | 4 | 115 | 1.05 | 0.98 |
| 162 | 1 | 19.45 | 10.76 | 0 | 0 | 4 | 115 | 1.05 | 0.98 |
| 163 | 1 | 46.70 | -26.83 | 0 | 0 | 4 | 115 | 1.05 | 0.98 |
| 164 | 2 | 16.25 | 8.99 | 0 | 0 | 4 | 115 | 1.05 | 0.98 |
| 165 | 1 | 31.20 | 17.26 | 0 | 0 | 4 | 115 | 1.05 | 0.98 |
| 166 | 1 | 41.06 | 13.31 | 0 | 0 | 4 | 115 | 1.05 | 0.98 |
| 167 | 1 | 12.16 | 6.73 | 0 | 0 | 4 | 115 | 1.05 | 0.98 |
| 168 | 1 | 0.00 | 0.00 | 0 | 0 | 4 | 115 | 1.05 | 0.98 |
| 169 | 1 | 44.80 | 24.78 | 0 | 0 | 4 | 115 | 1.05 | 0.98 |
| 170 | 1 | 21.96 | -0.34 | 0 | 0 | 4 | 115 | 1.05 | 0.98 |
| 171 | 1 | 61.83 | 5.27 | 0 | 0 | 4 | 115 | 1.05 | 0.98 |
| 172 | 1 | 77.55 | 42.91 | 0 | 0 | 4 | 115 | 1.05 | 0.98 |
| 173 | 1 | 36.96 | -13.88 | 0 | 0 | 4 | 115 | 1.05 | 0.98 |
| 174 | 1 | 33.50 | -2.66 | 0 | 0 | 4 | 115 | 1.05 | 0.98 |
| 175 | 1 | 28.95 | -6.08 | 0 | 0 | 4 | 115 | 1.05 | 0.98 |
| 176 | 1 | 27.25 | -7.62 | 0 | 0 | 4 | 115 | 1.05 | 0.98 |
| 177 | 1 | 50.20 | 27.78 | 0 | 0 | 4 | 115 | 1.05 | 0.98 |

Table A.6 Bus data of Thailand power system-continued

| Bus | Type | $P_d$ | $Q_d$ | $G_s$ | $B_s$ | Area | kV | $V^{max}$ | $V^{min}$ |
|---|---|---|---|---|---|---|---|---|---|
| 178 | 1 | 62.06 | 34.34 | 0 | 0 | 4 | 115 | 1.05 | 0.98 |
| 179 | 1 | 46.66 | 19.53 | 0 | 0 | 4 | 115 | 1.05 | 0.98 |
| 180 | 1 | 22.42 | 12.40 | 0 | 0 | 4 | 115 | 1.05 | 0.98 |
| 181 | 1 | 26.98 | 2.36 | 0 | 0 | 4 | 115 | 1.05 | 0.98 |
| 182 | 1 | 13.28 | 7.35 | 0 | 0 | 4 | 115 | 1.05 | 0.98 |
| 183 | 1 | 5.93 | 3.28 | 0 | 0 | 4 | 115 | 1.05 | 0.98 |
| 184 | 1 | 30.52 | 10.60 | 0 | 0 | 4 | 115 | 1.05 | 0.98 |
| 185 | 1 | 19.47 | 10.77 | 0 | 0 | 4 | 115 | 1.05 | 0.98 |
| 186 | 1 | 33.92 | 12.68 | 0 | 0 | 4 | 115 | 1.05 | 0.98 |
| 187 | 1 | 12.95 | 7.16 | 0 | 0 | 4 | 115 | 1.05 | 0.98 |
| 188 | 1 | 9.61 | 5.31 | 0 | 0 | 4 | 115 | 1.05 | 0.98 |
| 189 | 1 | 27.93 | 9.19 | 0 | 0 | 4 | 115 | 1.05 | 0.98 |
| 190 | 1 | 33.47 | 12.23 | 0 | 0 | 4 | 115 | 1.05 | 0.98 |
| 191 | 2 | 0.00 | 0.00 | 0 | 0 | 4 | 230 | 1.05 | 0.98 |
| 192 | 1 | 0.00 | 0.00 | 0 | 0 | 4 | 230 | 1.05 | 0.98 |
| 193 | 1 | 0.00 | 0.00 | 0 | 0 | 4 | 230 | 1.05 | 0.98 |
| 194 | 1 | 0.00 | 0.00 | 0 | 0 | 4 | 230 | 1.05 | 0.98 |
| 195 | 2 | 0.00 | 0.00 | 0 | 0 | 4 | 230 | 1.05 | 0.98 |
| 196 | 1 | 0.00 | 0.00 | 0 | 0 | 4 | 230 | 1.05 | 0.98 |
| 197 | 1 | 0.00 | 0.00 | 0 | 0 | 4 | 230 | 1.05 | 0.98 |
| 198 | 2 | 0.00 | 0.00 | 0 | 0 | 4 | 230 | 1.05 | 0.98 |
| 199 | 1 | 45.05 | 24.93 | 0 | 0 | 4 | 230 | 1.05 | 0.98 |
| 200 | 2 | 0.00 | 0.00 | 0 | 0 | 4 | 230 | 1.05 | 0.98 |
| 201 | 2 | 0.00 | 0.00 | 0 | 0 | 4 | 500 | 1.05 | 0.98 |
| 202 | 1 | 0.00 | 0.00 | 0 | 0 | 4 | 500 | 1.06 | 0.98 |
| 203 | 1 | 29.32 | 16.22 | 0 | 0 | 5 | 69 | 1.05 | 0.98 |
| 204 | 1 | 0.00 | 0.00 | 0 | 0 | 5 | 69 | 1.05 | 0.98 |
| 205 | 1 | 0.80 | 0.44 | 0 | 0 | 5 | 69 | 1.05 | 0.98 |
| 206 | 1 | 26.37 | 14.59 | 0 | 0 | 5 | 115 | 1.05 | 0.98 |
| 207 | 1 | 110.53 | 15.36 | 0 | 0 | 5 | 115 | 1.05 | 0.98 |
| 208 | 1 | 45.50 | 9.57 | 0 | 0 | 5 | 115 | 1.05 | 0.98 |
| 209 | 1 | 35.86 | 7.36 | 0 | 0 | 5 | 115 | 1.05 | 0.98 |
| 210 | 1 | 58.93 | 25.32 | 0 | 0 | 5 | 115 | 1.05 | 0.98 |
| 211 | 2 | 343.96 | 42.75 | 0 | 0 | 5 | 115 | 1.066 | 0.996 |
| 212 | 1 | 32.50 | -6.98 | 0 | 0 | 5 | 115 | 1.05 | 0.98 |
| 213 | 1 | 27.07 | 11.86 | 0 | 0 | 5 | 115 | 1.05 | 0.98 |
| 214 | 1 | 30.50 | -13.41 | 0 | 0 | 5 | 115 | 1.05 | 0.98 |
| 215 | 1 | 43.84 | 1.55 | 0 | 0 | 5 | 115 | 1.05 | 0.98 |
| 216 | 1 | 33.87 | 6.26 | 0 | 0 | 5 | 115 | 1.05 | 0.98 |
| 217 | 1 | 35.00 | -9.58 | 0 | 0 | 5 | 115 | 1.05 | 0.98 |
| 218 | 1 | 18.71 | -6.30 | 0 | 0 | 5 | 115 | 1.05 | 0.98 |
| 219 | 1 | 412.14 | 45.26 | 0 | 0 | 5 | 115 | 1.05 | 0.98 |
| 220 | 1 | 86.55 | 2.49 | 0 | 0 | 5 | 115 | 1.05 | 0.98 |
| 221 | 1 | 45.13 | -7.09 | 0 | 0 | 5 | 115 | 1.05 | 0.98 |
| 222 | 1 | 18.44 | -5.40 | 0 | 0 | 5 | 115 | 1.05 | 0.98 |
| 223 | 1 | 74.41 | 41.17 | 0 | 0 | 5 | 115 | 1.05 | 0.98 |
| 224 | 1 | 60.00 | 4.02 | 0 | 0 | 5 | 115 | 1.05 | 0.98 |

Table A.6 Bus data of Thailand power system-continued

| Bus | Type | $P_d$ | $Q_d$ | $G_s$ | $B_s$ | Area | kV | $V^{max}$ | $V^{min}$ |
|---|---|---|---|---|---|---|---|---|---|
| 225 | 2 | 208.10 | 47.04 | 0 | 0 | 5 | 115 | 1.05 | 0.98 |
| 226 | 1 | 0.00 | 0.00 | 0 | 0 | 5 | 230 | 1.05 | 0.98 |
| 227 | 1 | 0.00 | -66.99 | 0 | 0 | 5 | 230 | 1.05 | 0.98 |
| 228 | 1 | 0.00 | 0.00 | 0 | 0 | 5 | 230 | 1.05 | 0.98 |
| 229 | 1 | 0.00 | 0.00 | 0 | 0 | 5 | 230 | 1.05 | 0.98 |
| 230 | 1 | 0.00 | 0.00 | 0 | 0 | 5 | 230 | 1.05 | 0.98 |
| 231 | 2 | 0.00 | 0.00 | 0 | 0 | 5 | 230 | 1.05 | 0.98 |
| 232 | 2 | 0.00 | 0.00 | 0 | 0 | 5 | 230 | 1.05 | 0.98 |
| 233 | 1 | 0.00 | 0.00 | 0 | 0 | 5 | 500 | 1.06 | 0.98 |
| 234 | 2 | 245.91 | 45.26 | 0 | 0 | 6 | 115 | 1.068 | 0.998 |
| 235 | 1 | 73.66 | -4.17 | 0 | 0 | 6 | 115 | 1.05 | 0.98 |
| 236 | 1 | 81.50 | 45.10 | 0 | 0 | 6 | 115 | 1.05 | 0.98 |
| 237 | 1 | 103.93 | 24.32 | 0 | 0 | 6 | 115 | 1.05 | 0.98 |
| 238 | 1 | 0.00 | 0.00 | 0 | 0 | 6 | 115 | 1.05 | 0.98 |
| 239 | 2 | 266.03 | 101.79 | 0 | 0 | 6 | 115 | 1.071 | 1.001 |
| 240 | 1 | 34.29 | -3.73 | 0 | 0 | 6 | 115 | 1.05 | 0.98 |
| 241 | 1 | 95.49 | -6.35 | 0 | 0 | 6 | 115 | 1.05 | 0.98 |
| 242 | 1 | 27.06 | 14.97 | 0 | 0 | 6 | 115 | 1.05 | 0.98 |
| 243 | 1 | 45.06 | 17.52 | 0 | 0 | 6 | 115 | 1.05 | 0.98 |
| 244 | 2 | 398.41 | 153.44 | 0 | 0 | 6 | 115 | 1.05 | 0.98 |
| 245 | 2 | 0.00 | 0.00 | 0 | 0 | 6 | 115 | 1.05 | 0.98 |
| 246 | 1 | 41.05 | -11.34 | 0 | 0 | 6 | 115 | 1.05 | 0.98 |
| 247 | 1 | 41.14 | 1.22 | 0 | 0 | 6 | 115 | 1.05 | 0.98 |
| 248 | 2 | 131.30 | 38.59 | 0 | 0 | 6 | 115 | 1.067 | 0.997 |
| 249 | 2 | 121.78 | 25.68 | 0 | 0 | 6 | 115 | 1.0555 | 0.986 |
| 250 | 1 | 0.00 | 0.00 | 0 | 0 | 6 | 115 | 1.05 | 0.98 |
| 251 | 2 | 67.06 | 3.05 | 0 | 0 | 6 | 115 | 1.063 | 0.993 |
| 252 | 1 | 9.60 | 5.31 | 0 | 0 | 6 | 115 | 1.05 | 0.98 |
| 253 | 1 | 28.48 | 8.34 | 0 | 0 | 6 | 115 | 1.05 | 0.98 |
| 254 | 2 | 0.00 | 0.00 | 0 | 0 | 6 | 115 | 1.05 | 0.98 |
| 255 | 1 | 48.62 | -1.48 | 0 | 0 | 6 | 115 | 1.05 | 0.98 |
| 256 | 1 | 38.92 | -9.92 | 0 | 0 | 6 | 115 | 1.05 | 0.98 |
| 257 | 1 | 18.90 | -5.15 | 0 | 0 | 6 | 115 | 1.05 | 0.98 |
| 258 | 2 | 0.00 | 0.00 | 0 | 0 | 6 | 115 | 1.05 | 0.98 |
| 259 | 2 | 267.28 | 40.68 | 0 | 0 | 6 | 115 | 1.07 | 1 |
| 260 | 1 | 0.00 | -66.99 | 0 | 0 | 6 | 230 | 1.05 | 0.98 |
| 261 | 2 | 120.00 | 66.39 | 0 | 0 | 6 | 230 | 1.05 | 0.98 |
| 262 | 2 | 0.00 | 0.00 | 0 | 0 | 6 | 230 | 1.05 | 0.98 |
| 263 | 2 | 0.00 | 0.00 | 0 | 0 | 6 | 230 | 1.05 | 0.98 |
| 264 | 1 | 0.00 | 0.00 | 0 | 0 | 6 | 230 | 1.05 | 0.98 |
| 265 | 1 | 0.00 | 0.00 | 0 | 0 | 6 | 230 | 1.05 | 0.98 |
| 266 | 2 | 0.00 | 0.00 | 0 | 0 | 6 | 230 | 1.05 | 0.98 |
| 267 | 1 | 0.00 | 0.00 | 0 | 0 | 6 | 230 | 1.05 | 0.98 |
| 268 | 2 | 0.00 | 0.00 | 0 | 0 | 6 | 230 | 1.05 | 0.98 |
| 269 | 1 | 0.00 | 0.00 | 0 | 0 | 6 | 230 | 1.05 | 0.98 |
| 270 | 1 | 0.00 | 0.00 | 0 | 0 | 6 | 500 | 1.05 | 0.98 |
| 271 | 2 | 0.00 | 0.00 | 0 | 0 | 6 | 230 | 1.05 | 0.98 |

Table A.6 Bus data of Thailand power system-continued

| Bus | Type | $P_d$ | $Q_d$ | $G_s$ | $B_s$ | Area | kV | $V^{max}$ | $V^{min}$ |
|---|---|---|---|---|---|---|---|---|---|
| 272 | 2 | 0.00 | 0.00 | 0 | 0 | 6 | 230 | 1.05 | 0.98 |
| 273 | 2 | 0.00 | 0.00 | 0 | 0 | 6 | 230 | 1.05 | 0.98 |
| 274 | 2 | 0.00 | 0.00 | 0 | 0 | 6 | 115 | 1.05 | 0.98 |
| 275 | 1 | 0.00 | 0.00 | 0 | 0 | 6 | 230 | 1.05 | 0.98 |
| 276 | 1 | 58.40 | 27.78 | 0 | 0 | 7 | 115 | 1.05 | 0.98 |
| 277 | 1 | 171.40 | 49.04 | 0 | 0 | 7 | 115 | 1.05 | 0.98 |
| 278 | 1 | 92.60 | 51.23 | 0 | 0 | 7 | 115 | 1.05 | 0.98 |
| 279 | 1 | 36.63 | 20.27 | 0 | 0 | 7 | 115 | 1.05 | 0.98 |
| 280 | 1 | 29.68 | -5.91 | 0 | 0 | 7 | 115 | 1.05 | 0.98 |
| 281 | 2 | 8.02 | 4.44 | 0 | 0 | 7 | 115 | 1.05 | 0.98 |
| 282 | 1 | 23.34 | 6.67 | 0 | 0 | 7 | 115 | 1.05 | 0.98 |
| 283 | 1 | 70.17 | -25.30 | 0 | 0 | 7 | 115 | 1.05 | 0.98 |
| 284 | 1 | 7.74 | 4.28 | 0 | 0 | 7 | 115 | 1.05 | 0.98 |
| 285 | 1 | 116.76 | -11.45 | 0 | 0 | 7 | 115 | 1.05 | 0.98 |
| 286 | 1 | 42.90 | 11.25 | 0 | 0 | 7 | 115 | 1.05 | 0.98 |
| 287 | 1 | 30.04 | 16.62 | 0 | 0 | 7 | 115 | 1.05 | 0.98 |
| 288 | 1 | 26.31 | 10.31 | 0 | 0 | 7 | 115 | 1.05 | 0.98 |
| 289 | 1 | 30.30 | 7.44 | 0 | 0 | 7 | 115 | 1.05 | 0.98 |
| 290 | 1 | 164.67 | 35.28 | 0 | 0 | 7 | 115 | 1.05 | 0.98 |
| 291 | 1 | 430.53 | -15.09 | 0 | 0 | 7 | 115 | 1.05 | 0.98 |
| 292 | 1 | 64.75 | -9.58 | 0 | 0 | 7 | 115 | 1.05 | 0.98 |
| 293 | 1 | 62.04 | 0.87 | 0 | 0 | 7 | 115 | 1.05 | 0.98 |
| 294 | 1 | 79.66 | -42.38 | 0 | 0 | 7 | 115 | 1.05 | 0.98 |
| 295 | 1 | 54.39 | -14.94 | 0 | 0 | 7 | 115 | 1.05 | 0.98 |
| 296 | 1 | 137.46 | 53.16 | 0 | 0 | 7 | 115 | 1.05 | 0.98 |
| 297 | 1 | 44.15 | 5.70 | 0 | 0 | 7 | 115 | 1.05 | 0.98 |
| 298 | 1 | 0.78 | 0.43 | 0 | 0 | 7 | 115 | 1.05 | 0.98 |
| 299 | 1 | 33.02 | 18.27 | 0 | 0 | 7 | 115 | 1.05 | 0.98 |
| 300 | 2 | 2.34 | 1.29 | 0 | 0 | 7 | 115 | 1.05 | 0.98 |
| 301 | 1 | 0.00 | 0.00 | 0 | 0 | 7 | 230 | 1.05 | 0.98 |
| 302 | 2 | 0.00 | 0.00 | 0 | 0 | 7 | 230 | 1.05 | 0.98 |
| 303 | 1 | 0.00 | 0.00 | 0 | 0 | 7 | 230 | 1.05 | 0.98 |
| 304 | 2 | 0.00 | 0.00 | 0 | 0 | 7 | 230 | 1.05 | 0.98 |
| 305 | 1 | 0.00 | 0.00 | 0 | 0 | 7 | 230 | 1.05 | 0.98 |
| 306 | 1 | 0.00 | 0.00 | 0 | 0 | 7 | 230 | 1.05 | 0.98 |
| 307 | 2 | 0.00 | 0.00 | 0 | 0 | 7 | 230 | 1.05 | 0.98 |
| 308 | 1 | 0.00 | 0.00 | 0 | 0 | 7 | 230 | 1.05 | 0.98 |
| 309 | 1 | 0.00 | 0.00 | 0 | 0 | 7 | 230 | 1.05 | 0.98 |
| 310 | 2 | 0.00 | 0.00 | 0 | 0 | 7 | 230 | 1.05 | 0.98 |
| 311 | 1 | 0.00 | 0.00 | 0 | 0 | 7 | 500 | 1.05 | 0.98 |
| 312 | 3 | 0.00 | 0.00 | 0 | 0 | 7 | 500 | 1.05 | 0.98 |
| 313 | 2 | 0.00 | 0.00 | 0 | 0 | 7 | 230 | 1.05 | 0.98 |

Table A.7 Generator data of Thailand power system

| Gen | Bus | $P_g$ | $Q_g^{max}$ | $Q_g^{min}$ | Vg | Base | $P_g^{max}$ | $P_g^{min}$ |
|---|---|---|---|---|---|---|---|---|
| 1 | 39 | 1756 | 1310 | -660 | 1.02 | 2910.5 | 2271 | 0 |
| 2 | 2 | 90 | 55 | -27 | 1.028 | 188.6 | 180 | 0 |
| 3 | 53 | 39.5 | 19.4 | -8 | 1.049 | 45 | 40 | 0 |
| 4 | 98 | 249.5 | 242 | -120 | 1.02 | 556 | 500 | 0 |
| 5 | 45 | 5.5 | 3.6 | 0 | 1.025 | 7 | 6 | 0 |
| 6 | 101 | 509 | 372 | -240 | 1.04 | 902 | 710 | 0 |
| 7 | 73 | 59 | 64 | -44 | 1.045 | 144 | 136 | 0 |
| 8 | 85 | 29.5 | 18.6 | -9 | 1.025 | 42 | 36 | 0 |
| 9 | 89 | 15.5 | 12.9 | -9 | 1.045 | 31.5 | 30 | 0 |
| 10 | 109 | 125 | 60 | -30 | 1.048 | 144 | 138 | 0 |
| 11 | 105 | 79 | 93 | -44 | 1.049 | 185 | 160 | 0 |
| 12 | 111 | 209 | 130 | -64 | 1.048 | 252 | 220 | 0 |
| 13 | 108 | 24 | 32.09 | -14 | 1.05 | 55.3 | 45 | 0 |
| 14 | 113 | 59 | 44.7 | -21 | 1.043 | 84.72 | 72 | 0 |
| 15 | 144 | 225 | 180 | -90 | 1.04 | 446 | 300 | 0 |
| 16 | 117 | 71.5 | 46.5 | -23 | 1.02 | 88.33 | 75 | 0 |
| 17 | 142 | 718.5 | 464.1 | -229 | 1.037 | 973.33 | 761 | 0 |
| 18 | 147 | 159 | 141 | -222 | 1.04 | 267 | 240 | 0 |
| 19 | 148 | 346 | 186 | -120 | 1.04 | 451.5 | 360 | 0 |
| 20 | 191 | 419 | 257.4 | -125 | 1.045 | 750.53 | 730 | 0 |
| 21 | 164 | 128.5 | 96.1 | -47 | 1.045 | 201.04 | 160 | 0 |
| 22 | 195 | 440 | 372 | -200 | 1.04 | 668 | 600 | 0 |
| 23 | 201 | 1140 | 1116 | -600 | 1.042 | 2000 | 1800 | 0 |
| 24 | 198 | 314 | 166.4 | -80 | 1.03 | 528 | 500 | 0 |
| 25 | 200 | 0 | 160 | -300 | 1.04 | 460 | 0 | 0 |
| 26 | 231 | 984 | 806 | -402 | 1.03 | 1534.4 | 1302 | 0 |
| 27 | 232 | 552 | 451 | -225 | 1.03 | 857.65 | 728 | 0 |
| 28 | 27 | 10 | 6.2 | -3 | 1.034 | 47.1 | 47 | 0 |
| 29 | 225 | 90 | 55 | -27 | 1.01 | 130.59 | 119 | 0 |
| 30 | 211 | 180 | 110 | -54 | 1.04 | 328.85 | 309 | 0 |
| 31 | 263 | 1052 | 1114 | -612 | 1.04 | 2216.4 | 1915 | 0 |
| 32 | 262 | 850 | 1128.4 | -558 | 1.04 | 2324 | 1177 | 0 |
| 33 | 245 | 11.5 | 7.6 | -6 | 1.025 | 15.6 | 13.6 | 0 |
| 34 | 268 | 1164 | 744 | -480 | 1.035 | 1496.2 | 1297.1 | 0 |
| 35 | 273 | 700 | 516 | -255 | 1.04 | 982 | 836 | 0 |
| 36 | 272 | 350 | 260 | -130 | 1.045 | 500 | 428 | 0 |
| 37 | 271 | 712 | 520 | -260 | 1.038 | 1000 | 855 | 0 |
| 38 | 254 | 221.87 | 135 | -66.5 | 1.036 | 491.28 | 472 | 0 |
| 39 | 248 | 25 | 22 | -11 | 1.032 | 55.76 | 51.2 | 0 |
| 40 | 251 | 180 | 110 | -54 | 1.028 | 402.6 | 387 | 0 |
| 41 | 259 | 302 | 186.4 | -91 | 1.032 | 651.78 | 621 | 0 |
| 42 | 266 | 300 | 184 | -90 | 1.036 | 626.7 | 598 | 0 |
| 43 | 274 | 41 | 25 | -12 | 1.04 | 137.88 | 136 | 0 |
| 44 | 258 | 70 | 43 | -21 | 1.046 | 247 | 243 | 0 |
| 45 | 261 | 60 | 37 | -18 | 1.029 | 352.9 | 351 | 0 |
| 46 | 244 | 180 | 110 | -54 | 1.018 | 352.94 | 335 | 0 |

Table A.7 Generator data of Thailand power system-continued

| Gen | Bus | $P_g$ | $Q_g^{max}$ | $Q_g^{min}$ | Vg | Base | $P_g^{max}$ | $P_g^{min}$ |
|---|---|---|---|---|---|---|---|---|
| 47 | 234 | 150 | 92 | -45 | 1.033 | 263.04 | 246 | 0 |
| 48 | 239 | 90 | 55 | -27 | 1.036 | 159.29 | 150 | 0 |
| 49 | 249 | 45 | 27 | -13 | 1.0205 | 168.24 | 166 | 0 |
| 50 | 302 | 0 | 300 | -50 | 1.03 | 350 | 0 | 0 |
| 51 | 304 | 199 | 114 | -57 | 1.047 | 333.3 | 300 | 0 |
| 52 | 281 | 12.8 | 9 | -4 | 1.01 | 21.2 | 17.5 | 0 |
| 53 | 307 | 1123.6 | 896 | -448 | 1.03 | 1705.9 | 1451 | 0 |
| 54 | 312 | 881.25 | 1358 | -678 | 1.033 | 2833 | 2484 | 0 |
| 55 | 310 | 349 | 342 | -171 | 1.04 | 850 | 720 | 0 |
| 56 | 300 | 37.5 | 12.6 | -6 | 1.035 | 41 | 38 | 0 |
| 57 | 313 | 700 | 495 | -242 | 1.025 | 944 | 800 | 0 |

Table A.8 Transmission line data of Thailand power system

| Line | From Bus | To Bus | *r* | *x* | *b* | Rating | Ratio |
|---|---|---|---|---|---|---|---|
| 1 | 28 | 1 | 0 | 0.055 | 0 | 300 | 1.000 |
| 2 | 28 | 1 | 0 | 0.055 | 0 | 300 | 1.000 |
| 3 | 29 | 2 | 0 | 0.065 | 0 | 200 | 1.000 |
| 4 | 29 | 2 | 0 | 0.065 | 0 | 200 | 1.000 |
| 5 | 29 | 2 | 0 | 0.065 | 0 | 200 | 1.000 |
| 6 | 29 | 2 | 0 | 0.065 | 0 | 200 | 1.000 |
| 7 | 30 | 3 | 0 | 0.064 | 0 | 200 | 1.000 |
| 8 | 30 | 3 | 0 | 0.065 | 0 | 200 | 1.000 |
| 9 | 32 | 4 | 0 | 0.04635 | 0 | 200 | 0.988 |
| 10 | 32 | 4 | 0 | 0.04685 | 0 | 200 | 0.988 |
| 11 | 34 | 5 | 0 | 0.0625 | 0 | 200 | 0.988 |
| 12 | 34 | 5 | 0 | 0.06583 | 0 | 200 | 0.988 |
| 13 | 36 | 6 | 0 | 0.0655 | 0 | 200 | 1.000 |
| 14 | 36 | 6 | 0 | 0.065 | 0 | 200 | 1.000 |
| 15 | 36 | 6 | 0 | 0.065 | 0 | 200 | 1.000 |
| 16 | 36 | 6 | 0 | 0.065 | 0 | 200 | 1.000 |
| 17 | 37 | 7 | 0 | 0.055 | 0 | 300 | 1.000 |
| 18 | 37 | 7 | 0 | 0.055 | 0 | 300 | 1.000 |
| 19 | 39 | 8 | 0 | 0.055 | 0 | 300 | 0.988 |
| 20 | 39 | 8 | 0 | 0.055 | 0 | 300 | 0.988 |
| 21 | 40 | 9 | 0 | 0.065 | 0 | 200 | 1.000 |
| 22 | 40 | 9 | 0 | 0.065 | 0 | 200 | 1.000 |
| 23 | 41 | 10 | 0 | 0.055 | 0 | 300 | 0.988 |
| 24 | 41 | 10 | 0 | 0.055 | 0 | 300 | 0.988 |
| 25 | 28 | 11 | 0 | 0.06465 | 0 | 200 | 1.000 |
| 26 | 28 | 11 | 0 | 0.06465 | 0 | 200 | 1.000 |
| 27 | 30 | 12 | 0 | 0.06625 | 0 | 200 | 1.000 |
| 28 | 30 | 12 | 0 | 0.065 | 0 | 200 | 1.000 |
| 29 | 32 | 13 | 0 | 0.06635 | 0 | 200 | 0.988 |
| 30 | 32 | 13 | 0 | 0.06758 | 0 | 200 | 0.988 |

Table A.8 Transmission line data of Thailand power system-continued

| Line | From Bus | To Bus | *r* | *x* | *b* | Rating | Ratio |
|---|---|---|---|---|---|---|---|
| 31 | 34 | 14 | 0 | 0.0705 | 0 | 200 | 0.988 |
| 32 | 34 | 14 | 0 | 0.069 | 0 | 200 | 0.988 |
| 33 | 39 | 15 | 0 | 0.055 | 0 | 300 | 0.988 |
| 34 | 39 | 15 | 0 | 0.055 | 0 | 300 | 0.988 |
| 35 | 40 | 16 | 0 | 0.065 | 0 | 200 | 1.000 |
| 36 | 40 | 16 | 0 | 0.06525 | 0 | 200 | 1.000 |
| 37 | 29 | 17 | 0 | 0.06225 | 0 | 200 | 1.000 |
| 38 | 29 | 17 | 0 | 0.065 | 0 | 200 | 1.000 |
| 39 | 29 | 17 | 0 | 0.065 | 0 | 200 | 1.000 |
| 40 | 30 | 18 | 0 | 0.06 | 0 | 200 | 1.000 |
| 41 | 30 | 18 | 0 | 0.06 | 0 | 200 | 1.000 |
| 42 | 31 | 19 | 0 | 0.055 | 0 | 300 | 0.988 |
| 43 | 31 | 19 | 0 | 0.055 | 0 | 300 | 0.988 |
| 44 | 31 | 19 | 0 | 0.055 | 0 | 300 | 0.988 |
| 45 | 33 | 20 | 0 | 0.061 | 0 | 200 | 1.000 |
| 46 | 33 | 20 | 0 | 0.061 | 0 | 200 | 1.000 |
| 47 | 35 | 21 | 0 | 0.055 | 0 | 300 | 1.000 |
| 48 | 35 | 21 | 0 | 0.055 | 0 | 300 | 1.000 |
| 49 | 36 | 22 | 0 | 0.065 | 0 | 200 | 1.000 |
| 50 | 36 | 22 | 0 | 0.065 | 0 | 200 | 1.000 |
| 51 | 38 | 23 | 0 | 0.055 | 0 | 300 | 1.000 |
| 52 | 38 | 23 | 0 | 0.055 | 0 | 300 | 1.000 |
| 53 | 39 | 24 | 0 | 0.055 | 0 | 300 | 0.988 |
| 54 | 39 | 24 | 0 | 0.055 | 0 | 300 | 0.988 |
| 55 | 41 | 25 | 0 | 0.055 | 0 | 300 | 0.988 |
| 56 | 41 | 25 | 0 | 0.055 | 0 | 300 | 0.988 |
| 57 | 42 | 26 | 0 | 0.06045 | 0 | 200 | 1.000 |
| 58 | 42 | 26 | 0 | 0.06045 | 0 | 200 | 1.000 |
| 59 | 36 | 27 | 0 | 0.055 | 0 | 300 | 1.000 |
| 60 | 36 | 27 | 0 | 0.055 | 0 | 300 | 1.000 |
| 61 | 28 | 35 | 0.00045 | 0.00478 | 0.01949 | 858 | 0.000 |
| 62 | 28 | 35 | 0.00045 | 0.00478 | 0.01949 | 858 | 0.000 |
| 63 | 28 | 35 | 0.00045 | 0.00478 | 0.01949 | 858 | 0.000 |
| 64 | 28 | 35 | 0.00045 | 0.00478 | 0.01949 | 858 | 0.000 |
| 65 | 28 | 37 | 0.00022 | 0.00232 | 0.00981 | 858 | 0.000 |
| 66 | 28 | 37 | 0.00022 | 0.00232 | 0.00981 | 858 | 0.000 |
| 67 | 29 | 35 | 0.00115 | 0.00826 | 0.01824 | 429 | 0.000 |
| 68 | 29 | 35 | 0.00115 | 0.00826 | 0.01824 | 429 | 0.000 |
| 69 | 29 | 41 | 0.00022 | 0.00227 | 0.0096 | 858 | 0.000 |
| 70 | 29 | 41 | 0.00022 | 0.00227 | 0.0096 | 858 | 0.000 |
| 71 | 29 | 262 | 0.0022 | 0.02316 | 0.09447 | 858 | 0.000 |
| 72 | 29 | 262 | 0.0022 | 0.02316 | 0.09447 | 858 | 0.000 |
| 73 | 30 | 34 | 0.00092 | 0.01073 | 0.0354 | 858 | 0.000 |
| 74 | 30 | 34 | 0.00092 | 0.01073 | 0.0354 | 858 | 0.000 |
| 75 | 30 | 38 | 0.00074 | 0.01381 | 0.07009 | 1716 | 0.000 |
| 76 | 30 | 38 | 0.00074 | 0.01381 | 0.07009 | 1716 | 0.000 |

Table A.8 Transmission line data of Thailand power system-continued

| Line | From Bus | To Bus | *r* | *x* | *b* | Rating | Ratio |
|---|---|---|---|---|---|---|---|
| 77 | 30 | 40 | 0.00038 | 0.0039 | 0.01712 | 858 | 0.000 |
| 78 | 30 | 40 | 0.00038 | 0.0039 | 0.01712 | 858 | 0.000 |
| 79 | 30 | 308 | 0.00058 | 0.00599 | 0.02528 | 858 | 0.000 |
| 80 | 31 | 32 | 0.00024 | 0.00402 | 0.02611 | 1716 | 0.000 |
| 81 | 31 | 32 | 0.00024 | 0.00402 | 0.02611 | 1716 | 0.000 |
| 82 | 31 | 32 | 0.00024 | 0.00402 | 0.02611 | 1716 | 0.000 |
| 83 | 31 | 34 | 0.00028 | 0.00472 | 0.03069 | 1716 | 0.000 |
| 84 | 31 | 38 | 0.00081 | 0.01526 | 0.07746 | 1716 | 0.000 |
| 85 | 31 | 38 | 0.00081 | 0.01526 | 0.07746 | 1716 | 0.000 |
| 86 | 32 | 34 | 0.00017 | 0.0029 | 0.01884 | 1716 | 0.000 |
| 87 | 33 | 35 | 0.00046 | 0.00861 | 0.04372 | 1716 | 0.000 |
| 88 | 43 | 33 | 0 | 0.02348 | 0 | 600 | 0.975 |
| 89 | 33 | 263 | 0.0021 | 0.02203 | 0.0905 | 858 | 0.000 |
| 90 | 35 | 42 | 0.00046 | 0.00861 | 0.04372 | 1716 | 0.000 |
| 91 | 35 | 263 | 0.00289 | 0.02995 | 0.12637 | 858 | 0.000 |
| 92 | 35 | 263 | 0.00289 | 0.02995 | 0.12637 | 858 | 0.000 |
| 93 | 36 | 231 | 0.00249 | 0.02625 | 0.10711 | 858 | 0.000 |
| 94 | 36 | 231 | 0.00249 | 0.02625 | 0.10711 | 858 | 0.000 |
| 95 | 36 | 232 | 0.00249 | 0.02625 | 0.10711 | 858 | 0.000 |
| 96 | 36 | 232 | 0.00249 | 0.02625 | 0.10711 | 858 | 0.000 |
| 97 | 36 | 265 | 0.0037 | 0.03899 | 0.15921 | 858 | 0.000 |
| 98 | 36 | 265 | 0.0037 | 0.03899 | 0.15921 | 858 | 0.000 |
| 99 | 44 | 38 | 0 | 0.024 | 0 | 750 | 1.000 |
| 100 | 44 | 38 | 0 | 0.024 | 0 | 750 | 1.000 |
| 101 | 44 | 38 | 0 | 0.024 | 0 | 750 | 1.000 |
| 102 | 38 | 227 | 0.00706 | 0.05079 | 0.11233 | 429 | 0.000 |
| 103 | 38 | 227 | 0.00706 | 0.05079 | 0.11233 | 429 | 0.000 |
| 104 | 38 | 301 | 0.00134 | 0.02218 | 0.14432 | 1716 | 0.000 |
| 105 | 38 | 301 | 0.00134 | 0.02218 | 0.14432 | 1716 | 0.000 |
| 106 | 39 | 40 | 0.00079 | 0.00762 | 0.03693 | 858 | 0.000 |
| 107 | 39 | 40 | 0.00079 | 0.008 | 0.03514 | 858 | 0.000 |
| 108 | 39 | 40 | 0.00079 | 0.008 | 0.03514 | 858 | 0.000 |
| 109 | 40 | 308 | 0.00089 | 0.00919 | 0.03879 | 858 | 0.000 |
| 110 | 43 | 42 | 0 | 0.02355 | 0 | 600 | 0.975 |
| 111 | 42 | 263 | 0.0021 | 0.02203 | 0.0905 | 858 | 0.000 |
| 112 | 43 | 202 | 0.0018 | 0.02341 | 2.2139 | 2832 | 0.000 |
| 113 | 43 | 233 | 0.00044 | 0.00521 | 0.57658 | 2832 | 0.000 |
| 114 | 43 | 233 | 0.00044 | 0.00521 | 0.57658 | 2832 | 0.000 |
| 115 | 43 | 233 | 0.00048 | 0.00571 | 0.63205 | 2832 | 0.000 |
| 116 | 43 | 270 | 0.00076 | 0.01337 | 1.5146 | 3736 | 0.000 |
| 117 | 44 | 233 | 0.00051 | 0.00617 | 0.67934 | 2832 | 0.000 |
| 118 | 44 | 233 | 0.00051 | 0.00617 | 0.67934 | 2832 | 0.000 |
| 119 | 44 | 311 | 0.00055 | 0.01038 | 1.1801 | 3736 | 0.000 |
| 120 | 44 | 311 | 0.00055 | 0.01038 | 1.1801 | 3736 | 0.000 |
| 121 | 68 | 45 | 0 | 0.26583 | 0 | 40 | 1.000 |
| 122 | 46 | 62 | 0.2399 | 0.30186 | 0.03228 | 67 | 0.000 |

Table A.8 Transmission line data of Thailand power system-continued

| Line | From Bus | To Bus | *r* | *x* | *b* | Rating | Ratio |
|---|---|---|---|---|---|---|---|
| 123 | 46 | 90 | 0.04208 | 0.18498 | 0.02773 | 163 | 0.000 |
| 124 | 46 | 94 | 0.04948 | 0.13894 | 0.01947 | 120 | 0.000 |
| 125 | 46 | 94 | 0.04948 | 0.13894 | 0.01947 | 120 | 0.000 |
| 126 | 47 | 52 | 0.03644 | 0.16016 | 0.024 | 163 | 0.000 |
| 127 | 48 | 70 | 0.04118 | 0.12123 | 0.01542 | 120 | 0.000 |
| 128 | 49 | 57 | 0.03986 | 0.11191 | 0.01568 | 120 | 0.000 |
| 129 | 49 | 59 | 0.09749 | 0.27416 | 0.03849 | 120 | 0.000 |
| 130 | 50 | 74 | 0.11062 | 0.32597 | 0.04169 | 120 | 0.000 |
| 131 | 51 | 64 | 0.15785 | 0.33573 | 0.04104 | 96 | 0.000 |
| 132 | 51 | 65 | 0.13994 | 0.39437 | 0.05551 | 120 | 0.000 |
| 133 | 51 | 65 | 0.13994 | 0.39437 | 0.05551 | 120 | 0.000 |
| 134 | 51 | 78 | 0.04675 | 0.1312 | 0.0184 | 120 | 0.000 |
| 135 | 51 | 87 | 0.06623 | 0.14053 | 0.01714 | 96 | 0.000 |
| 136 | 52 | 76 | 0.05494 | 0.16165 | 0.02061 | 120 | 0.000 |
| 137 | 95 | 52 | 0 | 0.06255 | 0 | 200 | 1.000 |
| 138 | 95 | 52 | 0 | 0.065 | 0 | 200 | 1.000 |
| 139 | 53 | 54 | 0.0515 | 0.15233 | 0.01921 | 120 | 0.000 |
| 140 | 54 | 57 | 0.08824 | 0.26126 | 0.03299 | 120 | 0.000 |
| 141 | 55 | 58 | 0.07535 | 0.21139 | 0.02974 | 120 | 0.000 |
| 142 | 55 | 58 | 0.07535 | 0.21139 | 0.02974 | 120 | 0.000 |
| 143 | 55 | 61 | 0.11921 | 0.1497 | 0.01599 | 67 | 0.000 |
| 144 | 55 | 79 | 0.03814 | 0.10702 | 0.01501 | 120 | 0.000 |
| 145 | 55 | 79 | 0.03814 | 0.10702 | 0.01501 | 120 | 0.000 |
| 146 | 55 | 80 | 0.07749 | 0.34157 | 0.05131 | 163 | 0.000 |
| 147 | 55 | 86 | 0.02634 | 0.11579 | 0.01733 | 163 | 0.000 |
| 148 | 56 | 91 | 0.03456 | 0.15189 | 0.02276 | 163 | 0.000 |
| 149 | 57 | 58 | 0.0071 | 0.01991 | 0.0028 | 120 | 0.000 |
| 150 | 57 | 58 | 0.0071 | 0.01991 | 0.0028 | 120 | 0.000 |
| 151 | 57 | 59 | 0.13646 | 0.38449 | 0.05411 | 120 | 0.000 |
| 152 | 57 | 61 | 0.22217 | 0.27944 | 0.02988 | 67 | 0.000 |
| 153 | 57 | 66 | 0.02983 | 0.08373 | 0.01173 | 120 | 0.000 |
| 154 | 57 | 66 | 0.02983 | 0.08373 | 0.01173 | 120 | 0.000 |
| 155 | 57 | 76 | 0.18895 | 0.23751 | 0.02538 | 67 | 0.000 |
| 156 | 57 | 89 | 0.14093 | 0.17702 | 0.01891 | 67 | 0.000 |
| 157 | 96 | 57 | 0 | 0.06 | 0 | 200 | 0.988 |
| 158 | 96 | 57 | 0 | 0.05858 | 0 | 200 | 0.988 |
| 159 | 96 | 57 | 0 | 0.05858 | 0 | 200 | 0.988 |
| 160 | 59 | 64 | 0.04624 | 0.12984 | 0.01819 | 120 | 0.000 |
| 161 | 59 | 65 | 0.05009 | 0.14065 | 0.01971 | 120 | 0.000 |
| 162 | 60 | 69 | 0.07868 | 0.23161 | 0.02956 | 120 | 0.000 |
| 163 | 61 | 79 | 0.0985 | 0.12308 | 0.01327 | 67 | 0.000 |
| 164 | 62 | 88 | 0.02818 | 0.12376 | 0.01854 | 163 | 0.000 |
| 165 | 63 | 81 | 0.18817 | 0.20989 | 0.02861 | 67 | 0.000 |
| 166 | 63 | 88 | 0.03707 | 0.16292 | 0.02442 | 163 | 0.000 |
| 167 | 99 | 63 | 0 | 0.065 | 0 | 200 | 1.000 |
| 168 | 64 | 65 | 0.00629 | 0.02764 | 0.00413 | 163 | 0.000 |

Table A.8 Transmission line data of Thailand power system-continued

| Line | From Bus | To Bus | *r* | *x* | *b* | Rating | Ratio |
|---|---|---|---|---|---|---|---|
| 169 | 64 | 65 | 0.00629 | 0.02764 | 0.00413 | 163 | 0.000 |
| 170 | 64 | 76 | 0.28604 | 0.36032 | 0.03855 | 67 | 0.000 |
| 171 | 65 | 72 | 0.07414 | 0.21354 | 0.02873 | 118 | 0.000 |
| 172 | 65 | 84 | 0.03028 | 0.08712 | 0.01171 | 118 | 0.000 |
| 173 | 100 | 65 | 0 | 0.06265 | 0 | 200 | 0.988 |
| 174 | 100 | 65 | 0 | 0.06065 | 0 | 200 | 0.988 |
| 175 | 100 | 65 | 0 | 0.0625 | 0 | 200 | 0.988 |
| 176 | 66 | 67 | 0.00186 | 0.01236 | 0.00317 | 326 | 0.000 |
| 177 | 66 | 67 | 0.00186 | 0.01236 | 0.00317 | 326 | 0.000 |
| 178 | 66 | 89 | 0.06223 | 0.07811 | 0.00834 | 67 | 0.000 |
| 179 | 66 | 92 | 0.0991 | 0.28137 | 0.03875 | 120 | 0.000 |
| 180 | 66 | 92 | 0.0991 | 0.28137 | 0.03875 | 120 | 0.000 |
| 181 | 66 | 93 | 0.08321 | 0.23387 | 0.03281 | 120 | 0.000 |
| 182 | 66 | 93 | 0.08321 | 0.23387 | 0.03281 | 120 | 0.000 |
| 183 | 101 | 67 | 0 | 0.065 | 0 | 200 | 1.000 |
| 184 | 101 | 67 | 0 | 0.06205 | 0 | 200 | 1.000 |
| 185 | 68 | 80 | 0.01824 | 0.08016 | 0.01199 | 163 | 0.000 |
| 186 | 68 | 86 | 0.03306 | 0.14534 | 0.02176 | 163 | 0.000 |
| 187 | 69 | 92 | 0.05211 | 0.1533 | 0.01955 | 120 | 0.000 |
| 188 | 69 | 93 | 0.03832 | 0.16843 | 0.02525 | 163 | 0.000 |
| 189 | 70 | 74 | 0.05575 | 0.16577 | 0.02069 | 120 | 0.000 |
| 190 | 70 | 93 | 0.03905 | 0.11607 | 0.01448 | 120 | 0.000 |
| 191 | 71 | 92 | 0.04543 | 0.1275 | 0.01788 | 120 | 0.000 |
| 192 | 71 | 92 | 0.1161 | 0.14579 | 0.01557 | 67 | 0.000 |
| 193 | 71 | 107 | 0.02608 | 0.07316 | 0.01026 | 120 | 0.000 |
| 194 | 71 | 107 | 0.06664 | 0.08364 | 0.00893 | 67 | 0.000 |
| 195 | 72 | 219 | 0.05816 | 0.16744 | 0.02251 | 118 | 0.000 |
| 196 | 73 | 91 | 0.07162 | 0.20112 | 0.02823 | 120 | 0.000 |
| 197 | 73 | 91 | 0.07162 | 0.20112 | 0.02823 | 120 | 0.000 |
| 198 | 74 | 80 | 0.05211 | 0.15345 | 0.01953 | 120 | 0.000 |
| 199 | 74 | 80 | 0.08514 | 0.18359 | 0.02169 | 96 | 0.000 |
| 200 | 74 | 93 | 0.14593 | 0.31516 | 0.0373 | 96 | 0.000 |
| 201 | 75 | 79 | 0.0527 | 0.2318 | 0.03478 | 163 | 0.000 |
| 202 | 75 | 79 | 0.0527 | 0.2318 | 0.03478 | 163 | 0.000 |
| 203 | 75 | 87 | 0.05021 | 0.22079 | 0.03312 | 163 | 0.000 |
| 204 | 77 | 79 | 0.02829 | 0.12429 | 0.01862 | 163 | 0.000 |
| 205 | 79 | 94 | 0.0701 | 0.19686 | 0.02763 | 120 | 0.000 |
| 206 | 79 | 94 | 0.0701 | 0.19686 | 0.02763 | 120 | 0.000 |
| 207 | 79 | 94 | 0.17734 | 0.22181 | 0.02394 | 67 | 0.000 |
| 208 | 102 | 79 | 0 | 0.065 | 0 | 200 | 1.000 |
| 209 | 102 | 79 | 0 | 0.06185 | 0 | 200 | 1.000 |
| 210 | 102 | 79 | 0 | 0.065 | 0 | 200 | 1.000 |
| 211 | 80 | 81 | 0.00503 | 0.03143 | 0.00919 | 326 | 0.000 |
| 212 | 80 | 81 | 0.00503 | 0.03143 | 0.00919 | 326 | 0.000 |
| 213 | 80 | 88 | 0.27801 | 0.24842 | 0.02458 | 81 | 0.000 |
| 214 | 103 | 81 | 0 | 0.065 | 0 | 200 | 1.000 |

Table A.8 Transmission line data of Thailand power system-continued

| Line | From Bus | To Bus | *r* | *x* | *b* | Rating | Ratio |
|---|---|---|---|---|---|---|---|
| 215 | 103 | 81 | 0 | 0.065 | 0 | 200 | 1.000 |
| 216 | 103 | 81 | 0 | 0.065 | 0 | 200 | 1.000 |
| 217 | 82 | 87 | 0.02954 | 0.12981 | 0.01945 | 163 | 0.000 |
| 218 | 83 | 91 | 0.06586 | 0.18493 | 0.02595 | 120 | 0.000 |
| 219 | 83 | 91 | 0.06586 | 0.18493 | 0.02595 | 120 | 0.000 |
| 220 | 83 | 94 | 0.08965 | 0.25164 | 0.03543 | 120 | 0.000 |
| 221 | 83 | 94 | 0.08965 | 0.25164 | 0.03543 | 120 | 0.000 |
| 222 | 84 | 219 | 0.10265 | 0.29597 | 0.03987 | 118 | 0.000 |
| 223 | 85 | 90 | 0.16392 | 0.19049 | 0.02386 | 67 | 0.000 |
| 224 | 85 | 90 | 0.16392 | 0.19049 | 0.02386 | 67 | 0.000 |
| 225 | 85 | 106 | 0.06081 | 0.17892 | 0.02282 | 120 | 0.000 |
| 226 | 90 | 91 | 0.02537 | 0.07117 | 0.00998 | 120 | 0.000 |
| 227 | 90 | 91 | 0.02537 | 0.07117 | 0.00998 | 120 | 0.000 |
| 228 | 90 | 94 | 0.09649 | 0.28487 | 0.03622 | 120 | 0.000 |
| 229 | 104 | 91 | 0 | 0.065 | 0 | 200 | 1.000 |
| 230 | 104 | 91 | 0 | 0.065 | 0 | 200 | 1.000 |
| 231 | 92 | 93 | 0.01108 | 0.03194 | 0.00427 | 118 | 0.000 |
| 232 | 93 | 107 | 0.07898 | 0.22195 | 0.03113 | 120 | 0.000 |
| 233 | 95 | 97 | 0.00972 | 0.07024 | 0.15458 | 429 | 0.000 |
| 234 | 95 | 97 | 0.00972 | 0.07024 | 0.15458 | 429 | 0.000 |
| 235 | 95 | 100 | 0.01009 | 0.07296 | 0.16061 | 429 | 0.000 |
| 236 | 95 | 100 | 0.01009 | 0.07296 | 0.16061 | 429 | 0.000 |
| 237 | 95 | 200 | 0.01852 | 0.13457 | 0.29807 | 429 | 0.000 |
| 238 | 95 | 200 | 0.01852 | 0.13457 | 0.29807 | 429 | 0.000 |
| 239 | 96 | 97 | 0.0007 | 0.00504 | 0.01106 | 429 | 0.000 |
| 240 | 96 | 97 | 0.0007 | 0.00504 | 0.01106 | 429 | 0.000 |
| 241 | 97 | 101 | 0.00146 | 0.01539 | 0.06276 | 858 | 0.000 |
| 242 | 97 | 101 | 0.00146 | 0.01539 | 0.06276 | 858 | 0.000 |
| 243 | 97 | 102 | 0.01115 | 0.08062 | 0.17758 | 429 | 0.000 |
| 244 | 97 | 102 | 0.01115 | 0.08062 | 0.17758 | 429 | 0.000 |
| 245 | 97 | 194 | 0.01765 | 0.12813 | 0.28355 | 429 | 0.000 |
| 246 | 97 | 194 | 0.01765 | 0.12813 | 0.28355 | 429 | 0.000 |
| 247 | 98 | 100 | 0.00649 | 0.04685 | 0.10295 | 429 | 0.000 |
| 248 | 98 | 100 | 0.00649 | 0.04685 | 0.10295 | 429 | 0.000 |
| 249 | 98 | 229 | 0.00641 | 0.04627 | 0.10168 | 429 | 0.000 |
| 250 | 98 | 229 | 0.00641 | 0.04627 | 0.10168 | 429 | 0.000 |
| 251 | 99 | 103 | 0.00876 | 0.06318 | 0.13947 | 429 | 0.000 |
| 252 | 99 | 110 | 0.00175 | 0.01258 | 0.02772 | 429 | 0.000 |
| 253 | 103 | 110 | 0.00831 | 0.05995 | 0.13233 | 429 | 0.000 |
| 254 | 104 | 109 | 0.0225 | 0.16373 | 0.36609 | 429 | 0.000 |
| 255 | 104 | 109 | 0.0225 | 0.16373 | 0.36609 | 429 | 0.000 |
| 256 | 105 | 107 | 0.07404 | 0.20803 | 0.02918 | 120 | 0.000 |
| 257 | 105 | 107 | 0.07404 | 0.20803 | 0.02918 | 120 | 0.000 |
| 258 | 105 | 107 | 0.18921 | 0.23784 | 0.02542 | 67 | 0.000 |
| 259 | 106 | 108 | 0.07091 | 0.2087 | 0.02663 | 120 | 0.000 |
| 260 | 110 | 111 | 0.00995 | 0.07176 | 0.15852 | 429 | 0.000 |

Table A.8 Transmission line data of Thailand power system-continued

| Line | From Bus | To Bus | *r* | *x* | *b* | Rating | Ratio |
|---|---|---|---|---|---|---|---|
| 261 | 110 | 111 | 0.00995 | 0.07176 | 0.15852 | 429 | 0.000 |
| 262 | 112 | 136 | 0.0136 | 0.03937 | 0.00518 | 120 | 0.000 |
| 263 | 112 | 136 | 0.0136 | 0.03937 | 0.00518 | 120 | 0.000 |
| 264 | 113 | 140 | 0.05389 | 0.10905 | 0.01464 | 96 | 0.000 |
| 265 | 113 | 140 | 0.05389 | 0.10905 | 0.01464 | 96 | 0.000 |
| 266 | 114 | 120 | 0.05879 | 0.16502 | 0.02316 | 120 | 0.000 |
| 267 | 114 | 136 | 0.17662 | 0.49874 | 0.0705 | 120 | 0.000 |
| 268 | 114 | 278 | 0.11783 | 0.35912 | 0.04293 | 120 | 0.000 |
| 269 | 114 | 278 | 0.11783 | 0.35912 | 0.04293 | 120 | 0.000 |
| 270 | 115 | 116 | 0.01136 | 0.02421 | 0.00292 | 96 | 0.000 |
| 271 | 115 | 116 | 0.00893 | 0.02625 | 0.00335 | 120 | 0.000 |
| 272 | 115 | 125 | 0.15526 | 0.26493 | 0.0288 | 82 | 0.000 |
| 273 | 115 | 133 | 0.07434 | 0.21874 | 0.02793 | 120 | 0.000 |
| 274 | 116 | 123 | 0.09608 | 0.26999 | 0.03796 | 120 | 0.000 |
| 275 | 116 | 123 | 0.09608 | 0.26999 | 0.03796 | 120 | 0.000 |
| 276 | 116 | 132 | 0.04452 | 0.13091 | 0.0167 | 120 | 0.000 |
| 277 | 116 | 134 | 0.0209 | 0.05863 | 0.00822 | 120 | 0.000 |
| 278 | 116 | 134 | 0.0209 | 0.05863 | 0.00822 | 120 | 0.000 |
| 279 | 141 | 116 | 0 | 0.065 | 0 | 200 | 1.000 |
| 280 | 141 | 116 | 0 | 0.06692 | 0 | 200 | 1.000 |
| 281 | 141 | 116 | 0 | 0.06658 | 0 | 200 | 1.000 |
| 282 | 142 | 117 | 0 | 0.13 | 0 | 100 | 1.000 |
| 283 | 142 | 117 | 0 | 0.11833 | 0 | 100 | 1.000 |
| 284 | 118 | 119 | 0.16073 | 0.27696 | 0.02953 | 82 | 0.000 |
| 285 | 118 | 124 | 0.18486 | 0.31872 | 0.034 | 82 | 0.000 |
| 286 | 144 | 118 | 0 | 0.065 | 0 | 200 | 1.000 |
| 287 | 144 | 118 | 0 | 0.065 | 0 | 200 | 1.000 |
| 288 | 119 | 125 | 0.12065 | 0.20573 | 0.02235 | 82 | 0.000 |
| 289 | 119 | 138 | 0.03105 | 0.13644 | 0.02044 | 163 | 0.000 |
| 290 | 120 | 136 | 0.1278 | 0.35972 | 0.05065 | 120 | 0.000 |
| 291 | 121 | 131 | 0.05146 | 0.22641 | 0.03393 | 163 | 0.000 |
| 292 | 121 | 131 | 0.05146 | 0.22641 | 0.03393 | 163 | 0.000 |
| 293 | 145 | 121 | 0 | 0.0647 | 0 | 200 | 1.000 |
| 294 | 145 | 121 | 0 | 0.06495 | 0 | 200 | 1.000 |
| 295 | 122 | 135 | 0.04695 | 0.13183 | 0.01847 | 120 | 0.000 |
| 296 | 122 | 139 | 0.08729 | 0.18627 | 0.02248 | 96 | 0.000 |
| 297 | 122 | 140 | 0.03983 | 0.17505 | 0.02624 | 163 | 0.000 |
| 298 | 123 | 139 | 0.03996 | 0.11749 | 0.01499 | 120 | 0.000 |
| 299 | 124 | 126 | 0.07686 | 0.21799 | 0.03001 | 120 | 0.000 |
| 300 | 124 | 126 | 0.07686 | 0.21799 | 0.03001 | 120 | 0.000 |
| 301 | 124 | 127 | 0.03407 | 0.23506 | 0.03257 | 215 | 0.000 |
| 302 | 124 | 127 | 0.03407 | 0.23506 | 0.03257 | 215 | 0.000 |
| 303 | 124 | 129 | 0.07363 | 0.20696 | 0.02901 | 120 | 0.000 |
| 304 | 124 | 129 | 0.07363 | 0.20696 | 0.02901 | 120 | 0.000 |
| 305 | 124 | 129 | 0.04958 | 0.21804 | 0.0327 | 163 | 0.000 |
| 306 | 124 | 129 | 0.04958 | 0.21804 | 0.0327 | 163 | 0.000 |

Table A.8 Transmission line data of Thailand power system-continued

| Line | From Bus | To Bus | *r* | *x* | *b* | Rating | Ratio |
|---|---|---|---|---|---|---|---|
| 307 | 124 | 137 | 0.08537 | 0.14551 | 0.0158 | 82 | 0.000 |
| 308 | 146 | 125 | 0 | 0.065 | 0 | 200 | 1.000 |
| 309 | 146 | 125 | 0 | 0.065 | 0 | 200 | 1.000 |
| 310 | 126 | 127 | 0.01806 | 0.05117 | 0.00703 | 120 | 0.000 |
| 311 | 128 | 136 | 0.00629 | 0.01822 | 0.0024 | 120 | 0.000 |
| 312 | 128 | 136 | 0.00629 | 0.01822 | 0.0024 | 120 | 0.000 |
| 313 | 147 | 129 | 0 | 0.06965 | 0 | 200 | 1.000 |
| 314 | 147 | 129 | 0 | 0.065 | 0 | 200 | 1.000 |
| 315 | 130 | 137 | 0.16706 | 0.35834 | 0.0431 | 96 | 0.000 |
| 316 | 136 | 137 | 0.21604 | 0.36926 | 0.0402 | 82 | 0.000 |
| 317 | 148 | 136 | 0 | 0.11817 | 0 | 100 | 0.988 |
| 318 | 148 | 136 | 0 | 0.125 | 0 | 100 | 0.988 |
| 319 | 148 | 136 | 0 | 0.125 | 0 | 100 | 0.988 |
| 320 | 149 | 138 | 0 | 0.065 | 0 | 200 | 1.000 |
| 321 | 149 | 138 | 0 | 0.065 | 0 | 200 | 1.000 |
| 322 | 139 | 140 | 0.00075 | 0.00472 | 0.00138 | 326 | 0.000 |
| 323 | 139 | 140 | 0.00075 | 0.00472 | 0.00138 | 326 | 0.000 |
| 324 | 150 | 140 | 0 | 0.065 | 0 | 200 | 1.000 |
| 325 | 150 | 140 | 0 | 0.065 | 0 | 200 | 1.000 |
| 326 | 141 | 143 | 0.0015 | 0.01168 | 0.0875 | 858 | 0.000 |
| 327 | 141 | 143 | 0.0015 | 0.01168 | 0.0875 | 858 | 0.000 |
| 328 | 141 | 146 | 0.00877 | 0.06327 | 0.13957 | 429 | 0.000 |
| 329 | 141 | 146 | 0.00877 | 0.06327 | 0.13957 | 429 | 0.000 |
| 330 | 142 | 145 | 0.00971 | 0.07048 | 0.15372 | 429 | 0.000 |
| 331 | 142 | 145 | 0.00971 | 0.07048 | 0.15372 | 429 | 0.000 |
| 332 | 142 | 148 | 0.00762 | 0.05519 | 0.12066 | 429 | 0.000 |
| 333 | 142 | 148 | 0.00762 | 0.05519 | 0.12066 | 429 | 0.000 |
| 334 | 143 | 149 | 0.01031 | 0.10941 | 0.45164 | 858 | 0.000 |
| 335 | 143 | 149 | 0.01031 | 0.10941 | 0.45164 | 858 | 0.000 |
| 336 | 143 | 150 | 0.01215 | 0.08775 | 0.19412 | 429 | 0.000 |
| 337 | 143 | 150 | 0.01215 | 0.08775 | 0.19412 | 429 | 0.000 |
| 338 | 144 | 149 | 0.00965 | 0.06962 | 0.15376 | 429 | 0.000 |
| 339 | 144 | 149 | 0.00965 | 0.06962 | 0.15376 | 429 | 0.000 |
| 340 | 145 | 146 | 0.00892 | 0.06472 | 0.1411 | 429 | 0.000 |
| 341 | 145 | 146 | 0.00892 | 0.06472 | 0.1411 | 429 | 0.000 |
| 342 | 145 | 149 | 0.00539 | 0.0388 | 0.08554 | 429 | 0.000 |
| 343 | 145 | 149 | 0.00539 | 0.0388 | 0.08554 | 429 | 0.000 |
| 344 | 147 | 148 | 0.00512 | 0.03688 | 0.08123 | 429 | 0.000 |
| 345 | 147 | 148 | 0.00512 | 0.03688 | 0.08123 | 429 | 0.000 |
| 346 | 148 | 149 | 0.00606 | 0.06391 | 0.26166 | 858 | 0.000 |
| 347 | 148 | 149 | 0.00606 | 0.06391 | 0.26166 | 858 | 0.000 |
| 348 | 148 | 302 | 0.02782 | 0.20472 | 0.45648 | 429 | 0.000 |
| 349 | 148 | 302 | 0.02782 | 0.20472 | 0.45648 | 429 | 0.000 |
| 350 | 151 | 187 | 0.03055 | 0.13423 | 0.02011 | 163 | 0.000 |
| 351 | 152 | 185 | 0.04742 | 0.13958 | 0.01792 | 118 | 0.000 |
| 352 | 152 | 188 | 0.06292 | 0.18458 | 0.02389 | 118 | 0.000 |

Table A.8 Transmission line data of Thailand power system-continued

| Line | From Bus | To Bus | *r* | *x* | *b* | Rating | Ratio |
|---|---|---|---|---|---|---|---|
| 353 | 191 | 152 | 0 | 0.11883 | 0 | 100 | 1.000 |
| 354 | 191 | 152 | 0 | 0.1185 | 0 | 100 | 1.000 |
| 355 | 153 | 187 | 0.06808 | 0.19117 | 0.02683 | 120 | 0.000 |
| 356 | 154 | 155 | 0.01157 | 0.03245 | 0.00455 | 120 | 0.000 |
| 357 | 154 | 155 | 0.01157 | 0.03245 | 0.00455 | 120 | 0.000 |
| 358 | 154 | 156 | 0.00503 | 0.03352 | 0.00861 | 326 | 0.000 |
| 359 | 154 | 156 | 0.00503 | 0.03352 | 0.00861 | 326 | 0.000 |
| 360 | 155 | 163 | 0.02648 | 0.07433 | 0.01041 | 120 | 0.000 |
| 361 | 155 | 163 | 0.02648 | 0.07433 | 0.01041 | 120 | 0.000 |
| 362 | 192 | 156 | 0 | 0.065 | 0 | 200 | 0.975 |
| 363 | 192 | 156 | 0 | 0.061 | 0 | 200 | 0.975 |
| 364 | 192 | 156 | 0 | 0.065 | 0 | 200 | 0.975 |
| 365 | 157 | 166 | 0.02766 | 0.12153 | 0.01821 | 163 | 0.000 |
| 366 | 157 | 174 | 0.08119 | 0.23905 | 0.03051 | 120 | 0.000 |
| 367 | 157 | 189 | 0.04271 | 0.18773 | 0.02814 | 163 | 0.000 |
| 368 | 193 | 157 | 0 | 0.065 | 0 | 200 | 0.975 |
| 369 | 193 | 157 | 0 | 0.065 | 0 | 200 | 0.975 |
| 370 | 158 | 163 | 0.05505 | 0.16189 | 0.02066 | 120 | 0.000 |
| 371 | 159 | 164 | 0.02954 | 0.12981 | 0.01945 | 163 | 0.000 |
| 372 | 159 | 164 | 0.02954 | 0.12981 | 0.01945 | 163 | 0.000 |
| 373 | 159 | 185 | 0.06211 | 0.18664 | 0.02299 | 118 | 0.000 |
| 374 | 160 | 162 | 0.09902 | 0.21113 | 0.02584 | 95 | 0.000 |
| 375 | 160 | 168 | 0.04184 | 0.12204 | 0.01594 | 118 | 0.000 |
| 376 | 160 | 183 | 0.05361 | 0.15722 | 0.02034 | 118 | 0.000 |
| 377 | 161 | 163 | 0.07454 | 0.20945 | 0.02938 | 120 | 0.000 |
| 378 | 161 | 163 | 0.07454 | 0.20945 | 0.02938 | 120 | 0.000 |
| 379 | 161 | 167 | 0.02161 | 0.06066 | 0.0085 | 120 | 0.000 |
| 380 | 161 | 167 | 0.02161 | 0.06066 | 0.0085 | 120 | 0.000 |
| 381 | 161 | 168 | 0.00849 | 0.05304 | 0.01552 | 326 | 0.000 |
| 382 | 161 | 168 | 0.00849 | 0.05304 | 0.01552 | 326 | 0.000 |
| 383 | 162 | 163 | 0.01634 | 0.04586 | 0.00642 | 120 | 0.000 |
| 384 | 164 | 177 | 0.04793 | 0.1411 | 0.01811 | 118 | 0.000 |
| 385 | 164 | 178 | 0.05272 | 0.15509 | 0.01977 | 120 | 0.000 |
| 386 | 165 | 175 | 0.05464 | 0.1607 | 0.0205 | 120 | 0.000 |
| 387 | 194 | 165 | 0 | 0.125 | 0 | 100 | 1.000 |
| 388 | 194 | 165 | 0 | 0.125 | 0 | 100 | 1.000 |
| 389 | 168 | 169 | 0.00799 | 0.03509 | 0.00525 | 163 | 0.000 |
| 390 | 168 | 169 | 0.00799 | 0.03509 | 0.00525 | 163 | 0.000 |
| 391 | 168 | 174 | 0.12152 | 0.34195 | 0.04812 | 120 | 0.000 |
| 392 | 168 | 174 | 0.12152 | 0.34195 | 0.04812 | 120 | 0.000 |
| 393 | 168 | 179 | 0.05585 | 0.15664 | 0.02202 | 120 | 0.000 |
| 394 | 168 | 179 | 0.05585 | 0.15664 | 0.02202 | 120 | 0.000 |
| 395 | 195 | 168 | 0 | 0.065 | 0 | 200 | 0.988 |
| 396 | 195 | 168 | 0 | 0.0627 | 0 | 200 | 0.988 |
| 397 | 195 | 168 | 0 | 0.06235 | 0 | 200 | 0.988 |
| 398 | 170 | 185 | 0.05832 | 0.25656 | 0.03851 | 163 | 0.000 |

Table A.8 Transmission line data of Thailand power system-continued

| Line | From Bus | To Bus | *r* | *x* | *b* | Rating | Ratio |
|---|---|---|---|---|---|---|---|
| 399 | 171 | 172 | 0.03005 | 0.13209 | 0.01977 | 163 | 0.000 |
| 400 | 171 | 186 | 0.0546 | 0.072 | 0.00747 | 72 | 0.000 |
| 401 | 172 | 180 | 0.04918 | 0.14461 | 0.01845 | 120 | 0.000 |
| 402 | 196 | 172 | 0 | 0.06495 | 0 | 200 | 0.975 |
| 403 | 196 | 172 | 0 | 0.0651 | 0 | 200 | 0.975 |
| 404 | 173 | 179 | 0.10912 | 0.32152 | 0.04112 | 120 | 0.000 |
| 405 | 175 | 176 | 0.09448 | 0.27881 | 0.03547 | 120 | 0.000 |
| 406 | 176 | 177 | 0.04776 | 0.14075 | 0.01788 | 120 | 0.000 |
| 407 | 177 | 178 | 0.01748 | 0.05143 | 0.0066 | 118 | 0.000 |
| 408 | 178 | 184 | 0.04083 | 0.12016 | 0.01543 | 118 | 0.000 |
| 409 | 197 | 178 | 0 | 0.0625 | 0 | 200 | 0.963 |
| 410 | 197 | 178 | 0 | 0.065 | 0 | 200 | 0.963 |
| 411 | 179 | 190 | 0.06323 | 0.17737 | 0.02494 | 120 | 0.000 |
| 412 | 179 | 190 | 0.06323 | 0.17737 | 0.02494 | 120 | 0.000 |
| 413 | 181 | 184 | 0.04246 | 0.12494 | 0.01604 | 118 | 0.000 |
| 414 | 181 | 190 | 0.04955 | 0.14585 | 0.01873 | 118 | 0.000 |
| 415 | 182 | 190 | 0.0613 | 0.17592 | 0.02381 | 118 | 0.000 |
| 416 | 182 | 190 | 0.0613 | 0.17592 | 0.02381 | 118 | 0.000 |
| 417 | 198 | 182 | 0 | 0.065 | 0 | 200 | 1.000 |
| 418 | 198 | 182 | 0 | 0.065 | 0 | 200 | 1.000 |
| 419 | 183 | 188 | 0.04063 | 0.11913 | 0.01541 | 118 | 0.000 |
| 420 | 184 | 185 | 0.07768 | 0.22881 | 0.02941 | 118 | 0.000 |
| 421 | 186 | 187 | 0.04746 | 0.13319 | 0.01868 | 120 | 0.000 |
| 422 | 186 | 187 | 0.04746 | 0.13319 | 0.01868 | 120 | 0.000 |
| 423 | 186 | 221 | 0.04513 | 0.13269 | 0.01693 | 120 | 0.000 |
| 424 | 200 | 187 | 0 | 0.0604 | 0 | 200 | 0.988 |
| 425 | 200 | 187 | 0 | 0.065 | 0 | 200 | 0.988 |
| 426 | 191 | 196 | 0.02153 | 0.15627 | 0.34985 | 429 | 0.000 |
| 427 | 191 | 196 | 0.02153 | 0.15627 | 0.34985 | 429 | 0.000 |
| 428 | 191 | 199 | 0.00545 | 0.04175 | 0.0811 | 429 | 0.000 |
| 429 | 192 | 195 | 0.01373 | 0.09943 | 0.21925 | 429 | 0.000 |
| 430 | 192 | 195 | 0.01373 | 0.09943 | 0.21925 | 429 | 0.000 |
| 431 | 193 | 195 | 0.01967 | 0.14297 | 0.31736 | 429 | 0.000 |
| 432 | 193 | 195 | 0.01967 | 0.14297 | 0.31736 | 429 | 0.000 |
| 433 | 194 | 197 | 0.01231 | 0.08909 | 0.19622 | 429 | 0.000 |
| 434 | 194 | 197 | 0.01231 | 0.08909 | 0.19622 | 429 | 0.000 |
| 435 | 195 | 197 | 0.01608 | 0.11664 | 0.25775 | 429 | 0.000 |
| 436 | 195 | 197 | 0.01608 | 0.11664 | 0.25775 | 429 | 0.000 |
| 437 | 201 | 195 | 0 | 0.02167 | 0 | 600 | 0.988 |
| 438 | 201 | 195 | 0 | 0.02167 | 0 | 600 | 0.988 |
| 439 | 196 | 197 | 0.02176 | 0.10422 | 0.21206 | 326 | 0.000 |
| 440 | 196 | 197 | 0.02176 | 0.10422 | 0.21206 | 326 | 0.000 |
| 441 | 196 | 199 | 0.01617 | 0.12454 | 0.24355 | 429 | 0.000 |
| 442 | 196 | 200 | 0.00484 | 0.03481 | 0.07693 | 429 | 0.000 |
| 443 | 196 | 200 | 0.00484 | 0.03481 | 0.07693 | 429 | 0.000 |
| 444 | 196 | 227 | 0.01255 | 0.09034 | 0.20142 | 429 | 0.000 |

Table A.8 Transmission line data of Thailand power system-continued

| Line | From Bus | To Bus | *r* | *x* | *b* | Rating | Ratio |
|---|---|---|---|---|---|---|---|
| 445 | 196 | 227 | 0.01255 | 0.09034 | 0.20142 | 429 | 0.000 |
| 446 | 197 | 198 | 0.01832 | 0.08764 | 0.17804 | 326 | 0.000 |
| 447 | 197 | 198 | 0.01832 | 0.08764 | 0.17804 | 326 | 0.000 |
| 448 | 202 | 200 | 0 | 0.02223 | 0 | 600 | 0.988 |
| 449 | 202 | 200 | 0 | 0.02244 | 0 | 600 | 0.988 |
| 450 | 202 | 200 | 0 | 0.02239 | 0 | 600 | 0.988 |
| 451 | 200 | 226 | 0.01462 | 0.10555 | 0.23455 | 429 | 0.000 |
| 452 | 200 | 226 | 0.01462 | 0.10555 | 0.23455 | 429 | 0.000 |
| 453 | 200 | 230 | 0.00724 | 0.07654 | 0.31397 | 858 | 0.000 |
| 454 | 200 | 230 | 0.00724 | 0.07654 | 0.31397 | 858 | 0.000 |
| 455 | 201 | 202 | 0.00264 | 0.03482 | 3.348 | 2832 | 0.000 |
| 456 | 201 | 202 | 0.0027 | 0.03566 | 3.434 | 2832 | 0.000 |
| 457 | 201 | 202 | 0.0027 | 0.03566 | 3.434 | 2832 | 0.000 |
| 458 | 202 | 233 | 0.00138 | 0.01646 | 1.8337 | 2832 | 0.000 |
| 459 | 202 | 233 | 0.00138 | 0.01646 | 1.8337 | 2832 | 0.000 |
| 460 | 226 | 203 | 0 | 0.106 | 0 | 100 | 1.000 |
| 461 | 204 | 205 | 0.14206 | 0.19104 | 0.00246 | 43 | 0.000 |
| 462 | 209 | 204 | 0 | 0.2996 | 0 | 25 | 1.000 |
| 463 | 206 | 208 | 0.07324 | 0.09492 | 0.01023 | 72 | 0.000 |
| 464 | 206 | 223 | 0.03332 | 0.09588 | 0.01288 | 118 | 0.000 |
| 465 | 206 | 223 | 0.03332 | 0.09588 | 0.01288 | 118 | 0.000 |
| 466 | 206 | 223 | 0.03393 | 0.09948 | 0.01287 | 118 | 0.000 |
| 467 | 226 | 206 | 0 | 0.061 | 0 | 200 | 0.975 |
| 468 | 226 | 206 | 0 | 0.065 | 0 | 200 | 0.975 |
| 469 | 226 | 206 | 0 | 0.065 | 0 | 200 | 0.975 |
| 470 | 207 | 208 | 0.03854 | 0.10813 | 0.01517 | 120 | 0.000 |
| 471 | 207 | 208 | 0.03854 | 0.10813 | 0.01517 | 120 | 0.000 |
| 472 | 207 | 213 | 0.03753 | 0.11034 | 0.01407 | 120 | 0.000 |
| 473 | 207 | 215 | 0.0432 | 0.12121 | 0.01701 | 120 | 0.000 |
| 474 | 207 | 215 | 0.0432 | 0.12121 | 0.01701 | 120 | 0.000 |
| 475 | 207 | 222 | 0.07989 | 0.10782 | 0.01064 | 72 | 0.000 |
| 476 | 207 | 223 | 0.1304 | 0.17208 | 0.01786 | 72 | 0.000 |
| 477 | 227 | 207 | 0 | 0.06205 | 0 | 200 | 0.963 |
| 478 | 227 | 207 | 0 | 0.06065 | 0 | 200 | 0.963 |
| 479 | 208 | 209 | 0.00346 | 0.0152 | 0.00228 | 163 | 0.000 |
| 480 | 208 | 209 | 0.00346 | 0.0152 | 0.00228 | 163 | 0.000 |
| 481 | 208 | 210 | 0.021 | 0.05893 | 0.00826 | 120 | 0.000 |
| 482 | 208 | 210 | 0.021 | 0.05893 | 0.00826 | 120 | 0.000 |
| 483 | 210 | 211 | 0.00107 | 0.00712 | 0.00183 | 326 | 0.000 |
| 484 | 210 | 211 | 0.00107 | 0.00712 | 0.00183 | 326 | 0.000 |
| 485 | 228 | 211 | 0 | 0.0605 | 0 | 200 | 0.988 |
| 486 | 228 | 211 | 0 | 0.0605 | 0 | 200 | 0.988 |
| 487 | 228 | 211 | 0 | 0.0625 | 0 | 200 | 0.988 |
| 488 | 228 | 211 | 0 | 0.0625 | 0 | 200 | 0.988 |
| 489 | 212 | 215 | 0.0826 | 0.24313 | 0.03105 | 120 | 0.000 |
| 490 | 214 | 221 | 0.07004 | 0.09718 | 0.00904 | 72 | 0.000 |

Table A.8 Transmission line data of Thailand power system-continued

| Line | From Bus | To Bus | *r* | *x* | *b* | Rating | Ratio |
|---|---|---|---|---|---|---|---|
| 491 | 216 | 220 | 0.02577 | 0.07576 | 0.00966 | 120 | 0.000 |
| 492 | 217 | 223 | 0.0207 | 0.06085 | 0.00776 | 120 | 0.000 |
| 493 | 218 | 223 | 0.04795 | 0.06651 | 0.00618 | 72 | 0.000 |
| 494 | 219 | 225 | 0.03287 | 0.09244 | 0.0129 | 118 | 0.000 |
| 495 | 219 | 225 | 0.03287 | 0.09244 | 0.0129 | 118 | 0.000 |
| 496 | 229 | 219 | 0 | 0.0585 | 0 | 200 | 0.988 |
| 497 | 229 | 219 | 0 | 0.06108 | 0 | 200 | 0.988 |
| 498 | 229 | 219 | 0 | 0.06042 | 0 | 200 | 0.988 |
| 499 | 220 | 225 | 0.01447 | 0.06358 | 0.00951 | 163 | 0.000 |
| 500 | 220 | 225 | 0.01447 | 0.06358 | 0.00951 | 163 | 0.000 |
| 501 | 220 | 225 | 0.02689 | 0.07885 | 0.0101 | 120 | 0.000 |
| 502 | 224 | 225 | 0.00547 | 0.01753 | 0.00244 | 118 | 0.000 |
| 503 | 230 | 225 | 0 | 0.065 | 0 | 200 | 0.988 |
| 504 | 230 | 225 | 0 | 0.065 | 0 | 200 | 0.988 |
| 505 | 230 | 225 | 0 | 0.0625 | 0 | 200 | 0.988 |
| 506 | 230 | 225 | 0 | 0.065 | 0 | 200 | 0.988 |
| 507 | 226 | 228 | 0.00493 | 0.03545 | 0.07836 | 429 | 0.000 |
| 508 | 226 | 228 | 0.00493 | 0.03545 | 0.07836 | 429 | 0.000 |
| 509 | 227 | 230 | 0.00518 | 0.03736 | 0.08206 | 429 | 0.000 |
| 510 | 227 | 230 | 0.00518 | 0.03736 | 0.08206 | 429 | 0.000 |
| 511 | 228 | 231 | 0.00112 | 0.01177 | 0.04798 | 858 | 0.000 |
| 512 | 228 | 231 | 0.00112 | 0.01177 | 0.04798 | 858 | 0.000 |
| 513 | 229 | 230 | 0.00309 | 0.02232 | 0.04901 | 429 | 0.000 |
| 514 | 229 | 230 | 0.00309 | 0.02232 | 0.04901 | 429 | 0.000 |
| 515 | 233 | 231 | 0 | 0.024 | 0 | 750 | 1.000 |
| 516 | 233 | 232 | 0 | 0.024 | 0 | 750 | 1.000 |
| 517 | 233 | 270 | 0.00095 | 0.01568 | 1.7691 | 3736 | 0.000 |
| 518 | 233 | 311 | 0.00096 | 0.01812 | 2.0724 | 3736 | 0.000 |
| 519 | 233 | 311 | 0.0011 | 0.02083 | 2.3903 | 3736 | 0.000 |
| 520 | 234 | 237 | 0.00676 | 0.04504 | 0.01156 | 326 | 0.000 |
| 521 | 234 | 237 | 0.00676 | 0.04504 | 0.01156 | 326 | 0.000 |
| 522 | 234 | 255 | 0.00315 | 0.01382 | 0.00207 | 163 | 0.000 |
| 523 | 234 | 255 | 0.00315 | 0.01382 | 0.00207 | 163 | 0.000 |
| 524 | 260 | 234 | 0 | 0.065 | 0 | 200 | 0.988 |
| 525 | 260 | 234 | 0 | 0.0601 | 0 | 200 | 0.988 |
| 526 | 260 | 234 | 0 | 0.0595 | 0 | 200 | 0.988 |
| 527 | 235 | 239 | 0.00849 | 0.05304 | 0.01552 | 326 | 0.000 |
| 528 | 235 | 239 | 0.00849 | 0.05304 | 0.01552 | 326 | 0.000 |
| 529 | 235 | 255 | 0.03368 | 0.09878 | 0.01266 | 120 | 0.000 |
| 530 | 261 | 236 | 0 | 0.065 | 0 | 200 | 1.000 |
| 531 | 261 | 236 | 0 | 0.065 | 0 | 200 | 1.000 |
| 532 | 237 | 242 | 0.01067 | 0.03201 | 0.00395 | 118 | 0.000 |
| 533 | 238 | 240 | 0.01634 | 0.04583 | 0.00643 | 120 | 0.000 |
| 534 | 238 | 240 | 0.01634 | 0.04583 | 0.00643 | 120 | 0.000 |
| 535 | 238 | 243 | 0.01598 | 0.07017 | 0.01051 | 163 | 0.000 |
| 536 | 238 | 243 | 0.01598 | 0.07017 | 0.01051 | 163 | 0.000 |

Table A.8 Transmission line data of Thailand power system-continued

| Line | From Bus | To Bus | *r* | *x* | *b* | Rating | Ratio |
|---|---|---|---|---|---|---|---|
| 537 | 263 | 238 | 0 | 0.0464 | 0 | 200 | 1.000 |
| 538 | 263 | 238 | 0 | 0.04625 | 0 | 200 | 1.000 |
| 539 | 264 | 239 | 0 | 0.0625 | 0 | 200 | 0.988 |
| 540 | 264 | 239 | 0 | 0.0625 | 0 | 200 | 0.988 |
| 541 | 264 | 239 | 0 | 0.065 | 0 | 200 | 0.988 |
| 542 | 264 | 239 | 0 | 0.065 | 0 | 200 | 0.988 |
| 543 | 240 | 258 | 0.03048 | 0.09145 | 0.01128 | 118 | 0.000 |
| 544 | 241 | 245 | 0.04789 | 0.07487 | 0.00857 | 78 | 0.000 |
| 545 | 241 | 246 | 0.05687 | 0.16714 | 0.02136 | 120 | 0.000 |
| 546 | 241 | 256 | 0.06243 | 0.18363 | 0.02344 | 120 | 0.000 |
| 547 | 241 | 259 | 0.04609 | 0.33245 | 0.04603 | 215 | 0.000 |
| 548 | 241 | 259 | 0.04609 | 0.33245 | 0.04603 | 215 | 0.000 |
| 549 | 242 | 252 | 0.01057 | 0.03171 | 0.00391 | 118 | 0.000 |
| 550 | 243 | 255 | 0.01346 | 0.05912 | 0.00885 | 163 | 0.000 |
| 551 | 265 | 244 | 0 | 0.065 | 0 | 200 | 0.988 |
| 552 | 265 | 244 | 0 | 0.065 | 0 | 200 | 0.988 |
| 553 | 265 | 244 | 0 | 0.065 | 0 | 200 | 0.988 |
| 554 | 246 | 249 | 0.04806 | 0.14124 | 0.01804 | 120 | 0.000 |
| 555 | 246 | 259 | 0.05747 | 0.16143 | 0.02262 | 120 | 0.000 |
| 556 | 246 | 259 | 0.05747 | 0.16143 | 0.02262 | 120 | 0.000 |
| 557 | 247 | 254 | 0.05737 | 0.16874 | 0.02153 | 120 | 0.000 |
| 558 | 247 | 258 | 0.04266 | 0.12801 | 0.01579 | 118 | 0.000 |
| 559 | 248 | 254 | 0.00377 | 0.02358 | 0.0069 | 326 | 0.000 |
| 560 | 248 | 254 | 0.00377 | 0.02358 | 0.0069 | 326 | 0.000 |
| 561 | 248 | 257 | 0.02479 | 0.15503 | 0.04542 | 326 | 0.000 |
| 562 | 267 | 248 | 0 | 0.065 | 0 | 200 | 1.000 |
| 563 | 267 | 248 | 0 | 0.065 | 0 | 200 | 1.000 |
| 564 | 249 | 251 | 0.00936 | 0.04113 | 0.00659 | 163 | 0.000 |
| 565 | 249 | 251 | 0.00936 | 0.04113 | 0.00659 | 163 | 0.000 |
| 566 | 250 | 251 | 0.00098 | 0.00964 | 0.00281 | 430 | 0.000 |
| 567 | 250 | 251 | 0.00098 | 0.00964 | 0.00281 | 430 | 0.000 |
| 568 | 268 | 250 | 0 | 0.0652 | 0 | 200 | 0.988 |
| 569 | 251 | 252 | 0.0166 | 0.07294 | 0.01092 | 163 | 0.000 |
| 570 | 252 | 253 | 0.01118 | 0.03354 | 0.00414 | 118 | 0.000 |
| 571 | 254 | 257 | 0.08975 | 0.26423 | 0.03376 | 120 | 0.000 |
| 572 | 268 | 259 | 0 | 0.06 | 0 | 200 | 1.000 |
| 573 | 268 | 259 | 0 | 0.06167 | 0 | 200 | 1.000 |
| 574 | 268 | 259 | 0 | 0.06558 | 0 | 200 | 1.000 |
| 575 | 260 | 263 | 0.00524 | 0.03769 | 0.08325 | 429 | 0.000 |
| 576 | 260 | 263 | 0.00524 | 0.03769 | 0.08325 | 429 | 0.000 |
| 577 | 260 | 263 | 0.00509 | 0.03665 | 0.08079 | 429 | 0.000 |
| 578 | 260 | 263 | 0.00509 | 0.03665 | 0.08079 | 429 | 0.000 |
| 579 | 260 | 264 | 0.0029 | 0.0209 | 0.04613 | 429 | 0.000 |
| 580 | 260 | 264 | 0.0029 | 0.0209 | 0.04613 | 429 | 0.000 |
| 581 | 260 | 273 | 0.00016 | 0.00166 | 0.00695 | 858 | 0.000 |
| 582 | 260 | 273 | 0.00016 | 0.00166 | 0.00695 | 858 | 0.000 |

Table A.8 Transmission line data of Thailand power system-continued

| Line | From Bus | To Bus | *r* | *x* | *b* | Rating | Ratio |
|---|---|---|---|---|---|---|---|
| 583 | 260 | 275 | 0.00016 | 0.00166 | 0.00695 | 858 | 0.000 |
| 584 | 260 | 275 | 0.00016 | 0.00166 | 0.00695 | 858 | 0.000 |
| 585 | 261 | 268 | 0.00065 | 0.00683 | 0.02784 | 858 | 0.000 |
| 586 | 261 | 268 | 0.00065 | 0.00683 | 0.02784 | 858 | 0.000 |
| 587 | 261 | 269 | 0.00077 | 0.01283 | 0.08345 | 1716 | 0.000 |
| 588 | 261 | 269 | 0.00077 | 0.01283 | 0.08345 | 1716 | 0.000 |
| 589 | 262 | 265 | 0.00044 | 0.00462 | 0.01885 | 858 | 0.000 |
| 590 | 262 | 265 | 0.00044 | 0.00462 | 0.01885 | 858 | 0.000 |
| 591 | 263 | 267 | 0.00379 | 0.03993 | 0.16308 | 858 | 0.000 |
| 592 | 263 | 267 | 0.00379 | 0.03993 | 0.16308 | 858 | 0.000 |
| 593 | 264 | 271 | 9.00E-05 | 0.001 | 0.00407 | 858 | 0.000 |
| 594 | 264 | 271 | 9.00E-05 | 0.001 | 0.00407 | 858 | 0.000 |
| 595 | 265 | 272 | 0.0022 | 0.01582 | 0.03484 | 429 | 0.000 |
| 596 | 265 | 272 | 0.0022 | 0.01582 | 0.03484 | 429 | 0.000 |
| 597 | 266 | 268 | 0.00062 | 0.00651 | 0.02656 | 858 | 0.000 |
| 598 | 266 | 268 | 0.00062 | 0.00651 | 0.02656 | 858 | 0.000 |
| 599 | 270 | 269 | 0 | 0.018 | 0 | 1000 | 1.000 |
| 600 | 270 | 269 | 0 | 0.018 | 0 | 1000 | 1.000 |
| 601 | 275 | 274 | 0 | 0.065 | 0 | 200 | 1.000 |
| 602 | 275 | 274 | 0 | 0.065 | 0 | 200 | 1.000 |
| 603 | 276 | 277 | 0.01184 | 0.03476 | 0.00428 | 179 | 0.000 |
| 604 | 276 | 277 | 0.0024 | 0.02521 | 0.00643 | 430 | 0.000 |
| 605 | 276 | 285 | 0.00519 | 0.05115 | 0.01489 | 430 | 0.000 |
| 606 | 276 | 289 | 0.03647 | 0.10943 | 0.0135 | 118 | 0.000 |
| 607 | 277 | 282 | 0.02212 | 0.06511 | 0.00828 | 120 | 0.000 |
| 608 | 277 | 285 | 0.00758 | 0.07982 | 0.02035 | 430 | 0.000 |
| 609 | 277 | 299 | 0.03327 | 0.09768 | 0.01249 | 120 | 0.000 |
| 610 | 301 | 277 | 0 | 0.06285 | 0 | 200 | 0.975 |
| 611 | 301 | 277 | 0 | 0.062 | 0 | 200 | 0.975 |
| 612 | 301 | 277 | 0 | 0.06183 | 0 | 200 | 0.975 |
| 613 | 278 | 287 | 0.0597 | 0.16757 | 0.02352 | 120 | 0.000 |
| 614 | 278 | 287 | 0.0597 | 0.16757 | 0.02352 | 120 | 0.000 |
| 615 | 302 | 278 | 0 | 0.065 | 0 | 200 | 1.000 |
| 616 | 302 | 278 | 0 | 0.065 | 0 | 200 | 1.000 |
| 617 | 279 | 280 | 0.02912 | 0.08554 | 0.01092 | 120 | 0.000 |
| 618 | 279 | 281 | 0.05805 | 0.1247 | 0.01483 | 96 | 0.000 |
| 619 | 279 | 286 | 0.032 | 0.09602 | 0.01184 | 118 | 0.000 |
| 620 | 280 | 288 | 0.02587 | 0.076 | 0.00971 | 120 | 0.000 |
| 621 | 303 | 280 | 0 | 0.065 | 0 | 200 | 1.000 |
| 622 | 303 | 280 | 0 | 0.065 | 0 | 200 | 1.000 |
| 623 | 283 | 299 | 0.01279 | 0.03753 | 0.0048 | 120 | 0.000 |
| 624 | 283 | 300 | 0.04624 | 0.13565 | 0.01739 | 120 | 0.000 |
| 625 | 304 | 284 | 0 | 0.1949 | 0 | 66.7 | 1.000 |
| 626 | 304 | 284 | 0 | 0.1949 | 0 | 66.7 | 1.000 |
| 627 | 285 | 292 | 0.001 | 0.01051 | 0.00268 | 430 | 0.000 |
| 628 | 285 | 292 | 0.001 | 0.01051 | 0.00268 | 430 | 0.000 |

Table A.8 Transmission line data of Thailand power system-continued

| Line | From Bus | To Bus | *r* | *x* | *b* | Rating | Ratio |
|---|---|---|---|---|---|---|---|
| 629 | 286 | 290 | 0.01697 | 0.10603 | 0.03104 | 326 | 0.000 |
| 630 | 286 | 290 | 0.01697 | 0.10603 | 0.03104 | 326 | 0.000 |
| 631 | 287 | 288 | 0.06334 | 0.17956 | 0.0247 | 120 | 0.000 |
| 632 | 305 | 287 | 0 | 0.123 | 0 | 100 | 0.975 |
| 633 | 305 | 287 | 0 | 0.123 | 0 | 100 | 0.975 |
| 634 | 289 | 290 | 0.00333 | 0.01465 | 0.00219 | 163 | 0.000 |
| 635 | 289 | 290 | 0.00333 | 0.01465 | 0.00219 | 163 | 0.000 |
| 636 | 289 | 297 | 0.0388 | 0.11828 | 0.01413 | 118 | 0.000 |
| 637 | 306 | 290 | 0 | 0.065 | 0 | 200 | 1.000 |
| 638 | 306 | 290 | 0 | 0.0625 | 0 | 200 | 1.000 |
| 639 | 291 | 295 | 0.00491 | 0.03268 | 0.00839 | 326 | 0.000 |
| 640 | 291 | 295 | 0.00491 | 0.03268 | 0.00839 | 326 | 0.000 |
| 641 | 308 | 291 | 0 | 0.0595 | 0 | 200 | 1.000 |
| 642 | 308 | 291 | 0 | 0.058 | 0 | 200 | 1.000 |
| 643 | 308 | 291 | 0 | 0.0595 | 0 | 200 | 1.000 |
| 644 | 308 | 291 | 0 | 0.0585 | 0 | 200 | 1.000 |
| 645 | 293 | 296 | 0.00762 | 0.0381 | 0.00795 | 163 | 0.000 |
| 646 | 293 | 296 | 0.00762 | 0.0381 | 0.00795 | 163 | 0.000 |
| 647 | 294 | 296 | 0.00347 | 0.01987 | 0.00522 | 326 | 0.000 |
| 648 | 294 | 296 | 0.00347 | 0.01987 | 0.00522 | 326 | 0.000 |
| 649 | 296 | 297 | 0.01626 | 0.04955 | 0.00592 | 118 | 0.000 |
| 650 | 309 | 296 | 0 | 0.065 | 0 | 200 | 1.000 |
| 651 | 309 | 296 | 0 | 0.065 | 0 | 200 | 1.000 |
| 652 | 309 | 296 | 0 | 0.065 | 0 | 200 | 1.000 |
| 653 | 298 | 300 | 0.03094 | 0.09075 | 0.01163 | 120 | 0.000 |
| 654 | 310 | 298 | 0 | 0.11967 | 0 | 100 | 1.000 |
| 655 | 301 | 306 | 0.00104 | 0.01726 | 0.11226 | 1716 | 0.000 |
| 656 | 301 | 306 | 0.00104 | 0.01726 | 0.11226 | 1716 | 0.000 |
| 657 | 301 | 310 | 0.01085 | 0.07847 | 0.17282 | 429 | 0.000 |
| 658 | 301 | 310 | 0.01085 | 0.07847 | 0.17282 | 429 | 0.000 |
| 659 | 301 | 310 | 0.01085 | 0.07847 | 0.17282 | 429 | 0.000 |
| 660 | 301 | 310 | 0.01085 | 0.07847 | 0.17282 | 429 | 0.000 |
| 661 | 302 | 305 | 0.00587 | 0.04255 | 0.09278 | 429 | 0.000 |
| 662 | 302 | 305 | 0.00587 | 0.04255 | 0.09278 | 429 | 0.000 |
| 663 | 303 | 305 | 0.00975 | 0.07046 | 0.15506 | 429 | 0.000 |
| 664 | 303 | 305 | 0.00975 | 0.07046 | 0.15506 | 429 | 0.000 |
| 665 | 303 | 306 | 0.01207 | 0.08734 | 0.19249 | 429 | 0.000 |
| 666 | 303 | 306 | 0.01207 | 0.08734 | 0.19249 | 429 | 0.000 |
| 667 | 304 | 310 | 0.00827 | 0.06016 | 0.13024 | 429 | 0.000 |
| 668 | 304 | 310 | 0.00827 | 0.06016 | 0.13024 | 429 | 0.000 |
| 669 | 306 | 307 | 0.0005 | 0.00828 | 0.05384 | 1716 | 0.000 |
| 670 | 306 | 307 | 0.0005 | 0.00828 | 0.05384 | 1716 | 0.000 |
| 671 | 306 | 313 | 0.00035 | 0.00368 | 0.01499 | 858 | 0.000 |
| 672 | 306 | 313 | 0.00035 | 0.00368 | 0.01499 | 858 | 0.000 |
| 673 | 307 | 309 | 0.0018 | 0.01891 | 0.07711 | 858 | 0.000 |
| 674 | 307 | 309 | 0.0018 | 0.01891 | 0.07711 | 858 | 0.000 |

Table A.8 Transmission line data of Thailand power system-continued

| Line | From Bus | To Bus | *r* | *x* | *b* | Rating | Ratio |
|---|---|---|---|---|---|---|---|
| 675 | 312 | 307 | 0 | 0.024 | 0 | 750 | 0.975 |
| 676 | 312 | 307 | 0 | 0.024 | 0 | 750 | 0.975 |
| 677 | 311 | 312 | 0.00012 | 0.00218 | 0.24702 | 3736 | 0.000 |
| 678 | 311 | 312 | 0.00012 | 0.00218 | 0.24702 | 3736 | 0.000 |

# BIOGRAPHY

Sataporn Limpatthamapanee was born in Nakhon Ratchasima Province, Thailand, on July 25, 1981. He received B.Eng. and M.Eng. degrees in electrical engineering from Chulalongkorn University, Thailand, in 2002 and 2007, respectively. He has joined Electricity Generating Authority of Thailand (EGAT) since 2002. Currently, he is an engineer in Electrical Maintenance Section, Hydro Power Plant Department, Generating Division, EGAT, and working toward the Ph.D. degree in electrical engineering at Chulalongkorn University. His research interests include power system operations, transfer capability, and power system security.